Light-driven Catalysis in Decarboxylative Small Molecule Functionalization

By

Kaitie Chase Cartwright

Submitted to the graduate degree program in chemistry and the graduate faculty of the University of Kansas in partial fulfillment of the requirements for the degree of Doctor of Philosophy.

_____

Chair: Jon A. Tunge

_____

Paul R. Hanson

_____

Michael A. Rubin

_____

Mikhail V. Barybin

_____

Shyam Sathyamoorthi

Date Defended: May 8, 2020

The dissertation committee for Kaitie Chase Cartwright certifies that this
is the approved version of the following dissertation:

Light-driven Catalysis in Decarboxylative Small Molecule Functionalization

_____

Jon A. Tunge

Date Approved: 8 May 2020

Abstract

Kaitie C. Cartwright and Jon A. Tunge

Department of Chemistry, May 8, 2020

The University of Kansas

Herein, the development and mechanistic elucidation of light-driven decarboxylative processes for the installation of olefins is described. The primary focus has been to devise methodology that allows for the installation of highly versatile functionalities and the synthesis of synthetically valuable building-blocks while adhering to the principles of green chemistry. This has been accomplished through the development of decarboxylative transformations that utilize light-driven catalysis. Through these developments, new approaches to olefin installation that improve upon the utility, economy, and environmental impact of traditional methods have been realized. In addition, new insights into catalyst reactivity have advanced the understanding of the reaction mechanisms and will ideally aid in further developments in the field.

Acknowledgement

I wish to express my deepest gratitude to Jon Tunge for his mentorship throughout my graduate studies. In addition to being an incredibly genuine and caring advisor, Jon's consistent guidance over my growth as a scientist as well as the incredible opportunities he has provided to me have led to a variety of my accomplishments over the past five years and I believe prepared me well for the next chapter in my chemistry journey. Jon's wealth of knowledge and curiosity towards devising and understanding new chemistry has consistently inspired me to continuously learn and discover. Thank you, Jon, for taking a chance on me five years ago, this has been an incredible experience.

Second, I would like to thank the professors that I have interacted with both in my courses as well as during my time at KU for a variety of rewarding discussions and for being an integral part of the learning process. I would also like to thank my committee members Jon Tunge, Paul Hanson, Michael Rubin, Mikhail Barybin, and Shyam Sathyamoorthi for your time and consideration during this process. Additionally, the work highlighted herein would not have been possible without the chemistry department staff and those that maintain the instrumentation facilities.

I would like to acknowledge my fellow KU graduate students that have been apart of this journey. Although I'm grateful for many people that have been part of this venture, there are several chemists I would like to highlight for their contributions and support. First, my lab daddy, Simon Lang, for his mentorship when I was just "a little guy" and continued friendship. Second, I'd like to thank all my co-authors for sharing in the pursuit of discovery and all the Tunge group members that aided in the maintenance of the lab and the laughs. I also wish to express my gratitude to Ashlie Walker, Angelika Trujillo, and Richard Welter who, despite only overlapping with me

at KU for a short time, have continuously supported my endeavors. To all my unmentioned past and present KU colleagues, thank you for the assistance, friendship, and the maintenance of the party spirit over the years.

I would like to pay special regard to my love Andy Edwards whose enthusiasm for chemistry and unrivaled attention to good lab technique has been enormously influential during my graduate school pursuits. Andy has not only been an editor, dear friend, and a constant source of valuable conversations but has also been my number one supporter throughout this process. I'm forever grateful for all that you have done and continue to do for me.

None of this would have been possible without my initial inspiration to pursue chemistry which was largely inspired and encouraged by the chemistry department at Sweet Briar College. I am indebted to everyone from my era of SBC chemistry for not only the influential experience but for the support and assistance throughout my seemingly unconventional path that led to my graduate studies at KU.

Lastly, I would like to thank those in my life that have supported and assisted me during my graduate studies despite having no idea what monopolized seemingly all my time. First, I wish to express my deepest gratitude to my mother, Mindy Cartwright, who has always fought for me to have countless opportunities and continued to support me after I learned to embrace her fierce independence and fight for myself. Also, I'd like to acknowledge all my family members that have supported me and accepted the reclusive nature I adopted during my graduate studies. I also wish to acknowledge the various roommates and acquaintances I've had during my time in Lawrence that have indirectly aided in this journey. Finally, I wish to pay special recognition to my angel, Sadie Mae, who moved to Lawrence with me and whose companionship throughout this experience will forever be treasured.

Table of Contents

Chapter 1: The Rise of Decarboxylation in Photoredox Catalysis

Chapter 2: Decarboxylative $C(sp^3)$–$C(sp^3)$ Cross-Coupling with π-electrophiles via Photoredox/Palladium Dual-Catalysis

Chapter 3: Photoredox-Promoted Kochi Decarboxylative Elimination

Chapter 4: Photoredox/Cobaloxime Dual Catalysis in Small Molecule Functionalization

Chapter 5: Acridinium/Cobaloxime Dual Catalysis for the Decarboxylative Elimination of Carboxylic Acids

Abbreviations

Ac	acetate
Acr$^+$	acridinium
ANDEN-Phenyl Trost	bis[2′-(diphenylphosphino)benzamido]-9,10-dihydro-9,10-ethanoanthracene
Ar	aryl
BINAP	2,2'-bis(diphenylphosphino)-1,1'-binaphthyl
Bn	benzyl
Boc	di-tert-butyl decarbonate
BOX	bis(oxazoline)
bpy	bipyridine
C	Celsius
cat.	catalyst
Cbz	barboxybenzyl
chgH	dicyclohexylglyoxime
Chiraphos	bis(diphenylphosphino)butane
cm^{-1}	inverse centimeter
COD	1,5 cyclooctadiene
Cy	cyclohexyl
Cz	carbazole
d	doublet (NMR)
DavePhos	2-Dicyclohexylphosphino-2′-(*N,N*-dimethylamino)biphenyl
dba	dibenzylideneacetone
DcA	decarboxylative allylation
DcB	decarboxylative benzylation
DCC	*N,N′*-Dicyclohexylcarbodiimide
DCE	dichloroethane
DCM	dichloromethane

Difluorophos	[4-(5-diphenylphosphanyl-2,2-difluoro-1,3-benzodioxol-4-yl)-2,2-difluoro-1,3-benzodioxol-5-yl]-diphenylphosphane
DIOP	2,3-*O*-Isopropylidene-2,3-dihydroxy-1,4-bis(diphenylphosphino)butane
DMAP	4-dimethylaminopyridine
DME	dimethoxyethane
DMF	dimethylformamide
dmgH	dimethylglyoxime
DMSO	dimethylsulfoxide
DPEPhos	bis[(2-diphenylphosphino)phenyl]
dpgH	diphenylglyoxime
dppe	1,2-bis(diphenylphosphino)ethane
dppf	1,1′-ferrocenediyl-bis(diphenylphosphine)
dtbbpy	di-tert-butyl-bipyridine
d.r.	diastereomeric ratio
DTMB	3,5-di-*tert*-butyl-4-methoxyphenyl
DuPhos	1,2-bis[(2S,5S)-2,5-dimethylphospholano]benzene
EDW	electron donating group
equiv.	equivalent
e.r.	enantiomeric ratio
ESITOF	electrospray ionization time-of-flight
Et	ethyl
EWG	electron withdrawing group
g	gram
GC	gas chromatography
h	hour
HiersoPHOS	1',4-bis(t-butyl)-1,2-bis(diphenylphosphino)-3'-(di-i-propylphosphino)ferrocene
HRMS	high resolution mass spectrometry

Hz	Hertz
IPN	4,6-dicyanobenzene
IR	infrared spectroscopy
kcal	kilocalorie
LED	light emitting diode
m	multiplet (NMR)
M	mols per liter
Me	methyl
MeCN	acetonitrile
MeOH	methanol
MeOBIPHEP	(6,6′-Dimethoxybiphenyl-2,2′-diyl)bis[bis(3,5-di-*tert*-butyl-4-methoxyphenyl)phosphine]
Mes	mesityl
mg	milligram
MHz	mega Hertz
min	minute
mL	milliliter
MonoPhos	(dinaphthalen-4-yl)dimethylamine
MOP	2-(diphenylphosphino)-2′-methoxy-1,1′-binaphthyl
MS	mass spectrometry
NMR	nuclear magnetic resonance
PC	photocatalyst
PG	protecting group
Phanephos	4,12-bis(diphenylphosphino)-[2.2]-paracyclophane
Ph	phenyl
PN	1,2-dicyanobenzene
ppy	phenylpyridine
q	quartet (NMR)
rt	room temperature

s	singlet (NMR)
salen	2,2′-ethylenebis(nitrilomethylidene)diphenol
SCE	saturated calomel electrode
SegPhos	5,5′-Bis(diphenylphosphino)-4,4′-bi-1,3-benzodioxole
STAB	sodium triacetoxyborohydride
SynPhos	6,6'-Bis(diphenylphosphino)-2,2',3,3'-tetrahydro-5,5'-bi-1,4-benzodioxin
t	triplet (NMR)
tBu	tert-butyl
TEMPO	2,2,6,6-tetramethylpiperidine 1-oxyl
Tf	trifyl
TFP	tri(2-furyl)phosphine
THF	tetrahydrofuran
TLC	thin layer chromatography
TOF	turn over frequency
TON	turn over number
TPN	1,4-dicyanobenzene
Tol	toluene
TunePhos	1,13-bis(diphenylphosphino)-7,8-dihydro-6H-dibenzo[f,h][1,5]dioxonin
UV-Vis.	ultraviolet–visible spectroscopy
V	Volt
W	Watt
Xantphos	4,5-Bis(diphenylphosphino)-9,9-dimethylxanthene
XPhos	2-Dicyclohexylphosphino-2′,4′,6′-triisopropylbipheny
{}	decoupling (NMR)
~	approximately
<	less than
>	greater than

# Chapter 1: The Rise of Decarboxylation in Photoredox Catalysis

1.1 Modern Photoredox Catalysis

Historically, light-mediated catalysis has enabled access to unique reaction pathways in organic synthesis that were previously difficult or unobtainable under thermal conditions.[1] Although known for several decades, the application of photoredox catalysis in organic synthesis was not explored extensively until the late 2000s.[2] New explorations into the application of photoredox catalysis to organic synthesis have led to a resurgence in radical chemistry and provided new advances in the realm of green chemistry as this strategy allows light energy to be converted into significant chemical energy.

These reactions operate by utilizing transition metal chromophores, such as ruthenium (Ru) and iridium (Ir) polypyridyl complexes,[2j] or organic dyes as catalyst.[2e] These catalysts absorb visible light, while common organic molecules do not, allowing for the selective excitation of the catalyst. This first excitation puts the catalyst in the singlet excited state (SES), which can then undergo intersystem crossing (ISC) to access the triplet excited state (TES) (Scheme 1.1).[2j] Once in the excited state, the catalyst exists both as an oxidant and a reductant simultaneously. The propensity of the catalyst to serve as an oxidant or a reductant can be determined based upon its' redox potentials with the most positive potential species being
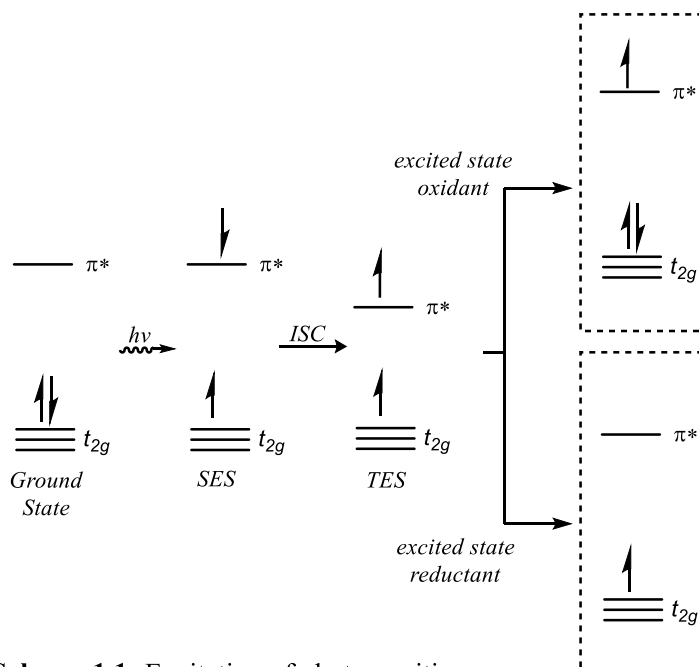

Scheme 1.1: Excitation of photosensitizers

reduced. When the excited state photocatalyst (PC) oxidizes a substrate (Sub), this process can be termed "direct reductive quenching" as the catalyst becomes reduced by one electron (Scheme 1.2). The reduced catalyst can then transfer this electron to another reagent to return to the ground state. Alternatively, the photocatalyst can serve as an excited state reductant and reduce a substrate which can be referred to as "direct oxidative quenching" (Scheme 1.2). The oxidized photocatalyst can then gain an electron from another species in the reaction media to return to the ground state. When substrate activation is achieved after the photocatalyst is quenched out of the excited state, the process can be referred to as an indirect quenching event (Scheme 1.2). This unique
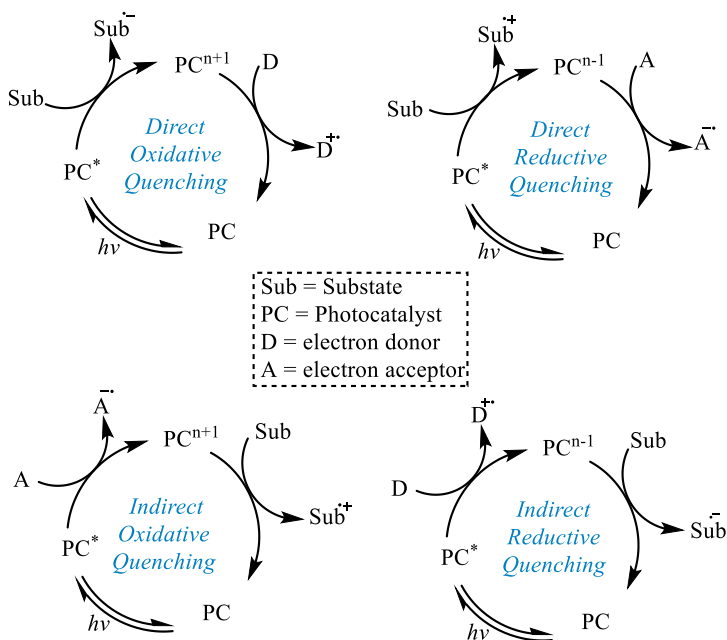
Scheme 1.2: Possible single electron transfer events in photocatalytic cycle

electronic duality provides access to net redox-neutral reaction conditions. Conversely, other redox methods, like electrochemistry, utilize a reaction environment that is either oxidizing or reducing but not both.[3]

A subsection of this field that has emerged during this modern renaissance is dual photoredox catalysis.[4] This methodology employs photoredox catalysis in conjunction with a second catalytic activation mode in order to achieve a synergistic effect. In this strategy, the photocatalyst can absorb light to activate a substrate while the second catalyst can dictate the reactivity of the resulting reactive intermediate. Often, the turnover of both catalysts is reliant on

one another, which can be advantageous as the formation of an excess quantity of reactive intermediates can be controlled and various oxidation states can be accessed. This also allows systems to be engineered such that additives are not needed to achieve substrate activation via an indirect quenching event as the co-catalyst can participate in the excited state quenching event. Utilizing photoredox catalysis in a dual catalytic design has been demonstrated to be operable with a broad range of co-catalyst and thus has served as a powerful approach towards the construction of complex organic molecules.

To date, photoredox catalysis has proven to be an invaluable strategy. These processes have clear benefits for sustainability as they employ light as the non-hazardous, energy efficient, and environmentally benign energy source instead of the high temperatures and harsh reaction conditions often required in thermal activation. Additionally, photoredox catalysis allows for the use of poorly reactive moieties, while also having high functional group tolerance allowing for safer, shorter, and more economical synthetic routes. However, despite the plethora of advancements, there are still challenges to be addressed in photoredox strategies. For one, these protocols have seen limited industrial application due to the difficulty achieving efficient irradiation on a large scale.[5] One solution to this problem is the use of flow-through technologies.[5] Another challenge is the extensive use of precious metal-containing photocatalysts, which are not sustainable materials.[2g,2j] These factors have resulted in a focus on organic dyes as photocatalysts and the engineering of organic dyes to have comparable activity to popular Ir- and Ru- based photocatalysts.[2c,2e,6] Ultimately, the field of photoredox catalysis provides an alternative to classical thermal reactions and can provide new opportunities towards accessing otherwise difficult reactivity while progressing towards greener and more economical processes.

1.2 Photoredox Catalysis in Decarboxylation

1.2.1 Modes of Decarboxylation

Carbon–Carbon (C–C) bond forming reactions are one of the most important synthetic transformations due to the prevalence of C–C bonds in organic scaffolds. One powerful strategy to create these sought-after bonds is through transition metal-catalyzed cross-coupling reactions.[7] Despite the high utility of these processes, traditional cross-coupling methods often utilize pre-activated coupling partners such as halides and highly reactive organometallic reagents (Scheme 1.3A).[7] This necessity not only places limitations on functional group compatibility but also results in the production of unwanted, sometimes toxic, stoichiometric side products. Carboxylic acids represent an alternative to halides or organometallic coupling partners as the extrusion of carbon dioxide (CO_2) can allow for the formation of carbon-metal intermediates reminiscent of those achieved with organometallic coupling partners but, with a benign and easily removed stoichiometric side-product (Scheme 1.3B).[8] Additionally, the high prevalence, versatility, and easy handling of carboxylic acids makes them an ideal choice for a coupling partner.
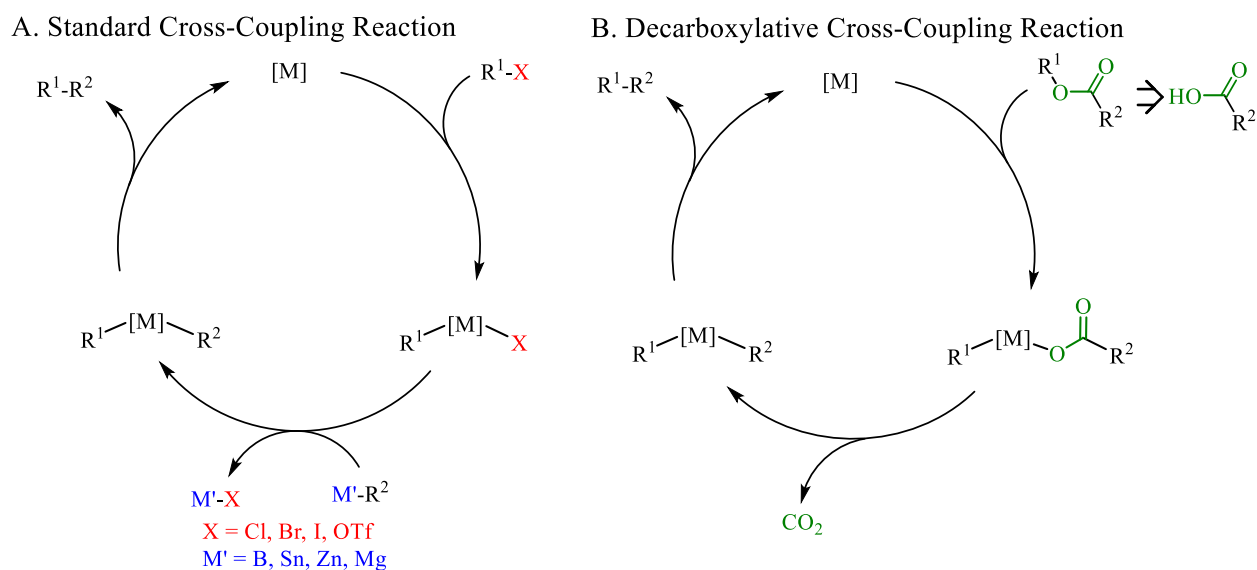
Scheme 1.3: Traditional and decarboxylative cross-coupling processes

Carboxylic acids are also unique in that, post the decarboxylation event, either nucleophilic or electrophilic synthetic equivalents can be generated (Scheme 1.4).[8,9] Perhaps one of the most versatile of these intermediates is the carbon radical, as the radical can itself participate in the bond
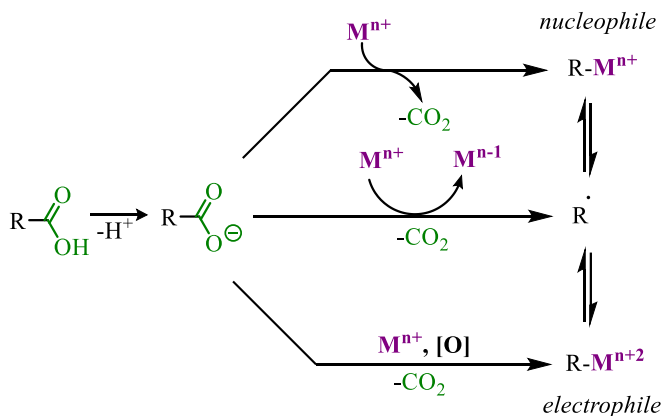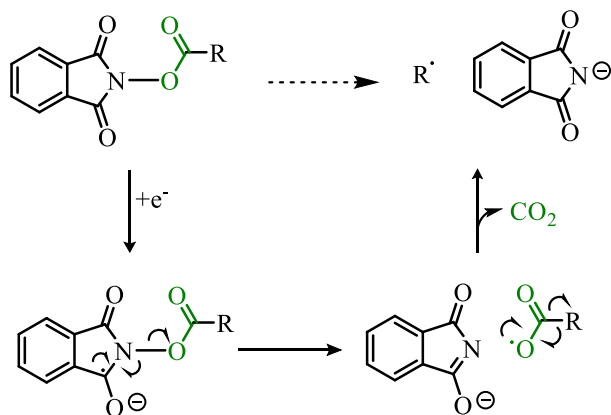

Scheme 1.4: Decarboxylation routes

forming process or can be further transformed via single electron reduction to an anion or single electron oxidation to a cation.[10] In addition, the radical decarboxylation process is facile and thus easier to achieve with an array of carboxylic acids compared to ionic pathways that rely on stabilization of the resulting reactive intermediate.[11] This mode of decarboxylation has received wide-spread attention over the last decade as a result of 1) the synthetic creativity and functionalization opportunity that can be achieved through utilizing carboxylic acids as masked carbon radicals and 2) the rise in photoredox catalysis and its' advantages in radical decarboxylation transformations.[2,12]

1.2.2 Reductive Radical Decarboxylation

Although the surge of photoredox-catalyzed synthetic transformations has recently led to extensive utilization of carboxylic acids as radical surrogates, methods that employ radical decarboxylation pathways have been known for many decades.[11a] One of the most famous classic examples is the Barton decarboxylation.[13] These reactions employ the use of a thiohydroximate ester more commonly referred to as the Barton ester. This functionality is poised to undergo fragmentation in the presence of a tin radical which facilitates the radical decarboxylation event to

provide the desired carbon radical intermediate. Hydrogen atom transfer (HAT) then results in the formation of a new C–H bond and propagates the radical chain process. Notable drawbacks to this methodology are the need to synthesize the Barton ester, the difficulty associated with handling and storing the Barton ester, as well as the stoichiometric and toxic side products that the process produces.[14]

Significant improvements to the Barton decarboxylation were reported by Okada in the late 80's and early 90's through employing *N*-(acyloxy)phthalimides (NHPI esters) which are more stable and easier to handle compared to the Barton ester and can be readily obtained from carboxylic acids.[15] These esters are unique in that they are posed to be reduced by one electron which facilitates the fragmentation event. Because a single electron reduction initiates the decarboxylation event, this C–C bond breaking strategy is termed a "reductive radical

Scheme 1.5: Redox-active ester facilitated decarboxylation

decarboxylation" and the functionality referred to as a "redox-active ester" (Scheme 1.5). Okada demonstrated that these redox-active esters can be used with a Ru photosensitizer to initiate the decarboxylation event and, when in the presence of electron deficient olefins, decarboxylative Michael addition reactions were achieved resulting in the formation of new $C(sp^3)$–$C(sp^3)$ bonds.[15b] Following this, Okada found this strategy can be employed for chlorination, phenylselenenylation, and to generate alkane products reminiscent of those from the Barton process.[15c-d] Okada's reports represent the first examples of decarboxylation in photoredox-catalyzed processes.

The NHPI redox-active ester model failed to gain popularity until recent years but has gone on to serve as a valuable strategy to utilize carboxylic acids as coupling partners in photoredox-catalyzed C–C bond forming reactions.[16] Typically, these operate via indirect reductive quenching. Thus, they rely on the photocatalyst to be reduced out of the excited state followed by an electron transfer from the reduced photocatalyst to the NHPI ester. This is typically done with amines that can undergo single electron oxidation to radical cations such as triethyl amine, diisopropylethylamine, and the Hantzsch ester (Scheme 1.6). Some of these methods employ the amines super-stoichiometrically but other processes have devised ways to use these reagents in electron transfer processes that render them sub-stoichiometric in these transformations.[17]
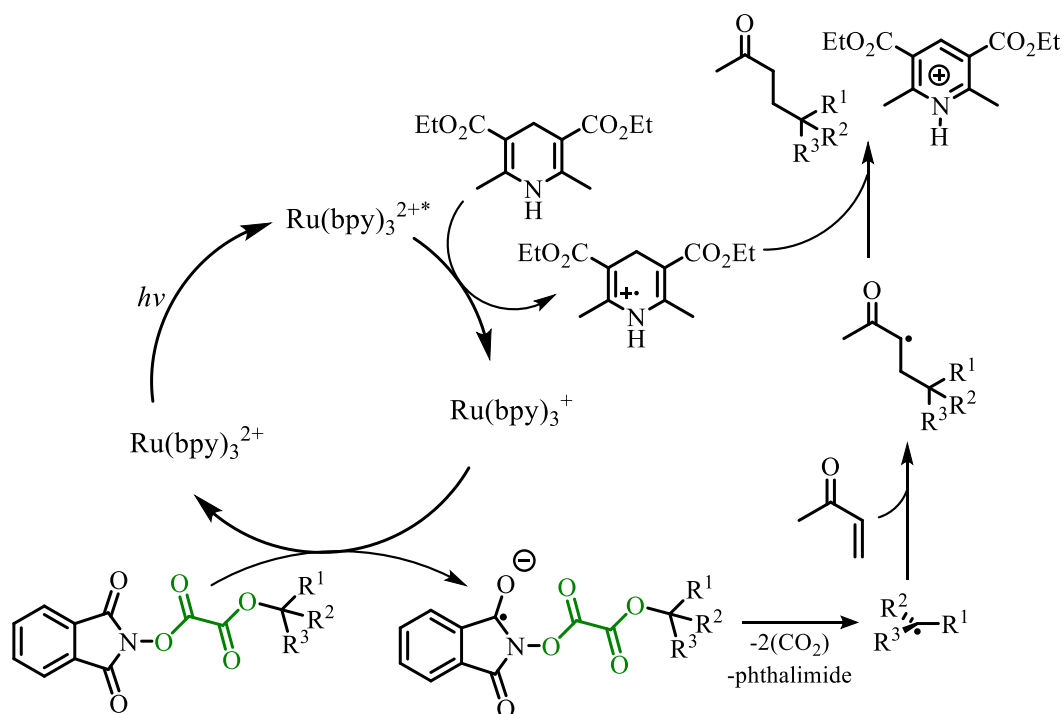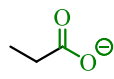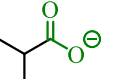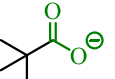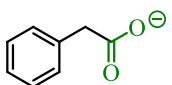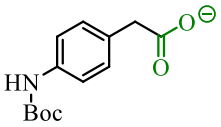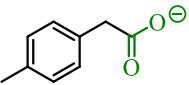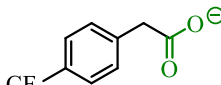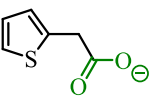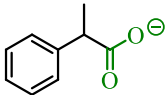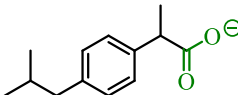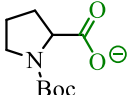

Scheme 1.6: NHPI ester in photoredox-catalyzed conjugate addition[17d]

Although this strategy has been highly successful for allowing carboxylic acids to serve as radical surrogates in synthesis, the poor atom economy of these processes must be noted. First, making the redox-active esters from carboxylic acids adds an additional synthetic step to the reaction sequence. But, perhaps more notable is the phthalimide waste generated in order to

achieve CO_2 extrusion (Scheme 1.5). The additional steps and atom loss detract from the strategy's idealness.[18]

1.2.3 Oxidative Radical Decarboxylation

A more direct approach towards homolytic C–C cleavage is oxidative radical decarboxylation which facilitates decarboxylation through direct substrate activation which would eliminate the need for any pre-activation of the carboxylic acid moiety. This strategy offers more ideal atom and step economy compared to the reductive radical decarboxylation processes. However, this decarboxylation strategy can be challenging as the oxidation potentials of carboxylates are quite high and a highly oxidizing photosensitizer would be needed to achieve the single electron oxidation of a carboxylate (Table 1.1).[19] Alternatively, more easily oxidized functionalities may be part of the substrate scaffold but this would limit the scope of applicable molecules.

Table 1.1: Oxidation potentials of tetrabutylammonium carboxylates vs. SCE

Oxidative radical decarboxylation occurs in nature and has been extensively studied in the context of biochemistry.[20] In organic chemistry, oxidative decarboxylation emerges in the Hunsdiecker-type reactions utilizing transition metal salts and persulfates to activate and oxidize

A. Minisci Reaction
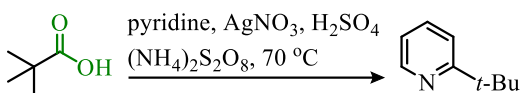
B. Kochi Decarboxylation

C. Kolbe Electrolysis
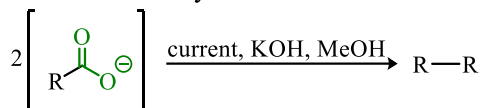
Scheme 1.7: Classic oxidative radical decarboxylation reactions

the carboxylate moiety (Scheme 1.7A & 1.7B).[11a,21a-d,22] Despite the appeal of direct activation of the carboxylate moiety, these classic synthetic methods have numerous drawbacks. Notably, they require a stoichiometric amount of toxic transition metals and elevated temperatures. Another classic oxidative radical decarboxylation process is Kolbe electrolysis (Scheme 1.7C).[21f-i] Through employing electrochemical means, the Kolbe electrolysis bypasses the use of the toxic reagents typically utilized in the Hunsdiecker-type processes. But, as mentioned previously, electrochemical methods operate under either oxidizing or reducing conditions (oxidiz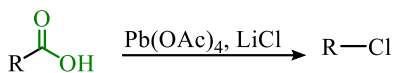ing conditions in Kolbe electrolysis) which can result in chemoselectivity problems. In these classic processes, poor control of the generated radicals' reactivity limits the synthetic utility. As such, utilizing the oxidative radical decarboxylation strategy in photoredox catalyzed systems is an attractive alternative to improve upon the utility of these methods while moving towards green synthetic processes.

During the past decade, the use of photoredox catalysis to facilitate oxidative radical decarboxylation emerged as a viable strategy to generate carbon radicals.[12] One of the first examples is from the Nishibayashi lab in 2013 in which aminobenzyl radicals were accessed from aminoarylacetic acids (Scheme 1.8).[23] In this report, oxidation of the amine functionality by the photocatalyst is proposed to facilitate decarboxylation. The resulting benzyl radical can then be trapped by electron deficient olefins. Moderate to good yields of the desired product are observed with competitive homocoupling of the resulting radical forming as a side product of the

transformation. Having the amine functionality is key to this strategy, as the iridium photosensitizer utilized, $[Ir(ppy)_2(bpy)]^+$ $[BF_4]^-$, can perform amine oxidation more efficiently while direct oxidation of the carboxylate moiety is largely endergonic and thus would be an inefficient pathway $(Ir(ppy)_2(bpy)^+$ E^{red} = +0.77 V, triethylamine E^{red} = +0.96 V, acetate E^{red} = +1.24 V vs. SCE).[24]

Scheme 1.8: Nishibayashi decarboxylative conjugate addition via oxidative substrate activation[22]

In 2014, MacMillian reported a decarboxylative arylation in which a direct single electron oxidation of the carboxylate moiety is proposed (Scheme 1.9).[25] Here, *N*-Boc amino acids are utilized to obtain α-amino radical intermediates. Cyanoaromatics that are capable of being reduced to radical anions were employed as the arene coupling partner. Due to the persistent radical feature of the cyanoarenes utilized, the cross-coupled products can be obtained in good yields.[26] Fluorescence quenching studies revealed that this process operates via an oxidative quenching pathway in which the Ir serves as an excited state reductant to generate the cyanoarene radical anion (Scheme 1.9). Once the Ir^{IV} is generated, the single electron oxidation of the carboxylate is needed to activate the substrate and turn over the catalyst. The direct single electron oxidation of the Boc-proline carboxylate is difficult as the oxidation potential (E^{red} = +0.95 V vs. SCE) is quite high. Thus, this strategy requires a strongly oxidizing photocatalyst. As a result, iridium sensitizers with fluorine substituents on the pyridine backbone were employed to provide the needed

efficiency for this oxidation Ir[p-F(t-Bu)ppy]$_3$ & Ir(dFppy)$_3$, $E_{1/2}^{red}$ [Ir^{IV}/Ir^{III}] = +0.97 V & +1.13 V vs. SCE in CH$_3$CN respectively).[25,27]

Scheme 1.9: MacMillian decarboxylative arylation of a-amino acids[24]

These seminal reports commenced the exploration of employing photoredox catalysis to enable the direct use of carboxylic acids as coupling partners in a variety of synthetic transformations. In the subsequent chapters, the development of methods that utilize photoredox catalysis to access carbon radicals directly from carboxylic acids for the instillation of olefin functionalities are described.

Chapter 2: Decarboxylative C(sp^3)–C(sp^3) Cross-Coupling with π-electrophiles via Photoredox/Palladium Dual-Catalysis
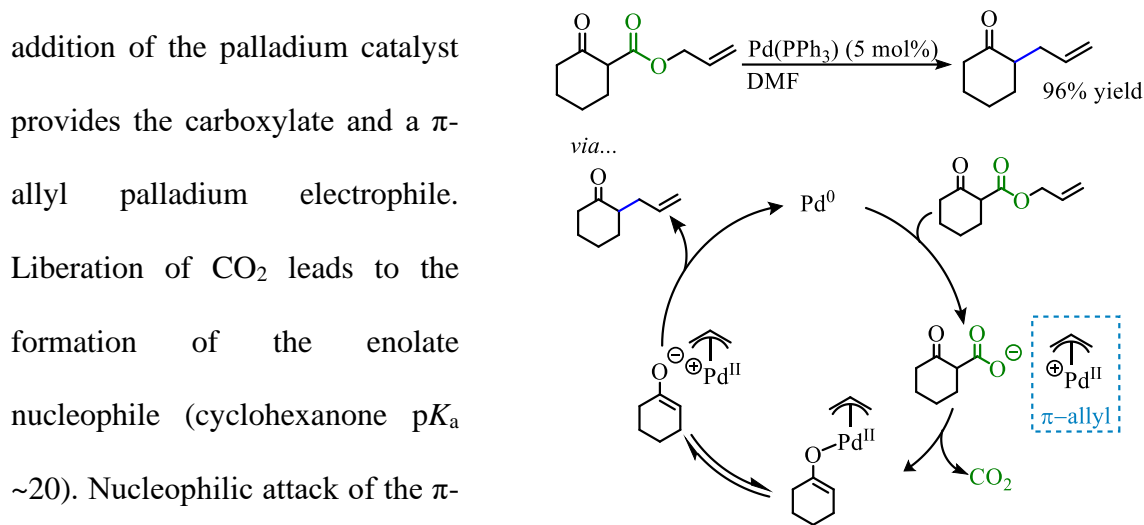
2.1 Introduction

In 2014, the Tunge lab introduced the use of carboxylic acid substrates in a dual-catalytic decarboxylative allylation.[28] Here, the photocatalyst is utilized to facilitate the radical decarboxylation event of amino alkanoic acids and esters that would otherwise be unreactive under thermal conditions. By employing this process in conjunction with a palladium (Pd) catalyst, the resulting radical species could be trapped by an electrophilic π-allyl-Pd. The cooperation of the two catalysts controls the production of the highly reactive radical intermediate, allowing for efficient cross-coupling. Since this initial report, the reaction has been further investigated resulting in an improvement on the methods utility. Reaction yields have been improved and the scope has been expanded to other classes of carboxylic acids as well as more diverse electrophiles. Additionally, mechanistic probes have provided new insights into the dominant reaction pathway and factors dictating the advantages and disadvantages of this methodology. In this chapter, the preceding work and the expansion upon the original photoredox/Pd dual catalysis report are described.

2.2 Decarboxylative Allylation (DcA) and Benzylation (DcB)

As discussed in *Section 1.2.1*, employing carboxylic acids as an alternative to pre-formed organometallics and halides represents a greener alternative to standard cross-coupling reactions (Scheme 1.3). One such reaction that has benefited from a decarboxylative variant is the Tsuji-Trost allylation.[29] This reaction is noteworthy as the method allows for the coupling of allylic electrophiles with nucleophiles chemo-, regio-, and stereoselectively.[30] To achieve new C–C bond
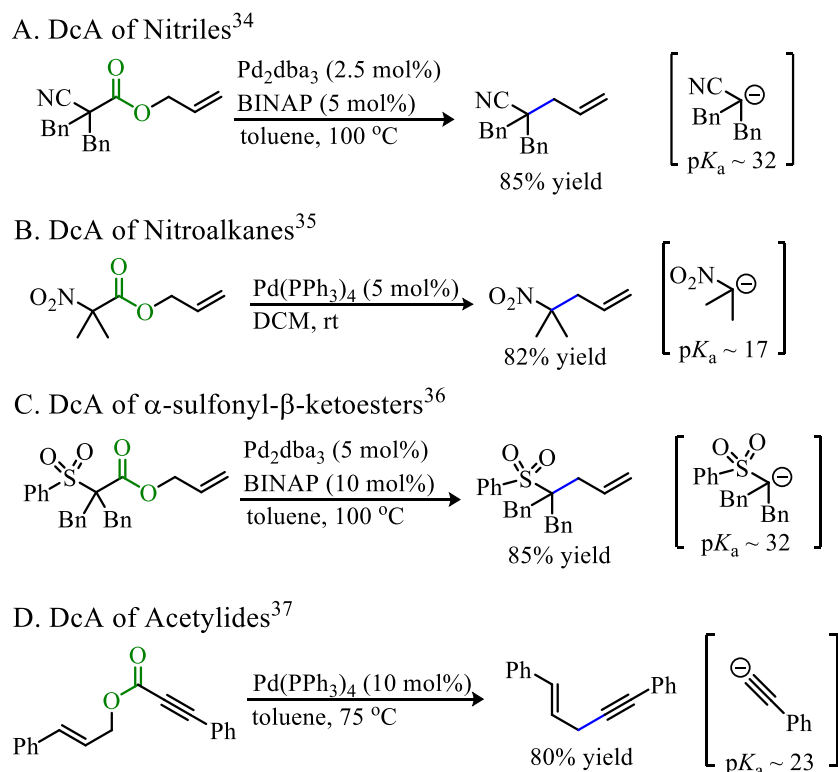
formations, these reactions are often limited to "soft" nucleophiles whose corresponding pK_a's are <20. Nucleophiles with higher pK_a's have been successfully utilized by employing preformed organometallic reagents.[31] Ultimately, these requirements limit the reactions utility as the conditions are highly alkaline, a stoichiometric amount of metal waste is produced, and pre-formed nucleophiles are frequently required. Alternatively, decarboxylative allylation (DcA) provides the carbon nucleophile *in situ* while producing easily removed byproduct, CO_2, thus improving upon the synthetic efficiency and economy of the traditional process.[29]

The first reports of a decarboxylative allylation utilize allyl esters of β-keto acids as substrates with a palladium catalyst to provide γ,δ-unsaturated ketones (Scheme 2.1).[32] Oxidative addition of the palladium catalyst provides the carboxylate and a π-allyl palladium electrophile. Liberation of CO_2 leads to the formation of the enolate nucleophile (cyclohexanone pK_a ~20). Nucleophilic attack of the π-allyl palladium provides the new C–C bond and returns the palladium catalyst to the cycle (Scheme 2.1). Following these initial

Scheme 2.1: Palladium-catalyzed DcA of enolate nucleophiles[32b]

reports, numerous methods for the facile allylation of enolate surrogates emerged.[29a,33] Although the vast majority of the DcA methods have focused on enolate nucleophiles, other carbon nucleophiles have been able to be generated via this method including α-cyano anions[32b,34], nitroalkanes,[35] α-sulfonyl anions[36], and acetylides[32b,37] (Scheme 2.2). However, accessing nucleophiles with higher pK_a's requires elevated temperatures to achieve decarboxylation. When

the pK_a of the nucleophile exceeds 35, the barrier to decarboxylation becomes too high to achieve under thermal control.

A. DcA of Nitriles[34]

85% yield

B. DcA of Nitroalkanes[35]

82% yield

C. DcA of α-sulfonyl-β-ketoesters[36]

85% yield

D. DcA of Acetylides[37]

80% yield

Scheme 2.2: DcA of nucelophiles with anion-stabilizing functionalities

These descendants of the initial reports from Tsuji rely on transition metals to undergo oxidative addition with allylic electrophiles resulting in π-allyl metal complexes. Similar reactions that arose in the early 1990's show benzylic electrophiles can be utilized to access π-benzyl metal complexes that, when intercepted by a nucleophile, can result in the incorporation of a benzylic moiety.[38] By utilizing benzylic acetates and carbonates as electrophiles in this mode of catalysis, the use of toxic aryl halides as coupling partners can be avoided.[39] These intermediates have been exploited in decarboxylative processes ultimately replacing the carboxylate with an aryl functionality (Scheme 2.3).[40] The higher barrier for oxidative addition with benzylic acetates and

carbonates relative to the allylic systems can be problematic and thus benzylations typically utilize benzylic acetates or carbonates that have extended π-systems and thus
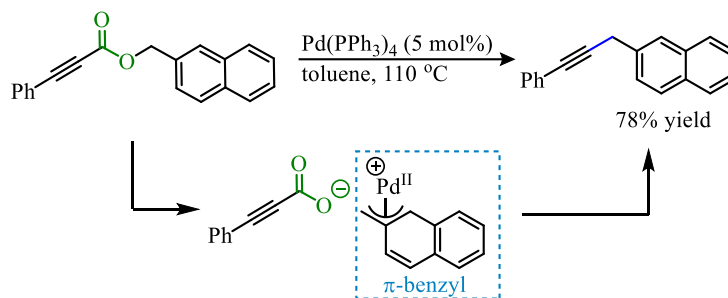
Scheme 2.3: Palladium-catalyzed DcB[40b]

lower resonance stabilization.[41] Additionally, elevated temperatures are typically employed to achieve oxidative addition. One solution to this problem is to utilize benzylic halides that are easier to ionize.[42]

Even with the significant attention DcA and DcB have received over the past several decades, limitations to this methodology still need to be addressed to achieve high synthetic utility. Most notable of these limitations is the need for anion-stabilizing functionalities in the carboxylic acid substrates to allow for anionic decarboxylation to be achieved. The pK_a limitation is unfortunate as carboxylic acids represent an abundant feed stock and functionalizing similar scaffolds via base-promoted alkylation would not provide that same regioselectivity that decarboxylation achieves (Figure 2.1). To improve upon the utility of DcA and DcB in complex molecular synthesis, innovations to these processes that improve upon their generality are required.
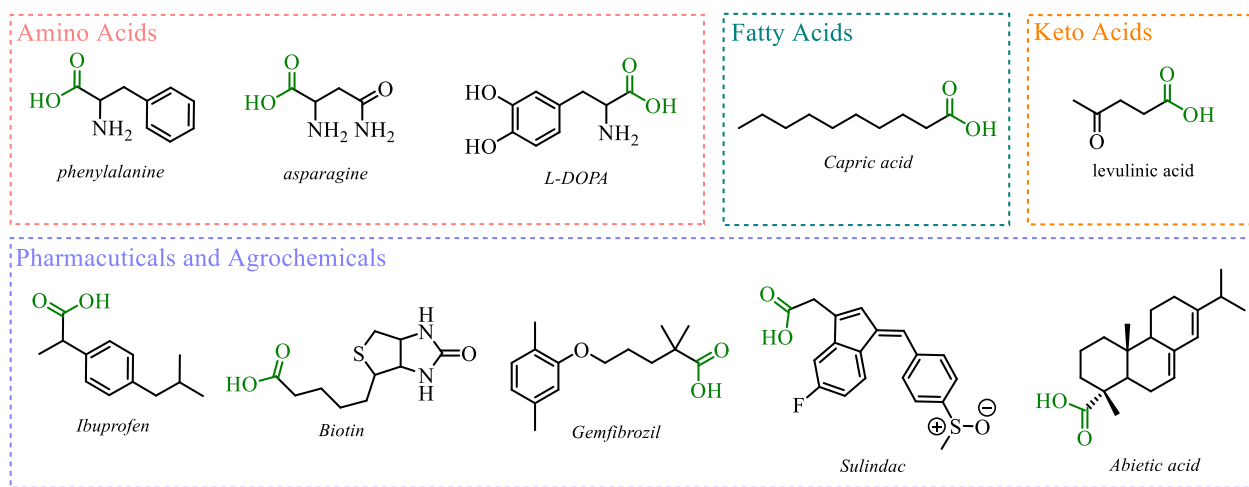
**Figure 2.1**: Classes of carboxylic acids that are not accessible nucleophiles in thermal DcA and DcB

15

2.3 Ir/Pd Catalyzed DcA

In order to access other classes of carboxylic acid nucleophiles in the DcA, the possibility

of exploiting a radical decarboxylation was explored. Using a radical decarboxylation approach,

carbon radical intermediates would be obtained instead of carbanions which would avoid the

previously encountered pK_a limitation. The initial report by Tunge in 2014 introduced the use of

an Ir photosensitizer in conjunction with a Pd catalyst in order to achieve the $C(sp^3)$–$C(sp^3)$ bond

formation with amino alkanoic acids as carbon nucleophile surrogates and allylic electrophiles

(Scheme 2.4).[28]

**Scheme 2.4**: Ir/Pd catalyzed DcA of amino alkanoic esters
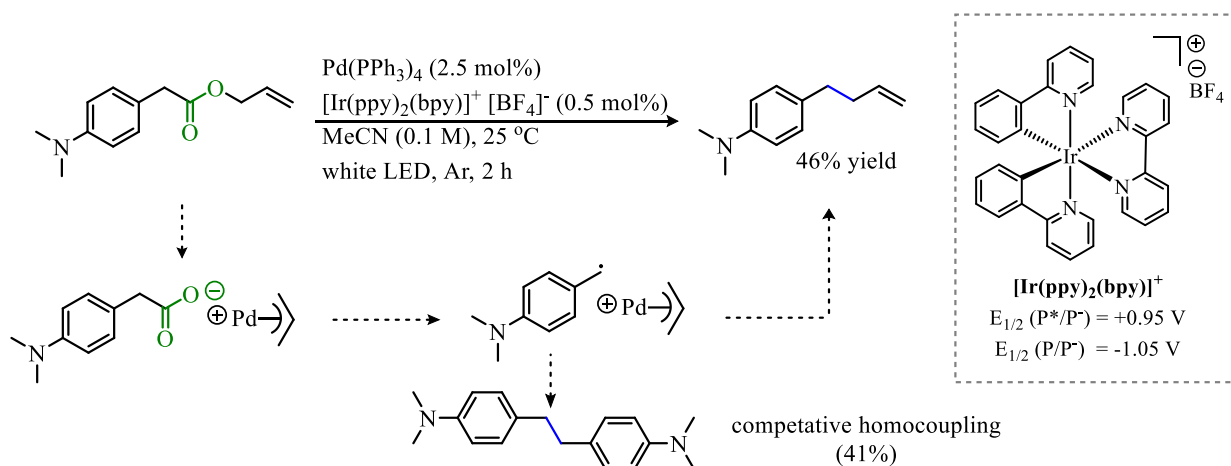
In these reactions, the allylic ester substrates and the Pd catalyst are proposed to undergo

oxidative addition to liberate a carboxylate and the π-allyl-Pd intermediate. The amino and para-

amino-phenylacetic carboxylates are not able to undergo thermal decarboxylation. Instead, the

amine functionalities on these substrates are posed to undergo single electron oxidation facilitated

by Ir(ppy)$_2$(bpy)$^+$ BF$_4^-$. The amine oxidation promotes decarboxylation, making this process a

photoredox-promoted oxidative radical decarboxylation similar to what was proposed by

Nishibayashi (Scheme 1.8).[23] The facile radical decarboxylation results in a reactive carbon radical

intermediate that can undergo addition to the π-allyl-Pd species resulting in the allylated product.

The Ir photocatalyst and Pd catalyst rely on each other for catalyst turn over. The explored scope of this process was limited to α-tert-amino and aminobenzylic radicals (Figure 2.2). The yields of these reactions ranged from 40%–60% yield and faced considerable competitive homocoupling. The dimerization of the free-radicals generated limits the efficiency of these cross-couplings.

| 49% yield | 50% yield | 57% yield | 55% yield |
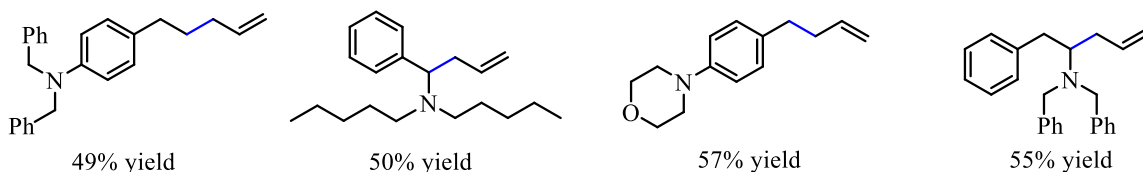
Figure 2.2: Select DcA products[28]

In 2015, the DcA of a wider array of α-amino acid substrates were allylated by Tunge under similar reaction conditions (Scheme 2.5).[43] The most notable difference between the 2014 and 2015 reports is the switch to a more oxidizing Ir photosensitizer, $[Ir[dF(CF_3)ppy]_2(dtbbpy)]^+$. Switching to a more oxidizing catalyst provides the opportunity for direct oxidation of the carboxylate (α-aminocarboxylates ~+0.95 V vs. SCE)[19] however, it is still plausible that an amine oxidation pathway facilitates decarboxylation. The change in catalyst system allowed for greater generality in the scope of amino acids and higher yields than the original catalyst pairing (Scheme 2.5).


Select Examples:

| 65% yield | 83% yield | 77% yield | 58% yield |
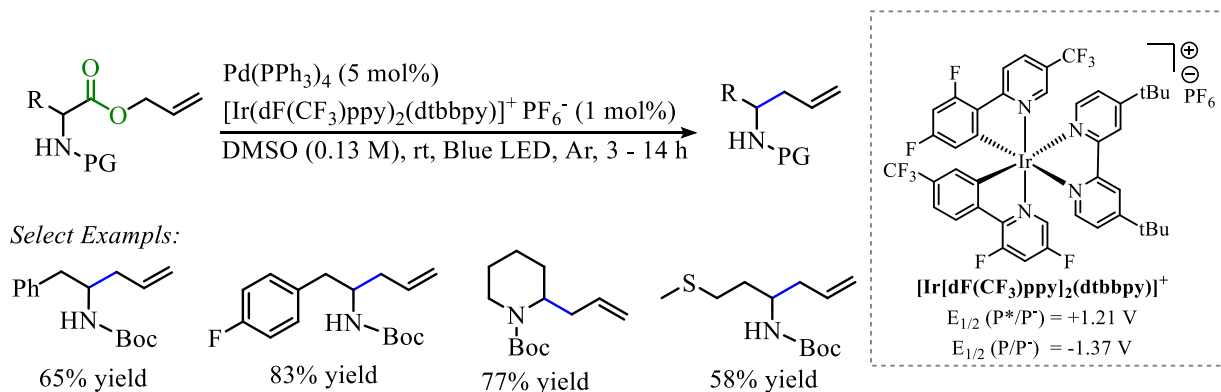
Scheme 2.5: Ir/Pd DcA of *N*-protected α-amino acids[43]

Despite this major advancement in DcA, the Ir/Pd methodology faces several limitations. For one, the reaction is limited in scope to substrates that produce amine-stabilized radical intermediates which, perform with variable success. Utilizing the established dual catalytic system with other classes of carboxylic acid substrates as well as more complex π-electrophiles was not realized. Lastly, using the limited Ir resource in the catalyst system is not a sustainable choice.[44] Nonetheless, this seminal work represents one of the first photoredox-transition metal dual catalytic processes that does not invoke additional additives or activating groups to propagate catalysis and provides an elegant design scaffold to build upon.

2.4 Organophotoredox/Pd Catalyzed Cross-Coupling with Carboxylic Acids and π-Electrophilic Carbonates

Initially, a return to the catalyst system was undertaken in order to address the challenges that plague the first-generation photoredox/Pd dual-catalytic DcA. Early in 2016, the Zhang lab reported a series of carbazolyl dicyanobenzene-based donor-acceptor fluorophores that possess similar potentials to the Ir photosensitizers that were found to be successful in oxidative radical decarboxylation methodology (Figure 2.3).[44] In fact, Zhang showed the utility of these organophotoredox catalyst in one of MacMillian's decarboxylative cross-coupling reactions.[44,45] Two catalysts, 4CzIPN and 4DPAIPN, were identified as providing comparable product yields to what is obtained with the $[Ir[dF(CF_3)ppy]_2(dtbbpy)]^+$ photosensitizer initially employed (Table 2.1).
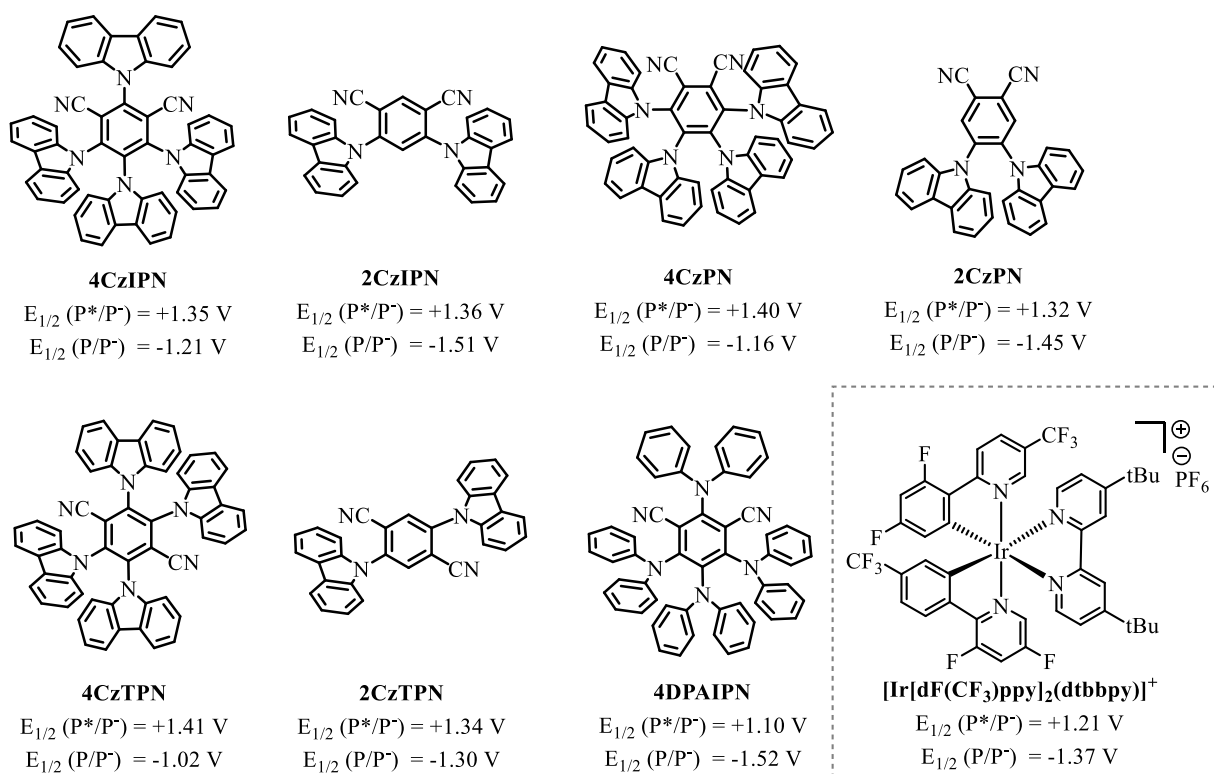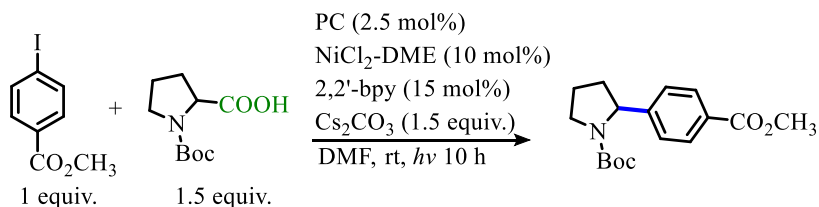
Figure 2.3: Carbazole dicyanobenzene-based D-A fluorophores

Not only do these catalysts represent a more sustainable photocatalyst option compared to Ir but they are also easy to synthesize and economical. For instance, 4CzIPN can be synthesized from 2,4,5,6-tetrafluoro-1,3-benzenedicarbonitrile and carbazole via nucleophilic aromatic substitution, costing ~$4/gram.[44] As a result of the synthetic simplicity, as well as the range of potentials that can be accessed with this family of photocatalyst, the return to

| PC	Yield
4CzIPN	85%
4DPAIPN	87%
2CzIPN	56%
4CzPN	15%
2CzPN	20%
4CzTPN	12%
2CzTPN	<5%
[Ir[dF(CF$_3$)ppy]$_2$(dtbbpy)]$^+$	83%

Table 2.1: D-A fluorophores in decarboxylative coupling

photoredox-facilitated dual-catalytic DcA was centered around the use of the carbazolyl dicyanobenzene-based donor-acceptor fluorophores.

2.4.1 Development of Protocol[46]

Initial investigations were directed toward the allylation of 4-tert-butylcyclohexylcarboxylic acid (**1a**) as it represents a carboxylic acid that does not have any additional radical stabilizing functionalities. The allyl ester (**2a**) was first subjected to reaction conditions reminiscent of the optimal conditions for the Ir/Pd DcA process, but 4CzIPN was utilized as the photosensitizer (Scheme 2.6). The reaction resulted in 66% conversion providing 26% of the allylated product in the final reaction mixture. Interestingly, the homocoupled product that plagued the Ir/Pd methodology was not observed in this reaction, which is surprising as the radical generated is highly reactive. Although dimerization is not observed, an alkane and alkene product were part of the final reaction mixture (Scheme 2.6). These side products can possible arise from unproductive pathways such as radical disproportionation, β-hydride elimination, or reductive elimination from a Pd-hydride.[47] Despite the low conversion observed, the formation of the allylated product from a substrate with no radical-stabilizing functionalities as well as the seemingly different reactivity accessed from the switch in photosensitizer encourage a further evaluation of using Pd catalyst in conjunction with the 4CzIPN.
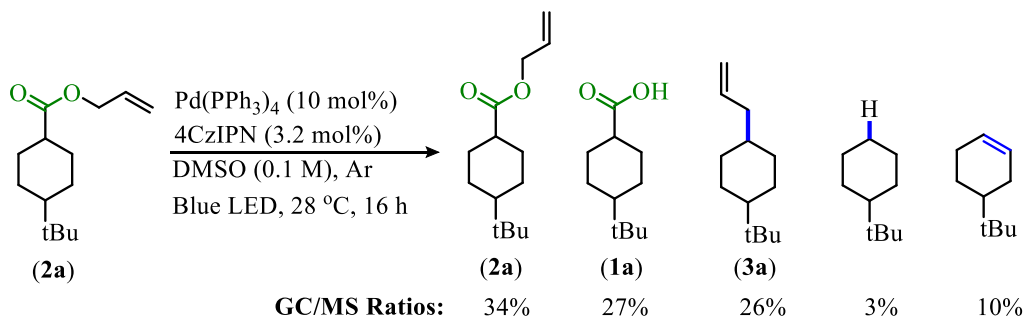
Scheme 2.6: Initial exploration of intramolecular DcA

Utilizing Pd(OAc)$_2$ as the pre-catalyst, a variety of ligands were screened in the DcA reaction of **2a** (Table 2.2). Of the ligands explored, the highest conversions were seen with bidentate phosphine ligands. Bidentate phosphine ligands that provided the highest quantity of allylated product include BINAP, (R)-C$_3$-TunePhos, (R)-SegPhos, (S)-SynPhos, (R)-Tol-BINAP, DTBM SegPhos, and DPEPhos (Table 2.2, Entries 1-7). These ligands all possess similar scaffolds and are pictured next to the reaction table.

Optimal ligands:

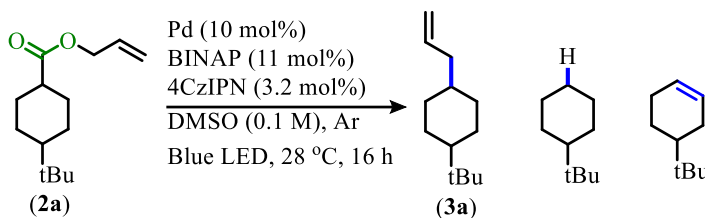| Entry	Ligand	(3a)	alkane	alkene	(2a)	(1a)
1	BINAP	82	9	9	0	0
2	(R)-C$_3$-TunePhos	78	8	14	0	0
3	(R)-SegPhos	76	9	15	0	0
4	(S)-SynPhos	75	8	17	0	0
5	(R)-Tol-BINAP	73	8	19	0	0
6	DTBM SegPhos	70	8	22	0	0
7	DPEPhos	70	8	22	0	trace
8	Xantphos	56	12	32	0	0
9	DifluoroPhos	51	3	6	0	14
10	(S,S)-DIOP	40	5	9	0	45
11	(S,S)-ChiraPhos	32	29	39	0	0
12	RMOP	19	21	10	50	0
13	PhanePhos	9	1	3	0	87
14	tBu-BOX	0	50	50	0	0
15	(R,R)-ANDEN-PhenylTrost	0	0	0	0	100
16	HiersoPhos	0	0	0	0	100
17	MeOBIPHEP[c]	trace	trace	trace	0	trace
18	MonoPhos	0	0	0	>99	trace
19	Phosphoramidite[d]	0	0	0	>99	trace
20	PCy$_3$	0	0	0	100	0
21	PhDavePhos	0	0	0	100	0
22	TFP	0	0	0	100	0
23	P(p-CF$_3$Ph)$_3$	0	0	0	100	0
24	XPhos	0	0	0	100	0
25	tBuXantphos	0	0	0	100	0
26	dppe	0	0	0	100	0

Table 2.2: Palladium catalyst ligand examination
[a] All reactions were performed on 0.2 mmol scale and product ratios were determined by GC/MS. [b] Monodentate ligand loading 22 mol%. [c] Many side products. [d] (+)-*N,N*-Bis[(1R)-1-phenylethyl]-dinaphtho[2,1-d:1',2'f][1,3,2]dioxaphosphepin-4-amine.

Interestingly, a higher quantity of alkene side product is observed from the more sterically demanding (R)-Tol-BINAP and DTBM SegPhos (Entries 5 & 6 respectively) as compared with their less sterically demanding counterparts (Entries 1 & 3 respectively). Although PhanePhos,

ANDEN-PhenylTrost, and HiersoPhos, allowed for compete de-allylation of the allylic ester, decarboxylation did not occur to any considerable extent (Table 2.2, Entries 13-16). The monophoshine ligands screened resulted in little-to-no conversion from the allyl ester (Table 2.2, Entries 12, 18-20, 22-23). It is also noteworthy that switching to a nitrogen-based ligand did not provide the allylated product but did result in complete conversion to the alkane and alkene side products in a 1:1 ratio (Table 2.2, Entry 14). Due to its superior performance, high availability, and low expense relative to the other ligands screened, BINAP was selected as the optimal ligand.

The pre-catalyst utilized was also revisited (Table 2.3). The ligand exploration was conducted utilizing Pd(OAc)$_2$ which is a relatively inexpensive and air-stable palladium source. However, the reaction was also performed with other Pd^{II} and Pd^0 sources to ensure the optimal pre-catalyst was identified. Comparable DcA of **2a** was observed with Pd^0 sources Pd(dba)$_2$ and Pd$_2$(dba)$_3$ (Table 2.3, Entries 2-3). But, switching to a PdCl$_2$ source resulted in more alkene product and less allylation (Table 2.3, Entry 4). Based on this analysis, the Pd(OAc)$_2$/BINAP catalyst was selected as the optimal Pd catalyst choice to pair with 4CzIPN.

Entry	Pd	(3a)	alkane	alkene	(2a)	(1a)
1	Pd(OAc)$_2$	82	9	9	0	0
2	Pd(dba)$_2$	77	15	8	0	0
3	Pd$_2$(dba)$_3$	75	17	8	0	0
4	PdCl$_2$	59	10	31	0	0

Table 2.3: Palladium pre-catalyst screening
All product ratios reported were determine by GC/MS.

Having identified a promising catalyst system, the ideal concentrations of the catalysts were investigated. Both the ratio of Pd to 4CzIPN as well as the ratio of catalyst to substrate have the be considered. The highest conversion to allylated product **3a** was observed when the loading of Pd catalyst exceeds the loading of 4CzIPN (Table 2.4, Entries 1-5). Catalyst loadings in which the 4CzIPN to Pd ratio was 1:1 and 2:1 saw significantly lower conversions (Table 2.4, Entries 6 & 7 respectively). The ideal catalyst ratio was 0.32:1 4CzIPN to Pd (Table 2.4, Entries 1, 3, 5). Relative to the substrate, the highest quantity of allylated product was observed when 10–20 mol% of Pd catalyst and 2.3–6.4 mol% of 4CzIPN were utilized (Table 2.4, Entries 1 & 3). Further decreasing the loading leads to a lower quantity of **3a** in favor of the alkane and alkene side products and ultimately poor conversion (Table 2.4, Entries 5 & 8). After assessing the cost of catalyst loading to quantity of allylated product observed, a 10 mol% Pd catalyst loading and 3.2 mol% 4CzIPN was found to be optimal. Note that the ligand loading relative to the palladium pre-catalyst was always in a slight excess which was done to aid in reduction of the pre-catalyst from Pd^{II} to Pd^0.[48]
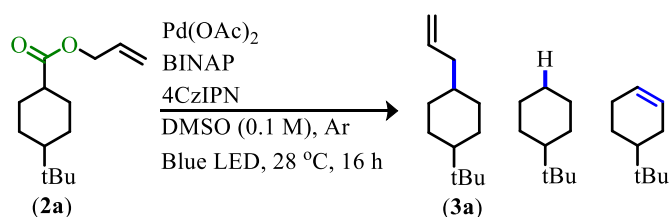
Entry	Pd(OAc)$_2$ (mol%)	BINAP (mol%)	4CzIPN (mol%)	(3a)	alkane	alkene
1	20	21	6.4	86	5	8
2	10	11	5	67	12	7
3	10	11	3.2	82	9	9
4	10	10	0.6	64	7	11
5	5	6	1.6	71	15	14
6	5	6	5	28	9	9
7	5	6	10	20	6	6
8	2.5	3.5	0.6	1	1	1

Table 2.4: Catalyst loading
All product ratios reported were determine by GC/MS and represent percents out of 100. Product mixtures that don't add to 100% contained unconverted allylester and free carboxylic acid.

In addition to the use of 4CzIPN, other carbazole dicyanobenzene D-A fluorophores in the DcA of **2a** were evaluated (Table 2.5). The 4CzPN is the only other carbazole catalyst that provided considerable conversion but was greatly inferior to 4CzIPN (Table 2.5, Entry 2). Like 4CzIPN, 4CzPN is more oxidizing and less reducing than the Ir catalysts employed in the first-generation methodology. Compared to 4CzIPN, the 4CzPN is slightly more oxidizing and slightly less reducing. Interestingly, 4DPAIPN performed poorly in this reaction but Zhang reports this catalyst and 4CzIPN having optimal performance in MacMillians decarboxylative $C(sp^3)$-$C(sp^2)$ coupling with amino acids and aryl iodides (Table 2.5, Entry 3).[44,45] It should be noted that 4DPAIPN is much less oxidizing and more reducing than 4CzIPN and this difference in potentials may be a poor match for the DcA. Lastly, it is notable that the $Ir[dF(CF_3)ppy]_2(dtbbpy)^+ PF_6^-$ performs comparably to 4CzIPN under these conditions, but the 4CzIPN is a less expensive $(Ir[dF(CF_3)ppy]_2(dtbbpy)^+ PF_6^- = \$834/g$ vs. 4CzIPN = \$4/g) and more sustainable option (Table 2.5, Entry 5).[44]
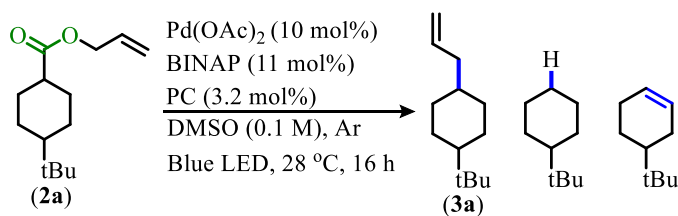
Entry	PC	(3a)	alkane	alkene	(2a)	(1a)
1	4CzIPN	82	9	9	0	0
2	4CzPN	48	4	4	24	19
3	4DPAIPN	0	1	1	98	0
4	2CzTPN	5	2	1	92	0
5	$Ir[dF(CF_3)ppy]_2(dtbbpy)^+PF_6^-$	84	6	10	0	0

Table 2.5: Carbazole-based donor-acceptor fluorophores in DcA
All product ratios reported were determine by GC/MS.

To improve upon the economy and operational simplicity, an intermolecular variant of the reaction with the carboxylic acid (**1a**) and various allylic electrophiles and bases were investigated

(Table 2.6). To our delight, the reaction proceeds well intermolecularly. Allyl methyl carbonate

was identified as the ideal allylic electrophile choice (Table 2.6, Entry 1). The choice in base also

had an influence on reaction success with sodium carbonate proving to be the ideal choice (Table

2.6, Entry 1). Lastly, the reaction was found to produce comparable results in acetonitrile, which

was preferred over the use of dimethyl sulfoxide as it is easier to remove.

Entry	Electrophile	base	(3a)	alkane	alkene
1	allyl methyl carbonate	Na_2CO_3	84	5	11
2	allyl chloride	Na_2CO_3	68	9	23
3	allyl phosphate	Na_2CO_3	43	0	0
4	allyl methyl carbonate	Cs_2CO_3	71	8	21
5	allyl methyl carbonate	NaOAc	61	7	9
6	allyl methyl carbonate	Na_2HPO_4	57	4	8
7	allyl methyl carbonate	K_2CO_3	56	6	11
8	allyl methyl carbonate	Na_3PO_4	56	5	17
9	allyl methyl carbonate	Li_2CO_3	54	5	7
10	allyl methyl carbonate	LiOAc	32	3	5

Table 2.6: Intermolecular DcA
All product ratios reported were determine by GC/MS.

2.4.2 Exploration of 4CzIPN/Pd DcA with Carboxylic Acid Nucleophiles

   With new dual-catalytic DcA conditions established, attention was given to the allylation

of a variety of carboxylic acids (Table 2.7). Initial focus was paid to the allylation of *N*-protected

amino acids (**3b-r**). With the amino acid substrates, the DcA proceeded well providing high yields

and no alkene or alkane side products were observed. Amino acid substrates that were employed

in the first-generation Ir/Pd methodology were able to be allylated in higher yields with the new

conditions. For instance, product **3b** saw a 20% increase in yield and **3d** a 71% increase in yield.

Under the newly developed reaction conditions, carbamate functionalities result in higher yields

than their amide counterparts whereas the first-generation Ir/Pd conditions result in comparable yields for both protecting groups (**3b-c**, **3l-m**).[43] Despite this, the *N*-Boc and *N*-Cbz protected amino acid substrates generally performed well with a variety of different side chain functionalities and steric demand. Additionally, cyclic scaffolds were efficiently allylated (**3n-q**). Interestingly, the cyclopropane amino acid substrate **3n** was allylated in only 21% yield which could be due to reduced stability of a radical located in an orbital with increased s character. Larger ring sizes such as a cyclobutane (**3o**), cyclopentane (**3p**), and cyclohexane (**3q**) all could be allylated in high yields. The DcA of **1b-Boc** was also successfully run in batch on 1 mmol scale providing **3b** in 93% yield.

In addition to the successful decarboxylative allylation of amino acids, other carboxylic acids that produce more reactive radical intermediates were allylated with this methodology (**3r-3gg**). Substrates that produced α-oxy radicals were generally allylated in moderate yields (**3r-v**). Carboxylic acid substrates that provide benzylic radicals upon decarboxylation could be allylated in moderate to good yields (**3w-3aa**). Of these, the disubstituted benzylic acids produced yields exceeding 60% (**3w-3y**). This is noteworthy because previously in the Tunge lab, *para*-aminophenylacetic acid allyl esters that produce α-benzylic radical intermediates were allylated with yields around 50% as a result of competitive homocoupling (Scheme 2.4). Dimeric products were not observed with the disubstituted benzylic acids under the new DcA conditions but, it is worth noting that increasing the concentration of the photocatalyst does lead to dimer formation (DcA of **1w** with 6.4 mol% 4CzIPN produced 54% yield **3w** and 31% yield of the homocoupled product). Although dimer formation can be avoided with these substrates, the alkane and alkene side products do arise. The unsubstituted benzylic acid substrate (**1z**) was able to be allylated in 31% yield (**3aa**) but, this substrate did produce the homocoupled product in 48% yield. Thus,

increasing the reactivity of the radical intermediate leads to competitive dimerization under these reaction conditions.
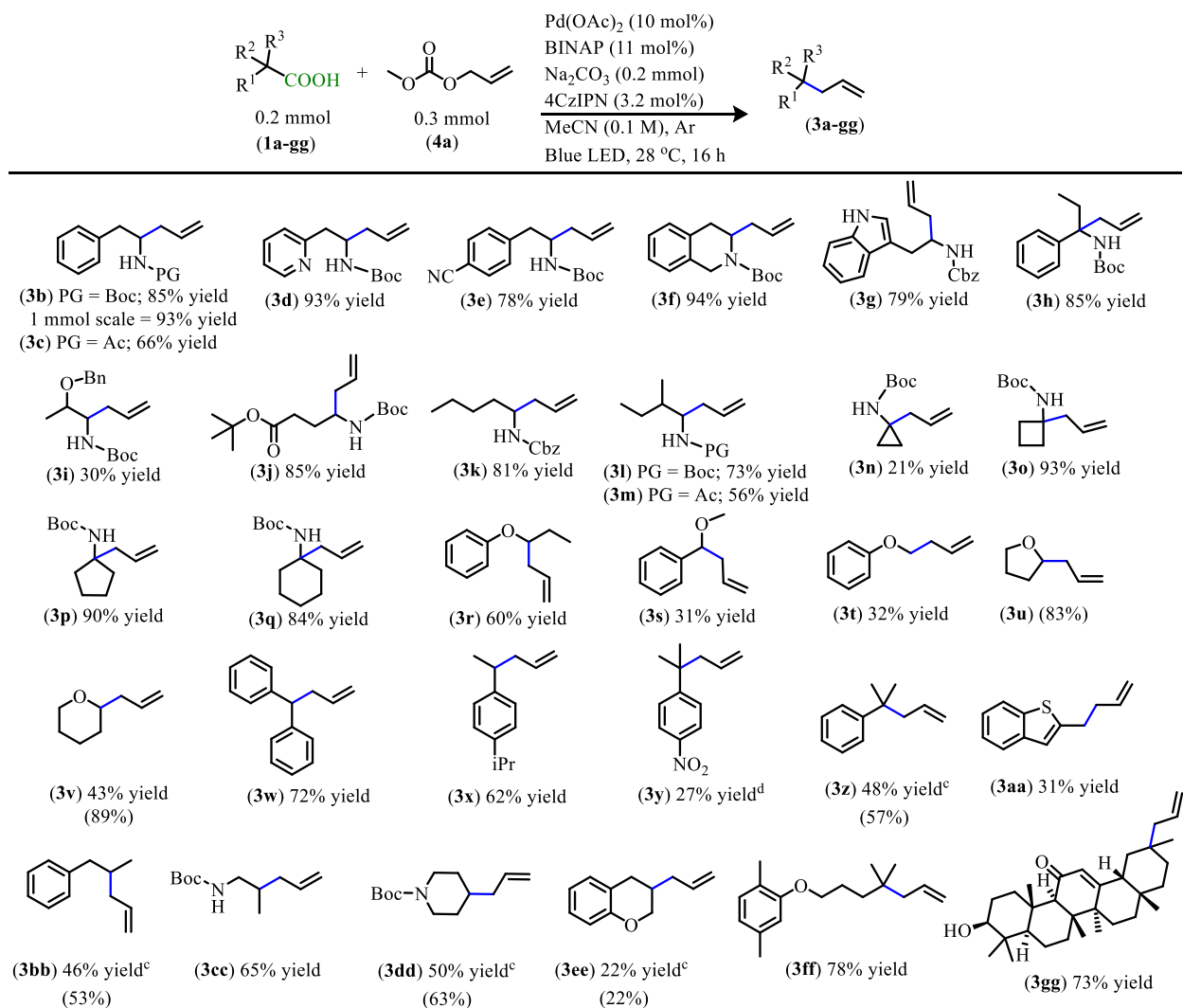
Table 2.7: Products from DcA of carboxylic acids

[a] Isolated yields are shown. [b] (Yields) were determined by q^{1}H NMR with pyridine as the internal standard for products that were found to be volatile. [c] Yields are an average of two reactions. [d] Product was isolated with alkane side product and mass adjusted.

The dual catalytic DcA was also viable with carboxylic acids that possess weak radical-stabilizing functionalities (**3a, 3bb-3gg**). The trisubstituted carboxylic acids **1ff** and **1gg** produced the highest yields of allylated product (78% yield of **3ff**, 73% yield of **3gg**). The disubstituted carboxylic acids of this group, such as β-amino acid (**1bb**) and γ-amino acid (**1cc**), were allylated

in moderate yields (65% yield of **3cc** and 50% yield of **3dd**). Unfortunately, unsubstituted acids that do not possess functionalities to stabilize the resulting radical intermediate result in poor conversion, only producing trace amounts of allylated product. An artifact of this reactivity difference is the ability to perform the DcA of a disubstituted acid **1v** selectively in the presence of the unsubstituted acid **1gg**, which remained intact during the reaction (Scheme 2.7). When carboxylic acid **1gg** was subjected to the DcA conditions independently, a 27% yield was obtained after one week of irradiation.
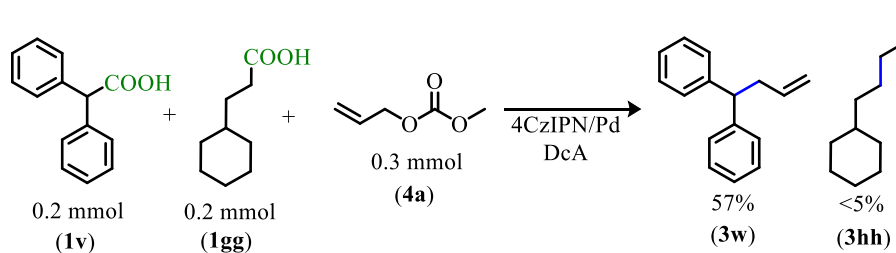
Scheme 2.7:Preferential DcA of disubstituted carboxylic acid

Despite the ability of the reaction to efficiently allow for the DcA of carboxylic acid nucleophiles that are not accessible under thermal conditions, utilizing this method towards the DcA of carboxylic acids with anion-stabilizing functionalities has not been as fruitful (Scheme 2.8). Product **3w,** whose corresponding alkane has a pK_a >30, has been synthesized under thermal conditions by Walsh however, it was only isolated in 10% yield.[49] Under the 4CzIPN/Pd conditions, **3w** can be obtained in 72% yield making the dual-catalytic methodology advantageous in this case (Scheme 2.8 A). But, the synthesis of **3y** under the dual-catalytic methodology provided only 27% yield and a comparable yield was able to be obtained without the 4CzIPN catalyst but with irradiation. This product has been synthesized by Tunge under thermal conditions in 93% yield (Scheme 2.8 B).[50] When subjecting substrates with a nitrile (**1hh**) or sulfone functionality (**2c** & **2d**) to the 4CzIPN/Pd DcA conditions, little to no allylation was observed (Scheme 2.8 C &

D). However, these substrates can be allylated via anionic decarboxylation (Scheme 2.2 A &
C).[36,37]
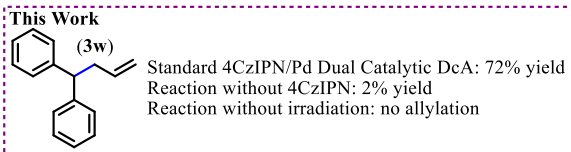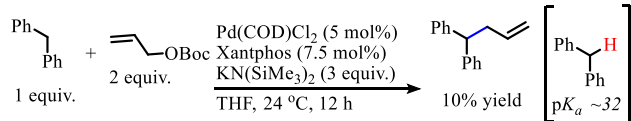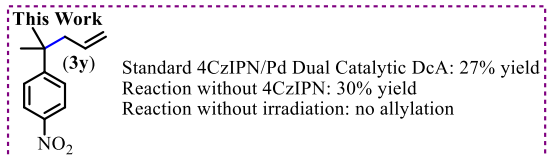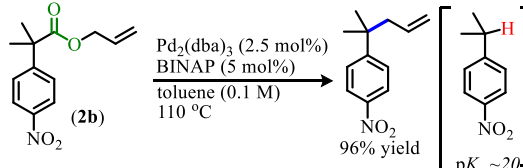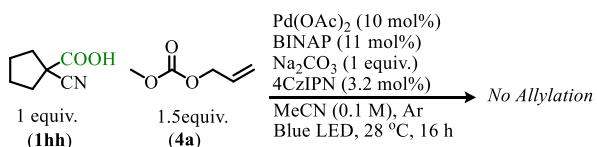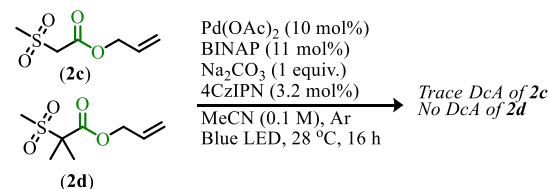
Scheme 2.8: Comparison of 4CzIPN/Pd DcA of various carboxylic acid nucleophiles to the thermal allylation

The allylation of sp^2 and sp-hybridized carboxylic acids was also attempted under these conditions (Scheme 2.9).[51] However, these did not produce allylated product. While the sp^2 acids (**1ii** & **1jj**) underwent poor conversion with no allylation, it is interesting to note that relatively high conversion was observed for the sp acid (**1kk**) but, resulted exclusively in the dimeric product.
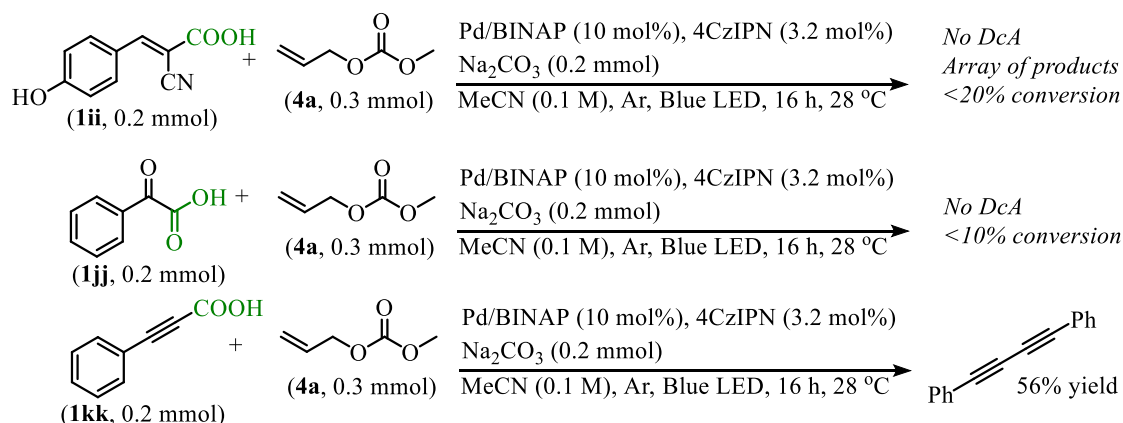
Scheme 2.9: Carboxylic acids on sp^2 and sp-hybridized carbons as nucleophiles

In the first-generation methodology, the possibility of an asymmetric allylation was explored however, it was found that only the incredibly sterically demanding ANDEN-PhenylTrost ligand provided any selectivity.[43] Performing the 4CzIPN/Pd DcA enantioselectively was also investigated, primarily with (R)-BINAP. However, these reactions resulted in <60:40 e.r. (explored with substrates **1b-Boc**, **1f-Boc**, and **1s**).

Despite these limitations, the now realized 4CzIPN/Pd dual catalytic DcA represents a mild, economical, and efficient process for the installation of an allylic functional handle onto a variety of molecular scaffolds using readily available carboxylic acid substrates.

2.4.3 Exploration with Allylic and Benzylic Carbonates

This new mode of catalysis has allowed for an advancement in the utility of DcA methodology by allowing for more generality in the nucleophiles employed, but this process has also proven to be advantageous in the installation of more diverse electrophiles. There are a few examples of substituted allylic functionalities being installed on carboxylic acid nucleophiles via this mode of catalysis. However, these examples have substitutions exclusively in the 2-position.[43,52] The use of more diverse allylic electrophiles remained underexplored. Additionally, using this mode of catalysis in DcB was not previously realized. Thus, another compelling aspect of this 4CzIPN/Pd dual-catalyzed cross-coupling chemistry is the ability to achieve the decarboxylative coupling between amino acid **1f** and a variety of allylic and benzylic electrophiles (**4b-x**, Table 2.8).

Allylic carbonates with substituents in the 2-position proceeded well with the electron withdrawing phenyl substituent yielding more allylated product (**5c**, 82% yield) compared to the 2-methyl allyl carbonate (**5b**, 64% yield). Having Cl in the 2-position unfortunately resulted in

only 14% yield (**5d**) which could be due to poor chemoselectivity when a vinyl halide is in the reaction mixture. Allylic carbonates substituted in the 1- and 3-position also operated well. With hydrocarbon substituents, the yields of allylated products ranged from 65-85% (**5e-5h**). Additionally, comparably results were observed, regardless of the geometric configuration of the alkene or the structure of the allylic carbonate (branched/linear) and produced the *E*-configured olefin and the linear product despite the variation in the carbonate starting material (**5e-5h**). This tolerance of various carbonate scaffolds makes utilizing versatile allylic carbonates easy. For instance, a large variety of branched allylic carbonates can be synthesized from allylic alcohols easily accessible via Grignard addition of vinyl magnesium bromide to aldehydes. Cyclic allylic carbonates also provided allylated products however, the yields were about half what is realized with their linear counterparts.

Utilizing branched allylic carbonates turned out to be quite advantageous. Apart from the ability to access more diverse electrophiles from aldehyde starting materials, utilizing branched carbonates provided cleaner reactions then their 3-substituted allyl carbonate counterparts in several instances. For example, using carbonates derived from cinnamyl alcohols produced a complex mixture of products under these reaction conditions and provided poor yields of allylated product. But, the styrenyl products could be obtained and easily isolated in good yields when switching to the branched carbonates (**5k-5o**, 70-95% yield). In addition to the styrenyl functionalities, dienyl functional handles can also be incorporated (**5p** & **5q**). The α,α-diallyl-substituted carbonate does produce a superior yield of diene product (**5p**, 72% yield) as opposed to carbonate **4q** which is substituted in the 3-position (**5q**, 45% yield).

Pd(OAc)$_2$ (10 mol%)
BINAP (11 mol%)
Na$_2$CO$_3$ (0.2 mmol)
4CzIPN (3.2 mol%)
MeCN (0.1 M), Ar
Blue LED, 28 °C, 16 h

0.2 mmol + 0.3 mmol

R^1, R^2, R^3

Carbonate	Product	Carbonate	Product
(4b)	(5b) 64% yield	(4i)	(5i) 41% yield
(4c)	(5c) 82% yield	(4j)	(5j) 33% yield
(4d)	(5d) 14% yield	(4k)	(5k) 92% yield, 75:25 E:Z
(4e)	(5e) 65% yield	(4l)	(5l) 79% yield, 68:32 E:Z
(4f)	(5f) 77% yield	(4m)	(5m) 86% yield, 91:9 E:Z
(4e')	(5e) 72% yield	(4n)	(5n) 72% yield, 76:24 E:Z
(4g)	(5g) 81% yield	(4o)	(5o) 81% yield, >95:5 E:Z
(4h)	(5h) 80% yield	(4p)	(5p) 72% yield, 67:33 E:Z
		(4q)	(5q) 45% yield, E/Z

Table 2.8: DcA of **1f** with various allylic carbonates
[a] Isolated yields are shown. [b] Isomer ratios were determined by ^{1}H NMR.

Under these reaction conditions, the conjugated olefin products do result in a mixture of geometric isomers that is suspected to be a result of a background photoisomerization facilitated by 4CzIPN.[53] With the styrenyl substrates, higher yields and greater *E*-selectivity were obtained when the aryl moiety posed electron-withdrawing functionalities (**5n** & **5o**, 86% and 81% yield respectively, >90:10 *E:Z*) as opposed to electron-donating functionalities (**5l** & **5n**, 79% and 72% yield respectively, ~70:30 *E:Z*). With the dienyl substrates, *E/Z*-isomer mixtures were also observed with little selectivity (**5p**-**5q**).

Lastly, decarboxylative benzylation (DcB) utilizing Pd-π-benzyl electrophiles can also be achieved with this methodology (Table 2.9).[40] Similar to many thermal DcB reactions, benzyl carbonates with extend conjugation proceed to high conversion whereas those with greater resonance stabilization, such as benzyl, 4-phenylbenzyl, and 3-pyridinyl methyl carbonate, do not react efficiently under these conditions. Nonetheless, DcB can be achieved under the mild 4CzIPN/Pd dual catalytic reaction conditions, representing one of the first examples of radical additions to Pd-π-benzyl intermediates.

The highest yielding benzylations are those that install naphthalene (**5r**, 71% yield) and phenanthroline tethers (**5t**, 78% yield). The benzylic carbonates in these reactions proceed to full conversion, producing the benzyl dimer along with the cross-coupled product. The regiochemistry of the carbonate leaving group does influence the reaction yield. With the naphthalene system, the higher yield is obtained when the naphthalene is substituted in the 2-position (**4r**) vs. the 1-position (**4s**) (**5r** and **5s** isolated in 71% and 35% yield respectively). Similarly, the 9-anthracene carbonate (**4u**) provides the cross-coupled product (**5u**) in 21% yield.

Heteroaromatic systems could also undergo successful DcB, however, with yields between 20-40% (**5w-5aa**). Compared to the aromatic hydrocarbon systems, the heteroaromatic benzylic

carbonates produce a variety of side products. Like the naphthyl system, the regiochemistry of the alkylcarbonate influences the yield of the reaction. With the furan carbonate, the alkylcarbonate in the 2-position (**4w**) provides higher yields than the 3-position (**4x**). The pyrrole system was found to perform best when the amine was Boc protected, but ultimately the benzylated product was isolated in low yield reminiscent of what was observed with the furan carbonate (**5y**).
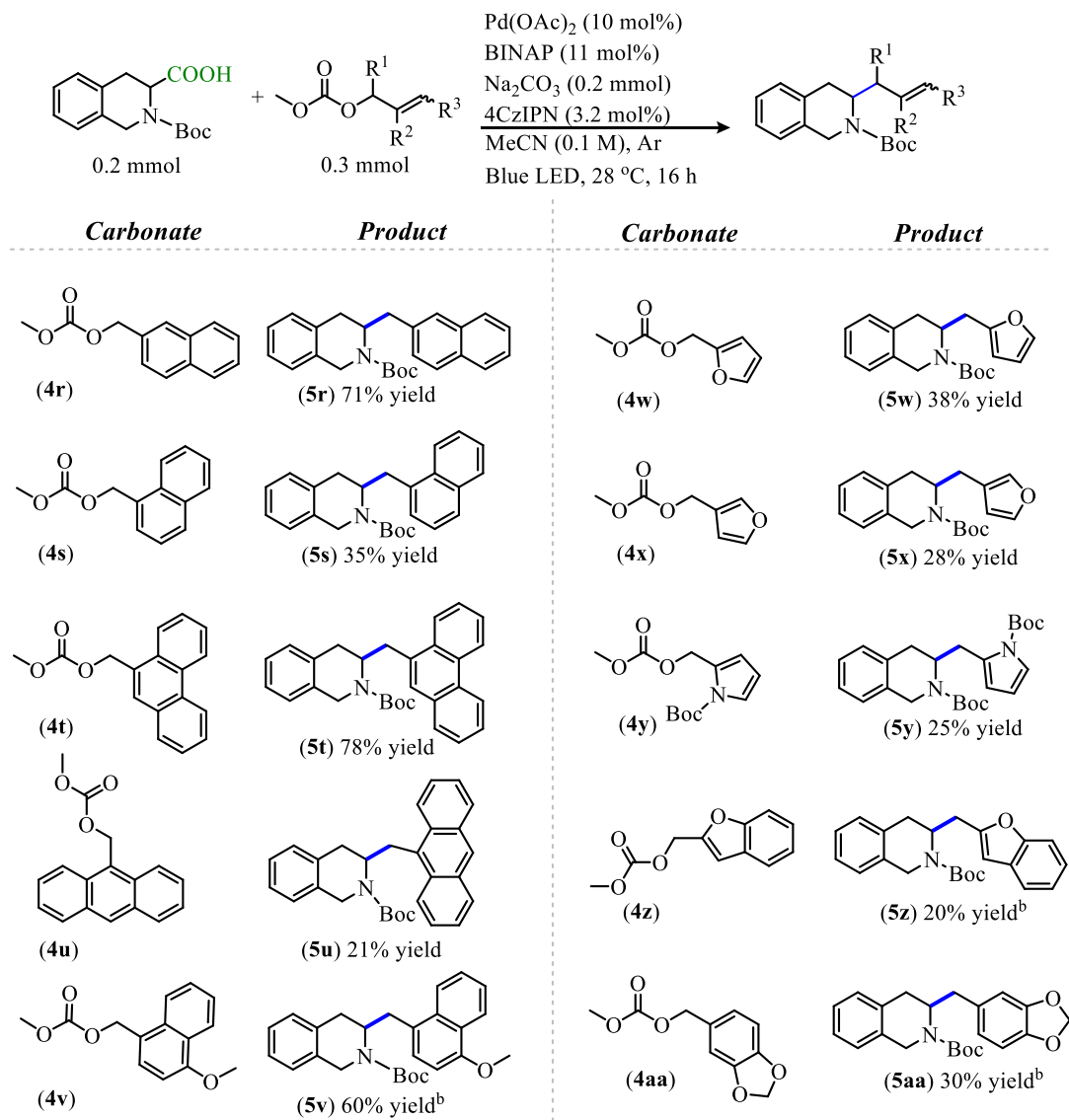
Table 2.9: DcB of **1f** with various benzylic carbonates
[a] Isolated yields are shown. [b] Isolated with various oligamers and yields adjusted. [c] Reaction performed with DTMB SEGPHOS ligand >90% pure.

The possibility of the DcB to be performed asymmetrically was also investigated. The DcB reaction of **1f** with **4r** was run with (R)-BINAP and resulted in a 55:44 e.r. of **5r**. Like what was observed in the DcA, performing this reaction with a chiral ligand did not provide a high degree of enantioselectivity.

2.4.4 Mechanistic Elucidation

Due to the unique abilities of this system, the operating mechanistic pathway was probed. First, it is important to note that the reaction does not proceed (<5% yield) without the presence of Pd, photocatalyst, or light, indicating that this process does rely on a light-promoted dual catalytic system (Table 2.10). Further, when the radical trap TEMPO is incorporated into the reaction the allylated product is not produced (Figure 2.4). Instead, conversion is interrupted and <10% yield of TEMPO trapped products were observed by ^{1}H NMR. Taken together, the pathway appears to proceed via a radical pathway that requires both the 4CzIPN and Pd to propagate.
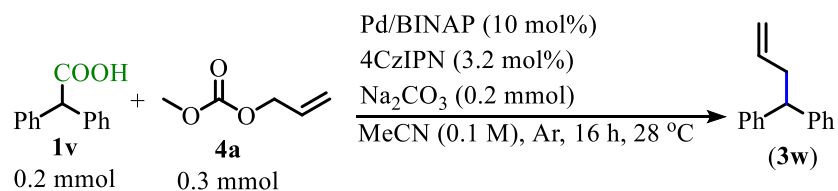
Pd/BINAP	4CzIPN	Blue LED	Yield 3w
✓	✓	✓	72%
✓	✓	-	0%
✓	-	✓	2%
-	✓	✓	0%

Table 2.10: Reaction dependence on dual catalytic system
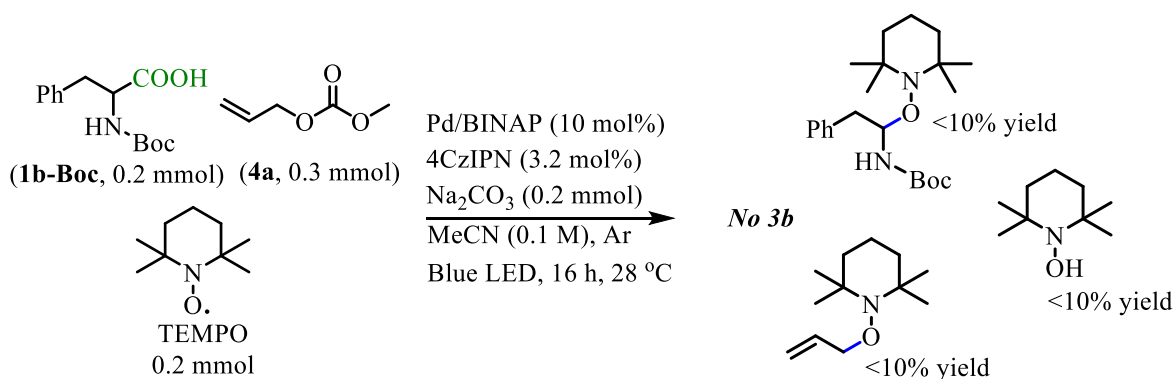
Figure 2.4: DcA in the presence of TEMPO

Generally, the side products that emerge in this reaction are the alkene and alkane products (Section 2.4.1). In addition to these side products, a side reaction with 4CzIPN was also observed (Scheme 2.10). Coupling between 4CzIPN and carbon radical intermediates was observed previously by König (Scheme 2.10A),[54] and this type of pathway was observed under the DcA conditions as well. Some of the 4CzIPN catalyst was found to have been allylated in the final reaction mixture of the DcA of **1b-Boc** (Scheme 2.10B). It was unclear if the "Allyl-4CzIPN" was active in the DcA or if this side reaction results in degradation of the photocatalyst's activity. To investigate this, the "Allyl-4CzIPN" was isolated and utilized as a catalyst under the standard DcA conditions. This revealed the allylated catalyst to be less efficient than 4CzIPN (Scheme 2.10C). Thus, this off-cycle allylation pathway is believed to deactivate the catalyst as the reaction progresses.

A. König Substitution of 4CzIPN

1 equiv.   4 equiv.   64% yield

Cs₂CO₃ (4 equiv.)
DMA, Blue LED, 3 h

B. Observed Side Raction in DcA

(**1w**, 0.2 mmol)   (**4a**, 0.3 mmol)

Pd/BINAP (10 mol%)
4CzIPN (6.4 mol%)
Na₂CO₃ (0.2 mmol)
MeCN (0.1 M), Ar
Blue LED, 16 h, 28 °C

54% yield
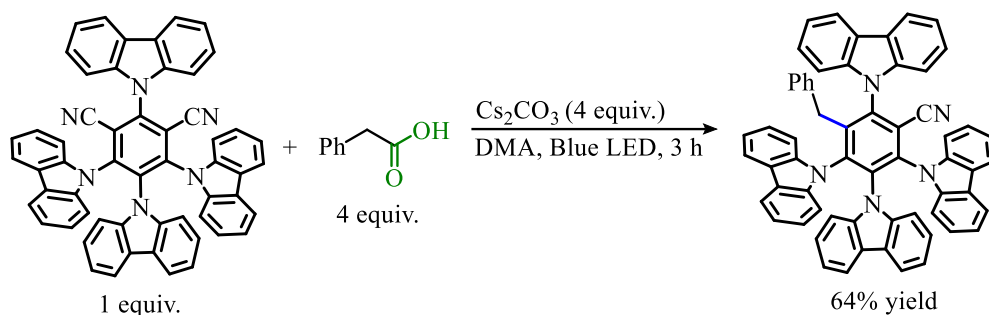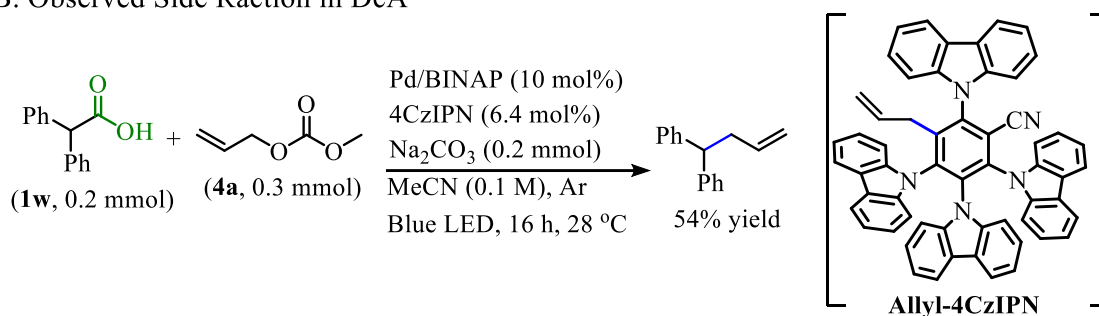
Allyl-4CzIPN

C. Allyl-4CzIPN Catalyzed DcA

(**1b-Boc**, 0.2 mmol)   (**4a**, 0.3 mmol)

Pd/BINAP (10 mol%)
Allyl-4CzIPN (6 mol%)
Na₂CO₃ (0.2 mmol)
MeCN (0.1 M), Ar
Blue LED, 16 h, 28 °C

24% yield **3b**
(standard conditions: 85% yield)
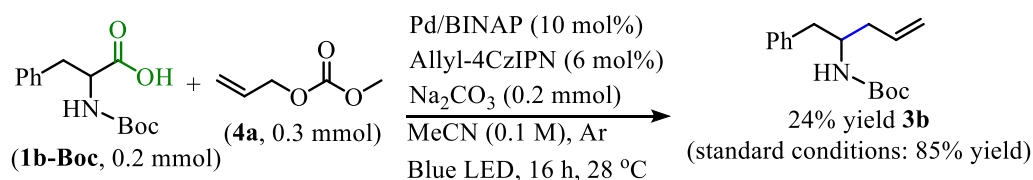
Scheme 2.10: Background substitution reaction with 4CzIPN

In an effort to better understand the catalytic processes occurring, a variety of fluorescent quenching experiments were undertaken. An oxidative radical decarboxylation process was anticipated to be part of the catalytic pathway and thus, finding that tetrabutylammonium diphenylcarboxylate (**1v⁻ ⁺NBu₄**) quenches 4CzIPN was not surprising (Figure 2.5). However, it was found that various Pd species performed as far more efficient quenchers than the carboxylate salt (Figure 2.6).
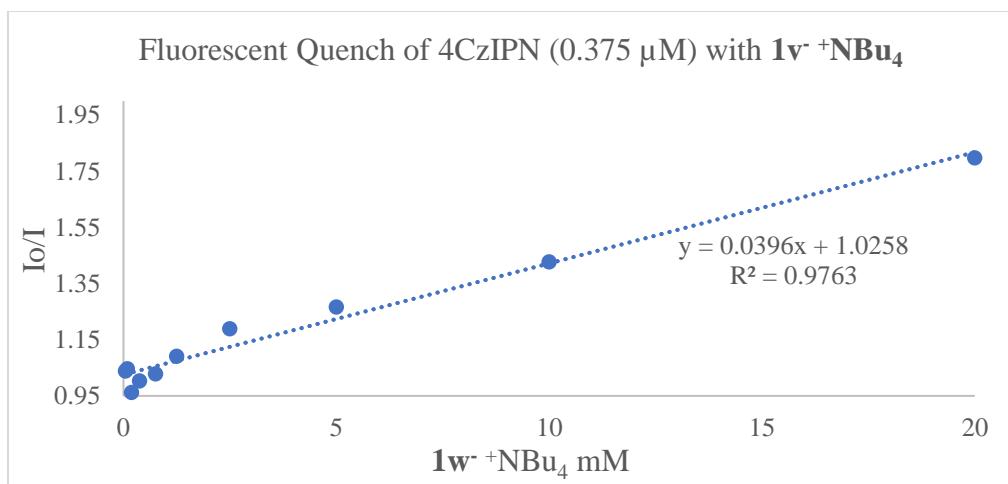
Figure 2.5: Stern-Volmer plot of 4CzIPN quenched with **1v⁻ ⁺NBu₄**
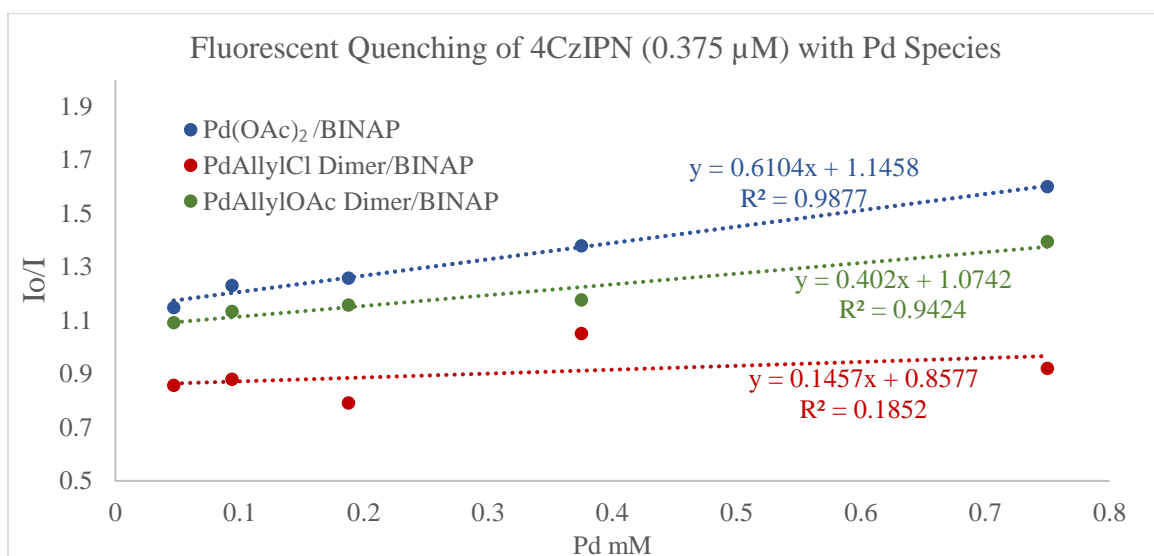
Figure 2.6: Stern-Volmer plot of 4CzIPN quenching by Pd species

When these reactions are assembled, an initial stirring of the Pd(OAc)₂ pre-catalyst and BINAP is performed to allow for reduction of the Pd^{II} to Pd^{0}. But, this process is not anticipated to fully reduce the Pd^{II} species and thus higher oxidation states of Pd are expected to be present at the onset of the reaction.[48] The mixture of Pd(OAc)₂/BINAP was found to be an efficient quencher of 4CzIPN (~10 fold more efficient than carboxylate, Figure 2.6). Similar Pd species are reported to have reduction potentials between -1.1 and -1.3 V vs. SCE[55], which places the potentials for the Pd^{II} catalyst reduction close to the excited state oxidation potential of 4CzIPN (-1.04 V vs. SCE)[44].

The 4CzIPN radical cation (+1.52 V vs. SCE)[44] should easily oxidize the carboxylate (+1.0 to +1.3

V vs. SCE)[19] in the reaction thus turning over the catalyst. A process of this nature is expected to

result in full reduction of the Pd[II] pre-catalyst to Pd[0] (Scheme 2.11A). Also, it is important to note

that the Pd catalyst and 4CzIPN can participate in an off-cycle pathway (Scheme 2.11B).

A. Hypothetical Pre-Reduction Pathway   B. Pd/4CzIPN Electron Transfer Pathway
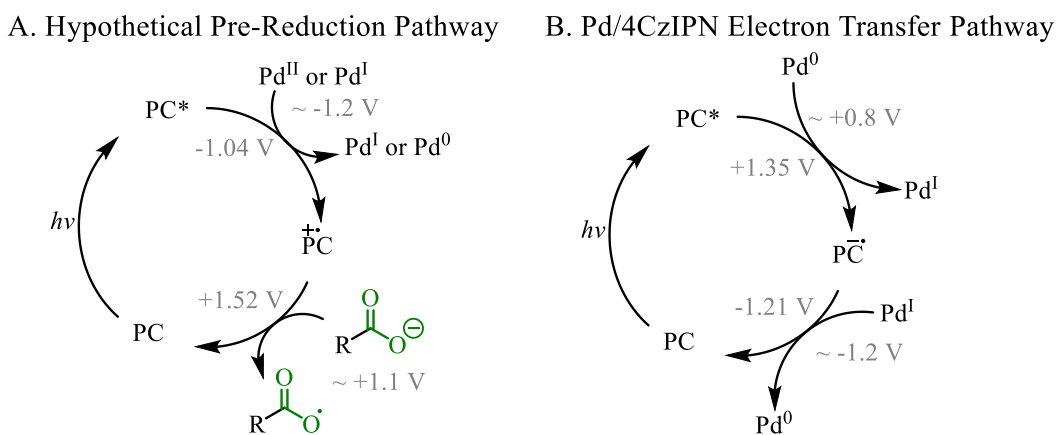
Scheme 2.11: Off-cycle reaction pathways

Once Pd[0] is formed, oxidative addition with the allyl carbonate is expected to provide

cationic π-allyl-Pd. The reduction of this species is not expected as its reported potential is -1.35

V vs. SCE and thus not a favorable match for 4CzIPN.[56] In agreement with this reduction potential

mismatch, [π-allyl-PdCl]$_2$/BINAP is not an efficient quencher of 4CzIPN (Figure 2.6). However,

[π-allyl-Pd(OAc)]$_2$/BINAP was found to be an efficient quencher of 4CzIPN (~10 fold more

efficient than carboxylate, Figure 2.6). The high quenching ability of the [π-allyl-

Pd(OAc)]$_2$/BINAP species points to a carboxylate oxidation pathway reminiscent of metal-

carboxylate species.[57]

After the decarboxylation event, there are several possibilities for the C–C bond formation.

First, the possibility of a radical-polar cross-over event must be considered.[10] But, due to the large

negative reduction potentials of most the alkyl radicals utilized herein (< -1.3 V vs. SCE)[58], this

pathway is not favorable. An alternate route is the radical addition to the cationic π-allyl-Pd. This

addition can occur at the allyl ligand resulting in the new C–C bond or coordination to the Pd center followed by inner sphere reductive elimination to form the new C–C bond.[43,59] In either event, the cross-coupled product would be liberated and a Pd^I species remains. This species is expected to have a reduction potential around -1.26 V vs. SCE[54] which would be well matched with the 4CzIPN radical anion (-1.21 V vs. SCE)[44].

Taken together, we believe the dominant catalytic pathway to proceed via a reductive quenching pathway in which the excited 4CzIPN is quenched by the π-allyl-Pd carboxylate species (Scheme 2.12). After, oxidation of this species facilitates decarboxylation and the formation of a carbon radical and π-allyl-Pd^{II} cation. Rebound of the radical with the π-allyl-Pd results in the formation of the allylated product and Pd^I. The Pd^I can be reduced by one electron via the 4CzIPN radical anion to complete both catalytic cycles. Alternatively, this process can proceed via an oxidative quenching pathway in which Pd^I quenches the 4CzIPN out of the excited state (Scheme 2.13).
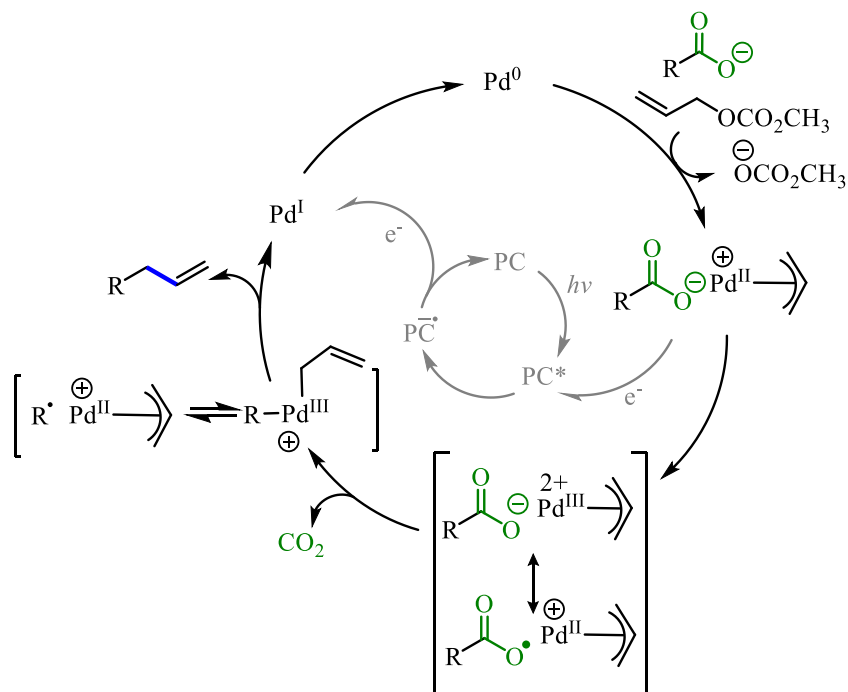
Scheme 2.12: Proposed dominant catalytic cycle (reductive quenching)
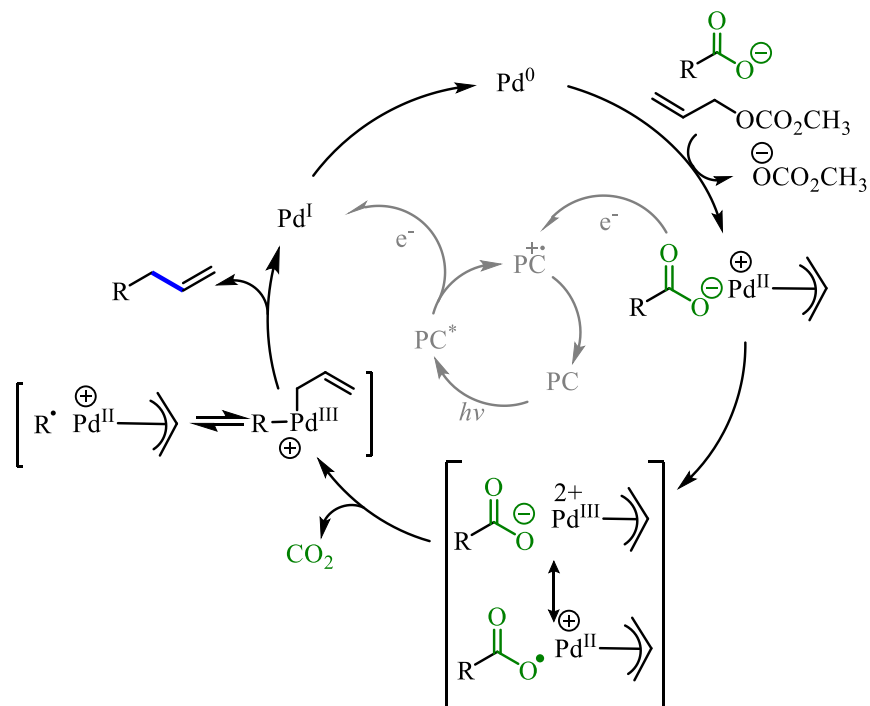
Scheme 2.13: Alternative catalytic cycle (oxidative quenching)

2.5 Organophotoredox/First-row Transition Metal DcA

Outside of Pd, alternative transition metal catalysts that could be utilized as co-catalysts with 4CzIPN were considered. Nickel (Ni) was an attractive choice as Ni represents a less expensive alternative to Pd and has been successfully employed in a verity of light-promoted dual-catalytic functionalization reactions.[60] The photoredox DcA of **2e-Boc** was initial performed under similar conditions to the optimal Pd conditions but with various Ni catalysts (Table 2.11). The allylation product **3b** was obtained from several reactions but high conversion was only observed when Ni(COD)₂ was employed as the pre-catalyst and with certain phosphine ligands (Table 2.11, Entries 1-3). The most successful catalyst in producing the DcA product **3b** was Ni(Xantphos) (Table 2.11, Entry 1). Utilizing a ligand of a similar scaffold but with a larger bite-angle resulted in inferior conversion (Table 2.11, Entry 5), while employing a similar ligand with a smaller bite angle resulted in high conversion but a lower quantity of **3b** relative to Xantphos (Table 2.10,

Entry 3). Nitrogen-based ligands perform very poorly in this chemistry (Table 2.11, Entries 6, 11, 14-16). This was an unexpected discovery as the Ni(dtbbpy)Cl₂ catalyst has been highly successful in photoredox/Ni dual catalytic processes particularly with 4CzIPN. The increase in electron donation from the phosphine ligand system to the Ni may be advantageous for the DcA chemistry.
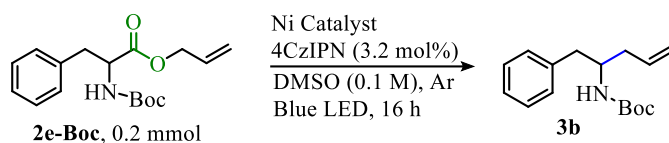
Entry	Ni (10 mol%)	Ligand (11 mol%)	3b	2b	other[b]
1	Ni(COD)$_2$	Xantphos	75	3	22
2	Ni(COD)$_2$	dppf	37	0	63
3	Ni(COD)$_2$	BINAP	34	6	59
4	Ni(COD)$_2$	(S,S)-DIOP	14	59	27
5	Ni(COD)$_2$	BISBI	11	64	25
6	Ni(COD)$_2$	tBu-PHOX	9	91	0
7	Ni(COD)$_2$	(R)-MOP	6	54	40
8	Ni(COD)$_2$	DBFPhos	2	94	4
9	Ni(COD)$_2$	PPh$_3$	1	99	0
10	Ni(COD)$_2$	(S,S)-DACHPhenylTrost	1	81	18
11	Ni(COD)$_2$	diphenyl-BOX	0	99	1
12	NiCl$_2$(dme)	Xantphos	0	100	0
13	NiCl$_2$(dme)	BINAP	0	100	0
14	NiCl$_2$(dme)	tBu-BOX	0	100	0
15	NiCl$_2$(dme)	diphenyl-BOX	0	100	0
16	NiCl$_2$ glyme	dtbbpy	0	100	0
17	Ni(dtbbpy)Cl$_2$		0	100	0

Table 2.11: Ni catalyst screening in photoredox/trasition metal-catalyzed DcA
[a] Reported ratios were determed by GC/MS. [b] Products that make up the "other" catagory include the alkene, alkane, free carboxylic acid, and various oligamers. [c] Product **3b** from the reaction in entry 1 was isolated and obtained in 33% yield.

Apart from a ligand screening, other changes in the reaction conditions were employed (Table 2.11). With regards to catalyst loading, the DcA was most efficient when the Ni concentration exceeded that of 4CzIPN (Table 2.12, Entries 1-3). This observation was also made for the Pd system. This reaction also proved to be highly solvent dependent, operating best in DMSO (Table 2.12, Entries 1-6). The reaction does proceed with high conversion when acetonitrile (MeCN) is employed, but the allylated product is produced as a minor product of the

reaction matrix. Although the Ni(dtbbpy)Cl$_2$ was found to have low utility in the DcA, it is interesting to note that when the reaction is run with K$_3$PO$_4$, the reaction proceeds with high conversion. But the alkene product and the free acid are the major products of the reaction (Table 2.12, Entries 7-9). The 4CzIPN/Ni conditions were applied to an intermolecular reaction as well as other carboxylic acid nucleophiles, but these resulted in little to no allylation. Allylic ester substrates derived from amino acids are the only substrates that provide >10% yield of the DcA product under these conditions. Thus, at this time, the Ni catalyzed process has lower utility that the Pd system.

2e-Boc, 0.2 mmol → Ni Catalyst / 4CzIPN / DMSO (0.1 M), Ar / Blue LED, 16 h → **3b**
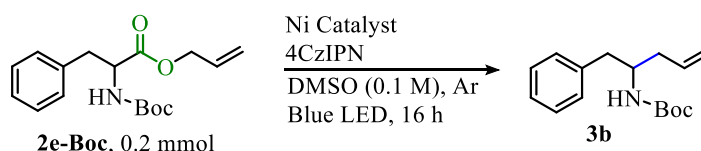
Entry	Ni (mol%)	4CzIPN (mol%)	Solvent	Additive[b]	3b	Enecarbamate	2b	Other[c]
1	Ni(Xantphos) (10 mol%)	6.4 mol%	DMSO	-	74	-	2	24
2	Ni(Xantphos) (15 mol%)	3.2 mol%	DMSO	-	63	-	0	37
3	Ni(Xantphos) (5 mol%)	10 mol%	DMSO	-	24	-	76	0
4	Ni(Xantphos) (10mol%)	3.2 mol%	MeCN	-	6	-	25	69
5	Ni(Xantphos) (10 mol%)	3.2 mol%	THF	-	0	-	100	0
6	Ni(Xantphos) (10 mol%)	3.2 mol%	DCM	-	0	-	100	0
7[d]	Ni(dtbbpy)Cl$_2$ (10 mol%)	3.2 mol%	DMSO	K$_3$PO$_4$	12	(49 *E*, 39 *Z*)	trace	0
8[d]	Ni(dtbbpy)Cl$_2$ (20 mol%)	3.2 mol%	DMSO	K$_3$PO$_4$	7	(49 *E*, 44 *Z*)	trace	0
9[d]	Ni(dtbbpy)Cl$_2$ (10 mol%)	3.2 mol%	DMSO	K$_3$PO$_4$	0	0	100	0
10[d]	Ni(dtbbpy)Cl$_2$ (10 mol%)	3.2 mol%	THF	K$_3$PO$_4$	3	(2 *E*, 16 *Z*)	78	1
11[d]	Ni(dtbbpy)Cl$_2$ (10 mol%)	3.2 mol%	DCM	K$_3$PO$_4$	0	0	97	3
12[d]	Ni(dtbbpy)Cl$_2$ (10 mol%)	3.2 mol%	MeCN	K$_3$PO$_4$	5	(15 *E*, 40 *Z*)	14	27

Table 2.12: Reaction condition modification in 4CzIPN/Ni DcA

[a] Product ratios determined by GC/MS. [b] K$_3$PO$_4$ was utilized in 2 equivalents in all entries except entry 9 in which 10 mol% was used. [c] Other products include alkene, alkane, free carboxylic acid and oligamer side products. [d] Reactions contained free acid 1b but this product is not part of the reported GC/MS ratios; enecarbamate products <60 % yield.

In addition to Ni, employing a cobalt (Co)/photoredox dual-catalytic system towards DcA was explored. Inspiration for this systems design came from Gryko's deallylation reactions that utilize vitamin B12 as a catalyst.[61] In this reaction design, a highly nucleophilic Co^{I} anion is

invoked to achieve a Sn2' addition to an allylic moiety. Following the same principle, a photoredox/Co reaction was envisioned in which vitamin B12 could be reduced to the reactive Co^I by single electron transfer which could then perform nucleophilic addition to the allyl electrophile. The Co-allyl species could then activate the allyl functionality for radical addition ultimately providing the allylated product (Scheme 2.14).
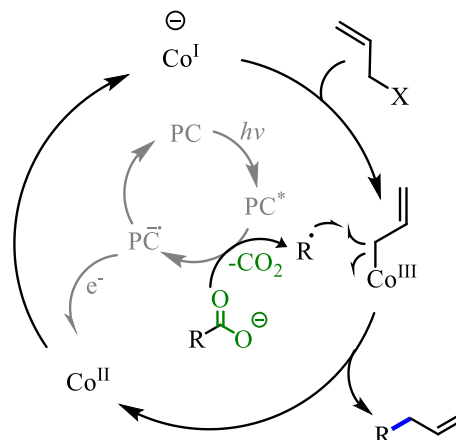
Scheme 2.14: General Co/PC mechanistic outline

Initial attempts at employing a photoredox/Co system in DcA resulted in low conversions and exclusive formation of the alkene, alkane, and homocoupled products. Ultimately, allylation could be achieve if carboxylate salts not prone to elimination were utilized as pro-nucleophiles (**1v⁻ Na⁺ salt**). The success of the carboxylate salts could possibly be due to avoiding undesired competitive protonation of the nucleophilic Co^I species when acids are utilized. In addition, the Co-catalyzed DcA reaction only proceeds with allyl halides as the electrophilic allyl source. The lack of reactivity seen with allyl esters as well as allyl carbonate and acetate suggest a halide reduction pathway may be operable instead of nucleophilic addition towards the Co–allyl intermediate.[62]

Photosensitizers from several different families were paired with vitamin B12 in the allylation of **1v⁻ Na⁺** (Table 2.13).[2c,2e] Of these, the 4CzIPN as well as an acridinium catalyst performed comparably with allyl bromide however, the yield of **3w** could be improved to 40% with a switch to allyl chloride as the electrophile source (Table 2.13, Entry 4).

44

Ph–C(O)–O⁻ ⊕ Na (Ph, Ph) + X–allyl →[B12 (3 mol%), PC, MeCN (0.1 M), Blue LED, 28 °C] Ph–CH(Ph)–CH₂–CH=CH₂ (**3w**)

0.2 mmol (**1v⁻ Na⁺**)   0.2 mmol
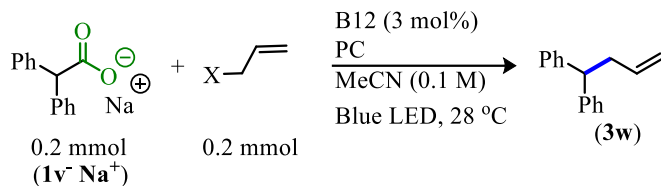
Entry	PC	X	3w Yield[a]
1	4CzIPN	Br	22%
2	4CzIPN	Cl	17%
3	Mes-2,7-Me₂-Acr-Me⁺ ClO₄⁻	Br	19%
4	Mes-2,7-Me₂-Acr-Me⁺ ClO₄⁻	Cl	40%
5[b]	Mes-2,7-Me₂-Acr-Me⁺ ClO₄⁻	Cl	20%
6	TPT[c]	Cl	0%

Table 2.13: Photocatalyst and allyl halide pairing with B12-catalyzed DcA
[a] Yields were determined by ¹H NMR with pyridine internal standard; product in entry 4 was isolated in 40% yield. [b] Reaction also contained Zn (10 mol%) and NH₄Cl (20 mol%). [c] 2,4,6-triphenylpyrylium tetrafluoroborate.

Changing the solvent to toluene, DMSO, methanol, or water resulted in inferior yields to what was obtained with MeCN (<20%). In addition, modifying the reaction concentration to 0.2 M or 0.05 M also lead to diminished yields. The potassium and lithium salts of **1w** were also subjected to the conditions outlined in Table 2.13 Entry 4, but the change in counter ion lead to <20% yield of **3w**.

Apart from vitamin B12, other cobalt catalysts were investigated for this allylation process (Table 2.14). Other Co catalysts screened had similar reactivity to what was observed with B12 but ultimately, B12 was the superior catalyst. Changes to the catalyst loadings did not improve the DcA (Table 2.15). Currently, the B12/Acr⁺ system provides full conversion of **1v⁻ Na⁺** but experiences competitive homocoupling. Also, the scope is limited to salts that do not possess any protons in the β-position. In sum, the Co methodology currently suffers from low utility and the undesired reaction pathways will have to be better inhibited for this reaction to be of general use.

Reaction scheme:

Ph–CH(Ph)–C(=O)–O⁻ Na⁺ (0.2 mmol, **1v⁻ Na⁺**) + X–CH₂–CH=CH₂ (0.2 mmol) → Ph–CH(Ph)–CH₂–CH=CH₂ (**3w**)

Conditions: Mes-2,7-Me$_2$-Acr-Me$^+$ ClO$_4^-$ (5 mol%), Co catalyst, MeCN (0.1 M), Blue LED, 28 °C
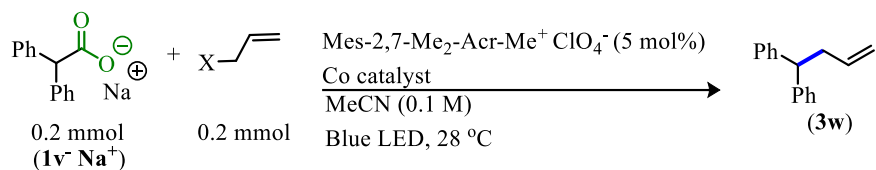
Entry	Co (3 mol%)	X	3w Yeild[b]
1	Co(Salen)$_2$	Br	21%
2	Co(dmgH)$_2$ClPy	Br	26%
3	*none*	Cl	1%
4	Co(dmgH)$_2$Cl(*N*-Me-Imidzole)	Cl	21%
5	Co(dmgH)$_2$ClPy	Cl	6%
6	Co(dpgH)$_2$ClPy	Cl	35%
7	Co(dmgBF$_2$)$_2$(NCCH$_3$)$_2$	Cl	2%
8	Co(acac)$_2$	Cl	10%

Table 2.14: Co catalyts in DcA

[a] Yields were determined by ^{1}H NMR with pyridine internal standard. [b] Cobaloxime catalysts in entry 4, 6, and 7 were previously synthesized in house following literature procedure.[63]

Reaction scheme:

Ph–CH(Ph)–C(=O)–O⁻ Na⁺ (0.2 mmol, **1v⁻ Na⁺**) + Cl–CH₂–CH=CH₂ (0.2 mmol) → Ph–CH(Ph)–CH₂–CH=CH₂ (**3w**)

Conditions: Mes-2,7-Me$_2$-Acr-Me$^+$ ClO$_4^-$, B12, MeCN (0.1 M), Blue LED, 28 °C
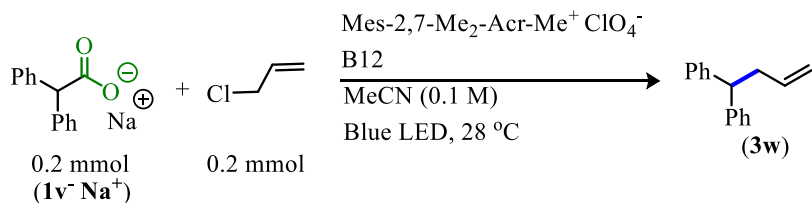
Entry	B12	Acr$^+$	3w Yield[a]
1	3 mol%	5 mol%	40%
2	6 mol%	10 mol%	14%
3	6 mol%	5 mol%	30%
4	6 mol%	5 mol%	31%
5	9 mol%	5 mol%	35%
6	9 mol%	2.5 mol%	11%
7	9 mol%	10 mol%	14%

Table 2.15: Catalyst loading variations

[a] Yields were determined by q[1]H NMR with pyridine internal standard.

2.6 Three-Component DcA

The 4CzIPN/Pd dual-catalytic system has greatly advanced the utility of the photoredox/transition metal DcA reaction. In addition to this advancement, these reaction conditions can be utilized in a three-component one-pot decarboxylative coupling reaction allowing for the rapid construction of more complex molecular scaffolds from readily accessible starting materials.[64] In this reaction sequence, two new $C(sp^3)$–$C(sp^3)$ bonds are formed while the only stoichiometric byproduct is CO_2.[65]

The general design plan for a three-component decarboxylative coupling employs the use of an activated olefin that can undergo efficient radical addition (Scheme 2.15). Once the decarboxylation event occurs, the activated olefin must be trapped by the carbon radical before the radical addition to the π-allyl-Pd occurs. The higher concentration of the activated olefin substrate (1 equiv.) relative to the π-allyl-Pd should aid in this event. After the first C–C bond formation, the second radical species can either undergo addition to the π-allyl-Pd or a radical-polar cross-over pathway may be at play in which the carbon radical is reduced to a carbanion which can undergo ionic addition with the π-allyl-Pd to form the second C–C bond.[10] A radical-polar crossover event is favorable with electrophilic olefins that result in α-carbonyl radical intermediates (~-0.6 V vs. SCE)[66] or α,α-dinitrile radical intermediates (~-0.7 V vs. SCE)[66] as these alkyl radicals can be reduced by 4CzIPN (< -1.0 V vs. SCE)[44].

A. Radical Pathway
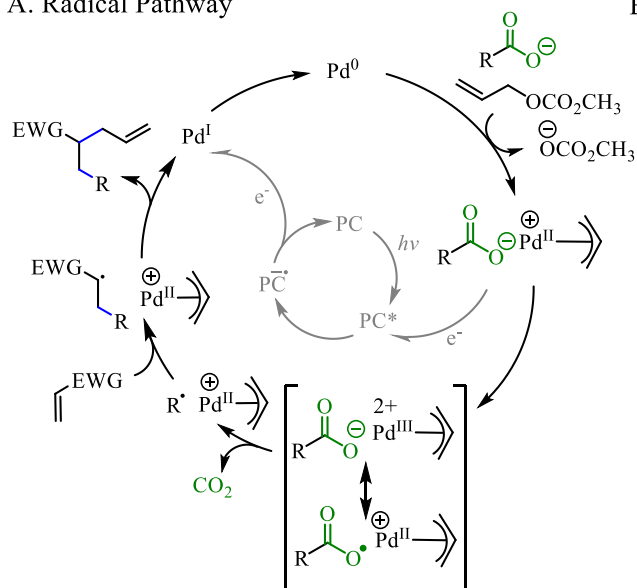
B. Radical-Polar Crossover
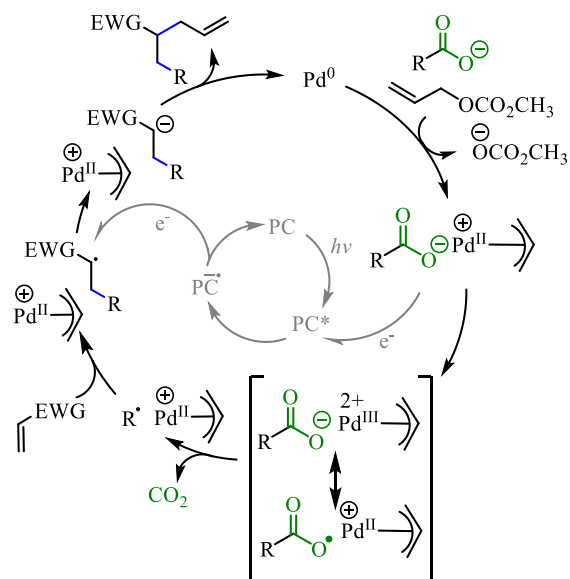
Scheme 2.15: Proposed three-component coupling pathways

Initial reactions utilized benzylidene malononitrile in 1 equivalent as the additional coupling component (Table 2.16). The malononitrile was able to be incorporated into the DcA with moderate to good yields with allyl methyl carbonate and different carboxylic acids (**6a-6c**). In these reactions, two main side products results. One is the direct DcA of the carboxylic acid, but this is consistently observed as a minor product indicating the radical generated post-decarboxylation is more efficiently trapped by the malononitrile then the π-allyl-Pd. The other side product was a diallylated benzyl malononitrile presumably arising from a background reaction of the π-allyl-Pd with the olefin.

Allylic carbonates with substituents in the 1-, 2-, and 3- position could also be employed in the three-part coupling (Table 2.16, **6d-6f**). In fact, the more substituted allylic carbonates **4b**, **4g**, **4h**, and **4i** generally resulted in higher yields than was observed with allyl methyl carbonate (**4a**) (**6c** vs. **6d-6f**). The direct DcA of **1t** was observed in some of these reactions as well but only as a minor product. Thus, these reactions are selective for the three-component coupling.
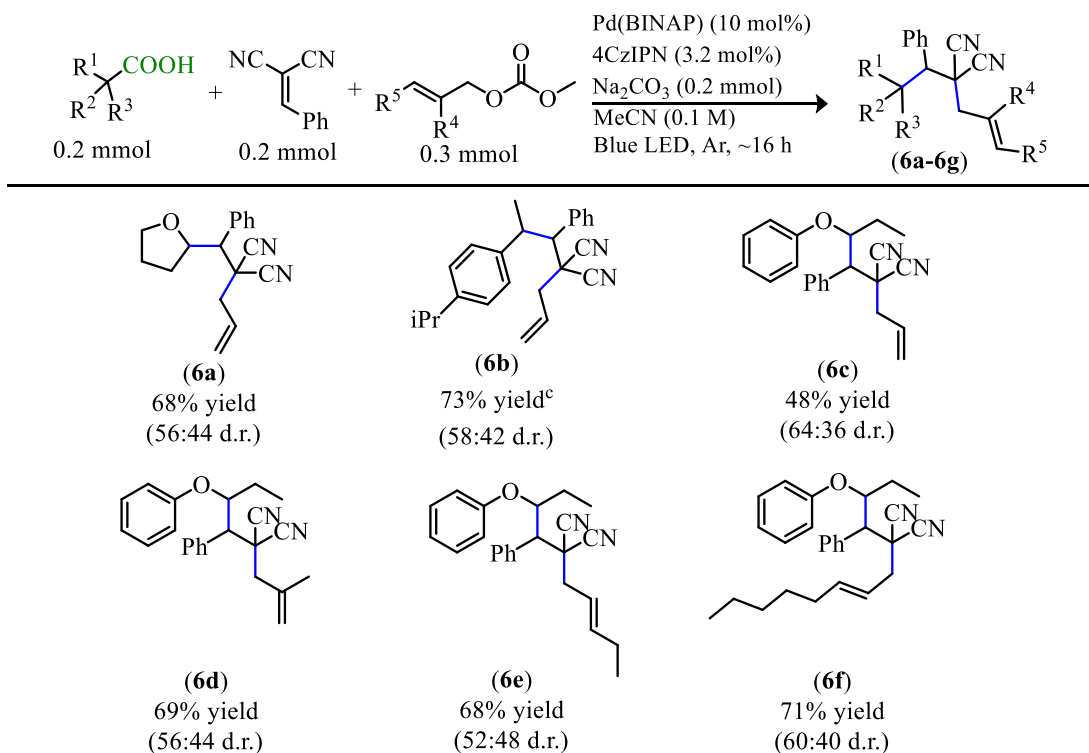
Table 2.16: Three-component DcA with benzilidene malononitrile

[a] Isolated yields shown. [b] Diastereomeric ratio (d.r.) was determined by ^{1}H NMR.

[c] Isolated with diallylbenzylmaolononitrile side product and mass adjusted.

The diallylated benzyl malononitrile product observed when **4a** was utilized was not observed with other allylic carbonates. However, the allylic carbonates utilized in these reactions generally did not proceed to full conversion which contrasts what was observed with allyl methyl carbonate.

Other electrophilic olefins were also able to be utilized in the three-component coupling (Table 2.17). Interestingly, methyl benzylidenecyanoacetate[67] resulted in two regioisomers (**6g.1** & **6g.2**). This result is possibly indicative of an allyl radical present in the reaction. However, this is the only case where two regioisomers were observed. The three-component coupling was also operable with 2-methacrolein and styrene, both resulting in product yields of ~30% (**6h** & **6i**). Although the three-component coupling product was observed with styrene, stilbene did not undergo the desired coupling reaction. Instead, 18% yield of difunctionalized side product **6j** was

collected which incorporated the allylic functionality as well as the methoxy nucleophile resulting from decarboxylation of the methyl carbonate. The remaining stilbene was recovered from the reaction.
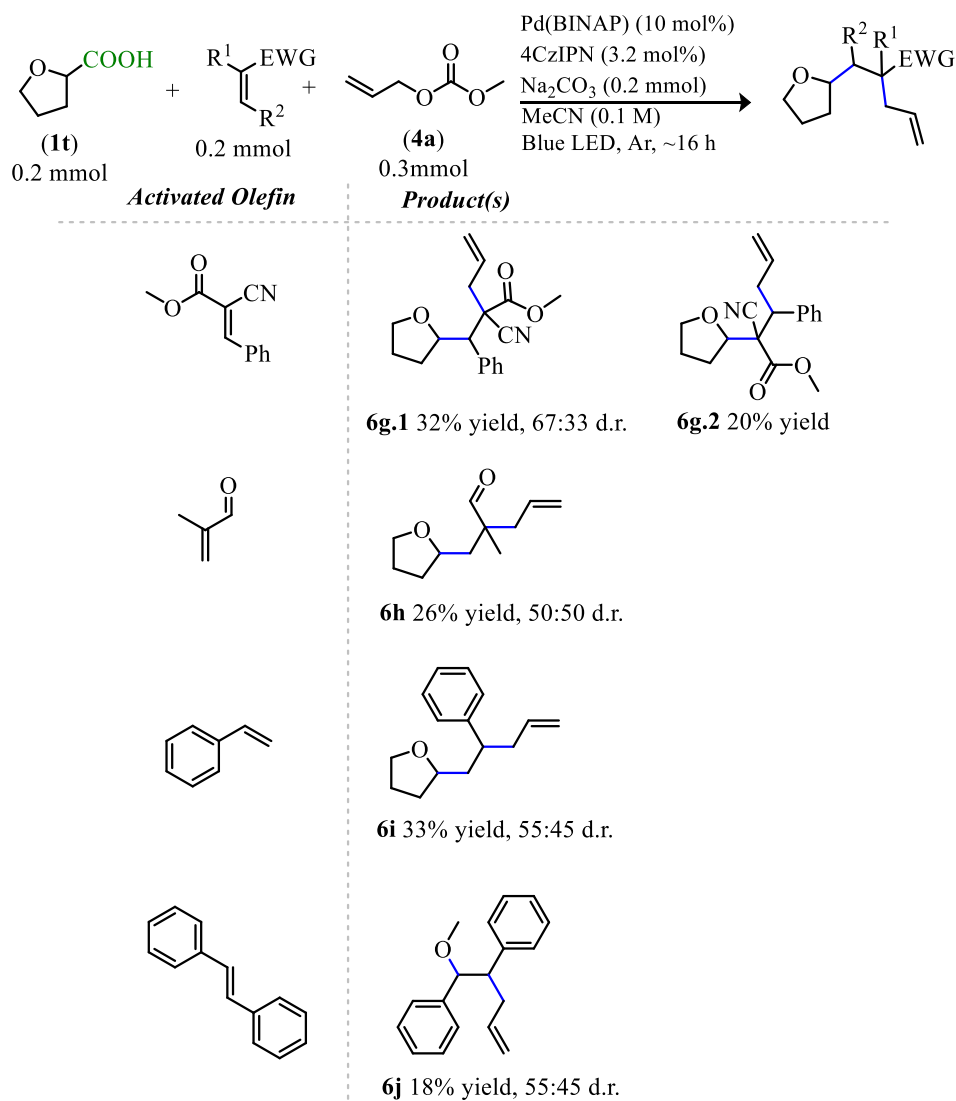
Table 2.17: Three-component DcA with electrophilic olefins

[a] Isolated yields shown. [b] Diastereomeric ratio (d.r.) determined by ^{1}H NMR.

This extension of the 4CzIPN/Pd DcA methodology to a multicomponent reaction allows for the rapid construction of densely functionalized molecular scaffolds. In addition to the installation of various allylic functional handles, the nitrile functionality incorporated through the use of malononitrile-derived olefins can be further diversifies in a variety of ways such as

hydrolysis, reduction, and as an electrophile in nucleophilic addition.[68] This method also provides an opportunity to use readily available reactants with diverse molecular scaffolds in the difunctionalization of electrophilic olefins. By employing the photoredox dual-catalytic strategy, three reactants were able to be linked via the formation of two new $C(sp^3)$–$C(sp^3)$ bonds in a single synthetic step under mild conditions.

2.7 Conclusions

A catalytic, mild, minimal waste producing, and operationally simplistic method towards the installation of allylic, dienyl, styrenyl, and benzylic functionalities on a variety of molecular scaffolds using carboxylic acid as latent carbon radicals has been realized. This method improved previously reported methodology through: 1) utilizing a more sustainable and less expensive photocatalyst, 2) providing increased yields across a broader carboxylic acid substrate scope, 3) is operational with a variety of π-electrophiles in addition to activated olefins in a multicomponent coupling, and 4) provided increased understanding of the dominant catalytic process. The methodology herein provides a simple and general approach toward building molecular complexity from easily accessible and inexpensive starting materials that would be otherwise difficult to achieve.

2.8 Experimental

2.8.1 General Considerations

All *N*-Boc and *N*-Cbz amino acids are commercially available and were used without further purification. *N*-Acetyl amino acids, 1-[(1,1-dimethylethoxy)carbonyl]-L-prolyl-L-phenylalanine, *N*-acetyl-norleucine, and *N*-acetyl-glutamic acid are commercially available and

were used without further purification, other acyl protected variants were previously made in the Tunge lab.[69] All additional carboxylic acid substrates are commercially available and were utilized without further purification. Allylmethylcarbonate (**4a**) was purchased from Oakwood and used without further purification. Allylic carbonates **4b**, **4c**, **4d**, **4e**, **4f**, **4i**, **4p** were made previously in the Tunge lab.[70] The carbazole fluorophore photocatalyst were synthesized from corresponding fluorocyanobenzenes and carbazole purchased from Sigma-Aldrich following reported literature procedure.[44] Allylic esters **2a-2e** were synthesized via DCC couplings from the corresponding carboxylic acids following reported literature procedure.[28] The $Pd(OAc)_2$ (reagent grade, >99%) pre-catalyst was purchased from Sigma-Aldrich. The BINAP ligand (95%) was purchased from Chem-Impex. Anhydrous solvents were purchased from Acros. Final decarboxylative allylation and benzylation reactions were run in a screw threaded tube from Chemglass (CLS-4208). Kessil H150 Blue LED grow lights provided 450 nm light. One light was used per reaction vessel and placed 2 mm from the surface of the light. A 2.0 mL solution of MeCN had an internal temperature of 28 °C after 1 hour of irradiation in the glass reaction tube under the standard LED configuration. Purification was accomplished with column chromatography using silica gel (60 Å porosity, 230 x 400 mesh, standard grade) which was purchased from Sorbent Technologies (catalog # 30930M-25). ^{1}H and ^{13}C NMR spectra were obtained on a Bruker ADVANCE 500 DRX equipped with a QNP cryoprobe. These spectra were referenced to residual protio solvent signals. HRMS data was obtained on an ESI LC-TOF Micromass LCT (Waters). HRMS data was collected using ESI mass spectrometry. GC/MS data was acquired on Shimadzu GCMS-QP2010 SE. Fluorescence quenching analysis for Stern-Volmer relationship data was obtained using PTI fluorometer (S/N 1266) with LPS-220 lamp and 710 photomultiplier system.

2.8.2 General Procedure for the Synthesis of Branched Allylic Alcohols from Aldehydes

A flame-dried Schlenk flask with stir bar under an atmosphere N_2 was charged with aldehyde (9.4 mmol, 1 equiv.) and THF (70 mL, 0.13 M). The reaction mixture was cooled to 0 ^{o}C using an ice bath. Vinyl magnesium bromide (13.2 mmol, 1.4 equiv.) was added via syringe and the reaction was allowed to warm to room temperature while stirring for approximately 14 hours. The reaction was quenched with 1M HCl (~20 mL) and the THF was removed under reduce pressure. The remaining aqueous solution was extracted with DCM (3x, ~20 mL), dried with $MgSO_4$ and concentrated under reduced pressure. The resulting allylic alcohols were utilized without further purification in the synthesis of allylic carbonates.

2.8.3 General Procedure for the Reduction of Aromatic Aldehydes

A round bottom flask with stir bar was charged with the corresponding aldehyde (2.4 mmol, 1 equiv.) and THF (10 mL, 0.24 M). The reaction mixture was cooled to 0 ^{o}C. Sodium borohydride (3.6 mmol, 0.14 g, 1.5 equiv.) was then added and the reaction was stirred while warming to room temperature for 1 hour. After, the reaction was quenched with H_2O (~10 mL) and THF removed under reduced pressure. The remaining aqueous solution was extracted with DCM (3x, ~10 mL), dried with $MgSO_4$, and concentrated under reduced pressure to provide the desired benzylic alcohol. The benzylic alcohols synthesized were used without further purification in the synthesis of benzylic carbonates.

2.8.4 Synthesis of Allylic and Benzylic Carbonates

Allylic and benzylic carbonates were prepared from the corresponding allylic and benzylic alcohols according to the modified literature procedure reported by Trost.[71] A flame-dried Schlenk

flask with stir bar under an atmosphere of N_2 was changed with the allylic or benzylic alcohol (1 equiv.) and anhydrous DCM (0.2 M). The resulting solution was cooled to 0 °C. Methyl chloroformate (2 equiv.) was then added via syringe followed by the dropwise addition of pyridine (5 equiv.) via syringe. After, the reaction was allowed to stir for approximately 14 hours while it warmed to room temperature. The reaction mixture was then quenched with saturated aqueous ammonium chloride (approximately half the reaction volume). The organics were collected, and the aqueous collection was extracted with DCM (3x, 20 mL). The combined organics were dried over $MgSO_4$ and concentrated under reduced pressure to provide the crude product. Products were purified via silica flash chromatography in 1:5-1:20 EtOAc:Hexanes.
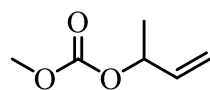
4e' (KC-7-126)

Product matched previously reported literature specification.[72]

^{1}H NMR (500 MHz, CDCl$_3$): δ 5.92-5.80 (m, 1H), 5.35-5.25 (dt, 1H), 5.22-5.14 (m, 2H), 3.78 (s, 3H), 1.37 (d, 3H).

^{13}C NMR{^{1}H} (126 MHz, CDCl$_3$): δ 155.3, 137.2, 116.7, 75.4, 55.2, 20.2.
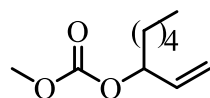
4g (KC-7-144)

Product matched previously reported literature specification.[73]

^{1}H NMR (500 MHz, CDCl$_3$): δ 5.86-5.74 (m, 1H), 5.30 (dt, 1H), 5.20 (dt, 1H), 5.04 (q, 1H), 3.78 (s, 3H), 1.75-1.55 (m, 2H), 1.40-1.23 (m, 6H), 0.88 (t, 3H).

^{13}C NMR{^{1}H} (126 MHz, CDCl$_3$): δ 155.5, 136.2, 117.5, 79.8, 54.8, 34.3, 31.7, 24.8, 22.6, 14.1.
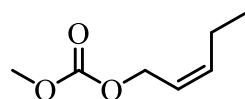
4h (KC-7-115)

Product matched previously reported literature specification.[74]

^{1}H NMR (500 MHz, CDCl$_3$): δ 5.72-5.59 (m, 1H), 5.59-5.44 (m, 1H), 4.74-4.60 (m, 2H), 3.77 (s, 3H), 2.19-2.04 (m, 2H), 1.03-0.91 (t, 3H).

^{13}C NMR{^{1}H} (126 MHz, CDCl$_3$): δ 156.2, 138.1, 122.5, 64.0, 55.1, 21.3, 14.4.
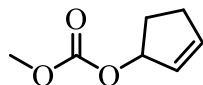
4j (KC-7-187)

Product matched previously reported literature specification.[74]

^{1}H NMR (500 MHz, CDCl$_3$): δ 6.17-6.12 (m, 1H), 5.90-5.84 (m, 1H), 5.66-5.58 (m, 1H), 3.77 (s, 3H), 2.60-2.47 (m, 1H), 2.38-2.22 (m, 2H), 1.97-1.86 (m, 1H).

^{13}C NMR{^{1}H} (126 MHz, CDCl$_3$): δ 155.7, 138.7, 128.8, 84.4, 54.6, 31.2, 29.8.
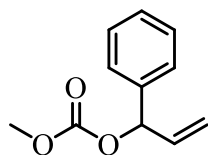
4k (KC-7-163)

Product matched previously reported literature specification.[73]

^{1}H NMR (500 MHz, CDCl$_3$): δ 7.44-7.29 (m, 5H), 6.12-5.98 (m, 2H), 5.35 (dt, 1H), 5.28 (dt, 1H), 3.79 (3H).

^{13}C NMR{^{1}H} (126 MHz, CDCl$_3$): δ 155.2, 138.4, 135.9, 128.8, 127.2, 117.6, 80.3, 55.0.
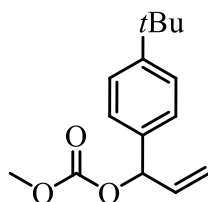
4l (KC-7-165)

Product matched previously reported literature specification.[73]

^{1}H NMR (500 MHz, CDCl$_3$): δ 7.41-7.36 (m, 2H), 7.33-7.27 (m, 2H), 6.10-5.99 (m, 2H), 5.39-5.31 (m, 1H), 5.29-5.23 (m, 1H), 3.77 (s, 3H), 1.31 (s, 9H).

^{13}C NMR{^{1}H} (126 MHz, CDCl$_3$): δ 155.4, 152.7, 135.7, 135.1, 126.7, 125.5, 117.1, 80.0, 54.7, 34.9, 31.2.
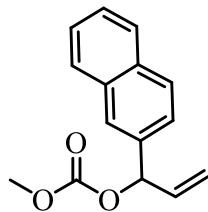
4m (KC-7-159)

Product matched previously reported literature specification.[73]

^{1}H NMR (500 MHz, CDCl$_3$): δ 7.77-7.58 (m, 4H), 7.41-7.26 (m, 3H), 6.17-6.07 (m, 1H), 6.04-5.89 (m, 1H), 5.28 (dt, 1H), 5.17 (dt, 1H), 3.62 (s, 3H).

^{13}C NMR{^{1}H} (126 MHz, CDCl$_3$): δ 155.2, 135.9, 133.3, 128.7, 128.3, 127.8, 126.5, 124.8, 117.9, 80.5, 55.0.
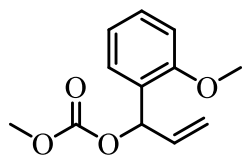
4n (KC-8-014)

Product matched previously reported literature specification.[75]

^{1}H NMR (500 MHz, CDCl$_3$): δ 7.36 (dd, J = 7.6, 1.7 Hz, 1H), 7.32–7.26 (m, 2H), 6.97 (t, J = 7.5 Hz, 1H), 6.89 (d, J = 8.2 Hz, 1H), 6.05 (ddd, J = 16.6, 10.4, 5.8 Hz, 1H), 5.31 (dt, J = 17.2, 1.4 Hz, 1H), 5.21 (dt, J = 10.4, 1.3 Hz, 1H), 3.85 (s, 3H), 3.78 (s, 3H).

^{13}C NMR{^{1}H} (126 MHz, CDCl$_3$): δ 156.6, 155.2, 135.5, 129.5, 127.4, 120.9, 116.7, 111.0, 74.6, 55.7, 54.9.
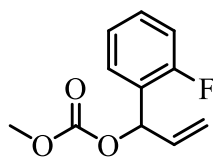
4o (KC-8-015)

Product matched previously reported literature specification.[75]

^{1}H NMR (500 MHz, CDCl$_3$): δ 7.41 (td, J = 7.5, 1.8 Hz, 1H), 7.38–7.26 (m, 1H), 7.19–7.11 (m, 1H), 7.06 (ddd, J = 9.7, 8.2, 1.2 Hz, 1H), 6.39 (dd, J = 6.1, 1.5 Hz, 1H), 6.06 (ddd, J = 16.8, 10.4, 6.0 Hz, 1H), 5.36 (dq, J = 17.2, 1.0 Hz, 1H), 5.29 (dt, J = 10.4, 1.2 Hz, 1H), 3.79 (s, 3H).

^{13}C NMR{^{1}H} (126 MHz, CDCl$_3$): δ 160.1 (d, *J* = 248.6 Hz), 154.9, 134.7, 130.2 (d, *J* = 8.4 Hz), 128.3 (d, *J* = 3.9 Hz), 125.9 (d, *J* = 13.5 Hz), 124.5 (d, *J* = 3.9 Hz), 117.9, 115.8 (d, 21.5 Hz), 74.3, 55.0.
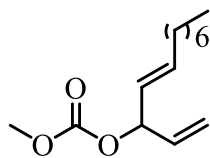
4q (KC-7-295)

^{1}H NMR (500 MHz, CDCl$_3$): δ 5.92–5.74 (m, 2H), 5.52–5.43 (m, 2H), 5.34–5.19 (m, 2H), 3.77 (s, 3H), 2.05 (q, J = 7.5 Hz, 2H), 1.37 (p, J = 6.9 Hz, 2H), 1.32–1.21 (m, 8H), 0.88 (t, J = 6.8 Hz, 3H).

^{13}C NMR{^{1}H} (126 MHz, CDCl$_3$): δ 155.2, 136.4, 135.5, 126.3, 117.5, 79.5, 54.4, 32.4, 31.9, 29.2, 28.9, 22.8, 14.2.

HRMS (ESITOF) m/z: Calc'd C$_{14}$H$_{23}$O$_3$ (M-H) = 239.1647, found 239.1636.

IR (film): 2956, 2927, 2856, 1751, 1700, 1647, 1559, 1507, 1465, 1437, 1262, 966, 934 cm^{-1}.
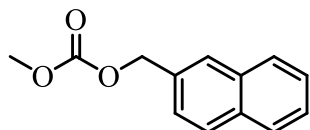
4r (KC-6-138)

Product matched previously reported literature specification.[76]

^{1}H NMR (500 MHz, CDCl$_3$): δ 7.88-7.80 (m, 4H), 7.55-7.44 (m, 3H), 5.33 (s, 2H), 3.81 (s, 3H).

^{13}C NMR{^{1}H} (126 MHz, CDCl$_3$): δ 156.7, 133.4, 133.3, 132.8, 128.6, 128.2, 127.9, 127.6, 126.5, 126.5, 125.9, 69.9, 55.1.
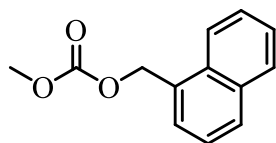
4s (KC-7-119)

Product matched previously reported literature specification.[77]

^{1}H NMR (500 MHz, CDCl$_3$): δ 8.15–7.98 (m, 1H), 7.98–7.79 (m, 2H), 7.65–7.38 (m, 5H), 5.64 (s, 2H), 3.80 (s, 3H).

^{13}C NMR{^{1}H} (126 MHz, CDCl$_3$): δ 155.9, 133.9, 131.7, 130.9, 129.8, 128.9, 127.9, 126.9, 126.1, 125.4, 123.6, 68.1, 55.0.
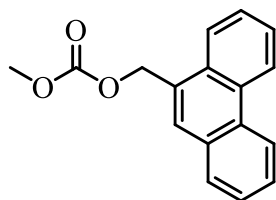
4t (KC-7-243)

^{1}H NMR (500 MHz, CDCl$_3$): δ 8.74 (dd, J = 7.4, 1.9 Hz, 1H), 8.68 (d, J = 8.3 Hz, 1H), 8.13–8.02 (m, 1H), 7.90 (dd, J = 7.9, 1.4 Hz, 1H), 7.87 (s, 1H), 7.75–7.64 (m, 3H), 7.61 (ddd, J = 8.0, 6.8, 1.2 Hz, 1H), 5.69 (s, 2H), 3.82 (s, 3H).

^{13}C NMR{^{1}H} (126 MHz, CDCl$_3$): δ 155.9, 131.2, 130.9, 130.8, 130.3, 129.3, 129.1, 128.8, 127.5, 127.2, 127.0, 126.9, 124.3, 123.4, 122.7, 68.5, 55.1.

HRMS (ESITOF) m/z: Calc'd C$_{17}$H$_{13}$O$_3$ (M-H) = 265.0865, found 265.0872.

IR (film): 2974, 1751, 1696, 1684, 1653, 1559, 1534, 1507, 1465, 1395, 1268, 1219 cm^{-1}.
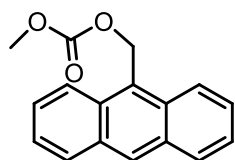
4u (KC-7-282)

^{1}H NMR (500 MHz, CDCl$_3$): δ 8.53 (s, 1H), 8.39 (dq, J = 8.9, 1.0 Hz, 2H), 8.04 (ddt, J = 8.5, 1.4, 0.7 Hz, 2H), 7.59 (ddd, J = 8.9, 6.6, 1.4 Hz, 2H), 7.54–7.46 (m, 2H), 6.24 (s, 2H), 3.80 (s, 3H).

^{13}C NMR{^{1}H} (126 MHz, CDCl$_3$): δ 131.5, 131.3, 129.7, 129.3, 127.0, 125.3, 124.1, 62.5, 55.1.

HRMS (ESITOF) m/z: Calc'd C$_{17}$H$_{14}$O$_3$ (M+) = 266.0943, found 266.0945.

IR (film): 3065, 1749, 1704, 1680, 1653, 1559, 1534, 1507, 1457, 1267, 1258, 936 cm^{-1}.
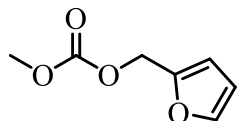
4v (KC-6-194)

Product matched previously reported literature specification.[78]

^{1}H NMR (500 MHz, CDCl$_3$): δ 7.50 (dt, J = 1.6, 0.8 Hz, 1H), 7.40 (t, J = 1.7 Hz, 1H), 6.45 (dd, J = 1.8, 0.8 Hz, 1H), 5.04 (s, 2H), 3.78 (s, 3H).

^{13}C NMR{^{1}H} (126 MHz, CDCl$_3$): δ 155.4, 148.7, 143.4, 111.3, 110.5, 61.2, 54.8.
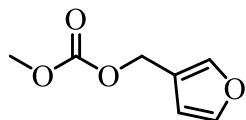
4w (KC-7-028)

Product matched previously reported literature specification.[79]

^{1}H NMR (500 MHz, CDCl$_3$): δ 7.59–7.43 (m, 1H), 7.40 (t, J = 1.7 Hz, 1H), 6.46 (dd, J = 1.9, 0.9 Hz, 1H), 5.04 (s, 2H), 3.79 (s, 3H).

^{13}C NMR{^{1}H} (126 MHz, CDCl$_3$): δ 155.9, 143.6, 142.1, 119.4, 110.6, 61.1, 55.1.
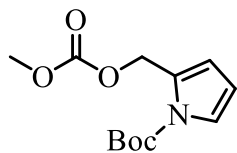
4x (KC-7-186)

^{1}H NMR (500 MHz, CDCl$_3$): δ 7.29 (dd, J = 3.3, 1.8 Hz, 1H), 6.44–6.23 (m, 1H), 6.13 (t, J = 3.3 Hz, 1H), 5.33 (d, J = 0.7 Hz, 2H), 3.79 (s, 3H), 1.59 (s, 9H).

^{13}C NMR{^{1}H} (126 MHz, CDCl$_3$): δ 155.7, 149.0, 128.2, 123.2, 116.7, 109.7, 84.4, 61.8, 55.3, 28.0.

HRMS (ESITOF) m/z: Calc'd C$_{12}$H$_{17}$NO$_5$Na (M+Na) = 278.1004, found 278.0992.

IR (film): 2980, 1749, 1700, 1647, 1559, 1507, 1457, 1373, 1345, 1319, 1272, 1138, 936 cm^{-1}.

2.8.5 4CzIPN/Pd Dual Catalytic DcA and DcB of Carboxylic Acids

In an Ar atmosphere glove box, a 10 mL screw threaded glass tube equipped with stir bar was charged with Pd(OAc)$_2$ (10 mol%, 0.02 mmol, 0.0045 g), BINAP (11 mol%, 0.022 mmol, 0.0145 g), and MeCN (1 mL). The reaction vessel was sealed and allowed to stir for 30 minutes during which time the reaction mixture goes from a yellow, heterogenous solution to a homogenous orange solution. After the pre-stir, the corresponding allylic or benzylic carbonate (1.5 equiv., 0.3 mmol), the corresponding carboxylic acid (1 equiv., 0.2 mmol), sodium carbonate (1 equiv., 0.2 mmol), and 4CzIPN (3.2 mol%, 0.0064 mmol, 0.005 g) were added to the tube followed by MeCN (1 mL) so that the total reaction volume is 2 mL (0.1 M). The tube is sealed

and removed from the glovebox. The reaction was stirred and irradiated with one 32 W Kessil blue LED lamp for 16 hours (see Appendix **A3** for light apparatus). The reaction temperature reaches 28 °C after the first hour of irradiation and maintains this temperature. After such time, the reaction is removed from the light, the tube opened, and the solvent removed under reduced pressure. The resulting product is purified via silica gel flash chromatography in either 1:5-1:40 EtOAc:Hexanes or 1:10 Et$_2$O:Pentane for products with molecular weights under 150 g/mol.
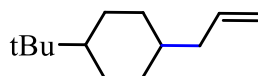
3a (KC-7-280)

Product matched previously reported literature specification.[80]

^{1}H NMR (500 MHz, CDCl$_3$): Mix of diastereomers (60:40 d.r.): δ 5.89–5.72 (m, 1H), 5.08–4.94 (m, 2H), [2.12 (dt) & 1.96 (dt), ∑2H], 1.83–1.63 (m, 4H), 1.54–1.41 (m, 2H), 1.35–1.20 (m, 2H), 1.19–1.07 (m, 1H), 0.87–0.85 (m, 9H).

^{13}C NMR{^{1}H} (126 MHz, CDCl$_3$): Mix of diastereomers (60:40 d.r.): δ 138.8, 138.0, 115.3, 115.1, 48.6, 48.3, 42.0, 38.0, 35.8, 33.6, 32.5, 30.3, 27.7, 27.7, 27.4, 27.4, 21.7.
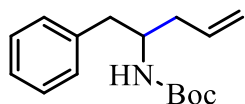
3b (KC-5-278)

Product matched previously reported literature specification.[43]

^{1}H NMR (500 MHz, CDCl$_3$): δ 7.23-7.11 (m, 2H), 7.14–7.04 (m, 3H), 5.69 (ddt, 1H), 5.32–4.66 (m, 2H), 4.30 (broad s, 1H), 3.80 (broad s, 1H), 2.66 (td, 2H), 2.15 (dt, 1H), 2.08–1.94 (m, 1H), 1.30 (s, 9H).

^{13}C NMR{^{1}H} (126 MHz, CDCl$_3$): δ 155.5, 138.2, 134.3, 129.6, 128.5, 126.5, 118.1, 79.2, 51.2, 40.6, 38.3, 28.4.
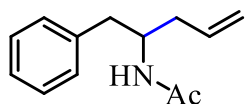
3c (KC-5-292)

Product matched previously reported literature specification.[43]

^{1}H NMR (500 MHz, CDCl$_3$): δ 7.33–7.27 (m, 2H), 7.25–7.15 (m, 3H), 6.06–5.54 (m, 1H), 5.30 (s, 1H), 5.27–4.82 (m, 2H), 4.70–4.01 (m, 1H), 2.81 (h, 2H), 2.31-2.24 (m, 1H), 2.21–2.00 (m, 1H), 1.92 (s, 3H).

^{13}C NMR{^{1}H} (126 MHz, CDCl$_3$): δ 169.6, 138.0, 134.5, 129.5, 128.6, 126.6, 118.2, 49.6, 40.1, 37.9, 23.6.
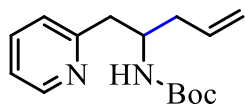
3d (KC-6-258)

Product matched previously reported literature specification.[43]

^{1}H NMR (500 MHz, CDCl$_3$): δ 8.52 (s, 1H), 7.58 (t, 1H), 7.22–6.82 (m, 2H), 5.80 (ddt, 1H), 5.28 (broad s, 1H), 5.05 (dd, 2H), 4.00 (p, 1H), 3.14–2.66 (m, 2H), 2.23 (qt, 2H), 1.36 (s, 9H).

^{13}C NMR{^{1}H} (126 MHz, CDCl$_3$): δ 159.0, 155.5, 149.3, 136.5, 134.8, 124.1, 121.5, 117.8, 79.0, 50.6, 42.0, 38.7, 28.3.
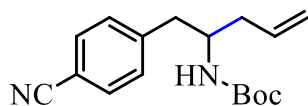
3e (KC-7-202)

Product matched previously reported literature specification.[43]

^{1}H NMR (500 MHz, CDCl$_3$): δ 7.57 (d, 2H), 7.30 (d, 2H), 5.77 (ddt, 1H), 5.22–4.96 (m, 2H), 4.42 (broad s, 1H), 3.90 (broad s, 1H), 2.83 (d, 2H), 2.24 (dt, 1H), 2.13 (dt, 1H), 1.37 (s, 9H).

^{13}C NMR{^{1}H} (126 MHz, CDCl$_3$): δ 155.4, 144.2, 134.0, 132.2, 130.4, 128.7, 119.1, 118.6, 110.4, 79.6, 51.0, 41.2, 38.4, 28.2.
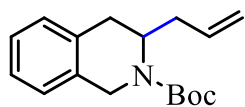
3f (KC-6-057)

Product matched previously reported literature specification.[43]

^{1}H NMR (500 MHz, CDCl$_3$): δ 7.21-7.14 (m, 2H), 7.11 (d, 2H), 5.78 (dq, 1H), 5.08–4.90 (m, 2H), 4.79 (broad s, 1H), 4.72–4.35 (m, 1H), 3.03 (dd, 1H), 2.69 (d, 1H), 2.46–2.15 (m, 1H), 2.04 (dt, 1H), 1.50 (s, 9H).

^{13}C NMR{^{1}H} (126 MHz, CDCl$_3$): δ 155.1, 135.3, 133.0, 129.5, 129.1, 126.7, 126.3, 117.3, 80.1, 50.0, 48.4, 43.2, 42.6, 37.0, 36.4, 32.9, 32.4, 28.5.
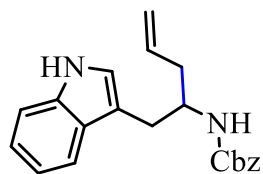
3g (KC-6-170)

^{1}H NMR (500 MHz, CDCl$_3$): δ 8.14 (broad s, 1H), 7.66 (d, 1H), 7.41–7.32 (m, 5H), 7.24–7.16 (m, 1H), 7.13 (d, 1H), 6.97 (broad s, 1H), 5.82 (ddt, 1H), 5.16–5.04 (m, 4H), 4.75 (d, 1H), 4.12–4.07 (m, 1H), 2.98 (tq, 2H), 2.35 (dt, 1H), 2.19 (dt, 1H).

^{13}C NMR{^{1}H} (126 MHz, CDCl$_3$): δ 156.1, 136.3, 134.6, 128.6, 128.2, 122.8, 122.1, 119.6, 119.1, 118.1, 112.0, 111.2, 66.6, 51.2, 38.5, 30.1.

HRMS (ESITOF) m/z: Calc'd C$_{21}$H$_{22}$N$_2$O$_2$Na (M+Na) = 357.1579, found 357.1582.

IR (film): 2925, 2854, 1700, 1653, 1559, 1521, 1507, 1457, 1430, 1419, 1340, 1260, 1219, 1058, 1027, 913 cm^{-1}.
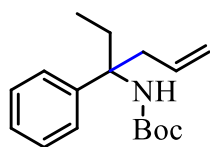
3h (KC-6-203)

^{1}H NMR (500 MHz, CDCl$_3$): Mix of rotamers: δ 7.43-7.27 (m, 3H), 7.18–7.00 (m, 2H), 5.55 (dq, 1H), 5.23–4.91 (m, 2H), 4.77 (broad s, 1H), 2.97–2.75 (m, 1H), 2.72 (q, 1H), 2.68–2.53 (m, 1H), 2.07–1.80 (m, 2H), 1.39 (broad d, 9H), 1.20 (t, 2H), 0.70 (t, 3H).

^{13}C NMR{^{1}H} (126 MHz, CDCl$_3$): Mix of rotamers: δ 162.2, 155.5, 133.7, 128.7, 128.2, 126.5, 125.8, 118.7, 82.0, 60.5, 41.6, 31.6, 28.5, 28.4, 8.1.

HRMS (ESITOF) m/z: Calc'd C$_{17}$H$_{29}$N$_2$O$_2$ (M+NH$_4$) = 293.2229, found 293.2212.

IR (film): 3422, 3356, 3287, 2976, 2935, 2880, 1724, 1699, 1494, 1446, 1391, 1365, 1271, 1252, 1170, 1082, 1001, 916 cm^{-1}.
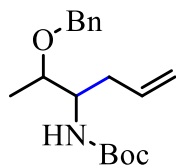
3i (KC-6-043)

^{1}H NMR (500 MHz, CDCl$_3$): δ 7.53–7.27 (m, 5H), 5.93–5.57 (m, 1H), 5.16–4.93 (m, 2H), 4.79 (d, 1H), 4.61 (d, 1H), 4.38 (d, 1H), 3.78–3.29 (m, 2H), 2.31 (hept, 2H), 1.43 (s, 9H), 1.20 (d, 3H).

^{13}C NMR{^{1}H} (126 MHz, CDCl$_3$): δ 156.2, 138.6, 135.3, 128.3, 127.8, 117.3, 79.3, 74.7, 71.0, 54.6, 37.6, 28.3, 16.3.

HRMS (ESITOF) m/z: Calc'd C$_{18}$H$_{28}$NO$_3$ (M+H) = 306.2069, found 306.2065.

IR (film): 3447, 3343, 2978, 2930, 2871, 1718, 1715, 1700, 1507, 1457, 1399, 1366, 1274, 1172, 1066, 993, 916 cm^{-1}.
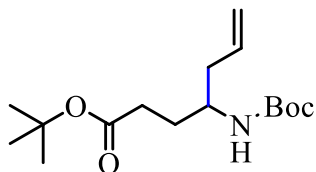
3j (KC-5-293)

^{1}H NMR (500 MHz, CDCl$_3$): δ 5.82–5.70 (m, 1H), 5.14–4.88 (m, 2H), 4.41 (d, 1H), 3.61 (tt, 1H), 2.27 (t, 2H), 2.20 (q, 2H), 1.79 (dtd, 1H), 1.61 (p, 1H), 1.43 (s, 9H), 1.41 (s, 9H).

^{13}C NMR{^{1}H} (126 MHz, CDCl$_3$): δ 172.8, 154.8, 134.1, 118.0, 80.4, 78.9, 50.0, 39.6, 32.3, 29.4, 28.3, 27.9.

HRMS (ESITOF) m/z: Calc'd C$_{16}$H$_{29}$NO$_4$Na (M+Na) = 322.1994, found 322.1981.

IR (film): 3354, 2978, 2933, 1717, 1691, 1525, 1452, 1392, 1367, 1251, 1220, 1170, 1053, 993, 914 cm^{-1}.
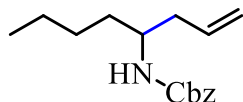
3k (KC-5-282)

Product matched previously reported literature specification.[81]

^{1}H NMR (500 MHz, CDCl$_3$): δ 7.56–7.28 (m, 5H), 5.77 (dq, 1H), 5.25–4.90 (m, 2H), 4.57 (d, 1H), 3.71 (q, 1H), 2.23 (ddt, 2H), 1.49 (dd, 1H), 1.43–1.18 (m, 6H), 0.90 (d, 3H).

^{13}C NMR{^{1}H} (126 MHz, CDCl$_3$): δ 156.1, 136.8, 134.4, 128.6, 128.2, 117.9, 66.6, 50.8, 39.6, 34.4, 28.2, 22.7, 14.1.
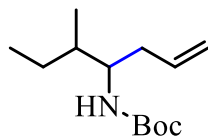
3l (KC-5-296)

^{1}H NMR (500 MHz, CDCl$_3$): (mix of rotamers) δ 5.76 (ddtd, 1H), 5.09–4.99 (m, 2H), 4.42-4.24 (m, 1H), 3.69-3.48 (m, 1H), 2.30-1.98 (m, 2H), 1.53-1.44 (m, 2H), 1.42 (s, 9H), 1.22–1.01 (m, 1H), 0.93–0.80 (m, 6H).

^{13}C NMR{^1H} (126 MHz, CDCl$_3$): (mix of rotamers) δ 155.9, 135.3, 117.2, 117.1, 79.0, 54.3, 53.4, 38.4, 38.0, 37.7, 36.2, 28.5, 26.4, 25.2, 15.3, 14.1, 11.8.

HRMS (ESITOF) m/z: Calc'd C$_{13}$H$_{24}$NO$_2$ (M-H) = 226.1807, found 226.1811.

IR (film): 2965, 2933, 1734, 1700, 1696, 1684, 1653, 1559, 1539, 1521, 1517, 1490, 1465, 1437, 1248, 1219, 1175 cm^{-1}.
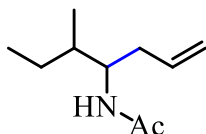
3m (KC-5-286)

^1H NMR (500 MHz, CD$_3$CN): Mix of diastereomers, (56:44 d.r.): δ 6.12 (broad d, 1H), 5.86–5.65 (m, 1H), 5.11–4.90 (m, 2H), [3.89 (tt) & 3.77 (tdd) ∑1H], 2.32–2.19 (m, 1H), 2.15–1.98 (m, 1H), 1.83 (d, 3H), [1.46 (dtd) & 1.37 (tt) ∑2H], 1.18–1.02 (m, 1H), 0.94–0.81 (m, 6H).

^{13}C NMR{^1H}(126 MHz, CD$_3$CN): Mix of diastereomers: δ 170.3, 170.1, 137.1, 136.9, 116.9, 116.8, 53.5, 52.5, 39.2, 39.0, 37.8, 36.3, 27.0, 26.0, 23.1, 15.5, 14.5, 12.0, 11.9.

HRMS (ESITOF) m/z: Calc'd C$_{10}$H$_{19}$NONa (M+Na) = 192.1364, found 192.1373.

IR (film): 3287, 3077, 2963, 2933, 2876, 1646, 1554, 1457, 1437, 1374, 1297, 1150, 993, 958, 913 cm^{-1}.
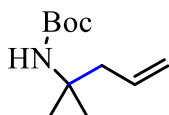
3n (KC-6-058)

Product matched previously reported literature specification.[82]

^1H NMR (500 MHz, CDCl$_3$): δ 5.89–5.69 (m, 1H), 5.15–4.95 (m, 2H), 4.86 (broad s, 1H), 2.30 (broad d, 2H), 1.43 (s, 9H), 0.73 (broad t, 2H), 0.64 (broad t, 2H).

^{13}C NMR {^1H}(126 MHz, CDCl$_3$): δ 155.7, 135.2, 117.3, 79.0, 40.6, 32.9, 28.2, 13.0.
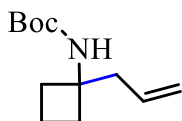
3o (KC-7-152)

^1H NMR (500 MHz, CDCl$_3$): δ 5.77 (ddt, 1H), 5.13–5.07 (m, 2H), 4.61 (broad s, 1H), 2.50 (d, 2H), 2.35–2.12 (m, 2H), 2.00 (ddd, 2H), 1.87 (ddq, 1H), 1.81–1.68 (m, 1H), 1.43 (s, 9H).

^{13}C NMR{^1H} (126 MHz, CDCl$_3$): δ 154.2, 134.1, 118.5, 79.1, 55.6, 42.2, 32.1, 28.7, 14.2.

HRMS (ESITOF) m/z: Calc'd C$_{12}$H$_{25}$N$_2$O$_2$ (M+NH$_4$) = 229.1916, found 229.1925.

IR (film): 3352, 3076, 2978, 2937, 1717, 1696, 1507, 1391, 1365, 1278, 1250, 1172, 1066, 995, 914 cm^{-1}.
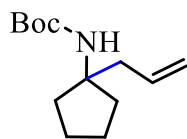
3p (KC-7-183)

^{1}H NMR (500 MHz, CDCl$_3$): δ 5.86–5.65 (m, 1H), 5.10–4.91 (m, 2H), 4.42 (broad s, 1H), 2.48 (d, 2H), 1.89-1.77 (m, 2H), 1.76–1.64 (m, 2H), 1.65-1.55 (m, 4H), 1.41 (s, 9H).

^{13}C NMR{^{1}H} (126 MHz, CDCl$_3$): δ 154.8, 134.9, 117.7, 79.0, 63.3, 42.0, 37.7, 28.5, 23.4.

HRMS (ESITOF) m/z: Calc'd C$_{13}$H$_{23}$NO$_2$Li (M+Li) = 232.1889, found 232.1887.

IR (film): 3448, 3357, 3075, 2976, 2872, 1718, 1695, 1517, 1490, 1452, 1390, 1365, 1276, 1245, 1172, 1091, 989, 912 cm^{-1}.
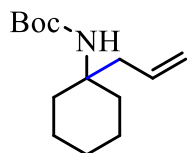
3q (KC-7-185)

^{1}H NMR (500 MHz, CDCl$_3$): δ 5.76 (ddt, 1H), 5.14–4.82 (m, 2H), 4.25 (broad s, 1H), 2.44 (d, 2H), 1.91 (d, 2H), 1.60–1.43 (m, 5H), 1.42 (s, 9H), 1.36–1.17 (m, 3H).

^{13}C NMR{^{1}H} (126 MHz, CDCl$_3$): δ 154.5, 134.2, 118.1, 78.6, 54.3, 35.0, 28.4, 25.8, 21.7.

HRMS (ESITOF) m/z: Calc'd C$_{14}$H$_{25}$NO$_2$Na (M+Na) = 262.1783, found 262.1786.

IR (film): 3450, 3366, 3075, 2977, 2931, 2858, 1722, 1700, 1496, 1448, 1390, 1365, 1248, 1220, 1167, 1086, 973, 913 cm^{-1}.
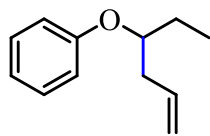
3r (KC-5-289)

^{1}H NMR (500 MHz, CDCl$_3$): δ 7.26–7.18 (m, 2H), 6.93–6.85 (m, 3H), 5.84 (ddt, 1H), 5.19–4.94 (m, 2H), 4.20 (p, 1H), 2.40 (dtdd, 2H), 1.76–1.62 (m, 2H), 0.95 (t, 3H).

^{13}C NMR{^{1}H} (126 MHz, CDCl$_3$): δ 158.6, 134.5, 129.5, 120.6, 117.3, 116.1, 78.8, 37.9, 26.5, 9.6.

HRMS (ESITOF) m/z: Calc'd C$_{12}$H$_{20}$ON (M+NH$_4$) = 194.1545, found 194.1535.

IR (film): 2971, 2331, 1700, 1653, 1599, 1559, 1496, 1241, 1220 cm^{-1}.
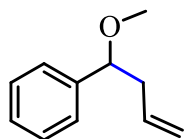
3s (KC-7-050)

Product matched previously reported literature specification.[83]

^{1}H NMR (500 MHz, CDCl$_3$): δ 7.39–7.34 (m, 2H), 7.31–7.25 (m, 3H), 5.82–5.71 (m, 1H), 5.04–4.93 (m, 2H), 4.20 (dd, 1H), 3.15 (s, 3H), 2.56–2.47 (m, 1H), 2.38 (dtt, 1H).

^{13}C NMR{^{1}H} (126 MHz, CDCl$_3$): δ 143.0, 136.1, 129.3, 128.5, 127.7, 117.1, 84.3, 56.7, 42.9.
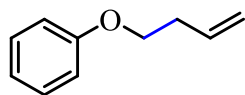
3t (KC-7-237)

Product matched previously reported literature specification.[81]

^{1}H NMR (500 MHz, CDCl$_3$): δ 7.38–7.24 (m, 2H), 7.02–6.87 (m, 3H), 5.92 (ddt, 1H), 5.23–5.07 (m, 2H), 4.02 (t, 2H), 2.55 (qt, 2H).

^{13}C NMR{^{1}H} (126 MHz, CDCl$_3$): δ 159.0, 134.6, 129.6, 120.9, 117.3, 114.9, 67.3, 33.8.
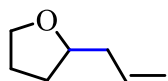
3u (KC-7-273)

Product matched previously reported literature specification.[85]

^{1}H NMR (500 MHz, CDCl$_3$): δ 5.93–5.79 (m, 1H), 5.16–4.99 (m, 2H), 3.85–3.76 (m, 2H), 3.71–3.59 (m, 1H), 2.03–1.94 (m, 6H).
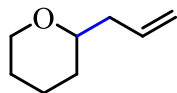
3v (KC-7-251)

Product matched previously reported literature specification.[86]

^{1}H NMR (500 MHz, CDCl$_3$): δ 5.77 (ddt, 1H), 5.05–4.91 (m, 2H), 3.91 (ddt, 1H), 3.36 (td, 1H), 3.28–3.21 (m, 1H), 2.25–2.17 (m, 1H), 2.15–2.06 (m, 1H), 1.78–1.72 (m, 1H), 1.54 (ddt, 1H), 1.46–1.37 (m, 2H), 1.26–1.15 (m, 1H).

^{13}C NMR{^{1}H} (126 MHz, CDCl$_3$): δ 135.3, 116.7, 68.8, 41.3, 31.6, 30.5, 26.2, 23.6.
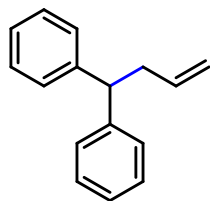
3w (KC-5-207)

Product matched previously reported literature specification.[87]

^{1}H NMR (500 MHz, CDCl$_3$): δ 7.41–7.26 (m, 10H), 5.81 (ddt, 1H), 5.12 (dq, 1H), 5.04 (ddt, 1H), 4.14–4.05 (m, 1H), 2.91 (ddt, 2H).

^{13}C NMR{^{1}H} (126 MHz, CDCl$_3$): δ 144.6, 137.0, 129.1, 128.5, 128.1, 126.3, 116.4, 51.4, 40.1.
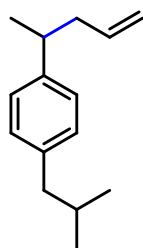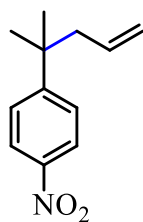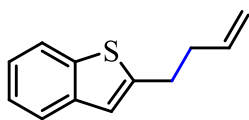

3x (KC-5-285)

Product matched previously reported literature specification.[88]

^{1}H NMR (500 MHz, CDCl$_3$): δ 7.08 (m, 4H), 5.78–5.66 (m, 1H), 5.03–4.92 (m, 2H), 2.76 (h, 1H), 2.49–2.42 (m, 2H), 2.42–2.33 (m, 1H), 2.26 (dtd, 1H), 1.85 (dh, 1H), 1.24 (dd, 3H), 0.90 (d, 6H).

^{13}C NMR{^{1}H} (126 MHz, CDCl$_3$): δ 144.4, 139.3, 137.5, 129.1, 126.8, 115.9, 45.2, 42.9, 39.5, 30.4, 22.6, 21.6.

3y (KC-8-048)

Product matched previously reported literature specification.[87] Note, the allylated product (**3y**) was isolated with the alkane product.

^{1}H NMR (500 MHz, CDCl$_3$): δ 8.18–8.13 (m, 3y & alkane, 4H), 7.51–7.47 (m, 3y, 2H), 7.40–7.34 (m, alkane, 2H), 5.57–5.42 (m, 3y, 1H), 5.01–4.92 (m, 3y, 2H), 3.02 (hept, alkane, 1H), 2.39 (dd, 3y, 2H), 1.35 (s, 3y, 6H), 1.29 (d, alkane, 2H).

^{13}C NMR{^{1}H} (126 MHz, CDCl$_3$): δ 157.2, 156.7, 134.3, 127.4, 127.0, 123.8, 123.4, 118.1, 48.7, 38.6, 34.4, 28.5, 23.7.
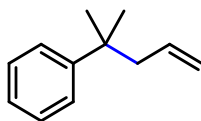
3z (KC-7-156)

Product matched previously reported literature specification.[87]

^{1}H NMR (500 MHz, CDCl$_3$): δ 7.39–7.26 (m, 4H), 7.22–7.15 (m, 1H), 5.56 (ddt, J = 17.3, 10.1, 7.2 Hz, 1H), 5.00–4.92 (m, 2H), 2.40–2.35 (m, 2H), 1.32 (s, 6H).

^{13}C NMR{^{1}H} (126 MHz, CDCl$_3$): δ 149.4, 135.7, 128.2, 126.0, 125.7, 117.0, 48.8, 37.7, 28.4, 22.0.
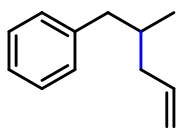
3aa (KC-7-230)

Product matched previously reported literature specification.[89]

^{1}H NMR (500 MHz, CDCl$_3$): δ 7.86 (ddd, J = 8.1, 3.4, 1.0 Hz, 1H), 7.75 (ddd, J = 15.6, 7.8, 1.2 Hz, 1H), 7.44–7.32 (m, 2H), 7.12 (s, 1H), 5.94 (ddt, J = 16.9, 10.2, 6.5 Hz, 1H), 5.12 (dq, J = 17.2, 1.9 Hz, 1H), 5.04 (ddt, J = 10.0, 2.8, 1.4 Hz, 1H), 2.98–2.92 (m, 2H), 2.53 (tdd, J = 7.6, 6.5, 1.2 Hz, 2H).

^{13}C NMR{^{1}H} (126 MHz, CDCl$_3$): δ 140.8, 139.4, 138.4, 136.6, 124.5, 124.2, 123.3, 122.0, 121.6, 115.6, 33.6, 28.5.

3bb (KC-7-278)

Product matched previously reported literature specification.[90]

^{1}H NMR (500 MHz, CDCl$_3$): δ 7.32–7.27 (m, 2H), 7.22–7.15 (m, 3H), 5.89–5.77 (m, 1H), 5.07–5.01 (m, 2H), 2.68 (dd, J = 13.4, 6.1 Hz, 1H), 2.44–2.32 (m, 1H), 2.14 (dddd, J = 13.7, 6.9, 5.5, 1.4 Hz, 1H), 2.00–1.92 (m, 1H), 1.89–1.79 (m, 1H), 0.89 (d, J = 6.6 Hz, 3H).

^{13}C NMR{^{1}H} (126 MHz, CDCl$_3$): δ 141.5, 137.5, 129.3, 128.3, 125.8, 116.1, 43.2, 41.1, 35.2, 19.6.
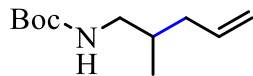
3cc (KC-6-046)

^{1}H NMR (500 MHz, CDCl$_3$): δ 5.77 (ddt, J = 17.1, 10.0, 7.1 Hz, 1H), 5.06–4.96 (m, 2H), 4.56 (broad s, 1H), 3.08 (dt, J = 12.9, 6.3 Hz, 1H), 2.94 (dt, J = 13.4, 6.6 Hz, 1H), 2.10 (dt, J = 13.4, 6.4 Hz, 1H), 1.90 (dt, J = 14.4, 7.4 Hz, 1H), 1.69 (dp, J = 11.6, 5.7, 4.7 Hz, 1H), 1.44 (s, 9H), 0.90 (d, J = 6.7 Hz, 3H).

^{13}C NMR{^{1}H} (126 MHz, CDCl$_3$): δ 156.2, 136.8, 116.5, 79.3, 46.2, 38.8, 33.9, 28.4, 17.3.

HRMS (ESITOF) m/z: Calc'd C$_{11}$H$_{21}$NO$_2$Na (M+Na) = 222.1470, found 222.1461.

IR (film): 2975, 2928, 1700, 1680, 1653, 1159, 1507, 1219, 1174 cm^{-1}.
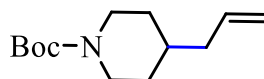
3dd (KC-7-275)

Product matched previously reported literature specification.[91]

^{1}H NMR (500 MHz, CDCl$_3$): δ 5.81–5.70 (m, 1H), 5.03–4.92 (m, 2H), 4.06 (broad s, 1H), 3.35 (t, J = 5.5 Hz, 2H), 2.72-2.61 (broad m, 1H), 1.99 (t, J = 7.0 Hz, 1H), 1.68-1.61 (m, 1H), 1.58-1.53 (m, 1H), 1.52-1.47 (m, 2H), 1.44 (s, 9H), 1.08 (qd, 2H).

^{13}C NMR{^{1}H} (126 MHz, CDCl$_3$): δ 155.0, 136.7, 115.7, 79.3, 41.0, 36.1, 32.0, 28.6, 24.6.
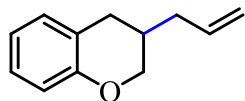
3ee (KC-7-281)

^{1}H NMR (500 MHz, CDCl$_3$): Mix of rotamers: δ 7.16–7.00 (m, 2H), 6.90–6.73 (m, 2H), 5.92–5.78 (m, 1H), 5.17–5.04 (m, 2H), 4.27–4.14 (m, 2H), 3.84–3.68 (m, 1H), 2.90–2.76 (m, 2H), 2.59–2.41 (m, 1H), 2.05–1.95 (m, 1H).

^{13}C NMR{^{1}H} (126 MHz, CDCl$_3$): Mix of rotamers: δ 154.7, 135.7, 130.0, 127.4, 121.7, 120.4, 117.0, 116.6, 70.3, 66.6, 36.4, 31.9, 31.2, 25.0, 22.5.

HRMS (ESITOF) m/z: Calc'd C$_{12}$H$_{14}$O (M+) = 174.1045, found 174.1050.

IR (film): 3076, 2975, 2923, 2860, 1739, 1647, 1583, 1490, 1457, 1267, 1228, 1118, 1066, 995, 916 cm^{-1}.
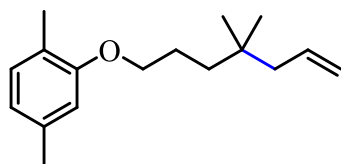
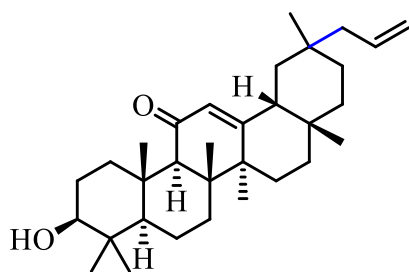**3ff (KC-5-291)**

^{1}H NMR (500 MHz, CDCl$_3$): δ 7.03 (d, 1H), 6.73–6.63 (m, 2H), 5.86 (ddt, 1H), 5.11–4.98 (m, 2H), 3.93 (t, 2H), 2.34 (s, 3H), 2.21 (s, 3H), 2.02 (d, 2H), 1.79 (dq, 2H), 1.42–1.35 (m, 2H), 0.93 (s, 6H).

^{13}C NMR{^{1}H} (126 MHz, CDCl$_3$): δ 157.5, 136.8, 136.0, 130.7, 124.0, 121.0, 117.2, 112.4, 69.0, 46.8, 38.2, 33.3, 27.4, 24.6, 21.7, 16.2.

HRMS (ESITOF) m/z: Calc'd C$_{17}$H$_{25}$O (M-H) = 245.1905, found 245.1909.

IR (film): 3074, 2954, 2925, 2868, 1616, 1586, 1509, 1471, 1414, 1387, 1285, 1265, 1158, 1130, 1039, 997, 912 cm^{-1}.

3gg (KC-7-207)

^{1}H NMR (500 MHz, CDCl$_3$): Mix of rotamers: δ 5.86–5.68 (m, 1H), 5.61-5.53 (m, 1H), 5.07–4.94 (m, 2H), 3.21 (dd, 1H), 2.78 (dt, 1H), 2.33 (s, 1H), 2.21-1.94 (m, 3H), 1.92 (d, 1H), 1.81 (tt, 1H), 1.71-1.54 (m, 6H), 1.51-1.37 (m, 4H), 1.36 (s, 3H), 1.31–1.23 (m, 3H), 1.20–1.14 (m, 2H), 1.12 (s, 6H), 1.05 (dt, 1H), 1.00 (s, 3H), 0.98–0.89 (m, 2H), 0.89-0.82 (m, 6H), 0.80 (s, 3H), 0.69 (d, 1H).

^{13}C NMR{^{1}H} (126 MHz, CDCl$_3$): Mix of rotamers: δ 200.5, 200.4, 170.6, 170.5, 134.9, 134.8, 128.4, 128.3, 128.2, 117.4, 117.3, 78.9, 61.9, 55.1, 55.1, 50.3, 47.3, 47.0, 45.5, 43.5, 43.5, 43.3, 42.8, 41.5, 41.0, 39.6, 37.2, 36.2, 36.0, 34.1, 33.7, 33.5, 33.0, 32.9, 32.9, 32.7, 32.4, 32.3, 29.6, 28.9, 28.9, 28.2, 27.5, 26.8, 26.6, 26.6, 26.5, 23.5, 22.5, 21.4, 18.9, 17.6, 16.5, 15.7.

HRMS (ESITOF) m/z: Calc'd C$_{32}$H$_{49}$O$_2$ (M-H) = 465.3733, found 465.3721.

IR (film): 2968, 2949, 2926, 2866, 1653, 1648, 1636, 1617, 1457, 1387, 1260, 1218, 1210, 1134, 1091, 1044, 994, 913, 801, 791, 785, 779, 775, 767, 744 cm^{-1}.
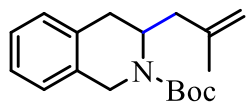
5b (KC-6-069)

^{1}H NMR (500 MHz, CDCl$_3$): δ 7.23–7.04 (m, 4H), 4.85-4.69 (m, 2H), 4.63-4.68 (m, 2H), 4.28 (d, *J* = 17.1 Hz, 1H), 3.02 (dd, *J* = 15.8, 5.8 Hz, 1H), 2.68 (dd, *J* = 15.7, 2.1 Hz, 1H), 2.21 (dd, *J* = 13.5, 7.5 Hz, 1H), 2.02–1.86 (m, 1H), 1.80 (s, 3H), 1.50 (s, 9H).

^{13}C NMR{^{1}H} (126 MHz, CDCl$_3$): δ 155.0, 133.3, 132.9, 129.6, 129.2, 126.7, 126.3, 113.4, 112.9, 79.8, 48.3, 46.8, 43.0, 42.5, 40.7, 40.0, 32.6, 32.2, 28.6, 22.2.

HRMS (ESITOF) m/z: Calc'd C$_{18}$H$_{26}$NO$_2$ (M+H) = 288.1964, found 288.1966.

IR (film): 3368, 3072, 2978, 2933, 2252, 1762, 1700, 1457, 1392, 1368, 1291, 1245, 1164, 1048, 947, 899 cm^{-1}.
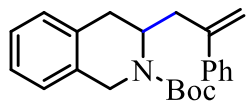
5c (KC-6-072)

^{1}H NMR (500 MHz, CDCl$_3$): Mix of rotamers: δ 7.46 (d, 2H), 7.34 (t, 2H), 7.32–7.24 (m, 1H), 7.23-7.12 (m, 3H), 7.06 (d, 1H), 5.34 (broad s, 1H), 4.92 (broad s, 1H), 4.85–4.42 (m, 2H), 4.32 (d, 1H), 2.90 (dd, 1H), 2.77 (dd, 1H), 2.70 (dd, 1H), 2.41 (dd, 1H), 1.42 (broad s, 9H).

^{13}C NMR{^{1}H} (126 MHz, CDCl$_3$): δ 154.5, 133.3, 129.4, 128.5, 127.7, 126.7, 126.3, 115.3, 79.9, 48.6, 42.8, 37.9, 32.2, 28.6.

HRMS (ESITOF) m/z: Calc'd C$_{23}$H$_{26}$NO$_2$ (M-H) = 348.1964, found 348.1980.

IR (film): 3392, 3010, 2978, 2930, 2850, 1761, 1695, 1684, 1448, 1392, 1367, 1245, 1218, 1166, 1123, 1067, 1029, 947, 901 cm^{-1}.
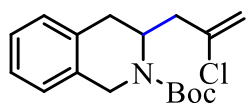
5d (KC-6-234)

^{1}H NMR (500 MHz, CDCl$_3$): Mix of rotamers: δ 7.24–7.07 (m, 4H), 5.20 (d, 1H), 5.06-4.96 (m, 1H), 4.95–4.69 (m, 2H), 4.27 (dd, 1H), 3.05 (td, 1H), 2.92–2.64 (m, 1H), 2.56–2.35 (m, 1H), 2.31–2.09 (m, 1H), 1.52-1.43 (m, 9H).

^{13}C NMR{^{1}H} (126 MHz, CDCl$_3$): Mix of rotamers: δ 139.7, 129.1, 128.5, 126.9, 126.7, 126.6, 126.5, 126.3, 115.0, 80.3, 48.5, 42.8, 42.1, 32.4, 29.9, 29.8, 28.7.

HRMS (ESITOF) m/z: Calc'd C$_{17}$H$_{26}$ClN$_2$O$_2$ (M+NH$_4$) = 290.1994, found 290.1996.

IR (film): 2977, 2902, 1700, 1684, 1653, 1558, 1534, 1507, 1457, 1219, 1162, 804 cm^{-1}.
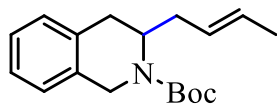
5e (KC-6-228)

^{1}H NMR (500 MHz, CDCl$_3$): Mix of rotamers: δ 7.22–7.05 (m, 4H), 5.46–5.30 (m, 2H), 4.87–4.69 (m, 1H), 4.63–4.30 (m, 1H), 4.23 (d, 1H), 3.02 (dd, 1H), 2.68 (d, 1H), 2.15 (dt,1H), 1.96 (t, 1H), 1.64 (broad s, 3H), 1.50 (broad s, 9H).

^{13}C NMR{^{1}H} (126 MHz, CDCl$_3$): Mix of rotamers: δ 155.2, 133.0, 129.6, 129.2, 127.8, 127.7, 126.6, 126.2, 79.7, 50.3, 48.6, 43.1, 42.5, 35.7, 35.2, 33.0, 32.3, 28.6, 18.1.

HRMS (ESITOF) m/z: Calc'd C$_{18}$H$_{25}$NO$_2$Na (M+Na) = 310.1783, found 310.1785.

IR (film): 3356, 2978, 2933, 2253, 1701, 1698, 1694, 1682, 1457, 1423, 1344, 1257, 1219, 1168, 1130, 1025, 968, 910 cm^{-1}.
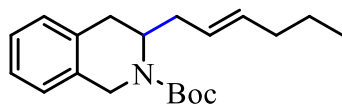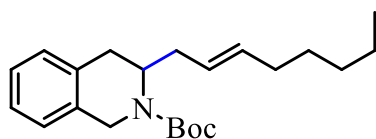
5f (KC-6-079)

^{1}H NMR (500 MHz, CDCl$_3$): δ 7.22–7.05 (m, 4H), 5.40–5.32 (m, 2H), 4.78 (broad s, 1H), 44.64-4.29 (m, 1H), 4.23 (d, 1H), 3.01 (dd, 1H), 2.69 (d, 1H), 2.16 (dt, 1H), 2.02-1.90 (m, 3H), 1.49 (s, 9H), 1.35 (h, 2H), 0.88 (t, 3H).

^{13}C NMR{^{1}H} (126 MHz, CDCl$_3$): δ 155.2, 133.3, 126.7, 126.2, 79.7, 34.8, 28.6, 22.7, 13.7.

HRMS (ESITOF) m/z: Calc'd C$_{20}$H$_{30}$NO$_2$ (M+H) = 316.2277, found 316.2266.

IR (film): 3031, 2963, 2930, 2873, 1703, 1695, 1457, 1392, 1368, 1340, 1255, 1219, 1167, 1127, 1020, 969, 938, 905, 857 cm^{-1}.
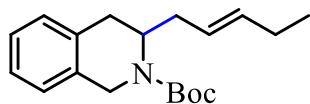
5g (KC-7-149)

^{1}H NMR (500 MHz, CDCl$_3$): δ 7.24–7.03 (m, 4H), 5.42–5.28 (m, 2H), 4.84–4.66 (m, 1H), 4.65–4.31 (m, 1H), 4.23 (d, 1H), 3.01 (dd, 1H), 2.69 (d, 1H), 2.21–2.12 (m, 1H), 2.01–1.88 (m, 3H), 1.49 (s, 9H), 1.38–1.16 (m, 7H), 0.89 (t, 3H).

^{13}C NMR{^{1}H} (126 MHz, CDCl$_3$): δ 155.2, 133.6, 133.1, 126.6, 126.4, 126.2, 79.7, 32.7, 31.5, 29.3, 28.6, 22.7, 14.2.

HRMS (ESITOF) m/z: Calc'd C$_{22}$H$_{33}$NO$_2$Li (M+Li) = 350.2671, found 350.2691.

IR (film): 3352, 2956, 2929, 2858, 1700, 1420, 1392, 1367, 1341, 1248, 1166, 1128, 969 cm^{-1}.

5h (KC-7-122)
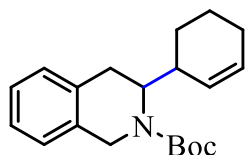
^{1}H NMR (500 MHz, CDCl$_3$): Mix of rotamers: δ 7.22–7.05 (m, 4H), 5.46–5.28 (m, 2H), 4.84–4.70 (m, 1H), 4.64–4.30 (m, 1H), 4.23 (d, 1H), 3.02 (dd, 1H), 2.68 (d, 1H), 2.16 (dt, 1H), 1.98 (dt, 2H), 1.49 (s, 9H), 0.95 (t, 3H).

^{13}C NMR{^{1}H} (126 MHz, CDCl$_3$): Mix of rotamers: δ 203.7, 183.5, 181.6, 177.6, 175.1, 174.7, 173.9, 128.3, 98.9, 97.1, 91.7, 91.2, 84.2, 83.7, 81.3, 80.8, 77.2, 74.3, 62.4.

HRMS (ESITOF) m/z: Calc'd C$_{19}$H$_{27}$NO$_2$ (M+) = 301.2042, found 301.2054.

IR (film): 3352, 3009, 2975, 2933, 1705, 1703, 1697, 1693, 1456, 1392, 1367, 1342, 1255, 1172, 1128, 1029, 939, 864 cm^{-1}.

**5i (KC-6-073)**

^{1}H NMR (500 MHz, CDCl$_3$): Mix of rotamers: δ 7.14–6.96 (m, 4H), 5.76–5.36 (m, 2H), 4.87 (dd, 1H), 4.29–4.05 (m, 1H), 2.98–2.66 (m, 2H), 2.03 (broad s, 1H), 1.93–1.86 (m, 2H), 1.71–1.48 (m, 3H), 1.46–1.35 (m, 9H), 1.27–1.11 (m, 3H).

^{13}C NMR{^{1}H} (126 MHz, CDCl$_3$): Mix of rotamers: δ 159.4, 130.0, 129.3, 129.0, 127.4, 126.3, 126.0, 79.6, 29.6, 28.4, 28.4, 28.3, 28.2, 28.2, 28.0, 28.0.

HRMS (ESITOF) m/z: Calc'd C$_{20}$H$_{28}$NO$_2$ (M+H) = 314.2120, found 314.2118.

IR (film): 2928, 2860, 1704, 1689, 1653, 1559, 1502, 1457, 1368, 1219, 1167 cm^{-1}.
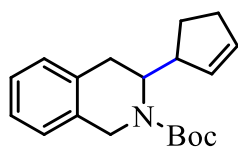
5j (KC-7-192)

^{1}H NMR (500 MHz, CDCl$_3$): Mix of rotamers: δ 7.22–7.04 (m, 4H), 5.85–5.48 (m, 2H), 5.09–4.54 (m, 2H), 4.37–4.03 (m, 2H), 3.05 (dd, 1H), 2.87–2.68 (m, 2H), 2.46–2.16 (m, 2H), 1.88 (dqd, 1H), 1.75–1.62 (m, 1H), 1.49 (s, 9H).

^{13}C NMR{^{1}H} (126 MHz, CDCl$_3$): Mix of rotamers: δ 155.2, 133.2, 132.9, 131.8, 129.5, 126.5, 126.2, 79.8, 46.7, 46.4, 38.8, 32.4, 32.0, 31.8, 28.6, 28.6, 28.0.

HRMS (ESITOF) m/z: Calc'd C$_{19}$H$_{25}$NO$_2$Na (M+Na) = 322.1783, found 322.1794.

IR (film): 2974, 2930, 2905, 2848, 1693, 1454, 1392, 1348, 1252, 1219, 1170, 1116, 1097, 978, 913, 882, 763 cm^{-1}.
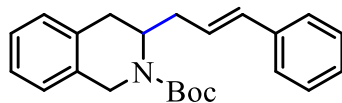
5k (KC-7-166)

^{1}H NMR (500 MHz, CDCl$_3$): Mix of *E/Z* isomers and rotamers: δ 7.41–7.27 (m, 3H), 7.25–6.93 (m, 6H), [6.51 (d) & 6.33 (d), ∑1H], 6.25–5.91 (m) & 5.65 (p), ∑1H], 5.04–4.46 (m, 2H), [4.31 (d) & 4.16–4.09 (m), ∑1H], 3.06 (ddd, 1H), 2.90–2.65 (m, 1H), 2.55–2.31 (m, 1H), 2.30–2.13 (m, 1H), 1.56–1.24 (m, 9H).

^{13}C NMR{^{1}H} (126 MHz, CDCl$_3$): Mix of *E/Z* isomers and rotamers: δ 155.1, 140.0, 137.5, 133.0, 132.3, 131.1, 128.7, 128.6, 128.1, 127.2, 126.7, 126.6, 126.4, 126.2, 116.4, 115.7, 79.9, 69.8, 55.0, 53.9, 52.8, 52.7, 52.5, 52.4, 50.8, 50.5, 48.6, 43.2, 43.0, 42.8, 42.5, 36.3, 35.8, 33.1, 32.6, 31.3, 31.0, 30.7, 29.8, 28.7, 28.6, 28.3.

HRMS (ESITOF) m/z: Calc'd C$_{23}$H$_{27}$NO$_2$Na (M+Na) = 372.1939, found 372.1938.

IR (film): 3065, 3027, 2977, 2930, 1699, 1457, 1419, 1405, 1368, 1340, 1255, 1219, 1166, 1123, 912 cm^{-1}.
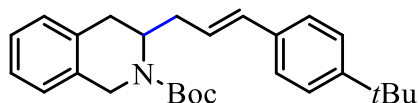
**5l (KC-7-172)**

^{1}H NMR (500 MHz, CDCl$_3$): Mix of *E/Z* isomers and rotamers: δ 7.37–7.27 (m, 3H), 7.25–6.97 (m, 6H), [6.48 (d) & 6.31 (d), ∑1H], [6.23–5.94 (m) & 5.62 (dt), ∑1H], 5.03–4.41 (m, 2H), [4.37–4.25 (m) & 4.18–4.10 (m), ∑1H], 3.33–2.99 (m, 1H), 2.89–2.67 (m, 1H), 2.56–2.33 (m, 1H), 2.28–2.14 (m, 1H), 1.55–1.45 (m, 9H), 1.35–1.27 (m, 9H).

^{13}C NMR{^{1}H} (126 MHz, CDCl$_3$): Mix of *E/Z* isomers and rotamers: δ 154.9, 150.0, 140.0, 138.4, 134.5, 132.7, 131.9, 130.6, 129.5, 129.5, 128.2, 127.7, 127.3, 127.2, 126.5, 126.3, 126.1, 126.0, 125.5, 125.2, 124.8, 115.9, 115.1, 79.7, 66.9, 53.7, 52.4, 52.1, 51.9, 42.9, 42.3, 34.3, 31.3, 31.2, 30.4, 29.6, 28.5, 28.4.

HRMS (ESITOF) m/z: Calc'd C$_{27}$H$_{35}$NO$_2$Na (M+Na) = 428.2565, found 428.2585.

IR (film): 3008, 2966, 2905, 2868, 2249, 1699, 1684, 1457, 1400, 1394, 1366, 1269, 1255, 1219, 1168, 1121, 1016, 968, 911, 857 cm^{-1}.
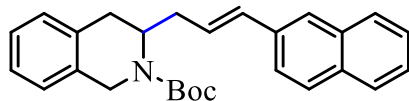
5m (KC-7-162)

^{1}H NMR (500 MHz, CDCl$_3$): Mix of *E/Z* isomers and rotamers: δ 7.83–7.74 (m, 3H), 7.66 (s, 1H), 7.57 (dd, 1H), 7.49–7.41 (m, 2H), 7.25–7.12 (m, 4H), [6.67 (d) & 6.49 (d), $\sum$1H], 6.40–6.21 (m, 1H), 5.16–4.47 (m, 2H), [4.36 (d) & 4.17 (d), $\sum$1H], 3.10 (td, 1H), 2.90–2.69 (m, 1H), 2.62–2.41 (m, 1H), 2.30 (broad s, 1H), [1.69-1.62 (m), & 1.53-1.42 (m), $\sum$9H].

^{13}C NMR{^{1}H} (126 MHz, CDCl$_3$): Mix of *E/Z* isomers and rotamers: δ 155.2, 133.7, 132.9, 128.2, 128.0, 127.7, 126.8, 126.4, 126.3, 125.7, 123.5, 80.0, 52.8, 52.6, 50.6, 50.5, 48.6, 43.2, 43.0, 42.9, 42.6, 36.4, 36.0, 33.2, 32.7, 29.8, 28.7, 28.4.

HRMS (ESITOF) m/z: Calc'd C$_{27}$H$_{29}$NO$_2$Na (M+Na) = 422.2096, found 422.2117.

IR (film): 3056, 3007, 2975, 2928, 2846, 1690, 1457, 1405, 1364, 1325, 1241, 1170, 1118, 1096, 1007, 963, 909, 859 cm^{-1}.
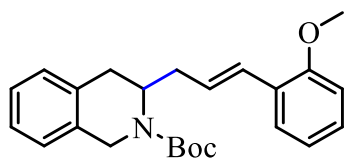
5n (KC-8-016)

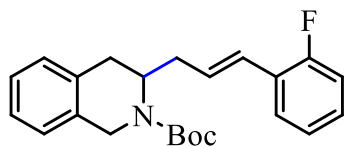^{1}H NMR (500 MHz, CDCl$_3$): Mix of *E/Z* isomers and rotamers: δ [7.44–7.36 (m) & 7.25–7.08 (m) & 7.04–6.79 (m), $\sum$8H], [6.67 (d) & 6.59 (d), $\sum$1H], [6.35–6.0 (m) & 5.75–5.66 (m), $\sum$1H], 5.10–4.56 (m, 2H), [4.35–4.27 (m) & 4.19–4.12 (m), $\sum$1H], [3.82 (s) & 3.80 (s) & 3.67 (s) & 3.61 (s), $\sum$3H], 3.12–2.97 (m, 1H), 2.88–2.65 (m, 1H), 2.48–2.34 (m, 1H), 2.37–2.16 (m, 1H), [1.55–1.44 (m) & 1.34–1.24 (m), $\sum$9H].

^{13}C NMR{^{1}H} (126 MHz, CDCl$_3$): Mix of *E/Z* isomers and rotamers: δ 156.4, 155.1, 139.7, 138.8, 133.1, 129.9, 129.7, 129.3, 128.2, 127.8, 127.6, 126.7, 126.5, 126.3, 126.2, 126.0, 121.0, 120.7, 120.1, 116.3, 111.1, 110.9, 79.8, 55.5, 55.5, 55.3, 55.2, 43.0, 42.3, 31.3, 30.9, 28.7, 28.5, 28.3.

HRMS (ESITOF) m/z: Calc'd C$_{23}$H$_{28}$NO$_3$ (M+H) = 366.2069, found 366.2052.

IR (film): 2974, 2836, 1695, 1688, 1554, 1489, 1457, 1395, 1363, 1243, 1219, 1169, 1117, 1096, 1028, 1006, 971 cm^{-1}.

5o (KC-8-017)

^{1}H NMR (500 MHz, CDCl$_3$): Mix of *E/Z* isomers and rotamers: δ [7.44–7.32 (m) & 7.23–7.10 (m) & 7.09–6.92 (m), ∑8H], 6.46 (d, 1H), 6.30–6.18 (m, 1H), 5.06–4.46 (m, 2H), 4.34–4.25 (m, 1H), 3.14–2.98 (m, 1H), 2.80–2.64 (m, 1H), 2.47–2.32 (m, 1H), 2.30–2.16 (m, 1H), [1.52–1.41 (m) & 1.33–1.22 (m), ∑9H].

^{13}C NMR{^{1}H} (126 MHz, CDCl$_3$): Mix of *E/Z* isomers and rotamers: δ 160.0 (d, *J* = 246.7 Hz), 155.1, 132.9, 130.0, 129.9, 129.7, 129.4 (d, *J* = 16.6 Hz), 127.3 (d, *J* = 4.5 Hz), 126.8, 126.4, 124.6 (d, 3.7 Hz), 124.1 (d, 4.0 Hz), 115.7, 115.6, 79.9, 63.6, 50.4, 48.6, 43.3, 42.7, 36.7, 36.2, 33.1, 32.7, 28.6.

HRMS (ESITOF) m/z: Calc'd C$_{22}$H$_{23}$FNO$_2$ (M-H) = 352.1713, found 352.1719.

IR (film): 2975, 2930, 2844, 1695, 1684, 1559, 1487, 1395, 1355, 1319, 1219, 1169, 1120, 1096, 1007, 968 cm^{-1}.
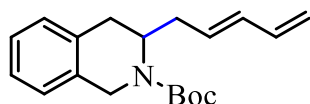
5p (KC-7-271)

^{1}H NMR (500 MHz, CDCl3): Mix of *E/Z*-isomers: δ 7.23–7.04 (m, 4H), 6.28 (dt, 1H), [6.06 (t) & 5.98 (dd), ∑1H], 5.72– 5.36 (m, 1H), 5.21–4.93 (m, 2H), 4.87–4.69 (m, 1H), 4.69–4.34 (m, 1H), [4.26 (d) & 4.25 (d), ∑1H], 3.03 (ddd, 1H), 2.69 (ddd, 1H), 2.35 (dtd, 1H), 2.26 (dt, 1H), [2.19 (broad s) & 2.08 (broad s), ∑1H], [1.50 (s) & 1.49 (s), ∑9H].

^{13}C NMR{^{1}H} (126 MHz, CDCl$_3$): Mix of *E/Z* isomers: δ 155.1, 137.1, 133.4, 132.9, 132.1, 131.6, 131.2, 129.5, 129.2, 126.7, 126.3, 115.9, 115.6, 79.8, 50.3, 48.5, 43.2, 42.7, 35.7, 35.3, 33.1, 32.4, 28.6.

HRMS (ESITOF) m/z: Calc'd C$_{19}$H$_{29}$N$_2$O$_2$ (M+NH$_4$) = 317.2229, found 317.2244.

IR (film): 2975, 2930, 2846, 2359, 1700, 1684, 1635, 1457, 1407, 1395, 1354, 1340, 1254, 1243, 1219, 1169, 1119, 1096, 1006, 904 cm^{-1}.


5q (KC-7-300)

^{1}H NMR (500 MHz, CDCl$_3$): δ Mix of *E/Z* isomers and rotamers: δ 7.23-7.02 (m, 4H), [6.37-6.15 (m) & 6.04-5.86 (m), ∑2H], 5.70-5.19 (m, 2H), 5.10-4.69 (m, 2H), 4.66-4.35 (m, 1H), 4.30-

4.05 (m, 1H), 3.09-2.82 (m, 2H), 2.76-2.61 (m, 1H), 2.36-1.91 (m, 3H), 1.52-1.46 (m, 9H), 1.37-1.57 (m, 10H), 0.92-0.83 (m, 3H).

^{13}C NMR{^{1}H} (126 MHz, CDCl$_3$): Mix of *E/Z* isomers and rotamers: δ 155.0, 139.4, 138.9, 133.0, 132.9, 132.8, 130.1, 129.4, 129.3, 129.1, 128.2, 126.5, 126.3, 126.1, 126.0, 125.9, 115.4, 114.9, 79.7, 51.2, 50.8, 50.2, 49.6, 49.3, 48.4, 43.1, 42.5, 32.8, 32.6, 31.9, 31.8, 29.7, 29.4, 29.2, 29.2, 28.5, 27.7, 22.7.

HRMS (ESITOF) m/z: Calc'd C$_{26}$H$_{39}$NO$_2$Li (M+Li) = 404.3141, found 404.3139.

IR (film): 2956, 2926, 2854, 1704, 1652, 1559, 1507, 1457, 1395, 1219, 1170, 1117 cm^{-1}.
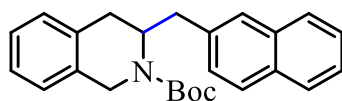
5r (KC-7-029)

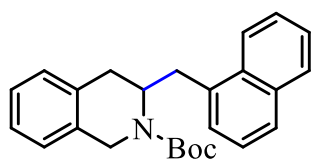^{1}H NMR (500 MHz, CDCl$_3$): Mix of rotamers: δ 7.84–7.74 (m, 3H), 7.54 (broad s, 1H), 7.45 (h, 2H), 7.38–7.27 (m, 1H), 7.25–7.16 (m, 3H), 7.15–7.11 (m, 1H), 4.93–4.57 (m, 2H), 4.44 (broad d, 1H), 3.03-2.89 (m, 2H), 2.67 (broad d, 2H), 1.46–1.34 (m, 9H).

^{13}C NMR{^{1}H} (126 MHz, CDCl$_3$): Mix of rotamers: δ 155.0, 133.7, 132.4, 128.2, 127.8, 127.7, 127.6, 126.9, 126.5, 126.0, 125.5, 80.0, 52.2, 43.2, 39.1, 32.6, 28.6, 28.5.

HRMS (ESITOF) m/z: Calc'd C$_{25}$H$_{27}$NO$_2$ (M+) = 373.2042, found 373.2046.

IR (film): 3052, 3010, 2976, 2923, 2856, 1700, 1507, 1457, 1392, 1367, 1243, 1218, 1167, 1123, 1016, 931, 891 cm^{-1}.

5s (KC-7-208)

^{1}H NMR (500 MHz, CDCl$_3$): Mix of rotamers: δ 8.28–8.06 (m, 1H), 7.91–7.82 (m, 1H), 7.75 (d, 1H), 7.50 (q, 2H), 7.36 (t, 1H), 7.30–7.20 (m, 3H), 7.15–7.06 (m, 2H), 5.02–4.68 (m, 2H), 4.52 (d, 1H), 3.42–3.16 (m, 1H), 3.03-2.78 (m, 2H), 2.71–2.46 (m, 1H), 1.57–1.19 (m, 9H).

^{13}C NMR{^{1}H} (126 MHz, CDCl$_3$): δ Mix of rotamers: 155.1, 135.1, 134.1, 133.2, 132.7, 132.4, 129.4, 128.9, 127.7, 127.4, 126.8, 126.5, 125.7, 124.1, 79.9, 50.4, 43.1, 36.0, 32.8, 28.6, 28.4.

HRMS (ESITOF) m/z: Calc'd C$_{25}$H$_{28}$NO$_2$ (M+H) = 374.2120, found 374.2123.

IR (film): 2975, 2930, 1690, 1457, 1457, 1391, 1363, 1291, 1219, 1165, 1118 cm^{-1}.
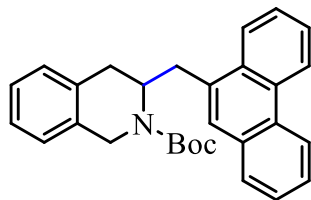
5t (KC-7-249)

^{1}H NMR (500 MHz, CDCl3): Mix of rotamers: δ 8.77 (d, 1H), 8.68 (d, 1H), 8.44–8.21 (m, 1H), 7.79 (d, 1H), 7.69 (d, 2H), 7.61 (dt, 2H), 7.44–7.27 (m, 4H), 7.18–7.05 (m, 1H), 5.13–4.71 (m, 2H), 4.59 (d, 1H), 3.54–3.27 (m, 1H), 3.04–2.80 (m, 2H), 2.69 (d, 1H), 1.62–1.24 (m, 9H).

^{13}C NMR{^{1}H} (126 MHz, CDCl$_3$): Mix of rotamers: δ 155.0, 133.3, 131.8, 131.4, 130.9, 130.0, 129.3, 128.2, 126.8, 126.6, 126.4, 124.6, 123.4, 122.5, 80.0, 50.0, 43.3, 36.5, 32.7, 28.7, 28.6, 28.5, 28.4.

HRMS (ESITOF) m/z: Calc'd $C_{29}H_{29}NO_2$ (M+) = 423.2198, found 423.2199.

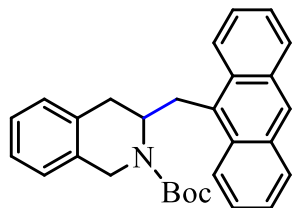IR (film): 2976, 2930, 1689, 1497, 1476, 1452, 1392, 1365, 1248, 1219, 1168, 1121, 1095, 1014 cm^{-1}.

5u (KC-7-293)

^{1}H NMR (500 MHz, CDCl$_3$): Mix of rotamers: δ 8.38 (s, 1H), 8.00 (d, 3H), 7.45 (t, 2H), 7.40 (d, J = 7.2 Hz, 2H), 7.32 (d, 2H), 7.25–7.20 (m, 2H), 6.92 (d, 1H), 5.01 (d, 2H), 4.62 (d, 1H), 3.81–3.63 (m, 2H), 2.93–2.72 (m, 1H), 2.50–2.31 (m, 1H), 1.63-1.32 (m, 9H).

^{13}C NMR{^{1}H} (126 MHz, CDCl$_3$): Mix of rotamers: δ 154.8, 134.3, 133.0, 131.7, 131.0, 130.6, 130.1, 129.2, 126.7, 126.6, 125.6, 125.0, 124.9, 51.1, 43.3, 32.3, 30.0, 28.6.

HRMS (ESITOF) m/z: Calc'd $C_{29}H_{28}NO_2$ (M-H) = 422.2120, found 422.2135.

IR (film): 2975, 2364, 1868, 1730, 1684, 1550, 1502, 1429, 1387, 1218, 1167, 1117, 1005 cm^{-1}.
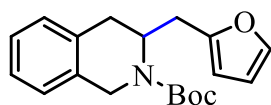
5v (KC-6-201)

^{1}H NMR (500 MHz, CDCl3): Mix of rotamers: δ 7.36 (s, 1H), 7.23–7.08 (m, 5H), 6.35-6.22 (m, 1H), 4.86–4.68 (m, 1H), 4.62–4.43 (m, 1H), 4.29 (d, 1H), 3.00 (dd, 1H), 2.68 (d, 1H), 2.60 (dd, 1H), 2.42–2.27 (m, 1H), 1.48 (d, 9H).

^{13}C NMR{^{1}H} (126 MHz, CDCl$_3$): Mix of rotamers: δ 155.0, 142.9, 140.0, 133.0, 128.8, 126.9, 126.6, 121.6, 111.4, 80.0, 51.0, 49.2, 43.4, 42.8, 32.6, 32.0, 28.6, 28.6, 27.9, 27.1.

HRMS (ESITOF) m/z: Calc'd C$_{19}$H$_{23}$NO$_3$Na (M+Na) = 336.1576, found 336.1566.

IR (film): 2878, 2930, 1764, 1692, 1456, 1411, 1367, 1245, 1164, 1121, 1011 cm^{-1}.

5w (KC-7-048)

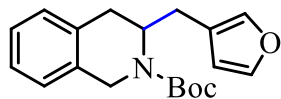^{1}H NMR (500 MHz, CD$_3$CN): Mix of rotamers: δ 7.42 (s, 1H), 7.23–7.08 (m, 5H), 6.35 (s, 1H), 4.76 (d, 1H), 4.66–4.51 (m, 1H), 4.23 (d, 1H), 2.99 (dd, 1H), 2.70 (dd, 1H), 2.54 (dd, 1H), 2.38 (dd, 1H), 1.39 (s, 9H).

^{13}C NMR{^{1}H} (126 MHz, CD$_3$CN): Mix of rotamers: δ 155.5, 143.9, 141.0, 134.3, 133.9, 130.1, 127.6, 127.0, 122.9, 112.5, 80.0, 51.6, 42.8, 33.5, 28.3.

HRMS (ESITOF) m/z: Calc'd C$_{19}$H$_{22}$NO$_3$ (M-H) = 312.1600, found 312.1597.

IR (film): 2976, 2930, 1771, 1734, 1700, 1684, 1653, 1559, 1456, 1419, 1395, 1363, 1244, 1219, 1165, 1097, 1010, 954 cm^{-1}.
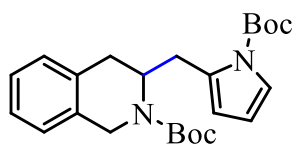
5x (KC-7-188)

^{1}H NMR (500 MHz, CDCl3): Mix of rotamers: δ 7.24–7.05 (m, 5H), [6.10–5.80 (m) & 5.72 – 5.35 (m), ∑2H], 5.10–4.64 (m, 2H), 4.60–4.19 (m, 1H), 3.37–2.64 (m, 4H), 1.65–1.48 (m, 9H), 1.41–1.21 (m, 9H).

^{13}C NMR{^{1}H} (126 MHz, CDCl$_3$): Mix of rotamers: δ 155.3, 155.2, 150.4, 149.6, 132.7, 129.4, 126.5, 126.5, 126.3, 121.3, 113.6, 110.5, 83.5, 49.4, 42.3, 34.1, 31.0, 28.6, 28.4, 28.3, 28.2, 16.5.

HRMS (ESITOF) m/z: Calc'd C$_{24}$H$_{32}$N$_2$O$_4$Na (M+Na) = 435.2260, found 435.2274.

IR (film): 2978, 2931, 2344, 1734, 1700, 1663, 1635, 1534, 1498, 1457, 1363, 1324, 1219, 1162, 1125 cm^{-1}.

2.8.6 Three-Component Decarboxylative Allylation

In an argon atmosphere glove box, a 10 mL screw threaded glass tube equipped with stir bar was charged with Pd(OAc)$_2$ (10 mol%, 0.02 mmol, 0.0045 g), BINAP (11 mol%, 0.022 mmol,

0.0145 g), and MeCN (1 mL). The reaction vessel was sealed and allowed to stir for 30 minutes during which time the reaction mixture goes from a yellow, heterogenous solution to a homogenous orange solution. After the pre-stir, the corresponding allylic or benzylic carbonate (1.5 equiv., 0.3 mmol), the corresponding carboxylic acid (1 equiv., 0.2 mmol), electrophilic olefin (1 equiv., 0.2 mmol), sodium carbonate (1 equiv., 0.2 mmol, 0.0212 g), and 4CzIPN (3.2 mol%, 0.0064 mmol, 0.005 g) were added to the tube followed by MeCN (1 mL) so that the total reaction volume is 2 mL (0.1 M). The tube is sealed and removed from the glovebox. The reaction was stirred and irradiated with one 32 W Kessil blue LED lamp for 16 hours and the reaction was found to reach 28 °C after the first hour of irradiation (see Appendix **A3**). After such time, the reaction is removed from the light, the tube opened, and the solvent removed under reduced pressure. The resulting product is purified via silica gel flash chromatography in 1:10-1:40 EtOAc:Hexanes.
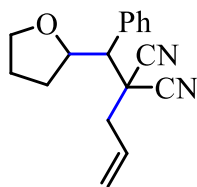
6a (MH-1-016)

^{1}H NMR (500 MHz, CDCl$_3$): Mix of diastereomers (56:44): δ 7.55–7.47 (m, 1H), 7.43–7.28 (m, 4H), 5.98–5.82 (m, 1H), 5.42–5.23 (m, 2H), [4.63 (ddd) & 4.57 (dt), $\sum$1H], [4.05 (ddd) & 3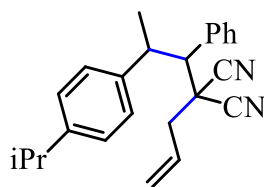.91 (ddd), $\sum$1H], 3.88–3.78 (m, 1H), 3.07–2.94 (m, 1H), 2.62 (dddt, 1H), 2.50 (dddt, 1H), [2.01 (dddd) & 1.89 (dddd), $\sum$3H], 1.84–1.73 (m, 1H), [1.65–1.53 (m) & 1.52–1.35 (m), $\sum$2H].


6b (MH-1-058)

^{1}H NMR (500 MHz, CDCl$_3$): Mix of diastereomers (58:43 d.r.): δ 7.47–7.30 (m, 3H), 7.22–7.00 (m, 4H), 6.92–6.81 (m, 2H), [5.87 (ddt) & 5.73 (ddt), $\sum$1H], [5.36 (dd) & 5.27–5.20 (m) & 5.08 (dd), $\sum$2H], 3.58–3.51 (m, 1H), [3.20 (d) & 3.12 (d), $\sum$1H], [2.50 (d) & 2.34 (d), $\sum$2H], 2.32–2.24

(m, ∑1H), 2.16–2.04 (m, 1H), [1.88 (hept) & 1.75 (hept), ∑1H], [1.68 (d) & 1.09 (d), ∑3H], [0.91 (dd) & 0.81 (dd), ∑6H].

^{13}C NMR{^{1}H} (126 MHz, CDCl$_3$): Mix of diastereomers (58:43 d.r.): δ 141.8, 140.4, 140.2, 140.0, 137.1, 136.3, 129.9, 129.4, 129.3, 129.1, 129.0, 128.9, 128.8, 128.7, 128.3, 128.9, 127.6, 123.2, 122.9, 58.2, 57.8, 45.3, 45.0, 44.7, 43.3, 42.6, 41.7, 30.4, 30.2, 22.3, 21.7, 21.5.
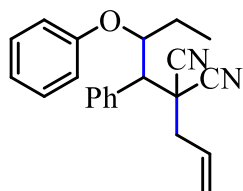
6c (MH-1-053)

^{1}H NMR (500 MHz, CDCl$_3$): Mix of diastereomers (64:36 d.r.): δ 7.76–7.65 (m, 1H), 7.50–7.38 (m, ∑H), 7.38–7.30 (m, 2H), 7.17–7.06 (m, 2H), 7.05–6.98 (m, 1H), 5.90 (ddt, 1H), 5.48–5.22 (m, 2H), [5.08 (dt) & 4.93 (dt), ∑1H], [3.54 (d) & 3.24 (d), ∑1H], 2.63–2.33 (m, 2H), 1.86–1.74 (m, 1H), 1.33–1.21 (m, 2H), 0.86–0.79 (m, 3H).

^{13}C NMR{^{1}H} (126 MHz, CDCl$_3$): Mix of diastereomers (64:36 d.r.): δ 157.0, 156.7, 134.7, 132.2, 131.3, 129.8, 129.8, 129.7, 129.5, 129.3, 129.1, 129.0, 128.9, 123.4, 123.2, 122.0, 121.9, 115.0, 78.8, 78.4, 53.5, 52.9, 41.9, 41.4, 40.3, 24.2, 23.3, 9.6, 7.1.
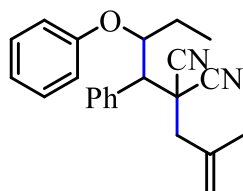
6d (LF-1-063)

^{1}H NMR (500 MHz, CDCl$_3$): Mix of diastereomers (56:44 d.r.): δ 7.71 (broad s, 1H), 7.48–7.39 (m, 4H), 7.34 (dd, 2H), 7.12 (dd, 3H), 7.02 (tdd, 1H), [5.14–5.07 (m) & 5.03 (s) & 5.00 (s) & 4.99–4.95 (m), ∑3H], [3.56 (d) & 3.25 (d), ∑1H], [2.58–2.46 (m) & 2.28 (d), ∑2H], [1.89 (s) & 1.88 (s), ∑3H], 1.86–1.72 (m, 1H), 1.35–1.19 (m, 1H), 0.88–0.78 (m, 3H).

^{13}C NMR{^{1}H} (126 MHz, CDCl$_3$): Mix of diastereomers (56:44 d.r.): δ157.0, 156.7, 137.8, 137.6, 135.0, 132.4, 131.5, 129.8, 129.7, 129.5, 129.3, 129.0, 122.0, 121.9, 118.8, 118.6, 116.3, 116.0, 115.5, 115.2, 78.7, 78.3, 54.7, 54.5, 45.5, 45.0, 40.5, 39.6, 31.1, 29.8, 24.3, 23.4, 23.2, 9.6, 7.1.
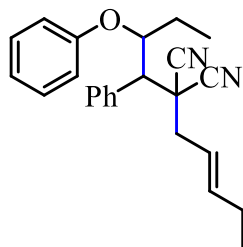
6e (LF-1-081)

^{1}H NMR (500 MHz, CDCl$_3$): Mix of diastereomers (52:48 d.r.): δ 7.74–7.66 (m, 1H), 7.48–7.37 (m, 4H), 7.37–7.31 (m, 2H), 7.11 (dd, 2H), 7.02 (tt, 1H), [5.77 (ddd) & 5.68 (ddd), ∑1H], 5.58–5.43 (m, 1H), [5.06 (dt) & 4.91 (dt), ∑1H], [3.52 (d) & 3.23 (d), ∑1H], [2.54–2.41 (m) & 2.30 (dd), ∑2H], 2.15–2.05 (m, 2H), 1.86–1.72 (m, 1H), 1.34–1.19 (m, 2H), 1.04–0.96 (m, 2H), 0.86–0.78 (m, 3H).

^{13}C NMR{^{1}H} (126 MHz, CDCl$_3$): Mix of diastereomers (52:48 d.r.): δ 157.1, 156.8, 141.6, 141.4, 134.9, 132.4, 131.4, 129.8, 129.8, 129.6, 129.4, 129.2, 129.0, 121.9, 121.9, 119.4, 119.3, 116.3, 116.0, 78.8, 78.4, 53.6, 52.8, 41.7, 40.9, 40.8, 40.5, 25.8, 25.7, 24.3, 23.3, 13.5, 9.6, 7.2.
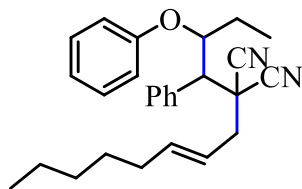
6f (LF-1-067)

^{1}H NMR (500 MHz, CDCl$_3$): Mix of diastereomers (60:40 d.r.) δ 7.76–7.64 (m, 1H), 7.49–7.37 (m, 4H), 7.37–7.32 (m, 2H), 7.17–7.06 (m, 2H), 7.06–6.97 (m, 1H), [5.76–5.69 (m) & 5.67–5.60 (m), ∑1H], 5.55–5.44 (m, 1H), [5.06 (dt) & 4.91 (dt), ∑1H], [3.52 (d) & 3.23 (d), ∑1H], [2.54–2.39 (m) & 2.34–2.28 (m), ∑1H], 2.12–2.01 (m, 2H), 1.86–1.72 (m, 1H), 1.43–1.34 (m, 2H), 1.34–1.27 (m, 4H), [0.91–0.85 (m) & 0.84–0.80 (m), ∑8H].

^{13}C NMR{^{1}H} (126 MHz, CDCl$_3$): Mix of diastereomers (60:40 d.r.) δ 157.1, 156.8, 140.3, 140.0, 134.9, 132.5, 131.4, 129.8, 129.8, 129.6, 129.4, 129.2, 129.0, 122.0, 121.9, 120.3, 120.1, 116.3, 116.0, 78.8, 78.4, 53.5, 52.8, 41.7, 41.1, 40.9, 40.6, 32.6, 31.4, 29.9, 28.8, 24.2, 23.3, 22.6, 14.2, 9.6, 7.2.
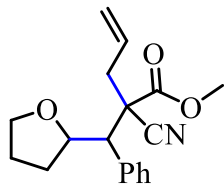
6g.1 (KC-8-066)

^{1}H NMR (500 MHz, CDCl$_3$): δ 7.33–7.24 (m, 5H), 5.87–5.75 (m, 1H), 5.26–5.14 (m, 2H), 4.55 (ddd, 1H), 3.98–3.91 (m, 1H), 3.87 (td, 1H), 3.47 (dd, 1H), 3.33 (s, 3H), 3.02 (d, 1H), 2.74 (dd, 1H), 1.86–1.73 (m, 2H), 1.67 (ddt, 1H), 1.33 (dq, 1H).

^{13}C NMR{^{1}H} (126 MHz, CDCl$_3$): δ 168.6, 137.7, 131.9, 129.1, 128.6, 128.1, 120.4, 118.7, 80.7, 68.7, 56.4, 56.2, 52.7, 41.6, 32.4, 25.1.
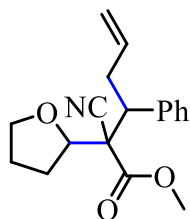
6g.2 (KC-8-066)

^{1}H NMR (500 MHz, CDCl$_3$): δ 7.55–7.26 (m, ∑5H), [5.82 (dddd) & 5.68 (dddd), ∑1H], [5.27–5.17 (m) & 5.12– 4.99 (m), ∑2H], [4.60 (ddd) & 4.51 (ddd), ∑1H], [3.79 (s) & 3.51 (s), ∑3H], 3.78–3.68 (m, ∑2H), [3.25 (d) & 3.15 (d), ∑1H], [2.87 (ddt) & 2.67 (dd), ∑1H], [2.25 (dd) & 1.98–1.90 (m), ∑2H], [1.91–1.69 (m) & 1.59–1.50 (m) & 1.41 (tdd), ∑4H].

^{13}C NMR{^{1}H} (126 MHz, CDCl$_3$): δ169.8, 168.6, 136.1, 135.6, 131.0, 130.9, 130.7, 128.5, 128.2, 128.1, 121.0, 120.2, 119.1, 118.7, 80.2, 69.0, 68.3, 56.5, 55.3, 53.9, 53.2, 53.1, 52.5, 41.8, 40.5, 30.7, 30.4, 25.8, 25.5.
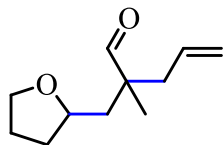
6h (KC-8-067)

^{1}H NMR (500 MHz, CDCl$_3$): δ [9.51 (s) & 9.49 (s), ∑1H], [5.82–5.60 (m, 1H), 5.15–5.00 (m, 2H), 3.97–3.84 (m, 1H), 3.78 (dtd, 1H), 3.66 (tt, 1H), 2.45–2.28 (m, 1H), 2.27–2.08 (m, 1H), 2.04–1.91 (m, 1H), 1.91–1.80 (m, 2H), 1.75–1.62 (m, 1H), 1.58 (dd, 1H), 1.48–1.37 (m, 1H), [1.13 (s) & 1.04 (s), ∑3H].

^{13}C NMR{^{1}H} (126 MHz, CDCl$_3$): δ 206.4, 206.3, 133.8, 133.3, 119.1, 118.8, 75.7, 75.6, 68.3, 68.3, 68.1, 68.0, 48.5, 48.4, 43.3, 42.5, 41.9, 39.0, 32.8, 32.7, 26.0, 20.4, 18.0.
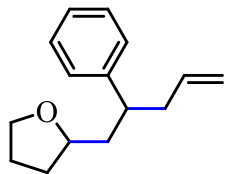
6i (KC-8-072)

^{1}H NMR (500 MHz, CDCl$_3$): Mix of diastereomers (55:45 d.r.) δ 7.29 (ddd, 2H), 7.18 (ddt, 3H), 5.76–5.56 (m, 1H), 5.02–4.84 (m, 2H), 3.83 (tdd, 1H), [3.63 (dddd) & 3.53 (dddd), ∑2H], [2.89 (dtd) & 2.77–2.63 (m), ∑1H], 2.50–2.30 (m, 2H), 2.06–1.66 (m, 5H), [1.50–1.38 (m) & 1.37–1.27 (m), ∑1H].

^{13}C NMR{^{1}H} (126 MHz, CDCl$_3$): Mix of diastereomers (55:45 d.r.) δ 144.9, 137.1, 136.8, 128.5, 128.4, 128.0, 127.7, 126.3, 126.2, 116.3, 116.1, 77.2, 67.5, 43.3, 43.0, 42.5, 41.9, 41.7, 41.5, 32.0, 31.2, 25.8.
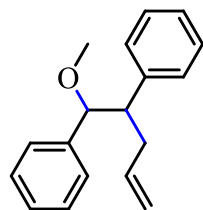
6j (KC-8-074)

^{1}H NMR (500 MHz, CDCl$_3$): Mix of diastereomers (55:45 d.r.): δ 7.34–7.27 (m, 2H), 7.24–6.94 (m, 8H), [5.78 (d) & 5.70 (d), ∑1H], 5.65–5.48 (m, 1H), 5.03–4.83 (m, 2H), [3.75 (s) & 3.62 (s), ∑3H], 3.23–3.10 (m, 1H), [2.78–2.67 (m) & 2.60–2.49 (m), ∑1H], 2.41–2.27 (m, 1H).

^{13}C NMR{^{1}H} (126 MHz, CDCl$_3$): Mix of diastereomers (55:45 d.r.): δ 155.3, 139.8, 139.5, 138.6, 138.4, 136.0, 135.7, 129.1, 129.0, 128.4, 128.4, 128.3, 128.2, 128.1, 128.0, 127.3, 127.2, 126.9, 126.9, 116.9, 116.7, 83.3, 82.7, 55.0, 54.8, 51.7, 51.5, 36.1, 35.7, 29.9.

Chapter 3: Photoredox-Promoted Kochi Decarboxylative Elimination

3.1 Introduction

The decomposition of organic carboxylic acids using metal salts has been established for many decades.[11a,21c,21d,22] Despite the synthetic appeal of replacing carboxylic acid moieties with alternative functionalities in a site-specific way, these types of reactions see little application in complex molecular synthesis due to aggressive reaction conditions and poor control of the intermediate's reactivity. Among these reports, there are numerous examples in which lead tetraacetate is utilized to facilitate decarboxylation liberating a carbon radical or carbocation. From these reactive intermediates, product mixtures containing the saturated alkane product, alkene product, and nucleophilic addition product(s) result. In order to improve upon the utility of these transformations and provide a complementary approach to alkene synthesis from carboxylic acids, an alternative method using photoredox catalysis to generate alkenes directly from carboxylic acids was developed. Herein, the establishment of the photoredox-facilitated decarboxylative elimination is described.

3.2 Kochi Decarboxylative Elimination

In the early 1950's, several reports illustrated that lead tetraacetate ($Pb(OAc)_4$) in the presence of carboxylic acids produces a carbon radical intermediate and CO_2.[92] Soon after these initial reports, the use of $Pb(OAc)_4$ for decarboxylative functionalization was investigated extensively by Kochi.[11a,57i,57j,93,94a-b] In these reactions, an array of products typically result, including an alkene and alkane as well as two ester products derived from nucleophilic addition by either the acetate or carboxylate ions present in the reaction solution (Scheme 3.1A). Kochi's investigations allowed for an enhanced understanding of the system's reactivity which allowed for optimization of the $Pb(OAc)_4$-facilitated decarboxylation conditions to achieve greater selectivity

of specific products. In order to gain the alkene as the major product of the reaction, Kochi outlines

a process in which copper acetate ($Cu(OAc)_2$) was utilized in the system (Scheme 3.1B).[11a,93]

Kochi goes on to refer to this oxidative elimination transformation as "decarboxylative

elimination."

A. $Pb(OAc)_4$-Facilitated Decomposition of Organic Acids
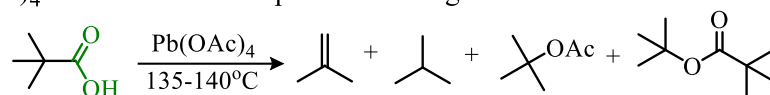
B. Kochi Decarboxylative Elimination
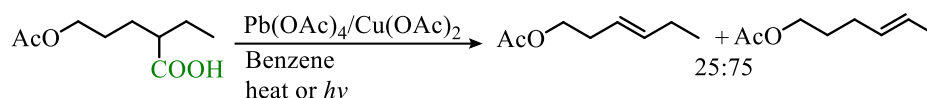
Scheme 3.1: $Pb(OAc)_4$ in decarboxylative elimination

This oxidative decarboxylative elimination sequence is proposed to proceed via the

formation of Pb-carboxylate which then undergoes a decarboxylative cleavage analogous to the

Kolbe electrolysis (Scheme 3.2).[57j,94] The resulting alkyl radical can be rapidly oxidized by

$Cu(OAc)_2$ which provides the alkene product. Cu^I is re-oxidized by Pb to return Cu^{II} to the cycle.

In these reactions, $Pb(OAc)_4$ serves as the stoichiometric oxidant (Scheme 3.2).

Formation of Pb-carboxylate:
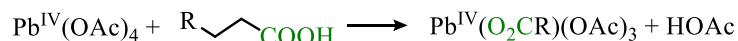
Decarboxylative Elimination:
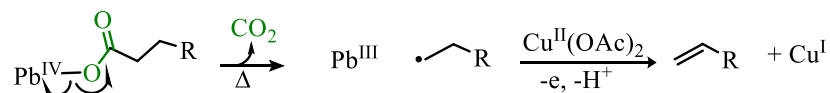
Oxidation of Cu with Pb:
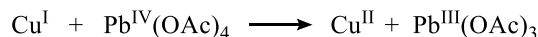
Scheme 3.2: Kochi decarboxylative elimination mechanistic outline

The use of a catalytic amount of $Cu(OAc)_2$ is crucial for the selective formation of the

alkene product. Presumably, this is due to two distinct differences between Pb^{IV} and Cu^{II}

86

oxidations. The first influencing factor is the much faster rate of alkyl radical trapping by Cu^{II} relative to Pb^{IV} (~100 fold).[93a,94c] In fact, Cu^{II} has been found to oxidize alkyl radicals at a rate near diffusion. The second influencing factor is the propensity for a discrete carbocation intermediate to form. Both the Pb^{IV} and Cu^{II} oxidation pathways are proposed to proceed through either a metal-alkyl intermediate or through electron transfer from the alkyl radical to generate a discrete carbocation (Scheme 3.3).
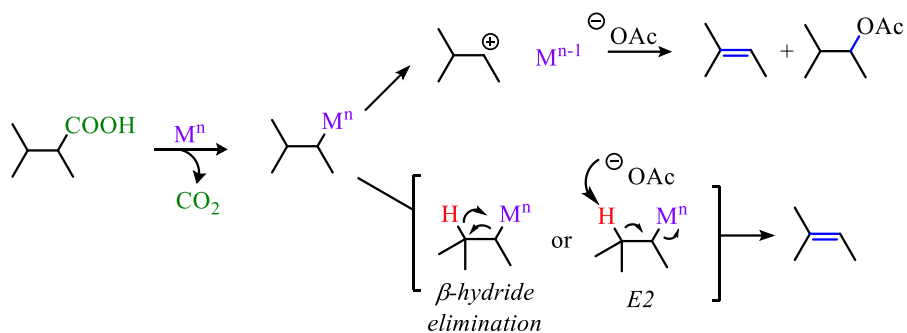
Scheme 3.3: Divergent mechanistic pathways in oxidative decarboxylative elimination

The dominate path is dependent on temperature, solvent, and the structure of the alkyl radical.[11a] All of these factors influence the cage escape of the oxidized intermediate as well as the stability of the carbocation intermediate. In addition to these factors, Cu has been found to have a greater propensity to form the Cu-alkyl as compared to Pb.[57j,95] In an evaluation of the decarboxylative elimination process with the Pb^{IV}/Cu^{II} conditions, Foster[96a] and Gream[96b] utilized a spirocyclic substrate to assess to quantity of rearrangement product compared to direct elimination (Scheme 3.4). A low yield of octalins resulted indicating the formation of a discrete carbocation to be unlikely along the dominant reaction pathway.[96]
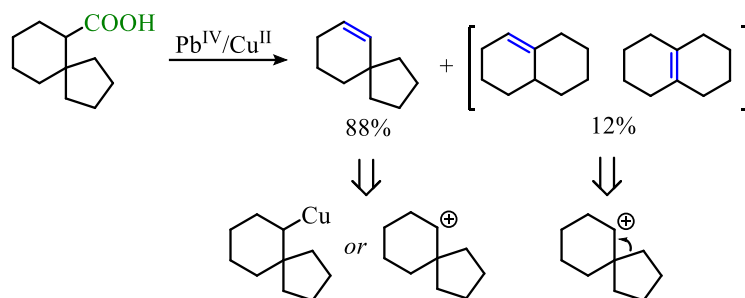
Scheme 3.4: Decarboxylative elimination with spirocyclic acid

For these reasons, the presence of Cu in these reactions allow for a high degree of alkene selectivity over the acetoxylated product. The acetoxylated product only becomes relevant when the carbocation is relatively stable or certain solvent systems are employed (Scheme 3.5).[97] Although a method to obtain the alkene as the major product has been reported, it is important to note that these reactions produce a mix of products. Additionally, high alkene selectivity is dependent on reaction conditions and the structure of the carboxylic acid substrate.
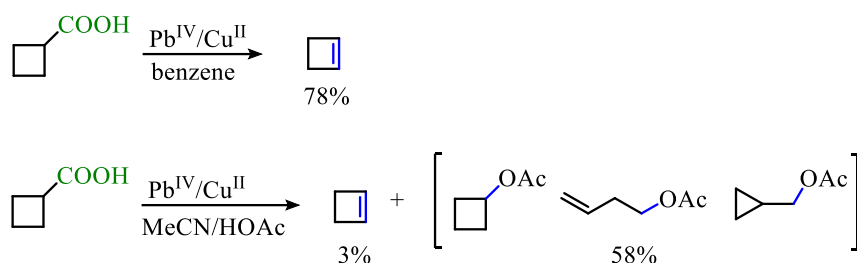
Scheme 3.5: Solvent influence on decarboxylative elimination

Due to the strongly oxidizing conditions, the use of elevated temperatures, limitations in scope, the formation of side products that are difficult to separate, and the use of a stoichiometric amount of a toxic Pb oxidant, this methodology has seen little application in synthesis.[98] Instead, chemists often elect to perform a two-step sequence transforming the carboxylic acid to a halogen which is then eliminated to form the desired alkene.[96]

3.3 Acridinium-Catalyzed Decarboxylative Elimination

To improve upon the synthetic utility of Kochi's methodology, the development of an alternative process that employs the use of a photoredox-facilitated decarboxylation process was undertaken.[100] By utilizing photoredox catalysis, the stoichiometric use of the highly toxic $Pb(OAc)_4$ can be avoided and the decarboxylation event can be achieved under mild reaction conditions. In order to maintain high atom economy, the reaction was envisioned to oxidize the carboxylate moiety directly through employing an oxidative radical decarboxylation pathway.[101] Once an alkyl radical is generated, a Cu source can be used to further oxidize the carbon radical to the desired alkene like in the Kochi decarboxylative elimination (Scheme 3.6). Using Cu as the terminal oxidant could also allow for re-oxidation of the photosensitizer to complete the catalytic cycle.
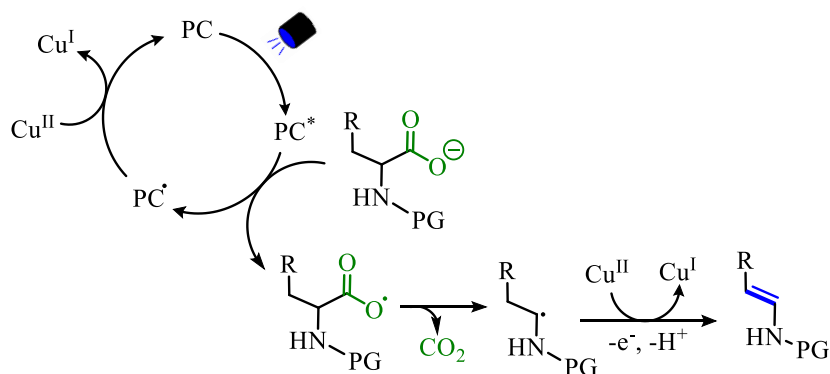
Scheme 3.6: Photoredox-facilitated Kochi decarboxylative elimination blue print

With this in mind, the acridinium family of photosensitizers emerged as ideal catalysts for this transformation as they are highly oxidizing ($E_{1/2}$ = > +2.0 V vs. SCE).[2e,2h,102] Their high positive excited state reduction potentials allows for the favorable single electron oxidations of the carboxylate moiety (Figure 3.1). Additionally, the resulting acridinium radical species is easy to re-oxidize ($E_{1/2}$ = -0.5 – -0.6 V vs. SCE) permitting for a facile electron transfer to the Cu oxidant (Figure 3.1).
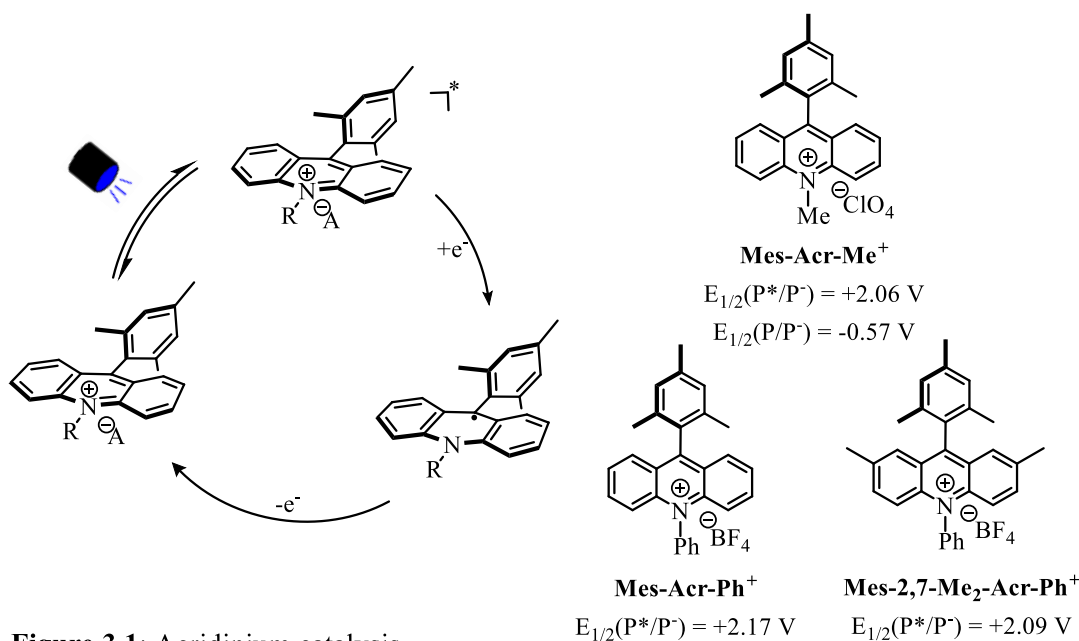
Figure 3.1: Acridinium catalysis

Mes-Acr-Me$^+$
$E_{1/2}(P^*/P^-) = +2.06$ V
$E_{1/2}(P/P^-) = -0.57$ V

Mes-Acr-Ph$^+$
$E_{1/2}(P^*/P^-) = +2.17$ V

Mes-2,7-Me$_2$-Acr-Ph$^+$
$E_{1/2}(P^*/P^-) = +2.09$ V

3.3.1 Development of Acridinium Catalyzed Decarboxylative Elimination of N-Acyl Amino Acids

Enamide synthesis was identified as an area that could benefit from a decarboxylative elimination procedure as commercially available amino acids could be converted directly into enamide building blocks in a single synthetic step. Many methods toward enamide synthesis have been reported (Figure 3.2).[103] Classical methods include condensation reactions of amines with aldehydes,[104] the Curtius rearrangement of acyl azides,[105] Wittig reactions of amides,[106] and the addition of Grignard reagents to *N,N*-dialkyl formamides.[107] Modern routes toward enamide and enecarbamate synthesis include transition metal-catalyzed cross coupling reactions,[108] isomerization of allylamines,[109] hydrogenation of ynamides,[110] hydroamination of alkynes,[111,112] and decarbonylative approaches.[113]
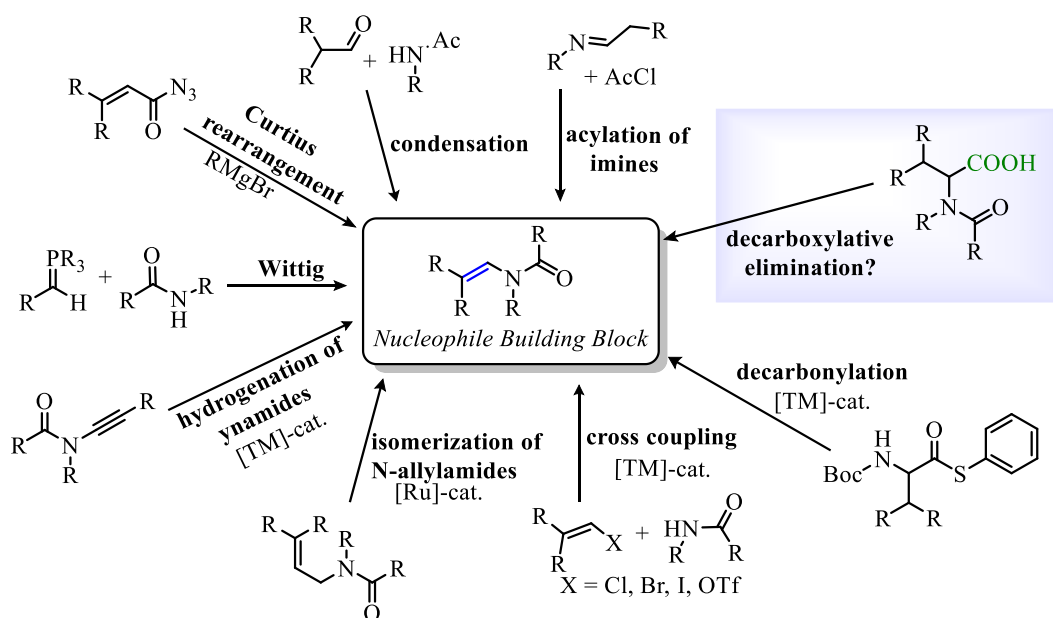
Figure 3.2: Synthesis of enamides and enecarbamates

Despite the vast attention enamide synthesis has received, the methods reported do not meet all ideal requirements, such as operational simplicity, easily accessible starting materials, configurational selectivity, mild and environmentally benign reaction conditions, as well as being economical. The production of enamides from amino acids is highly attractive because these starting materials are readily available, inexpensive, and possess a variety of side chain functionalities. Thus, operationally simple methods offering direct conversion of these substrates into synthetically useful enamines would be an advantageous addition to the enamide synthesis arsenal. Unfortunately, the Pb[IV]/Cu[II] Kochi decarboxylative elimination methodology was found to be incompatible with α-amino acids, since as the decarboxylation event with Pb-carboxylates leads to imine formation with these substrates (Scheme 3.8).[11a,114] As such, a photoredox-facilitated variant of the Kochi elimination could compensate for this limitation and allow for the facile synthesis of synthetically valuable enamide building-blocks.
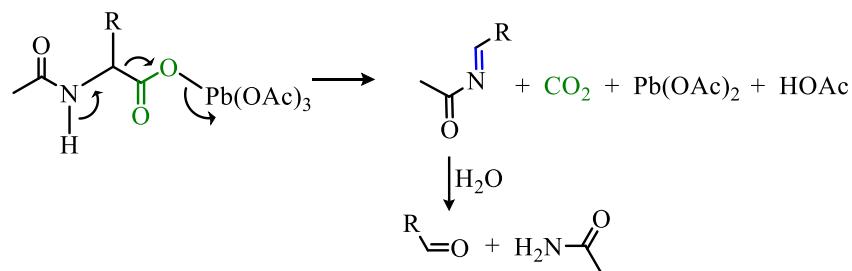
Scheme 3.8: Kochi elimination with α-amino acids

Initial explorations into the viability of a photoredox Kochi decarboxylative elimination exploited aspartic acid derivative (**1ll-Boc**) with $Cu(OAc)_2$ as the terminal oxidant (Table 3.1).[100] It was found that these reactions result in high conversion but in order to obtain respectable quantities of the enecarbamate product, the reaction solvent needs to be anhydrous to prevent hydrolysis. To overcome this, molecular sieves were incorporated into the reaction mixture. A screening of the acridinium photocatalysts revealed that the optimal catalyst for this transformation was Mes-2,7-Me$_2$-Acr-Ph$^+$ BF$_4^-$ (Table 3.1, Entry 3). Base was also utilized in the initial reaction investigations, but it was subsequently found that this reaction produced comparable yields without base (Table 3.1, Entry 4). This suggests that $Cu(OAc)_2$ not only serves as the terminal oxidant but also provides an acetate base to liberate carboxylate in this reaction.

Acetonitrile was utilized as the reaction solvent in the initial optimization studies because it has a high dielectric constant to allow for facile electron transfer in solution.[115] However, this reaction was operable in other reaction solvents, some with much lower dielectric constants than MeCN (Table 3.1, Entries 5-11). The yield of (**7a**) isolated when the reaction is run in Et$_2$O or toluene was found to be comparable to that obtained when the reaction was performed in MeCN (Table 3.1, Entries 8 & 10). The reaction provides moderate yields when run in MeOH (Table 3.1, Entry 11). Poor conversion resulted from the use of THF, DCM, DME, and DMF with yields of (**7a**) being <30% (Table 3.1, Entries 5-7, 9). It is important to note that the reaction does result in

92

a mixture of *E/Z*-isomers and the *E/Z*-selectivity was influenced by the change in reaction conditions. The nature of this *E/Z*-selectivity is discussed in detail in *Section 3.3.3*.

Reaction scheme: **1ll-Boc** → Cu(OAc)$_2$ (2.7 equiv.), PC (5 mol%), 32 W Blue LED, ~14 h, Ar, 28°C, Solvent (0.05 M) → **(7a-Boc)**
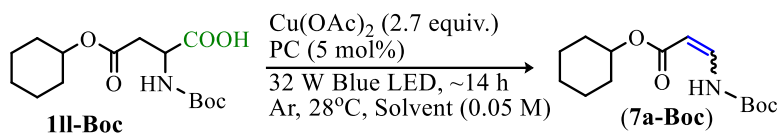
Entry	Na$_2$CO$_3$ (2 equiv.)	Photocatalyst	Solvent	Yield	Isomer Ratio (E:Z)
1	+	Mes-Acr-Ph$^+$ BF$_4^-$	MeCN	65%	49:51
2	+	Mes-Acr-Me$^+$ ClO$_4^-$	MeCN	71%	59:41
3	+	Mes-2,7-Me$_2$-Acr-Ph$^+$ BF$_4^-$	MeCN	91%	52:48
4	-	Mes-2,7-Me$_2$-Acr-Ph$^+$ BF$_4^-$	MeCN	90%	36:64
5	-	Mes-2,7-Me$_2$-Acr-Ph$^+$ BF$_4^-$	THF	24%	46:54
6	-	Mes-2,7-Me$_2$-Acr-Ph$^+$ BF$_4^-$	DCM	19%	37:63
7	-	Mes-2,7-Me$_2$-Acr-Ph$^+$ BF$_4^-$	DME	18%	0:100
8	-	Mes-2,7-Me$_2$-Acr-Ph$^+$ BF$_4^-$	Toluene	91%	45:55
9	-	Mes-2,7-Me$_2$-Acr-Ph$^+$ BF$_4^-$	DMF	29%	38:62
10	-	Mes-2,7-Me$_2$-Acr-Ph$^+$ BF$_4^-$	Ether	87%	38:62
11	-	Mes-2,7-Me$_2$-Acr-Ph$^+$ BF$_4^-$	MeOH	66%	88:12

Table 3.1: Acridinium catalyst and solvent investigations.
[a] Reactions were performed on the 0.4 mmol scale. [b] Isolated yields shown; isomers were isolated separately.

In addition to Cu(OAc)$_2$, other Cu salts were utilized under the photocatalytic conditions (Table 3.2). Of the copper salts examined, Cu(OAc)$_2$, Cu(acac)$_2$, and Cu(thiophene-2-carboxylate)$_2$ gave excellent yields (Table 3.2, Entries 1-3). Conversely, the copper halide salts did not perform well (Table 3.2, Entry 4, 8, 9), nor did Cu(SO$_4$)$_2$ or Cu(OTf)$_2$ (Table 3.2, Entry 5 & 11), suggesting that a counterion dependence exists for this transformation. It is noteworthy that CuOAc resulted in only slightly diminished yield (83%) compared to Cu(OAc)$_2$ (90%) (Table 3.2, Entry 6) and points to the possibility of CuOAc also being able to perform the oxidation of the carbon radicals and photocatalyst (Scheme 3.6). Despite the success of Cu(thiophene-2-carboxylate)$_2$ and Cu(acac)$_2$, Cu(OAc)$_2$ was chosen for further exploration of this reaction due to its lower expense and "greener alternative" label (Cu(thiophene-2-carboxylate)$_2$ = ~$79/gram,

Cu(acac)$_2$ = ~\$4/gram, Cu(OAc)$_2$ = ~\$2/gram).[116] Again, the *E/Z*-selectivity is influenced by the change in reaction conditions.
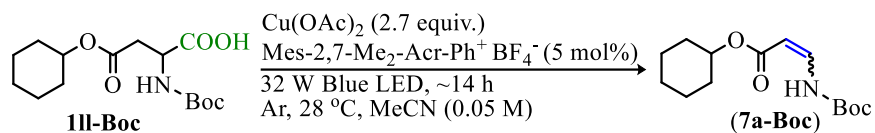
Entry	Cu	Yield	Isomer Ratio (E:Z)
1	Cu(OAc)$_2$	90%	36:64
2	Cu(acac)$_2$	98%	68:32
3	Cu(thiophene-2-carboxylate)$_2$	98%	38:62
4	Cu(Cl)$_2$	-	-
5	Cu(SO$_4$)	-	-
6	Cu(OAc)	83%	39:61
7	Cu(2-ethylhexanoate)	69%^{c}	48:52
8	Cu(I)	12%	33:67
9	Cu(Br)	17%^{c}	47:53
10	Cu(phthalocyanide)	13%	62:38
11	Cu(OTf)$_2$	-	-

Table 3.2: Copper salt performance in photocatalyzed decarboxylative elimation
^{a} Reactions were run on 0.2 mmol scale with 0.4 mmol of Na$_2$CO$_3$. ^{b} Isolated yields shown; isomers were isolated separately. ^{c} Yields determined by q^{1}H NMR with pyridine as the internal reference standard.

Other Cu salts and oxidizing agents were explored in the decarboxylative elimination as well. However, only the Cu salts with anionic oxygen ligands provided any reactivity while nitrogen-based ligand systems resulted in no reaction. This could be due to the much more negative reduction potential of Cu with nitrogen ligands (~-1.0 V vs. SCE) as compared to carboxylate ligands (~-0.25 V vs. SCE) and halide counter anions (~-0.06 V vs. SCE).[117] Other oxidants explored include ceric ammonium nitrate, ferrocenium hexafluorophosphate, and various quinones such as benzoquinone and 1,4-naphthylquinone, but these alternative oxidants did not have any reactivity in the photoredox-catalyzed decarboxylative elimination system.

Next, the optimal reagent concentrations were elucidated (Table 3.3). Previous optimizations were completed with 2.7 equivalents of Cu(OAc)$_2$ as 1 equivalent was suspected to be needed to oxidize the radical to the alkene while another equivalent would be needed to turn

over the photocatalyst (Scheme 3.6). But it was observed that the amount of Cu(OAc)$_2$ can be decreased to 1.5 equivalents and the same yields are observed (Table 3.3, Entry 2). Presumably, this seemingly sub-stoichiometric loading is allowed as the Cu(OAc) can also serve as an oxidant ultimately providing Cu^0. The Mes-2,7-Me$_2$-Acr-Ph$^+$ BF$_4^-$ loading could also be decreased to 2.5 mol% from the 5 mol% originally employed, and high reaction yields were maintained (Table 3.3, Entry 3). Further decreasing Cu(OAc)$_2$ and photocatalyst resulted in diminished yields (Table 3.3, Entry 4). Lastly, the reaction does not proceed without Cu(OAc)$_2$ and the reaction produces <10% yield of **7a** without the photocatalyst, indicating that both reagents are needed for the reaction to proceed (Table 3.3, Entry 5-6).
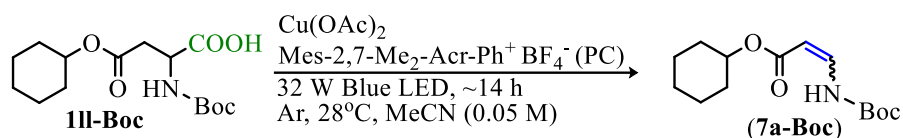
Entry	Cu(OAc)$_2$ (equiv.)	PC (mol%)	Yield	Isomer Ratio (E:Z)
1	4.2	5	95%	42:58
2	1.5	5	93%	40:60
3	1.5	2.5	94%	34:66
4	0.75	1.25	72%	35:65
5	-	2.5	0%	-
6	1.5	-	8%	50:50

Table 3.3: Reagent concentration optimization

Monitoring the model reaction over time revealed the reaction reaches completion after 14 hours of irradiation (Figure 3.3). The *E*-isomer was found to predominate at the onset of the reaction but as the reaction progressed, the *Z*-isomer prevails with a maximum selectivity of 34:66 *E:Z* observed after 14 hours of irradiation (see *Section 3.3.3* for further discussion of the isomer ratio). Allowing the reaction to be irradiated for 24 hours did not lead to significant changes in the yield or isomer ratio.
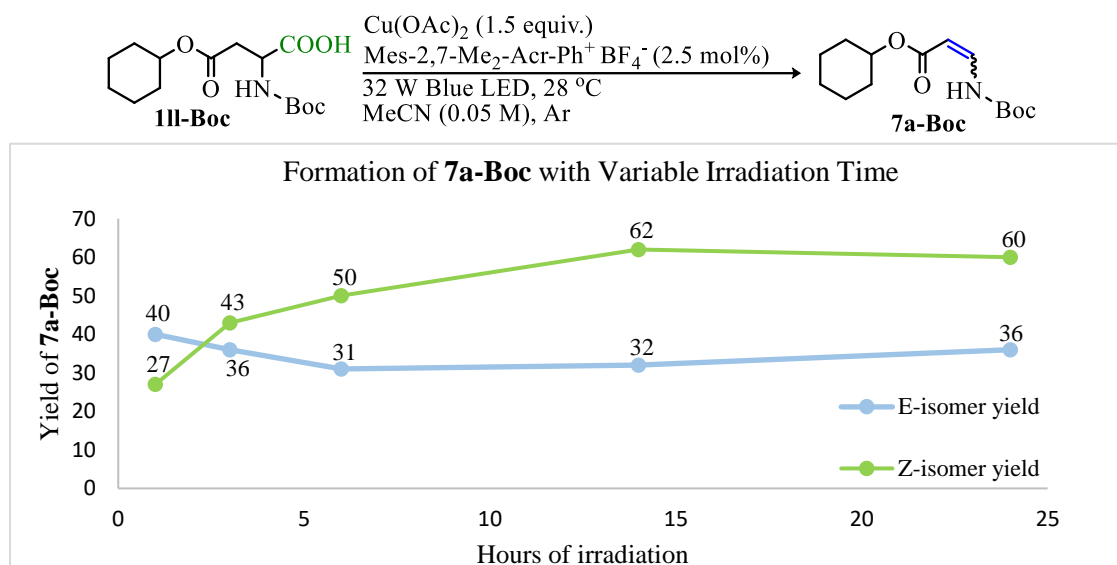
Figure 3.3: Acridinium-catalyzed decarboxylative elimination reaction time
ᵃ Isolated yields shown and *E/Z* isomers were isolated separately.

3.3.2 Decarboxylative Elimination for the Synthesis of Enecarbamates and Enamides

An assortment of *N*-protected amino acids were subjected to the optimal reaction conditions (Table 3.4). Aspartic acid derivatives produced excellent yields and displayed a small preference for the *Z*-isomer (**7a**−**7d**). Likewise, *N*-Boc asparagine provided a high yield of the corresponding enecarbamate and generated predominately the *Z*-isomer while only trace amounts of the *E*-isomer were observed (**7e-Boc**). Phenylalanine and its derivatives reacted smoothly, but these substrates favored the *E*-isomer (**7f**−**7j**). Conversely, when a pendant pyridine was present, the *Z*-isomer predominated while only trace amounts of the *E*-isomer were observed (**7k-Boc**). The variation in the isomer ratios is suspected to be a result of the hydrogen bonding ability of the amide proton with a nearby heteroatom, providing a thermodynamic preference for the *Z*-isomer. Amino acids with long side chains (**7m**−**7n**, **7u**−**7w**) also undergo elimination well providing moderate to good yields. In the case of cyclic amino acids, the alkene was able to be installed but in lower yields than the acyclic counterparts (**7s**−**7t**).

Cu(OAc)$_2$ (1.5 equiv.)

Mes-2,7-Me$_2$-Acr-Ph$^+$ BF$_4^-$ (2.5 mol%)

MeCN (0.05 M), 4Å Mol. Sieves

32 W Blue LED, 28 °C, 14 hr

(7a-Boc) 93%[c]
40:60 *E:Z*

(7b-Boc) 93%[c]
39:61 *E:Z*

(7c-Boc) 97%[c]
44:56 *E:Z*

(7d-Boc) 86%[c]
41:59 *E:Z*

(7e-Boc) 79%[c]
<1:99 *E:Z*

(7f-Boc) 87%
89:11 *E:Z*

(7g-Boc) 88%[c]
89:11 *E:Z*

(7h-Boc) 73%
89:11 *E:Z*

(7i-Boc) 85%
90:10 *E:Z*

(7j-Boc) 73%[c]
82:18 *E:Z*

(7k-Boc) 47%[c]
>1:99 *E:Z*

(7l-Boc) 76%
57:43 *E:Z*

(7m-Boc) 74%
63:37 *E:Z*

(7n-Boc) 58%
66:34 *E:Z*

(7o-Boc) R=H; 65%, 75:25 *E:Z*
(7p-Boc) R=CH$_3$; 30%

(7q-Boc) 80%
65:35 *E:Z*[d]

(7r-Cbz) 64%
53:47 *E:Z*

(7s-Boc) 54%

(7t-Boc) 48%

(7u-Boc) 65%, 70:30 *E:Z*
(7u-Ac) 62%, 76:24 *E:Z*
(7u-Cbz) 75%, 74:26 *E:Z*

Table 3.4: Scope of enamide and enecarbamate products
[a] Reactions were performed on 0.4 mmol scale. [b] Isomer ratios of mixed products were determined by ^{1}H NMR. [c] Isomers were isolated separately. [d] Major isomer was determined by NOESY.

In addition to screening various amino acids, the influences of several nitrogen protecting groups on alkene formation were probed. In the case of isoleucine, when the nitrogen was methylated this led to approximately a 50% yield decrease in alkene from the *N*-H variant (**7o-Boc** & **7p-Boc**) but did provide exclusively the *E*-isomer (**7p-Boc**). The decrease in efficiency observed with the tertiary amine may be due to a decrease in radical stabilization resulting from the increased strain experienced when the nitrogen lone pair is aligned with the radical. In the case of norluecine,
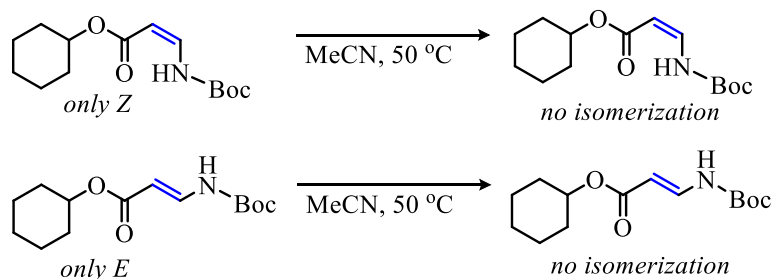
various protecting groups were utilized and with *N*-Boc, *N*-Cbz, and *N*-Ac functionalities, similar yields and *E/Z*-selectivity was observed (**7u**). However, when unprotected phenylalanine was subjected to the elimination conditions, no alkene product was observed.

The reaction was found to be easily assembled, tolerant to variations in the reaction conditions, and easy to purify. The reaction produces the enamides and enecarbamates as the sole product. Enamides and enecarbamates were purified with silica gel chromatography to separate the *E/Z*-isomers and obtain high analytical purity but these products can be easily separated from any remaining starting material, copper, and photocatalyst with only silica plug. Thus, column chromatography could be avoided, or the *E/Z*-isomers can be separated using column chromatography if desired.

3.3.3 Acridinium-Facilitated E/Z isomerization

Elucidating the factors dictating the *E/Z*-isomer mixtures was of interest. Both the *E*- and *Z*-isomers of **7a** were isolated separately for evaluation (Scheme 3.7). First, each isomer was taken in a solution of MeCN and heated at 50 °C for 14 hours, the duration of a typical elimination reaction. No isomerization of either the *E*- or *Z*-isomer was observed (Scheme 3.7A). Next, each isomer was independently dissolved in MeCN with Mes-2,7-Me$_2$-Acr-Ph$^+$ BF$_4^-$ (5 mol%) and irradiated. After 6 hours of irradiation, an *E/Z*-mixture of **7a** resulted from both the pure *E*- and *Z*-isomers (Scheme 3.7B). Thus, the isomerization was diagnosed to be an artifact of a background photochemical process in the decarboxylative elimination reactions.

A. Thermal Isomerization

MeCN, 50 °C

only Z → *no isomerization*

MeCN, 50 °C

only E → *no isomerization*

B. Photochemical Isomerization

Mes-2,7-Me$_2$-Acr-Ph$^+$ BF$_4^-$ (5 mol%)
MeCN, Blue LED, 28 °C, 6 h

only Z → *33:67 E:Z*

Mes-2,7-Me$_2$-Acr-Ph$^+$ BF$_4^-$ (5 mol%)
MeCN, Blue LED, 28 °C, 6 h

only E → *37:63 E:Z*
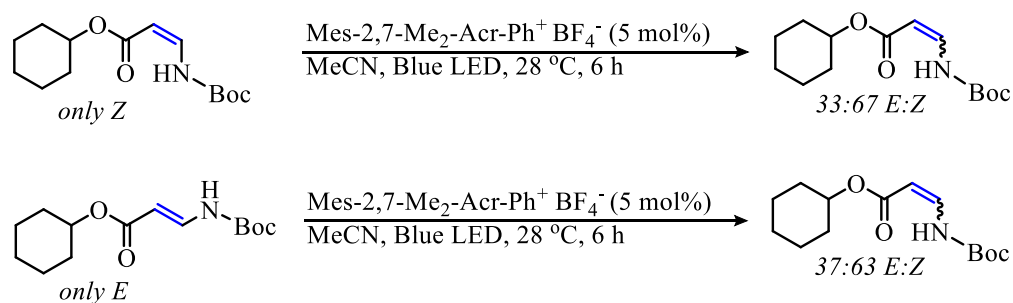
Scheme 3.7: Acridinium-faciliated *E/Z*-isomerization of **7a-Boc**

Isomerization facilitated by photosensitizers has been recently described by Weaver with iridium photosensitizers and carbinamines.[118] Upon studying this report, it became apparent that the isomerization could be facilitated by the acridinium in one of two ways (Scheme 3.8). The first possible path is through electron transfer (Scheme 3.8A). Such a pathway would be facilitated by amide oxidation to form a radical cation.[119,120] Formation of the iminium intermediate results in C–C σ-bond character, permitting free rotation. Quenching of the *Z*-configured radical cation by the reduced acridinium returns the photocatalyst to the ground state and results in the *Z*-configured product. The second possible pathway is an energy transfer process (Scheme 3.8B). Here, energy transfer from the excited state photocatalyst results in a diradical intermediate which can produce the *E*- or *Z*-isomer. In either case, the isomer ratio observed at the end of the elimination reaction is suspected to represent an equilibrium established between the conversion of *E* to *Z* which can be influenced by changes to the substrate and reaction conditions.

99

A. Electron Transfer Mechanism
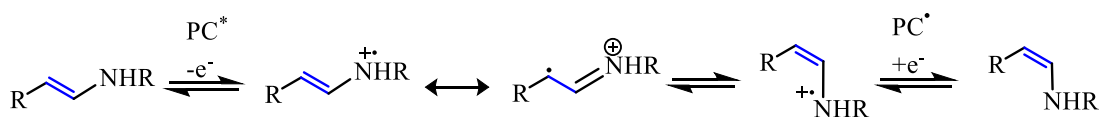
B. Energy Transfer Mechanism
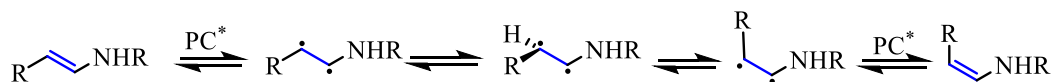
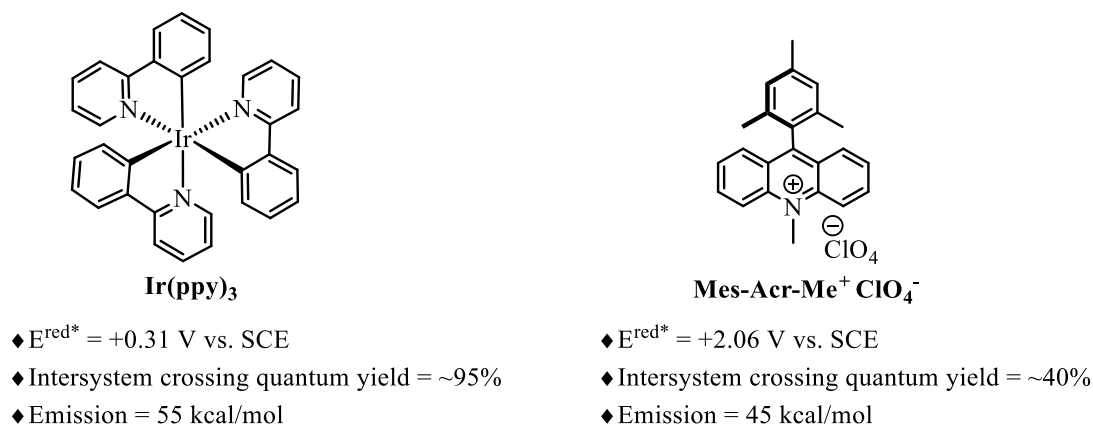**Scheme 3.8**: Possible mechanisms for acridinium-facilitated *E/Z*-isomerization

In Weavers report, evidence points to their system proceeding via an energy transfer pathway.[118] Similar reports of isomerizations proceeding though this pathway were also suggested by Yoon.[121] However, these reports are utilizing Ir photosensitizers which have very different photophysical properties than the acridinium employed in the decarboxylative elimination methodology (Figure 3.4). For one, the acridinium catalyst is far more oxidizing than the Ir catalysts, particularly the Ir(ppy)$_3$ catalyst employed by Weaver. Thus, the excited state acridinium can perform facile oxidation of the amine functionality whereas this oxidation is not favorable for with the Ir(ppy)$_3$ (amine to amine radical cation: ~ +0.7− +1.2 V vs. SCE; amide to amide radical cation: ~+1.2− +1.8 V vs. SCE).[120] Another important consideration is the significance of the triplet state with each class of photosensitizer. The Ir(ppy)$_3$ can undergo intersystem crossing in ~95% quantum yield making this species highly relevant.[122] Emissive energy from this catalyst is 55 $^{kcal}/_{mol}$.[122] Conversely, the acridinium Mes-Ace-Me$^+$ ClO$_4^-$ has been found to undergo intersystem crossing to the triplet state in ~40% quantum yield, making this species much less relevant.[102a,123] Further, the emissive energy from the Mes-Ace-Me$^+$ ClO$_4^-$ is reported to be 45 $^{kcal}/_{mol}$.[123] Most organic substrates have triplet energies exceeding 45 $^{kcal}/_{mol}$. For example, the C=C double bond of interest in the enamide system has a bond-dissociation energy of ~60 $^{kcal}/_{mol}$.[124]

Thus, an electron transfer pathway is suspected to be more likely in the acridinium-facilitated isomerization (Scheme 3.8A).

|	
Ir(ppy)₃	**Mes-Acr-Me⁺ ClO₄⁻**
◆ E^{red*} = +0.31 V vs. SCE	◆ E^{red*} = +2.06 V vs. SCE
◆ Intersystem crossing quantum yield = ~95%	◆ Intersystem crossing quantum yield = ~40%
◆ Emission = 55 kcal/mol	◆ Emission = 45 kcal/mol

**Figure 3.4**: Photophysical diverstiy between Ir and acridinium photosensitizers

In addition to the mechanistic speculation derived from the reported photophysics of the acridinium system, experimental observations made when evaluating the isomerization of phenylalanine derived **7f-Boc**, **7f-Ac**, and **7v-Ac** further point to an electron transfer pathway (Figure 3.5).[120b,125] Not only is the final *E/Z* ratio observed dependent on the identity of the nitrogen substituents, the rate at which the equilibrium *E/Z* ratio is reached is also dependent on the substituents. If the isomerization was facilitated by a triplet sensation of the alkene, little selectivity difference would be expected between the **7f-Boc** and **7f-Ac** as both enamines should have similar BDE as well as similar energy differences between *E*- and *Z*-isomers. Enamine **7v-Ac** could behave differently in an energy transfer process as a result of lower hyperconjugation stabilization of the diradical compared to **7f-Boc** and **7f-Ac**. But the resulting BDE difference is not expected to greatly exceed **7f**. However, **7f-Boc** and **7f-Ac** were found to reach different *E/Z* ratios and **7v-Ac** did not undergo isomerization (Figure 3.5A). Further, the rates at which **7f-Boc** and **7f-Ac** isomerize were different (Figure 3.5B, see Appendix **A4** for further discussion of this data). These experiments point to amine involvement in the isomerization process which is expected for the electron transfer mechanism and not the energy transfer mechanism (Scheme 3.8). Lastly, when

7f-Boc was subjected to Ir(ppy)₃, a high degree of *Z*-selectivity is achieved indicating vastly different isomerization behavior between the Ir and acridinium photosensitizers (Figure 3.5C).

A. Acridinium-Facilitated Isomerization of *N*-R Phenylalanine-Derived Enamides
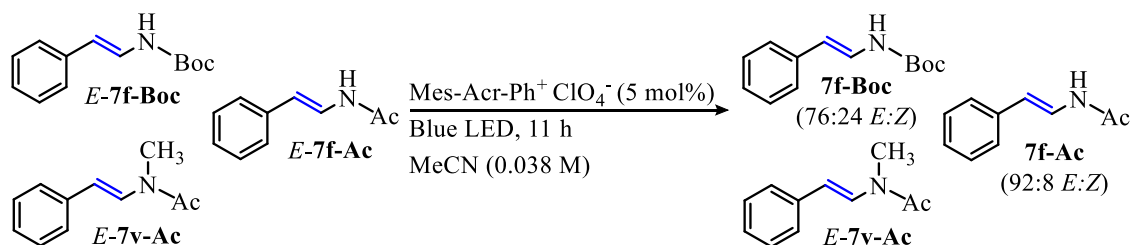
B. Rate of Acridinium-Facilitated Isomerization of *N*-R Phenylalanine-Derived Enamides
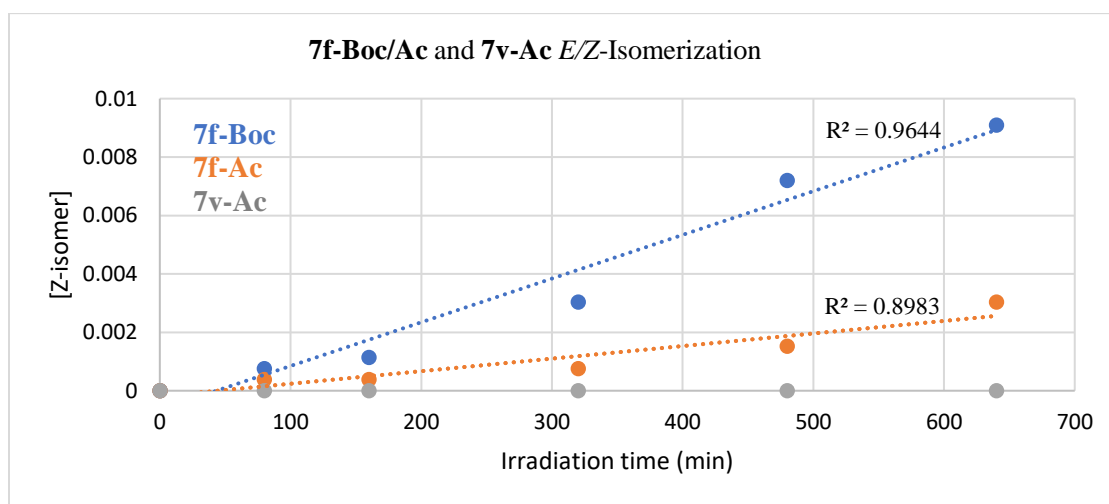
C. Ir-Facilitated Isomerization of **7f-Boc**
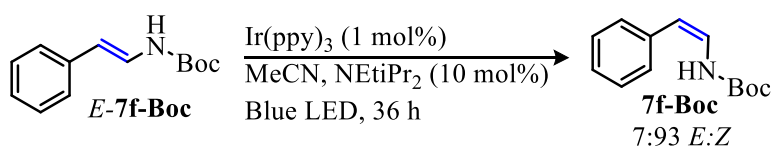
Figure 3.5: Photosensitizer-facilitated *E*/*Z*-isomerization with phenylalanine derived enamides

Although an artefact of utilizing the acridinium photosensitizers in the elimination is a mixture of *E/Z*-isomer products, this isomerization can be utilized for the enrichment of either isomer (Scheme 3.9). This was demonstrated through performing the decarboxylative elimination reaction and isolating the *E*-**7a-Boc** and *Z*-**7a-Boc** separately. The *E*-**7a-Boc** was then subjected to

the isomerization conditions and the *E/Z*-mixture that results was combined with the originally

isolated *Z*-**7a-Boc** to provide a 13:87 *E:Z* mix in 84% yield over two steps (Scheme 3.9).

Alternatively, the *E/Z*-mixtures can be converted to almost exclusively the *Z*-isomer if an Ir

photosensitizer is employed (Figure 3.5C).
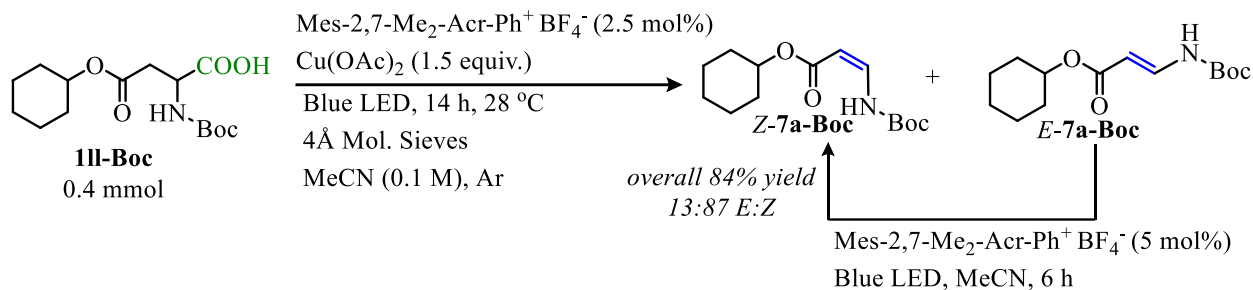
Scheme 3.9: Geomentric isomer enrichment
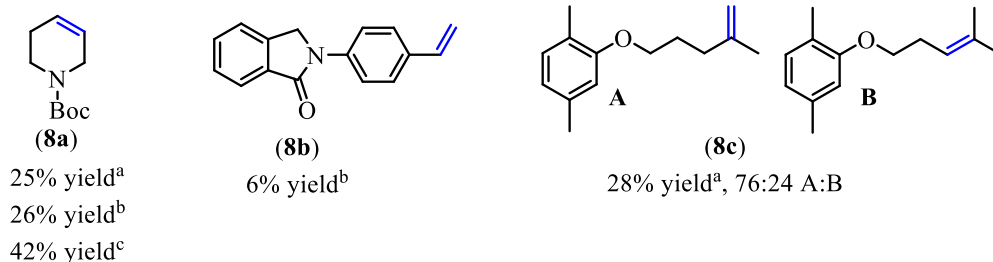
3.3.4 Decarboxylative Elimination of Carboxylic Acids

Apart from α-amino acids, other carboxylic acids were subjected to the decarboxylative

elimination conditions (Figure 3.6). Despite these substrates ability to undergo decarboxylative

elimination, the yields of alkene products obtained were significantly lower than what is observed

for the enamides. Nonetheless, there are a few notable observations that arose from these

substrates. For one, it was found that increasing the $Cu(OAc)_2$ and Acr^+ concentrations did not

improve the conversion to the alkene (Figure 3.6, **8a**). But, increasing the reaction temperature to

75 °C did allow for the yield to be increased by almost 50% (Figure 3.6, **8a**). When Gemfibrozil

(**1ff**) was utilized, a mixture of regioisomers results, with selective formation of the Hofmann

product observed (Figure 3.6, **8c**).

(8a)
25% yield[a]
26% yield[b]
42% yield[c]

(8b)
6% yield[b]

(8c)
28% yield[a], 76:24 A:B

Figure 3.6: Acridinium-catalyzed Cu decarboxylative elimination
[a] Reaction on 0.2 mmol scale with $Cu(OAc)_2$ (1.5 equiv.) and $Mes-2,7-Me_2-Acr-Ph^+$ BF_4^- (2.5 mol%).
[b] Reaction on 0.2 mmol scale with $Cu(OAc)_2$ (2.7 equiv.) and $Mes-2,7-Me_2-Acr-Ph^+$ BF_4^- (5 mol%).
[c] Reaction on 0.2 mmol scale with $Cu(OAc)_2$ (1.5 equiv.) and $Mes-2,7-Me_2-Acr-Ph^+$ BF_4^- (2.5 mol%) at 75 °C; yield was determined by q^1H NMR with pyridine internal reference standard.

3.3.5 Reaction Mechanism

The acridinium-catalyzed decarboxylative elimination is envisioned to proceed via the reaction schematic pictured in (Scheme 3.6). From the control experiments presented in Table 3.3 (Entries 5-6), the reliance on both the acridinium and the Cu source has been established. Additionally, the possibility for CuOAc to also facilitate the needed oxidation of the alkyl radical and the photocatalyst reveals that a pathway in which both Cu^{II} and Cu^I are participate is highly likely. Although this fits the mechanistic depiction in Scheme 3.6, the radical oxidation by Cu^{II} or Cu^I was left ambiguous.

As discussed in *Section 3.2*, the oxidation of the alkyl radical by Cu^{II} can proceed via either a discrete carbocation pathway or a Cu–alkyl intermediate that can undergo either β-hydride elimination or an E2 process to provide the alkene (Scheme 3.3). In Kochi's chemistry, the formation of the discrete carbocation is dependent on stability of the carbocation intermediate which can be provided by the substrate and/or reaction solvent. Also, elevated reaction temperatures favor the carbocation pathway.

To gain insight into the pathway by which the elimination proceeds, **1b-Boc** was subjected to the standard reaction conditions along with excess of a nucleophilic reagent (Scheme 3.10).[126]

In these reactions, no nucleophilic trapping product was observed and only the elimination product results.
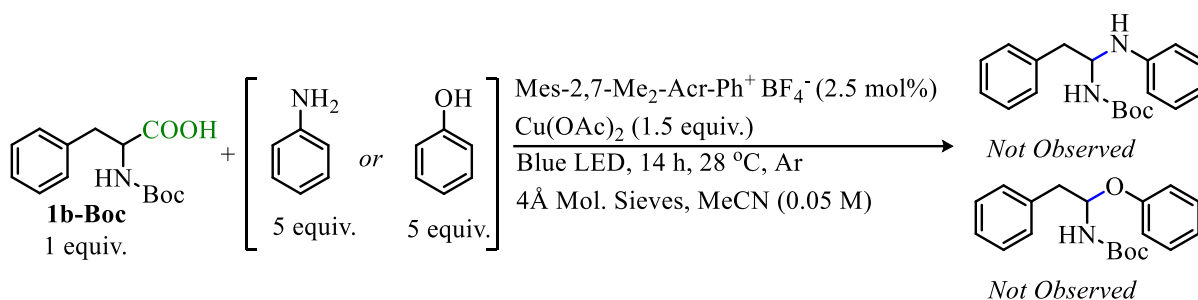
Scheme 3.10: Attempted carbocation trapping by a nucleophile

Despite the difficulty experienced in achieving nucleophilic addition, the reactivity was able to be adjusted to allow for the synthesis of the acetoxylated products (Scheme 3.11).[127] To achieve acetoxylation, carboxylic acids with carbocation-stabilizing functionalities that lack β-hydrogens performed best with no successful acetoxylation of the α-amino acids observed. Additionally, the acetoxylation reaction was performed at a higher temperature than the elimination reaction (45 °C vs. 28 °C, respectively) which has been proposed to favor discrete cation formation.[11a] Taken together, the decarboxylative elimination pathway is suspected to predominantly proceed via a Cu-alkyl species with little to no discrete carbocation formation.
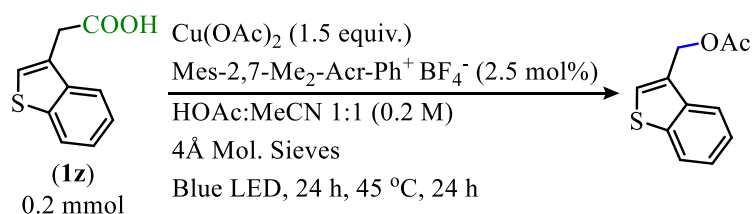
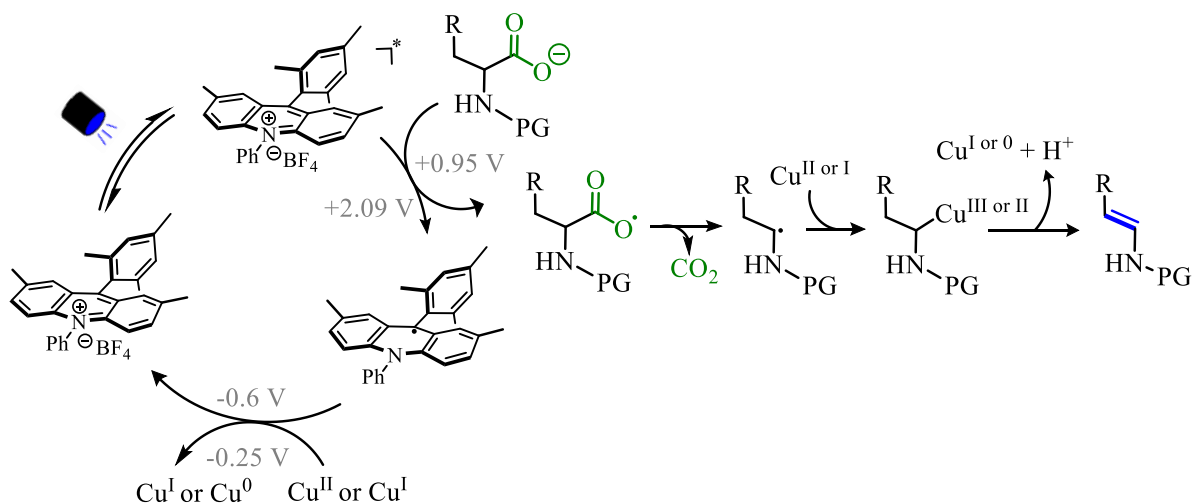Scheme 3.11: Decarboxylative acetoxylation

In addition to the nature of the radical oxidization, the possibility for the elimination of α-amino acids to proceed via the cleavage of either the α-C–H bond or the α-N–H bond needs to be considered. The breaking of the adjacent C–H bond would lead directly to the enamide product whereas breaking the N–H bond would provide an imine which could tautomerize to the enamide

product. If the reaction were to proceed exclusively through N–H bond breaking, tertiary amines would not allow for the elimination to proceed. However, tertiary amine enamide product **7p** was able to be synthesized in 30% under the reaction conditions (Table 3.4). Thus, although both pathways could be operable, an N–H breaking elimination pathway is not required for elimination to occur.

In sum, the dominant mechanistic pathway is expected to proceed via a reductive quenching pathway in which the excitation of the acridinium catalyst by blue light (+2.09 V vs. SCE)[102] allows for the single electron oxidation of the carboxylate (+0.95 V vs. SCE)[19] (Scheme 3.12). Facile decarboxylation would provide the α-amino radical intermediate which is expected to be trapped by Cu immediately.[93a,94c] A β-hydride elimination and/or an acetate-facilitated E2 pathway would give the enamide product. The Cu (Cu$^{II/I}$ ~-0.25 V vs. SCE)[117] also serves to reoxidize the acridinium (~-0.6 V vs. SCE)[2e,2h] by one electron returning it to its ground state (TON 36 in elimination of **1ll-Boc**). The Cu^{I} generated from this process can also serve as an oxidant and be active in subsequent eliminations to ultimately provide Cu^{0}.


Scheme 3.12: Expected dominant Cu/Acr^{+} decarboxylative elimination pathway

3.3.6 Dual-Catalytic Cu/Acr+ Decarboxylative Elimination

Replacing Pb(OAc)$_4$ with an acridinium catalyst has allowed for Kochi's decarboxylative elimination to proceed under mild condition while bypassing the stoichiometric amount of Pb which is highly toxic. However, the photoredox methodology does make use of a stoichiometric oxidant that detracts from the redox-neutral and minimal waste initiative of green method development. The possibility of rendering this reaction catalytic through the use of molecular oxygen as green and abundant terminal oxidant was explored. Although the reaction can proceed under an atmosphere or air, the reaction was inhibited when run under an atmosphere of oxygen, resulting in a less than 5% yield of enamide product.

In order to overcome this incompatibility, a different operational procedure was undertaken (Figure 3.7). The reaction was assembled with a substoichiometric loading of Cu(OAc)$_2$ and irradiated under an atmosphere of Ar until the Cu^{II} becomes reduced which can be observed visually by a change in color from blue-green to brown. After the reaction mixture became brown in color, irradiation was stopped, and the reaction was sparged with molecular oxygen. After about 30 minutes of sparging, the reaction mixture returned to its blue-green color indicating a reoxidation of the Cu^0 occurred. The atmosphere was then replaced with Ar and irradiation persisted.
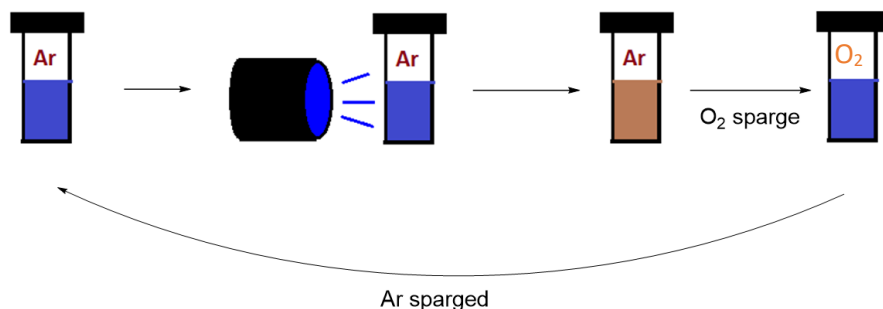
Figure 3.7: Cu-turnover with molecular O$_2$ in decarboxylative elimination

This process was first utilized with 33 mol% $Cu(OAc)_2$ and four re-oxidation cycles (Scheme 3.13). After four cycles of irradiation, **7a-Boc** was obtained in 71% yield and 69:31 *E:Z*. Thus, by employing this reoxidation process the $Cu(OAc)_2$ could be used substoichiometrically. However, when the $Cu(OAc)_2$ loading was further decreased to 10 mol% and seven irradiation cycles utilized, **7a-Boc** was only obtained in 29% yield (72:28 *E:Z*). Although $Cu(OAc)_2$ can be used catalytically, the operational simplicity and efficiency of this process is much lower than what can be accomplished when used stoichiometrically.
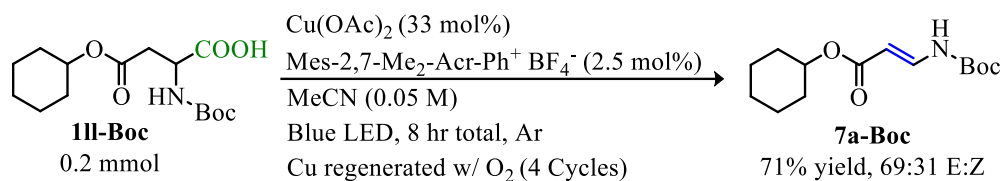

Scheme 3.13: Co-catalytic Cu/Acr$^+$ elimination with O_2 as the terminal oxidant

3.4 Conclusion

In conclusion, a photoinduced oxidative decarboxylation has been developed as a mild, inexpensive, and simple method for the generation of enamides from amino acids. The use of an acridinium photocatalyst replaces the need for toxic lead tetraacetate and allows the reaction to proceed using visible light as an economical and environmentally benign energy input. Moreover, the purification process is simple as the reaction does not produce any side products and the remaining reagents can be removed by simple filtration. Although a mix of *E/Z*-isomers results from a background photoisomerization, the isomers can be separated by column chromatography and the photoisomerization can be utilized for the enrichment of one isomer. This process offers an attractive route toward enamide and enecarbamate synthesis due to operational simplicity and high efficiency.

A drawback of this approach is the need for a terminal oxidant and thus this method operates under oxidative conditions. Around the time the photoredox-catalyzed Kochi decarboxylative elimination method described was reported, alternative photoredox-catalyzed decarboxylative elimination approaches began to emerge in the literature.[128] One such approach reported by Glorius[101a] also makes use of a Cu^{II} salt in conjunction with an organophotoredox catalyst, *N,N*-di(4-CF$_3$)phenyl dihydrophenazine, for the synthesis of alkenes from carboxylic acids (Scheme 3.15). However, this method makes use of redox-active esters in a reductive radical decarboxylation process detracting from the atom economy (see *Section 1.2.2* for discussion of redox-active esters in reductive decarboxylation). In addition, like the other decarboxylative elimination processes that have emerged recently, the Glorius method was not demonstrated to be a viable option for enamide synthesis.
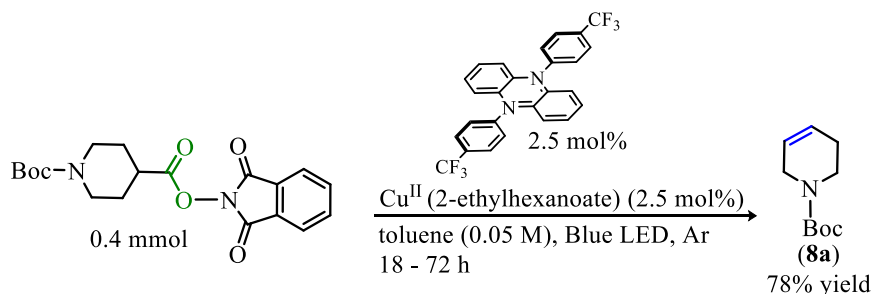
Scheme 3.14: Glorius decarboxylative elimination with redox-active esters

In an effort to maintain the high step and atom economy achieved when employing the direct decarboxylative approach while addressing the need for a terminal oxidant, this reaction was further investigated in the Tunge lab. An alternative dual-catalytic direct decarboxylative elimination was ultimately realized. The discovery of this complementary process is described in Chapter 5.

3.5 Experimental

3.5.1 General Considerations

Purification was accomplished with column chromatography using silica gel (60 Å porosity, 230 × 400 mesh, standard grade) which was purchased from Sorbent Technologies (catalog no. 30930M-25). TLC analysis was performed (fluorescence quenching and potassium permanganate acid stain) with silica gel HL TLC plates with UV254 purchased from Sorbent Technologies. Celite C212-500 (545 Filter Aid) was purchased from Fisher. 1 H and 13C NMR spectra were obtained on a Bruker ADVANCE 500 DRX equipped with a QNP cryoprobe. These spectra were referenced to residual protio solvent signals. HRMS data was obtained on an ESI LC-TOF Micromass LCT (Waters). HRMS data was collected using ESI mass spectrometry. Melting points were obtained with Digimelt MPA 160 SRS (no. 111278) and samples were loaded with borosilicate glass Kimble tube capillaries (no. 34505−9a). All *N*-protected amino acids apart from **1hh-Boc** and **1uu-Boc** were purchased and used without further purification. Photocatalysts Mes-Acr-Ph$^+$ BF$_4^-$ and Mes-2,7-Me$_2$-Mes-Acr-Ph$^+$ BF$_4^-$ were purchased from Sigma-Aldrich. Photocatalyst Mes-Acr-Me$^+$ ClO$_4^-$ was purchased from TCI. Anhydrous MeCN was purchased from Acros. Final decarboxylative elimination reactions were run in borosilicate glass Biotage microwave vials (Biotage no. 355631), with Biotage caps (Biotage no. 352298), and were sealed with crimper (no. 356671). Kessil H150 Blue LED grow lights provided 450 nm light. Reactions were run in the presence of 4 Å molecular sieves (3−5 mm beads) purchased from Alfa Aesar.

3.5.2 N-Boc Protection of Amino Acids

(tert-Butoxycarbonyl)leucine (**1uu-Boc**) was synthesized via boc-protection of leucine following literature procedure and NMR specra matched previously reported values.[129]

Synthesis of 2-((tert-Butoxycarbonyl)amino)-2-phenylbutanoic acid (**1h-Boc**). 2-Amino-2-phenylbutanoic acid (900 mg, 5.02 mmol) and K_2CO_3 (714 mg, 5.17 mmol) were added to a 100 mL flask equipped with magnetic stir bar. Then, H_2O (18 mL) was added and the solution stirred for 2 hours. The flask was then charged with a solution of Boc_2O (1.73 mL, 7.5 mmol) in THF (20 mL), and the reaction mixture was allowed to stir for approximately 14 hours. After, the reaction was refluxed for 2 days. Post reflux, the reaction was allowed to cool and the THF was removed *in vacuo*. To the aqueous solution, 10% NaOH was added until pH 12. The aqueous layer was then washed with DCM (∼10 mL, 2×) and acidified with citric acid until pH 3. The resulting solution was extracted with EtOAc (∼20 mL, 3×), washed with H_2O, dried with $MgSO_4$, and condensed. The white solid isolated was washed with hexanes and used without further purification. ^{1}H NMR (500 MHz, CD_3CN): δ [7.44, d, 2H], [7.36, t, 2H], [7.30, t, 1H], [6.18, broad s, 1H], [2.52−2.36, m, 2H], [1.37, s, 9H], [0.85, t, 3H]. $^{13}C\{^1H\}$ NMR (126 MHz, CD_3CN): δ 129.2, 128.5, 127.0, 80.2, 66.3, 28.4, 28.2, 8.7.

3.5.3 Acridinium-Catalyzed Kochi Decarboxylative Elimination

A microwave vial with stir bar was charged with amino acid (0.4 mmol, 1 equiv.), $Cu(OAc)_2$ (109 mg, 0.6 mmol, 1.5 equiv.), and Mes-2,7-Me_2-Acr-Ph$^+$ $^-BF_4$ (4.9 mg, 2.5 mol %). Anhydrous MeCN (8 mL) was added to the vial followed by the addition of microwave oven activated 4 Å molecular sieves. The vial was then sealed and sparged with argon for 5 minutes though the septa using a 20-gauge needle to bubble gas through the solvent and another needle to vent the vial. After the flask was sparged, the cap was wrapped with parafilm. The reaction was placed in front of a 450 nm 32 W blue LED light with no distance between the front of the light source and the glass wall of the reaction vessel for 14 hours. After irradiation, the reaction mixture

was filtered through a Celite plug using DCM as the wash solvent (~10 mL) to remove Cu salts. The filtrate was concentrated and purified via flash column chromatography on silica with 1:10−1:20 EtOAc:Hexanes.
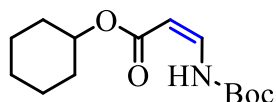

7a-Boc (KC-3-156)

^{1}H NMR (500 MHz, CD$_3$CN): *Z*-isomer (major): δ [9.58 (s, 1H)], [7.22 (dd, J = 11.71, 8.86 Hz, 1H)], [4.96 (d J = 8.96, 1H)], [4.76 (m, 1H)], [1.84 (m, 2H), 1.71 (m, 2H), 1.53 (m, 1H), 1.38 (m, 4H), 1.26 (m, 1H) Σ10], [1.47 (s, 9H)]. *E*-Isomer (minor): δ [7.95 (s, 1H)], [7.64 (dd, J = 14.07, 11.78 Hz, 1H)], [5.31 (d, J = 14.05 Hz, 1H)], [4.72 (m, 1H), 1.83 (m, 2H) 1.69 (m, 2H), 1.53 (m, 1H), 1.36 (m, 4H), 1.27 (m, 1H), Σ10], [1.44 (s, 9H)].

^{13}C{^{1}H} NMR (126 MHz, CD$_3$CN): *Z*-isomer: δ 169.4, 152.8, 141.2, 95.1, 82.6, 73.1, 32.2, 28.2, 26.0, 24.4. *E*-isomer: δ 167.6, 153.3, 140.8, 99.3, 82.3, 72.6, 32.4, 28.2, 26.1, 24.5.

IR (film): 3335, 2978, 2936, 2861, 1740, 1680, 1632, 1483, 1454, 1389, 1368, 1207, 1148, 1038, 1017, 970, 860 cm^{-1}.

HRMS (ESITOF) m/z: Calc'd for C$_{14}$H$_{23}$NO$_4$Na (M+Na)$^+$ 292.1525; Found = 292.1536.
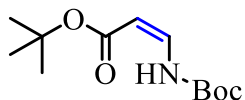
7b-Boc (KC-3-139)

^{1}H NMR (500 MHz, CD$_3$CN): *Z*-isomer (major): δ [9.61 (s, 1H)], [7.17 (dd, J = 11.65, 8.87 Hz, 1H)], [4.89 (d, J = 8.87, 1H)], [1.47 (s, 9H)], [1.45 (s, 9H)]. *E*-isomer (minor): δ [7.89 (s, 1H)], [7.56 (dd, J = 14.09, 11.75 Hz, 1H)], [5.25 (d, J = 14.05, 1H)], [1.45 (s, 9H)], [1.44 (s, 9H)].

^{13}C{^{1}H} NMR (126 MHz, CD$_3$CN): *Z*-isomer: δ 169.8, 152.9, 140.7, 96.3, 82.5, 81.2, 28.4, 28.2. *E*-isomer: δ 167.6, 153.1, 140.2, 100.6, 82.2, 80.0, 28.4, 28.2.

IR (film): 3337, 2978, 1740, 1678, 1632, 1481, 1381, 1368, 1238, 1219, 1146, 1055, 951, 872 cm^{-1}.

HRMS (ESI-TOF) m/z: Calc'd for C12H21NO4Na (M+Na)+ 266.1368; Found = 266.1368.
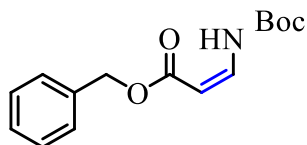
7c-Boc (KC-3-142)

^{1}H NMR (500 MHz, CD$_3$CN): Z-isomer: δ [9.54 (s, 1H)], [7.38 (d, 4H), 7.34 (m, 1H), Σ5H], [7.28 (dd, J = 11.81, 8.84 Hz, 1H)], [5.15 (s, 2H)], [5.05 (d, J = 8.88 Hz, 1H)], [1.48 (s, 9H)]. E-isomer: δ [8.02 (s, 1H)], [7.70 (dd, J = 14.02, 11.87 Hz, 1H)], [7.37 (d, 4H), 7.33 (m, 1H), Σ5H], [5.40 (d, J = 14.05, 1H)], [5.13 (s, 2H)], [1.45 (s, 9H)].

^{13}C{^{1}H} NMR (126 MHz, CD$_3$CN): Z-isomer: δ 169.7, 152.7, 142.0, 137.4, 129.5, 129.1, 94.1, 82.8, 66.4, 28.2. E-isomer: δ 168.0, 153.0, 141.5, 137.9, 129.4, 128.9, 98.3, 82.4, 66.2, 28.2.

IR (film): 3341, 2980, 2936, 1740, 1686, 1632, 1485, 1456, 1391, 1368, 1196, 1148, 1057, 976, 860 cm^{-1}.

HRMS (ESI-TOF) m/z: Calc'd for C$_{15}$H$_{19}$NO$_4$Na (M+Na)$^+$ 300.1212; Found = 300.1223.
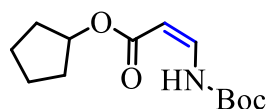
7d-Boc (KC-3-190)

^{1}H NMR (500 MHz, CD$_3$CN): Z-isomer: δ [9.58 (s, 1H)], [7.21 (dd, J = 11.68, 8.84 Hz, 1H)], [5.15 (m, 1H)], [4.94 (d, J= 8.86 Hz, 1H)], [1.87 (m, 2H), 1.67 (m, 6H), Σ8H], [1.47 (s, 9H)]. E-isomer: δ [7.95 (s, 1H)], [7.61 (dd, J = 14.09, 11.76 Hz, 1H)], [5.30 (d, J = 14.08 Hz, 1H)], [5.13 (m, 1H)], [1.84 (m, 2H), 1.66 (m, 6H), Σ5H], [1.45 (s, 9H)].

^{13}C{^{1}H} NMR (126 MHz, CD$_3$CN): Z-isomer: δ 169.8, 152.8, 141.2, 95.1, 82.6, 77.6, 33.3, 28.2, 24.4. E-isomer: δ 167.9, 153.1, 140.7, 99.3, 82.3, 77.1, 33.3, 28.2, 24.4.

IR (film): 3335, 2972, 2872, 1740, 1682, 1630, 1481, 1387, 1370, 1211, 1148, 1055, 1032, 974, 760 cm^{-1}.

HRMS (ESI-TOF) m/z: Calc'd for C$_{13}$H$_{21}$NO$_4$Na (M+Na)$^+$ 278.1368; Found = 278.1374.
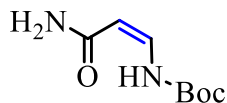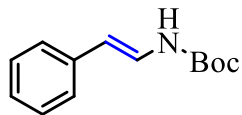

7e-Boc (KC-3-143)

^{1}H NMR (500 MHz, CD$_3$CN): δ [10.39 (s, 1H)], [7.06 (dd, J = 11.00, 8.76 Hz, 1H)], [6.10 (s, 1H), 5.57 (s, 1H), Σ2H], [4.99 (d, J = 8.79 Hz, 1H)], [1.45 (s, 9H)].

^{13}C{^{1}H} NMR (126 MHz, CD$_3$CN): δ 171.8, 153.2, 138.6, 97.0, 82.0, 28.2.

IR (film): 3630, 3366, 3279, 3090, 2261, 1728, 1668, 1630, 1595, 1391, 1267, 1221, 1157, 1036, 843 cm^{-1}.

HRMS (ESI-TOF) m/z: Calc'd for $C_8H_{14}N_2O_3Na$ (M+Na)$^+$ 209.0902; Found = 209.0898.

7f-Boc (KC-3-140)

^{1}H NMR (500 MHz, CD$_3$CN): Mix of E/Z isomers δ [7.54 (s, Σ1H)], [7.38−7.11 (m, Σ5H)], [7.17 (dd, J = 15.0, 10.0 Hz, maj.) and 6.60 (dd, J = 11.38, 9.81 Hz, min.), Σ1H], [6.01 (d, J = 14.69 Hz, maj.) and 5.55 (d, J = 9.78 Hz, min), Σ1H], [1.46 (s, Σ9H)].

^{13}C{^{1}H} NMR (126 MHz, CD$_3$CN): Mix of E/Z isomers δ 153.9, 138.0, 129.7, 129.5, 128.8, 127.3, 126.7, 125.9, 110.0, 80.8, 66.2, 28.4.

IR (film): 3630, 3538, 3368, 3277, 3090, 2980, 2936, 2261, 2114, 1944, 1881, 1701, 1483, 1451, 1370, 1153, 1101, 1030 cm^{-1}.

HRMS (ESI-TOF) m/z: Calc'd for $C_{13}H_{17}NO_2Na$ (M +Na)$^+$ 242.1157; Found = 242.1156.
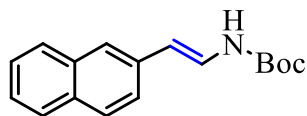
7g-Boc (KC-3-145)

^{1}H NMR (500 MHz, CD$_3$CN): *E*-isomer: δ [7.79 (m, 3H), 7.67 (m, 1H), 7.57 (dd, 1H), 7.42 (dddd, 2H), Σ7H], [7.33 (dd, J = 14.65, 10.68 Hz, 1H)], [6.17 (d, J = 14.70 Hz, 1H)], [1.48 (s, 9H)]. *Z*-isomer: δ [7.85 (ddd, 3H), 7.80 (m, 1H), 7.49 (m, 2H), 7.42 (dd, 1H), Σ7H], [6.70 (dd, J = 11.39, 9.77 Hz, 1H)], [5.69 (d, J = 9.85, 1H)], [1.47 (s, 9H)].

^{13}C{^{1}H} NMR (126 MHz, CD$_3$CN): *E*-isomer: δ 135.7, 134.8, 133.0, 129.4, 129.0, 128.4, 127.2, 126.1, 124.6, 124.6, 124.0, 110.1, 28.4. *Z*-isomer: δ 129.9, 129.1, 128.6, 128.4, 127.6, 127.2, 127.0, 126.7, 28.3.

IR (film): 3630, 3538, 3368, 3279, 3090, 2980, 2261, 2114, 1709, 1695, 1655, 1628, 1508, 1370, 1157, 1030, 858, 847 cm^{-1}.

HRMS (ESI-TOF) m/z: Calc'd for $C_{17}H_{19}NO_2Na$ (M+Na)$^+$ 292.1313; Found 292.1300.
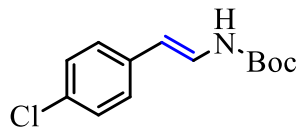
7h-Boc (KC-3-146)

^{1}H NMR (500 MHz, CD$_3$CN): Mix of E/Z isomers δ [7.58 (m Σ1H)], [7.37− 7.23 (m, Σ4H)], [7.18 (dd, J = 14.71, 10.65 Hz, maj.) and 6.62 (dd, J = 11.40, 9.83 Hz, min.) Σ1H], [5.98 (d, J = 14.70 Hz, maj.) and 5.51 (d, J = 9.83, min.), Σ1H], [1.45 (s, -Σ9H)].

^{13}C{^{1}H} NMR (126 MHz, CD$_3$CN): Mix of E/Z isomers δ 153.8, 137.0, 131.47, 129.4, 127.4, 126.6, 108.7, 81.0, 28.3.

IR (film): 3621, 3538, 3368, 3090, 2359, 2340, 2261, 2116, 1944, 1883, 1719, 1701, 1657, 1508, 1489, 1370, 1192, 1159, 1091, 1030, 843 cm^{-1}.

HRMS (ESI-TOF) m/z: Calc'd for C$_{14}$H$_{16}$N$_2$O$_2$Na (M+Na)$^+$ 267.1109; Found 267.1123.
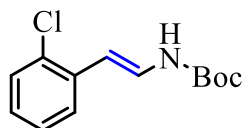
7i-Boc (KC-3-188)

^{1}H NMR (500 MHz, CD$_3$CN): δ [7.70 (s, Σ1H)], [7.56 (d) and 7.47 (ddd) and 7.38 (dd) and 7.34 (dd) and 7.20 (m) and 7.16 (td), Σ4H], [7.21 (m, maj.) and 6.77 (dd, J = 11.52, 9.67 Hz, min.), Σ1H], [6.40 (d, J = 14.65 Hz, maj.) and 5.64 (d, J = 9.69 Hz, min.), Σ1H], [1.49 (s, Σ9H)].

^{13}C{^{1}H} NMR (126 MHz, CD$_3$CN): Mix of E/Z isomers δ 153.8, 135.8, 132.1, 130.8, 130.5, 130.4, 129.1, 128.1, 128.0, 126.3, 105.8, 81.1, 28.3.

IR (film): 3304, 2978, 1701, 1653, 1508, 1466, 1368, 1316, 1273, 1246, 1155, 1055, 1034, 716 cm^{-1}.

HRMS (ESI-TOF) m/z: Calc'd for C$_{13}$H$_{16}$ClNO$_2$Na (M+Na)$^+$ 276.0767; Found 276.0778.
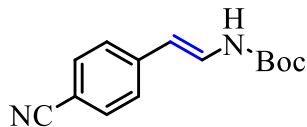
7j-Boc (KC-3-189)

^{1}H NMR (500 MHz, CD$_3$CN): *E*-isomer: δ [7.57 (d, 2H)], [7.46 (d, 2H)], [7.36 (dd, J = 14.65, 10.88 Hz, 1H)], [6.02 (d, J = 14.61 Hz, 1H)], [1.46 (s, 9H)]. *Z*-isomer: δ [7.67 (d, 2H)], [7.44 (d, 2H)], [6.73 (dd, J = 11.56, 9.85 Hz, 1H)], [5.55 (d, J = 9.83, 1H)], [1.46 (s, 9H).

^{13}C{^{1}H} NMR (126 MHz, CD$_3$CN): *E*-isomer: δ 153.6, 143.3, 133.3, 129.3, 126.3, 120.0, 109.1, 108.3, 81.3, 28.3. Z isomer: δ 153.9, 142.0, 133.4, 129.4, 127.1, 119.8, 109.9, 106.1, 81.5, 28.2.

IR (film): 3323, 2978, 2226, 1728, 1715, 1653, 1603, 1479, 1395, 1368, 1260, 1236, 1155, 1055, 1024, 764, 750 cm^{-1}.

HRMS (ESI-TOF) m/z: Calc'd for $C_{14}H_{16}N_2O_2Na$ (M+Na)$^+$ 267.1109; Found 267.1123.
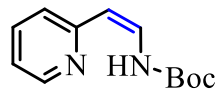
7k-Boc (KC-3-183)

^{1}H NMR (500 MHz, CD$_3$CN): δ [11.1 (s, 1H)], [8.50 (ddd, 1H), 7.68 (td, 1H), 7.15 (d, 1H), 7.10 (ddd, 1H), Σ4H], [6.95 (t, J = 9.95 Hz, 1H)], [5.53 (d, J = 9.14 Hz, 1H)], [1.49 (s, 9H)].

^{13}C{^{1}H} NMR (126 MHz, CD$_3$CN): δ 158.7, 153.8, 148.9, 137.8, 130.4, 123.9, 121.1, 104.1, 81.4, 28.4.

IR (film): 2979, 1724, 1648, 1592, 1557, 1472, 1392, 1368, 1272, 1224, 1148, 1050, 1024, 863 cm^{-1}.

HRMS (ESITOF) m/z: Calc'd for $C_{12}H_{16}N_2O_2Na$ (M+Na)$^+$ 243.1109; Found = 243.1113.
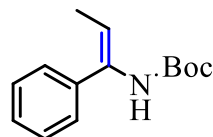
7l-Boc (KC-3-252)

^{1}H NMR (500 MHz, CD$_3$CN): Mix of E/Z isomers δ [7.41−7.24 (m, Σ5H)], [6.70 (broad d), Σ1H], [5.76 (broad s), Σ1H], [1.69 (dd, Σ3H)], [1.37 (broad d, Σ9H)].

^{13}C{^{1}H} NMR (126 MHz, CD$_3$CN): Mix of E/Z isomers δ 154.6, 129.6, 129.2, 129.0, 128.5, 128.2, 126.3, 79.8, 28.4, 13.8, 13.6.

IR (film): 2978, 2931, 2262, 1698, 1654, 1492, 1446, 1366, 1242, 1164, 1164, 1089, 1043, 1031 cm^{-1}.

HRMS (ESI-TOF) m/z: Calc'd for $C_{14}H_{19}NO_2Na$ (M+Na)$^+$ 256.1313; Found = 256.1321.
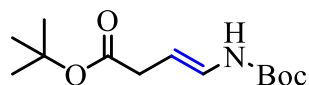
7m-Boc (KC-3-151)

^{1}H NMR (500 MHz, CD$_3$CN): Mix of E/Z isomers δ [7.24 (s, Σ1H)], [6.43 (dd, J = 14.40, 10.51 Hz, Σ1H)], [5.04 (dt, J = 14.08, 7.12 Hz, maj.) and 4.65 (q, J = 7.86 Hz, min.), Σ1H], [2.91 (dd) and 2.87 (dd), Σ2H], [1.43 (s) and 1.42 (s), Σ18H].

^{13}C{^{1}H} NMR (126 MHz, CD$_3$CN): Mix of E/Z isomers δ 172.3, 171.7, 153.9, 127.5, 126.0, 102.7, 100.6, 81.3, 80.9, 80.7, 80.4, 36.9, 33.4, 28.4, 28.2.

IR (film): 3337, 2978, 2934, 2359, 2261, 1726, 1713, 1608, 1508, 1456, 1393, 1368, 1290, 1244, 1147, 1069, 1045, 1018, 951, 866, 843 cm^{-1}.

HRMS (ESI-TOF) m/z: Calc'd for $C_{13}H_{23}NO_4Na$ (M+Na)$^+$ 280.1525; Found = 280.1535.
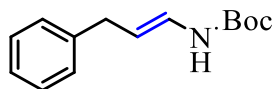
7n-Boc (KC-3-147)

^{1}H NMR (500 MHz, CD$_3$CN): Mix of E/Z isomers δ [7.33−7.14 (m, Σ5H)], [6.43 (dd, J = 14.01, 10.93 Hz, Σ1H], [5.16 (dt, J = 14.51, 7.25 Hz, maj.) and 4.70 (q, J = 8.16 Hz, min.), Σ1H], [3.34 (d) and 3.29 (d), Σ2H], [1.45 (s) and 1.42 (s), Σ9H].

^{13}C{^{1}H} NMR (126 MHz, CD$_3$CN): Mix of E/Z isomers δ 153.9, 142.4, 141.9, 129.4, 129.3, 129.2, 129.0, 126.8, 125.9, 123.9, 109.4, 107.6, 80.2, 36.5, 32.2, 28.4.

IR (film): 3621, 3530, 3366, 3090, 2261, 1944, 1881, 1719, 1676, 1495, 1452, 1368, 1236, 1163, 1042 cm^{-1}.

HRMS (ESI-TOF) m/z: Calc'd for $C_{14}H_{19}NO_2Na$ (M+Na)$^+$ 256.1313; Found = 256.1303.
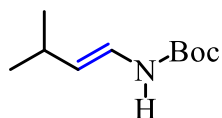
7o-Boc (KC-3-155)

^{1}H NMR (500 MHz, CD$_3$CN): Mix of E/Z isomers δ [7.00 (s, Σ1H)], [6.32 (dd, J = 14.09, 10.68 Hz, maj.) and 6.21 (t, J = 10.05 Hz, min.), Σ1H], [5.00 (dd, J = 14.32, 7.09 Hz, maj.) and 4.38 (t, J = 9.34 Hz, min.), Σ1H], [2.49 (m, min.) and 2.25 (m, maj.), Σ1H], [1.44 (s) and 1.42 (s), Σ9H], [0.96 (d, maj.) and 0.93 (d, min.), Σ6H].

^{13}C{^{1}H} NMR (126 MHz, CD$_3$CN): Mix of E/Z isomers δ 154.1, 122.8, 117.8, 80.1, 29.7, 28.5, 23.4.

IR (film): 3621, 3530, 3366, 3279, 3090, 2261, 1944, 1881, 1719, 1676, 1494, 1452, 1368, 1236, 1163, 1042 cm^{-1}.

HRMS (ESI-TOF) m/z: Calc'd for $C_{10}H_{19}NO_2Na$ (M+Na)$^+$ 208.1313; Found = 208.1323.
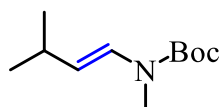
7p-Boc (KC-3-247)

^{1}H NMR (500 MHz, CD$_3$CN): δ [6.87 (broad s, Σ1H)], [4.82 (broad s, Σ1H)], [2.92 (s, Σ3H)], [2.33 (broad s, Σ1H)], [1.46 (s, Σ9H)], [0.99 (d, Σ6H)].

^{13}C{^{1}H} NMR (126 MHz, CD$_3$CN): δ 127.3, 116.7, 81.2, 30.3, 28.4, 23.9.

IR (film): 3105, 2959, 2930, 2862, 2358, 2278, 2138, 2083, 1701, 1654, 1388, 1367, 1326, 1150 cm^{-1}.

HRMS (ESI-TOF) m/z: Calc'd for $C_{11}H_{22}NO_2Na$ (M+Na)$^+$ 223.1548; Found = 223.1560.
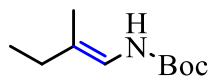
7q-Boc (KC-3-149)

^{1}H NMR (500 MHz, CD$_3$CN): Mix of E/Z isomers δ [6.68 (s, Σ1H)], [6.15 (d, maj.) and 6.10 (d, min.), Σ1H], [1.97 (m, Σ2H)], [1.63 (d, maj.) and 1.55 (d, min.), Σ3H], [1.43 (s, Σ9H)], [0.97 (t, maj.) and 0.94 (t, min.), CH3CH2−, Σ3H]

^{13}C{^{1}H} NMR (126 MHz, CD$_3$CN): Mix of E/Z isomers δ 154.3, 79.9, 30.1, 28.4, 24.0, 19.7, 14.6, 13.3, 12.3.

IR (film): 2978, 2937, 1701, 1497, 1368, 1153, 1051, 809 cm^{-1}.

HRMS (ESI-TOF) m/z: Calc'd for $C_{10}H_{19}NO_2Na$ (M+Na)$^+$ 208.1313; Found = 208.1340.
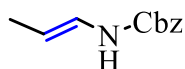
7r-Cbz (KC-3-158)

^{1}H NMR (500 MHz, CD$_3$CN): Mix of E/Z isomers δ [7.47−7.26 (m, Σ5H), [6.40 (m, Σ1H)], [5.11 (m, Σ2H)], [5.11 (m, maj.) and 4.67 (p, min.), Σ1H], [1.62 (dd, Σ3H)].

^{13}C{^{1}H} NMR (126 MHz, CD$_3$CN): Mix of E/Z isomers δ 155.0, 154.6, 137.9, 129.4, 128.9, 128.7, 125.4, 124.1, 106.2, 104.5, 167.3, 167.1, 14.9, 11.1.

IR (film): 3312, 3065, 3032, 2857, 1703, 1682, 1518, 1454, 1294, 1234, 1116, 1028, 947 cm^{-1}.

HRMS (ESI-TOF) m/z: Calc'd for $C_{11}H_{13}NO_2Na$ (M+Na)$^+$ 214.0844; Found = 214.0854.
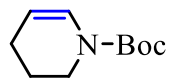
7s-Boc (KC-3-169)

^{1}H NMR (500 MHz, CD$_3$CN): δ [6.74 (dd, 1H)], [4.84 (d, 1H)], [3.50 (s, 2H)], [1.99 (m, 2H)], [1.77 (m, 2H)], [1.44 (s, 9H)].

^{13}C{^{1}H} NMR (126 MHz, CD$_3$CN): δ 153.4, 152.9, 126.4, 125.9, 106.6, 106.0, 80.9, 43.3, 42.2, 28.4, 22.5.

IR (film): 3458, 2976, 2934, 1697, 1651, 1406, 1368, 1302, 1254, 1234, 1167, 1115, 1072, 1053, 993, 878 cm^{-1}.

HRMS (ESITOF) m/z: Calc'd for $C_{10}H_{16}NO_2$ (M-H) 182.1181; Found = 182.1184.
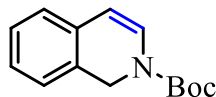
7t-Boc (KC-3-169)

Product matched previously reported specifications.[129]

^{1}H NMR (500 MHz, CD$_3$CN): δ 6.97-6.75 (m, 4H), 6.66 (broad s, 1H), 5.52 (broad s, 1H), 4.53 (s, 2H), 1.26 (broad s, 9H).

^{13}C{^{1}H} NMR (126 MHz, CD$_3$CN): δ 194.0, 132.3, 130.0, 128.6, 127.7, 126.7, 125.2, 82.1, 45.5, 28.6.
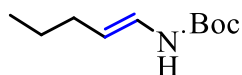
7u-Boc (KC-3-159)

^{1}H NMR (500 MHz, CD$_3$CN): δ [7.08 (s, maj.) and 6.96 (s, min.), Σ1H], [6.34 (m, Σ1H)], [5.00 (dt, J = 14.34, 7.20 Hz, maj.) and 5.12 (q, J = 7.99 Hz, min.), Σ1H], [1.94 (m, Σ2H), *overlaps with CH$_3$CN*], [1.43 (s) and 1.41 (s), Σ9H], [1.35 (m, Σ2H)], [0.90 (t) and 0.87 (t), Σ3H].

^{13}C{^{1}H} NMR (126 MHz, CD$_3$CN): Mix of E/Z isomers δ 154.0, 124.9, 123.2, 110.3, 109.1, 80.0, 32.5, 28.4, 24.0, 23.4, 13.8.

IR (film): 3327, 2961, 2930, 2872, 1701, 1676, 1508, 1452, 1368, 1242, 1165, 1047, 1022, 951 cm^{-1}.

HRMS (ESI-TOF) m/z: Calc'd for C$_{10}$H$_{19}$NO$_2$Na (M+Na)$^+$ 208.1313; Found = 208.1311.
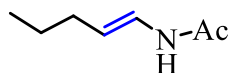
7u-Ac (KC-3-160)

^{1}H NMR (500 MHz, CD$_3$CN): δ [8.07 (s) and 7.89 (s), Σ1H], [6.62 (m, maj.) and 6.58 (m, min.), Σ1H], [5.15 (dt, J = 14.43, 7.23 Hz, maj.) and 4.64 (dt, J = 9.15, 7.64 Hz, min), Σ1H], [2.05−1.96 (m, Σ2H)], [1.96 (s) and 1.88 (s), Σ3H], [1.37 (m, Σ2H)], [0.92 (t) and 0.87 (t), Σ3H].

^{13}C{^{1}H} NMR (126 MHz, CD$_3$CN): Mix of E/Z isomers δ 168.5, 167.9, 123.9, 122.0, 112.4, 111.2, 32.5, 28.4, 23.8, 23.4, 22.9, 13.8.

IR (film): 3279, 3200, 3063, 2959, 2928, 2872, 1657, 1528, 1460, 1437, 1371, 1302, 1282, 1172, 1038, 955 cm^{-1}.

HRMS (ESITOF) m/z: Calc'd for C$_7$H$_{13}$NONa (M+Na)$^+$ 150.0895; Found = 150.0888.
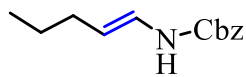
7u-Cbz (KC-3-158)

^{1}H NMR (500 MHz, CD$_3$CN): δ [7.45−7.29 (m, Σ5H)], [6.38 (m, Σ1H)], [5.10 (m, Σ2H)], [5.09 (m, maj.) and 4.60 (q, J = 7.99 Hz, min), Σ1H], [1.96 (m, Σ2H)], [1.35 (m, Σ2H)], [0.89 (t) and 0.87 (t), Σ3H].

^{13}C{^{1}H} NMR (126 MHz, CD$_3$CN): Mix of E/Z isomers δ 155.0, 154.6, 137.9, 129.4, 128.9, 128.7, 124.8, 123.1, 111.5, 110.4, 67.1, 32.4, 28.4, 23.9, 23.4, 13.8.

IR (film): 2963, 2123, 1714, 1679, 1521, 1237, 1051, 831 cm^{-1}.

HRMS (ESI-TOF) m/z: Calc'd for C$_{13}$H$_{17}$NO$_2$Na (M+Na)$^+$ 242.1157; Found = 242.1149.
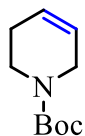
8a (KC-3-098)

Product matches previously reported literature specification.[101a]

^{1}H NMR (500 MHz, CD$_3$CN): δ 5.82 (dtd, 1H), 5.67 (m, 1H), 3.83 (t, 2H), 3.44 (t, 2H), 2.08 (tdtd, 2H), 1.43 (s, 9H).
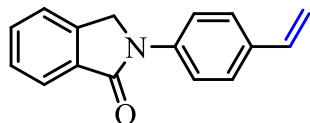
8b (KC-3-121)

Product matches previously reported literature specification.[131]

^{1}H NMR (500 MHz, CD$_3$CN): δ 7.94–7.87 (m, 2H), 7.84–7.77 (m, 1H), 7.65–7.62 (m, 2H), 7.59–7.49 (m, 3H), 6.76 (dd, 1H), 5.78 (dd, 1H), 5.23 (dd, 1H), 4.92 (s, 2H).
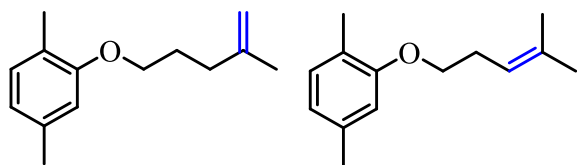
8c (KC-3-122)

Product matches previously reported literature specification.[101a]

^{1}H NMR (500 MHz, CD$_3$CN): δ 6.99 (dd, ∑1H), 6.75–6.68 (m, ∑1H), 6.68–6.59 (m, ∑1H), [5.25 (tdt) & 4.77–4.69 (m), ∑3H], 3.94 (dt, ∑2H), [3.42 (q) & 2.45 (tdd), ∑2H], [2.27 (s) & 2.11 (s) & 1.75 (s), ∑6H], 2.25–2.17 (m, maj., 2H), 1.94– 1.84 (m, maj., 2H), 1.72 (s, min. 3H), 1.66 (s, min., 3H), 1.12 (t, ∑3H).

Chapter 4: Photoredox/Cobaloxime Dual Catalysis in Small Molecule Functionalization[132]

4.1 Introduction

A significant ambition in catalysis is the growth of methods that achieve C–C and C–heteroatom linkages in a green and sustainable way.[133] Ideally, the protocol should be of low cost and produce minimal waste whilst maintaining high chemoselectivity.[18] One general strategy that has emerged to address this challenge is photoredox/transition metal dual-catalysis which allows for substrate activation and functionalization under relatively mild conditions while mostly reducing the cost/toxicity associated with traditional methods.[134] A subset of this reaction category involves the use of photoredox dual catalysis with dehydrogenative and cross-dehydrogenative couplings in an effort to progress towards the highly efficient but green method aspiration.[135] Traditional methods to achieve the same transformations typically employ a stoichiometric oxidant, elevated temperatures, and often exhibit poor chemoselectivity. The recent dual catalytic approaches have bypassed the need for a stoichiometric oxidant and have achieved high efficiency and selectivity via pairing a photosensitizer with a catalyst that is capable of proton reduction and ultimately producing H_2 as a traceless byproduct. Herein, the history, scope, limitations, and advantages of these recently reported strategies as well as mechanistic evaluations based on literature reported observations are described.

4.2 Cobaloximes in Photoredox-Driven Hydrogen Evolution

Inspiration for the oxidant-free dehydrogenative strategies in synthesis arises from the plethora of research in artificial photosynthesis,[136] light-driven water splitting,[137] and hydrogen production from acidic media[138]. These developments have been of interest to the scientific community due to their relevance in solar energy conversion.[139] The photocatalytic processes

established for these systems typically consist of 1) a photosensitizer, 2) a catalyst capable of promoting electron transfer, and 3) a sacrificial electron donor. A variety of chromophores have been employed in H_2 producing reactions including Pt-, Zn-, Ir-, and Ru-based photosensitizers as well as organic dyes such as Eosin Y and Rose Bengal.[140] A common choice for the electron relay catalysts, that has become of interest to the synthetic community, is a class of catalyst produced to mimic the reactivity of vitamin B12 called the cobaloximes.[141] Cobaloximes can participate in either a direct oxidative quenching or indirect reductive quenching event when paired with a photosensitizer and an electron donor (Scheme 4.1, also see *Section 1.1* for discussion of photoredox catalyzed pathways).[142]
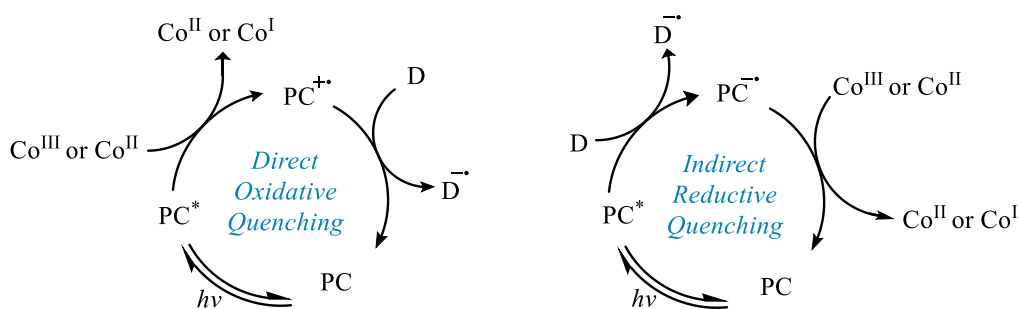
Scheme 4.1: Cobaloxime reduction in photoredox catalysis

The quintessential cobaloxime, Co(dmgH)$_2$ClPy (dmg = dimethylglyoxime), was first used for electrocatalytic H_2 production, but has since emerged in numerous photocatalytic H_2 production strategies.[143] There are several different pathways towards proton reduction that cobaloxime catalysts are proposed to follow.[141d,144] Generally, the first step involves a single electron reduction of the initial Co^{III} to Co^{II} (Scheme 4.1; equations 1 & 2). Next, the Co^{II} can become Co^{III}–H via either proton-coupled electron transfer (PCET) or through a single electron reduction of Co^{II} to an anionic Co^I followed by protonation (equations 1 & 2). The generation of this hydride intermediate is a common, but crucial step. However, the nature of this hydride is currently under debate.[145] From this key Co^{III}–H intermediate, H_2 production can be facilitated either via protonation of the

Co^{III}–H (equation 3), or via the single electron reduction of Co^{III}–H to Co^{II}–H followed by protonation (equations 4-6). A bimetallic pathway between two Co^{III}–H to generate H$_2$ and two Co^{II} complexes is also possible (equation 7).[146] The preferred pathway is thus dependent on the potentials of the photosensitizer used as well as the pH of the reaction matrix.[147] Regardless of the specific details of the mechanism, the photoredox/cobaloxime dual catalytic systems utilize light energy to obtain reduced cobalt species that presumably can allow access to the vital Co^{III}–H intermediate (equations 1 & 2).

Hydrogen Atom Transfer (HAT) Pathways:

$$Co^{III} + e^- \longrightarrow Co^{II} + e^- \longrightarrow \overset{\ominus}{Co}{}^{I} + HA \longrightarrow Co^{III}\text{–}H \qquad (1)$$

$$Co^{III} + e^- \longrightarrow Co^{II} + H^{\bullet} \longrightarrow Co^{III}\text{–}H \qquad (2)$$
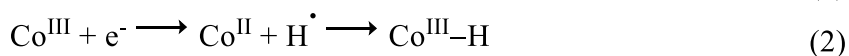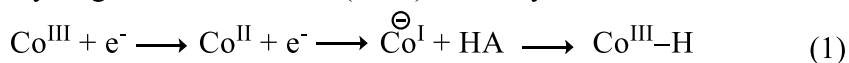
Hydrogen Evolution (HE) Pathways:

$$Co^{III}\text{–}H + HA \longrightarrow \overset{\oplus}{Co}{}^{III} + H_2 + A^{\ominus} \qquad (3)$$

$$Co^{III}\text{–}H + e^- \longrightarrow Co^{II}\text{–}H \qquad (4)$$

$$Co^{III}\text{–}H + \overset{\ominus}{Co}{}^{I} \longrightarrow Co^{II}\text{–}H \qquad (5)$$

$$Co^{II}\overset{\bullet-}{\text{–}}H + HA \longrightarrow Co^{II} + H_2 + A^{\ominus} \qquad (6)$$

$$Co^{II}\overset{\bullet-}{\text{–}}H + Co^{II}\overset{\bullet-}{\text{–}}H \longrightarrow 2(Co^{II}) + H_2 \qquad (7)$$
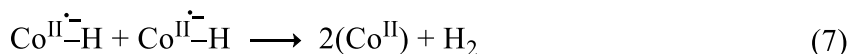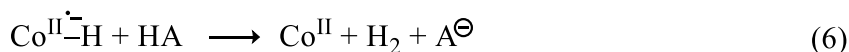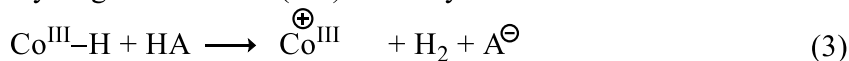
4.3 Merging Photoredox Catalysis and Cobaloxime Hydrogen Evolution Catalysis in Small Molecule Functionalization

Historically, hydrogen evolution using cobaloximes is made possible through intermediary cobalt hydrides (Co–H) generated from acid/water. Thus, translation of the fundamental chemistry of hydrogen evolution to organic synthesis could be achieved by the generation of identical cobalt hydrides from organic intermediates. In fact, it is well-established that, in the presence of an alkyl

radical intermediate, cobaloxime catalysts reversibly form Co^{III}–H and an olefin through a hydrogen atom transfer (HAT) reaction (Scheme 4.2A).[145,147] Through orchestrating a process in which the organic substrate and the cobaloxime can be activated by a photosensitizer, the proton reduction chemistry could provide access to highly useful products and synthetic intermediates while avoiding the need for a sacrificial electron donor utilized in hydrogen production (Scheme 4.1).

In 2014–2015, coupling the use of a photochemically-promoted cobaloxime-facilitated HAT with hydrogen evolution (HE) emerged as a viable strategy to achieve radical dehydrogenation without the need of a stoichiometric oxidant (Scheme 4.2B).[148] Over the past several years, this photoredox/cobalt dual catalytic strategy has been employed in a variety of small-molecule functionalizations. These new chemical methods that operate with a high degree of chemoselectivity, mild and oxidant-free conditions, and often producing hydrogen gas as sole by-product.

A. Reversible HAT with olefins and cobalt hydride
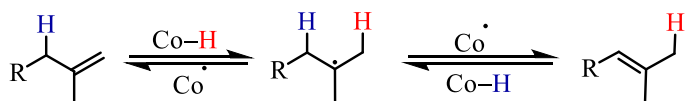
B. Photocatalyst-facilitated cobaloxime HAT/HE sequence
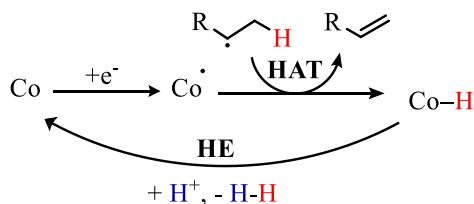
Scheme 4.2: Cobaloximes in alkene formation

4.3.1 Mechanistic Considerations: Cobaloxime Structure and Catalytically Relevant Species

In order to achieve the HAT/HE sequence in any given photoredox/cobaloxime dual catalytic system, the cobaloxime structure and its reactive intermediates must be defined. The cobaloximes employed are octahedral complexes containing an equatorial ligand system made up of two dioxime ligands connected either by hydrogen bonding or through BF_2 bridges (Figure 4.1). The north-facing axial orbital in these precatalysts is typically occupied by a halide. The south axial orbital is commonly occupied by a nitrogen base ligand, like pyridine, but can also be occupied by other bases or halides.
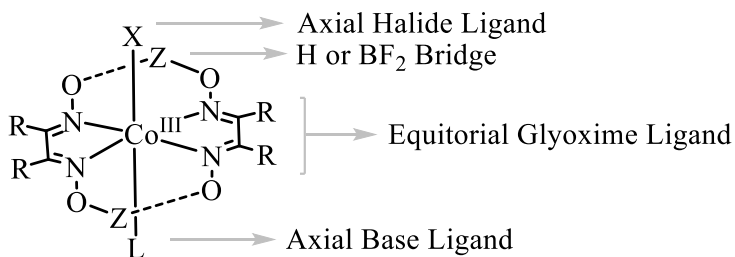
Figure 4.1: Cobaloxime anatomy

For clarity, the structures of common hypothetical intermediates for the cobaloxime catalyst are pictured (Figure 4.2). As discussed, the HE processes are expected to pass through the key Co^{III}–H (**B**) intermediate. There are two commonly suggested paths for the formation of this cobalt hydride. First, a single electron reduction of Co^{III} (**A**) produces Co^{II} (**C**) (equation 1& 2). This process is facile as even weakly reducing photosensitizers can facilitate this process. The resulting Co^{II} complex **C** can then abstract a hydrogen atom through concerted PCET (equation 2). Alternatively, if a strongly reducing photosensitizer is used, complex **C** can get further reduced to anionic Co^{I} (**E**). Protonation of this intermediate achieves the formation of the key Co^{III}–H (**B**) species (equation 1).[146] Both pathways involve a net hydrogen atom transfer thus, the term HAT is used to encompasses both possibilities.
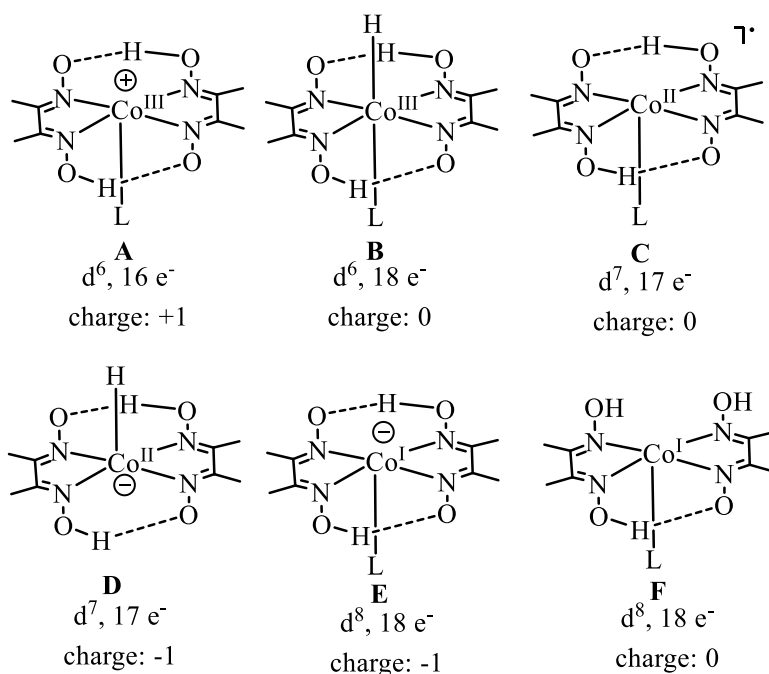
Figure 4.2: Commonly proposed cobaloxime intermediates

To determine the preferred sequence of events (equation 1 vs. 2) for the formation of cobalt hydride, the $Co^{II/I}$ (**C/E**) reduction potentials must be considered. Additionally, attention must be given to the pH of the media and the pK_a values of acidic components, including Co^{III}–H (**B**). Finally, while Co^{III}–H (**B**) is assumed to be the reactive species in solution, it has been suggested that this hydride tautomerizes to a Co^{I}(dmgH)(dmgH$_2$)L (**F**), further complicating interpretation of the cobalt speciation during catalysis.[145b]

After formation of Co^{III}–H (**B**), hydrogen evolution (HE) can occur through one of three pathways. The bimetallic hydrogen evolution resulting from reaction of two Co^{III} hydrides is generally slower than heterolytic pathways (equation 7).[146] Therefore, it is more common for the HE event to occur through protonation of Co^{III}–H (**B**) (equation 3) or via single electron reduction of Co^{III}–H to Co^{II}–H (**D**) followed by protonation (equation 4 & 6). To assess each possibility, the reduction potential of Co^{III}–H (**B**) and the basicities of Co^{III}–H (**B**) vs. Co^{II}–H (**C**) are crucial considerations. These properties are largely dependent on the electronic and steric attributes of the

axial ligand.[141d] Thus, changes in these ligands also influence the rate of HE. For example, the rate of HE has been observed to increase with electron-deficient axial ligands however, these complexes are less stable than the analogous electron-rich derivatives.[149] Ultimately, higher TONs are achieved with more stable cobaloximes that bear electron-donating ligands.[149]

The HE pathway and its efficiency is also influenced by the pH of the medium.[140g,150] The pH dependence is largely attributed to the ability to protonate cobalt hydride and release H_2. To this end, it is important to note that 1) the pK_a of the metal hydride tracks with Co^I bascicity[151] and increases as the $Co^{II/I}$ potentials become more negative, and 2) as the pK_a of the acidic proton increases, the acid's reduction potential (HA/H_2) will become more negative.[152] Lastly, the HE event can be influenced by solvent effects which are reported to be artifacts of differing solvent coordination and ability to stabilize different protonation states of cobaloxime intermediates.[153] To aid in the evaluation of HAT/HE methods, the potentials and pK_a values of common cobaloxime species as well as common photosensitizers have been compiled (Figure 4.3).

Co(dmgH)(dmgH₂)Cl₂
Co(III)/(II): -0.49 V[144]
Co(II)/(I): -0.80 V[144]

Co(dmgBF₂)₂(CH₃CN)₂
Co(III)/(II): 0.2 V[144]
Co(II)/(I): -0.55 V[144]
Co(III)-H/Co(II)-H: -1.10 V[144]
Co(I)-H pKa: 13.4[154c]
Co(II)-H pKa: 23.0

Co(dmgH)₂ClPy
Co(III)/(II): -0.68 V[144]
Co(II)/(I): -1.13 V[144]
Co(III)-H pKa: 7.7[154b]

Co(dmgH)₂Cl(DMAP)
Co(III)/(II): -0.84 V[144]
Co(II)/(I): -1.13 V[144]

Co(dmgH)₂Cl(4-OMe-Py)
Co(III)/(II): -0.78 V[144]
Co(II)/(I): -1.09 V[144]

Ru(bpy)₃Cl₂
$E^{II*/I}$: +0.77 V[154d,e]
$E^{III/II}$: +1.29 V[154d,e]
$E^{III/II}$: -0.81 V[154d,e]

Ir[dF(CF₃)ppy]₂(dtbpy)PF₆
$E^{III*/IV}$: -0.89 V[154d,e]
$E^{III*/II}$: +1.21 V[154d,e]
$E^{IV/III}$: +1.69 V[154d,e]
$E^{II/III}$: -1.37 V[154d,e]

Eosin Y
$E_{1/2}(P*/P^-)$: +0.83 V[154i,j]
$E_{1/2}(P*/P^+)$: -1.11 V[154i,j]
$E_{1/2}(P^-/P)$: -1.06 V[154i,j]
$E_{1/2}(P/P^+)$: +0.78 V[154i,j]

Mes-Acr-Me⁺
$E_{1/2}(P*/P^-)$: +2.06 V[154f,g,h]
$E_{1/2}(P^-/P)$: -0.57 V[154f,g,h]

QuH⁺ (R = H)
$E_{1/2}(P*/P')$: +2.46 V[154k]
QuCN⁺ (R = CN)
$E_{1/2}(P*/P')$: +2.72 V[154k,l]
$E_{1/2}(P'/P^+)$: -0.60 V[154k,l]

Figure 4.3: Catalysts commonly paired in photocatalytic H₂ evolution

4.3.2 Photoredox/Cobaloxime Catalysis in Alkene Synthesis

One of the initial reports of a HAT/HE sequence in small-molecule functionalization was Sorensen's acceptorless dehydrogenation (Scheme 4.3).[155] This reaction employed the tetrabutylammonium decatungstate photocatalyst to perform hydrogen atom abstraction of inactivated C–H bonds to provide aliphatic radical intermediates.[156] The C–H bond adjacent to the radical is weakened (<40 $^{kcal}/_{mol}$) and thus activated for cobaloxime-facilitated hydrogen atom abstraction.[157] This second HAT forms the desired olefin and two metal species that are capable of combining to release hydrogen.

A. Acceptorless Dehydrogenation of Cyclooctane

19% yield
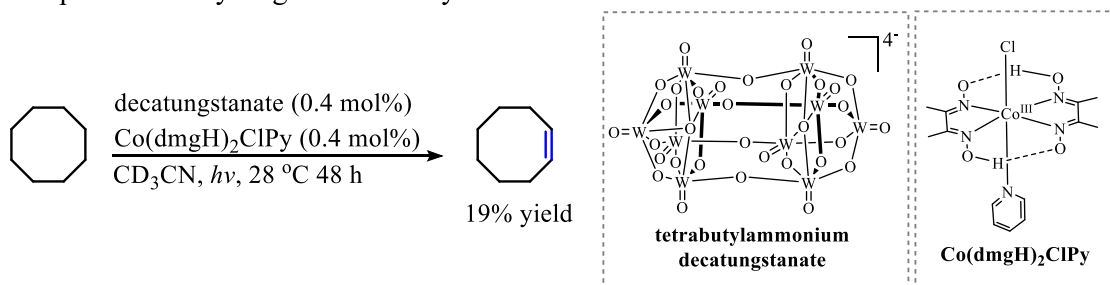
B. Hypothetical Mechanism

Scheme 4.3: Sorenson's Acceptorless Dehydrogenation

Exploration into the catalytically active pathways revealed that the presence of the cobaloxime catalyst, either Co(dmgH)$_2$ClPy or Co(dmgBF$_2$)(CH$_3$CN)$_2$, was crucial to the formation of the olefin products. In addition, UV/Vis continuous photolysis experiments displayed absorbances at 430 nm and 550 nm. These align with Co^{II} and Co^{I} species respectively. However,

the authors acknowledge that the $Co^{II/I}$ reduction is not favorable under their reaction conditions and this absorbance could also correlate with a dimeric cobalt species.[145a] Interestingly, an absorbance around 385 nm was found to be prominent when toluene was used as the reaction solvent. This was speculated to arise from a Co^{III} alkyl species that may be an important off-cycle species in these reactions.

Sorensen's initial dehydrogenation method relies on the challenging abstraction of strong C–H bonds by the decatungstate catalyst. As such, the reaction is typically characterized by low yields and no regioselectivity. Since the cobaloxime catalyst is not at fault for these deficiencies, recent focus has been on merging the cobaloxime HER with systems that form radical intermediates in a site-specific manner. To this end, Sorensen reported a tungsten/cobaloxime dual catalytic system for the dehydroformylation of aldehydes (Scheme 4.4).[158] In this case, the tungsten photocatalyst initiated the process by HAT from the aldehyde followed by loss of CO to provide the radical intermediate. The site-specific nature of this process resulted from of the weakness of the aldehyde C–H bond (approximately 87 $^{kcal}/_{mol}$), which selectively underwent homolytic activation by the decatungstate catalyst.[157] The olefin formation could then be accomplished through a second HAT by the catalytically active form of $Co(dmgH)_2ClPy$.
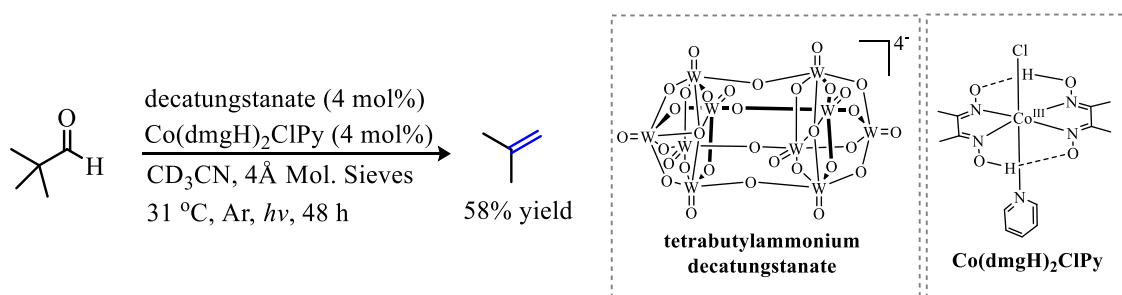
Scheme 4.4: Sorensen Dehydroformulation

In 2018, the use of a carboxylic acid to control site-specificity was introduced. In this strategy, decarboxylation provides the desired carbon radical intermediate. Such decarboxylative HE reactions were employed by Tunge[100] and Ritter[128a] for the direct olefination of carboxylic

acids (Scheme 4.6A & 4.6 B). Related methodology was also reported by Larionov in 2019 that

focuses on the decarboxylative elimination of biomass-derived feedstock carboxylic acids utilizing

various acridine/cobaloxime dual catalytic systems (Scheme 4.6C).[128b] In these methods, the acidic

proton of the acid moiety and the hydrogen atom adjacent to the carbon radical, formed upon

decarboxylation, are liberated as H_2. Thus, CO_2 and H_2 are the only stoichiometric by-products of

the reaction. Although similar in design, these methods possess independent sets of advantages

that may result from differences in the dominant HAT/HE pathway in each system arising from

the variations in catalyst choice (Scheme 4.6). The development of the Tunge olefination and

comparisons to related processes is detailed at length in Chapter 5.

A. Ritter Ir/Co Decarboxylative Elimination
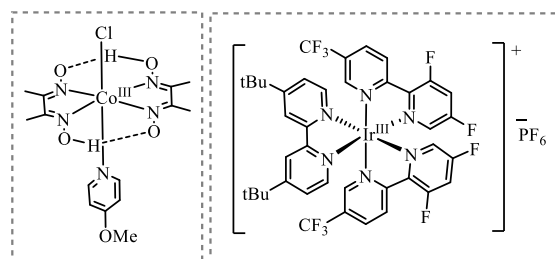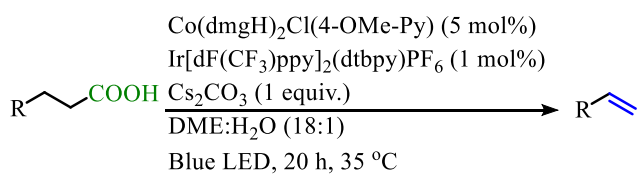
B. Tunge Acr$^+$/Co Decarboxylative Elimination
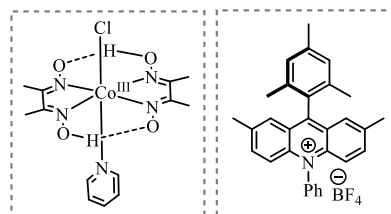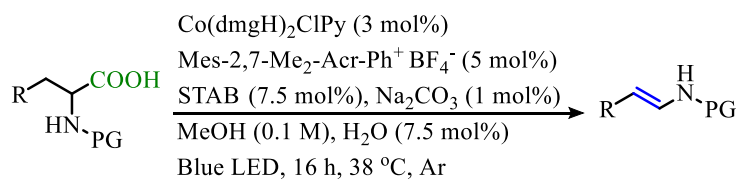
C. Larionov Decarboxylative Elimination
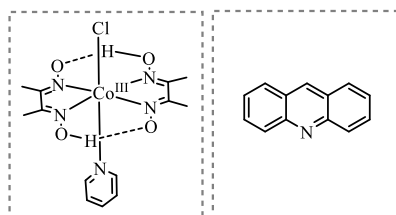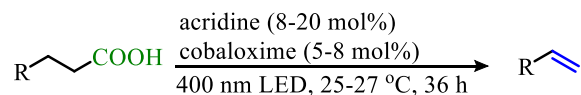
Scheme 4.6: Oxydent-free photoredox/cobalt decarboxylative elimination

In addition to these olefinations, similar dehydrogenative HAT/HE sequences have been

facilitated by amine oxidation using ruthenium-based photosensitizers in an oxidative quenching

manifold. In these systems, the amine dictates the regiochemistry of olefin formation. In 2017, Li

reported a dehydrogenation of *N*-heterocycles utilizing a Co(dmgH)$_2$ClPy/[Ru(bpy)$_3$]Cl$_2$·6H$_2$O dual catalytic system (Scheme 4.7).[159] The proposed catalytic cycle begins with a single electron reduction of Co$^{III/II}$ by the exited state photocatalyst. The amine is then oxidized to a radical cation thus returning the photocatalyst to its' ground state. From the *N*-radical cation intermediate, the HAT provided the observed olefin. Isomerization of the first olefin product allows a second facile dehydrogenation to occur resulting in the formation of an aromatic system.
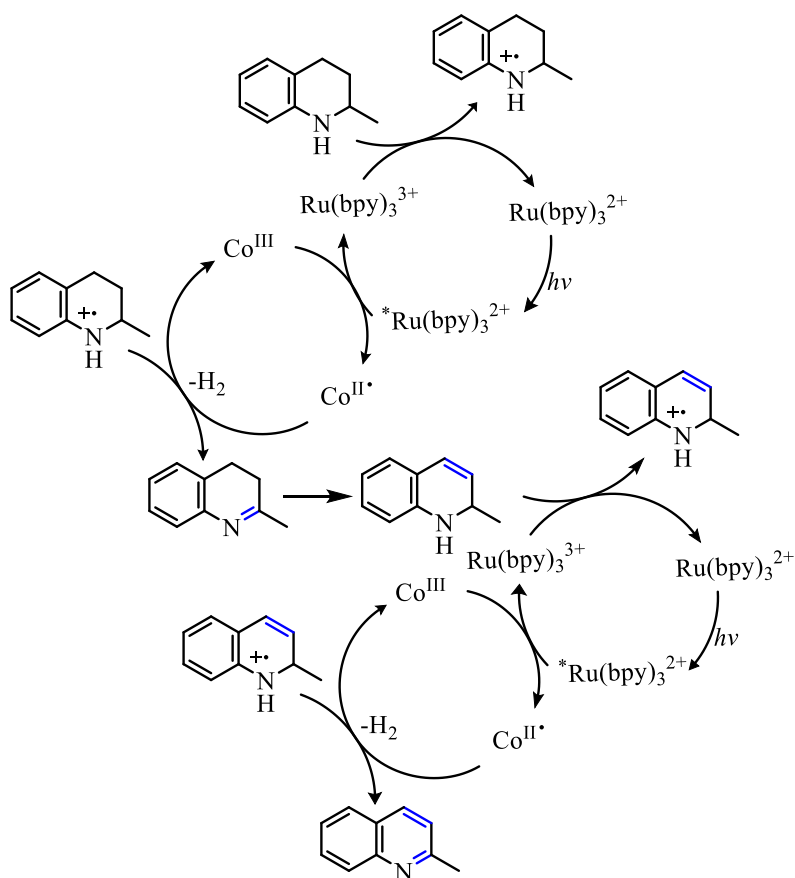
Scheme 4.7: Dehydrogenation of *N*-heterocycles

In 2018, Balaraman reported a similar dehydrogenation with diaryl hydrazines to provide azobenzenes using a Co(dmgH)$_2$ClPy/[Ru(bpy)$_3$]Cl$_2$ dual catalytic system (Scheme 9).[160] In this process, the formation of the key Co^{III}–H intermediate can be achieved through a HAT to Co^{II}. Here, the ruthenium photosensitizer is reducing enough to favorably perform a SET to Co^{III}–H to

generate Co^{II}–H which can then be protonated by the acidic N–H (Scheme 4.8). Liberation of H_2 results in the return of Co^{II}. Again, this pathway is suggested as the dominant path when photolytic HE is performed in the presence of highly reducing photosensitizers.[140h]
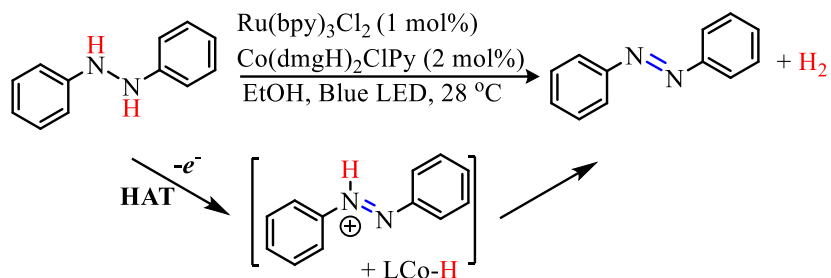
Scheme 4.8: Dehydrogenation of hydrazines

4.3.3 Imine/Oxonium Intermediates in Cross Dehydrogenative Coupling

The sequential amine oxidation/HAT pathway has also been utilized in the formation of iminium intermediates that were then intercepted by various carbon-based nucleophiles for $C(sp^2)$–$C(sp^3)$ and $C(sp^3)$–$C(sp^3)$ bond formation. This approach towards C–C bond formation is part of a common class of HAT/HE reactions referred to as cross-dehydrogenative coupling (CDC).[135] The CDC method is synthetically appealing as it doesn't require pre-functionalization of the substrates or a sacrificial oxidant, giving these reactions high atom economy while often avoiding the generation of toxic waste.[161]

The most common approach to making electrophilic intermediates in CDC to date follows reductive quenching pathways (Scheme 4.1). Most frequently, this is done utilizing the $Ru(bpy)_3^{2+}$ photosensitizer to oxidize an amine moiety to a radical cation. The amine radical cations can also be transformed to α-amino radical intermediates (~–1.0 V vs. SCE)[128a] through deprotonation by a base or disproportionation between the amine radical cation and another molecule of amine substrate. Regardless of the intermediate employed, the cobaloxime can generate the desired iminium ion intermediate for nucleophilic trapping (Scheme 4.9).
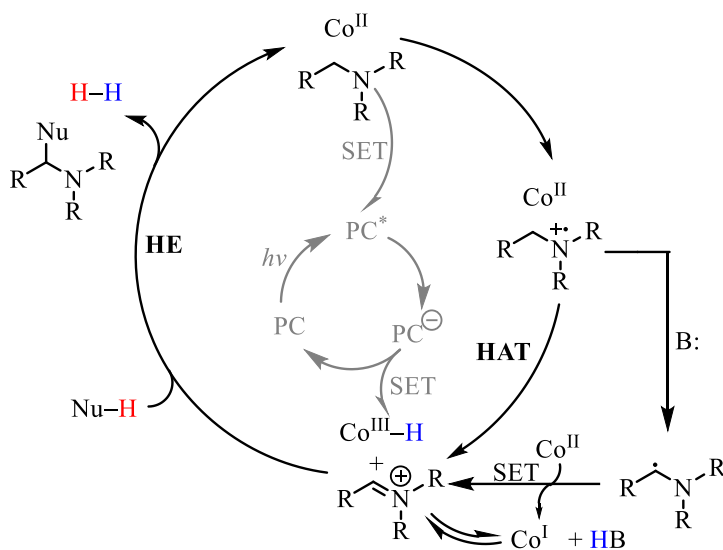
Scheme 4.9: General pathway for dehydrogenative imine ion formation

Wu reported one such example in 2014 with the coupling of various indole nucleophiles with an amine heterocycle using organic dye Eosin Y in tandem with $Co(dmgH)(dmgH_2)Cl_2$ (Scheme 4.10).[162] Quenching studies with the cobalt catalyst, amine substrate, and Eosin Y concluded that only the amine component was able to quench the excited state photocatalyst. Further, they found the reduced photocatalyst could be reoxidized by the starting Co^{III} catalyst to provide a Co^{II} intermediate. UV/Vis spectroscopic studies showed the presence of a Co^{II} complex with characteristic absorbance at 450 nm. The authors further proposed a Co^{I} intermediate to account for an absorbance observed at 550–650 nm. Based on these observations, the dominant catalytic pathway is believed to proceed through two single-electron transfers to reduce Co^{III} to anionic Co^{I}. However, it should be noted that the anionic Co^{I} (**E** in Figure 4.2) absorption assignment is also in line with a Co^{II} dimeric species and the Co^{I}–H (**F** in Figure 4.2).[145] A PCET could also account for the iminium ion formation from the amine radical cation species which would be more in line with the proposal by Eisenberg involving H_2 generation in a similar system.[140h]
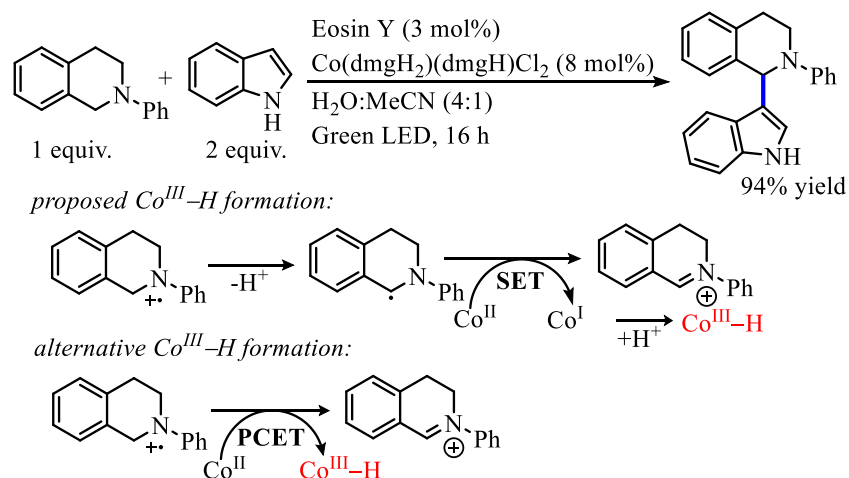
Scheme 4.10: Imine/indole coupling

In a report that combined the principles of Wu's coupling (Scheme 4.10) with Li's dehydrogenation (Scheme 4.7), Luo proposed the generation of iminum ions through PCET (Scheme 4.11).[159,162] Here, a Ru(bpy)$_3^{2+}$/Co(dmgH)$_2$ClPy system led to the oxidation of tetrahydroisoquinoline.[163] After HAT, iminium/enamine tautomerism results in a mixture of enamine and iminium. After coupling of these two reactive intermediates, dehydrogenation provided products resembling those in Li's report, making this a tandem CDC/dehydrogenation process.
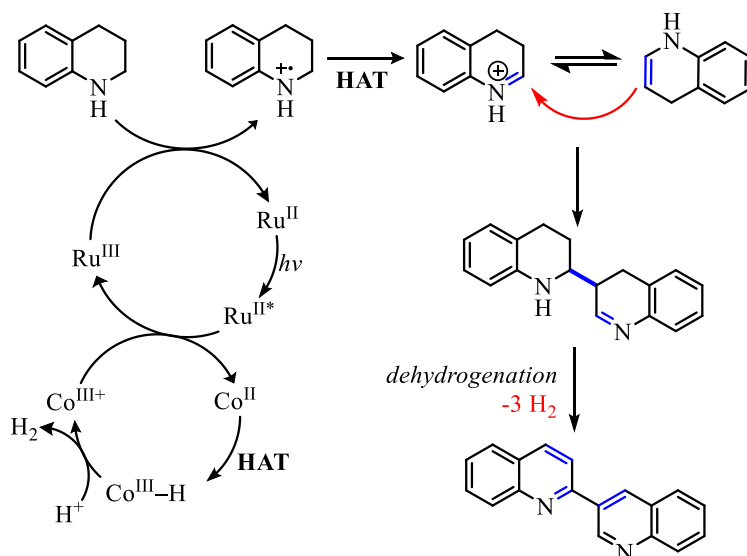
Scheme 4.11: Sequential dehydrogenation reactions of *N*-heterocycles

A 2017 report by Lei proposed yet another possible mechanism for the formation of iminium ions from amines in a dual catalytic system. Their method utilized $Ru(bpy)_3^{2+}$ and $Co(dmgH)(dmgH_2)Cl_2$ to synthesize α-aminophosphonates from *N,N*-alkylanilines (Scheme 4.12).[164] Here, a reductive quenching pathway is proposed to access an amine radical cation which the authors speculate to then form the α-amino radical following a deprotonation/SET sequence.[165] The mechanism proposed further invokes a $Co^{II/I}$ reduction facilitated by $Ru(bpy)_3^{2+}$ and oxidation of the intermediate α-amino radical by Co^{III}. However, the Co^{II} reduction by $Ru(bpy)_3^{2+}$ is not favorable. As such, a pathway that involves a $Co^{II/III}$ cycle, akin to that proposed by Luo (Scheme 4.11), maybe more likely. Regardless of the mechanism for its' formation, the iminium ion intermediate was trapped with trialkylphosphite nucleophiles to provide the desired products.
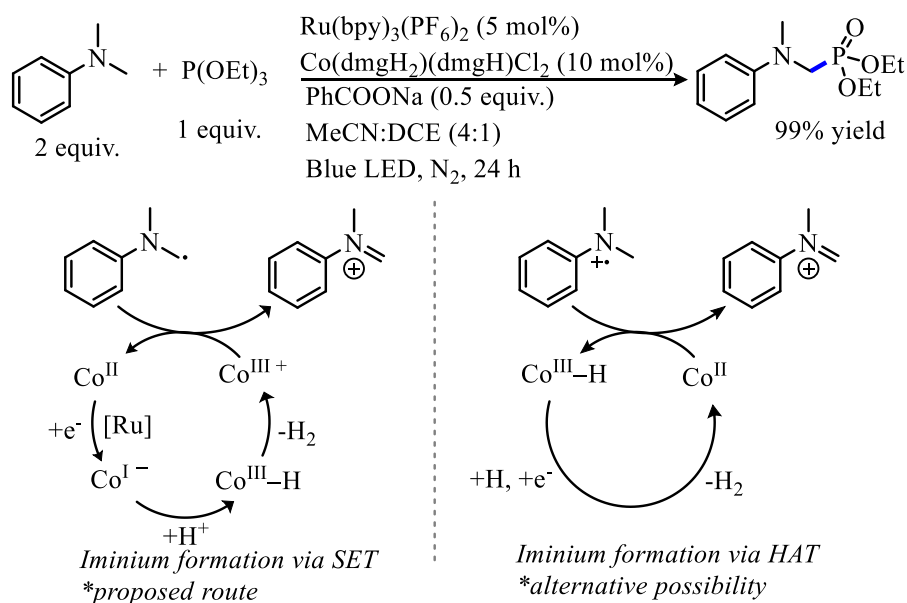
Scheme 4.12: Aminophosphonate synthesis

A report by Wu in 2015 highlights a coupling of amino esters with β-keto esters.[166] Again, the formation of an iminium ion intermediate through amine oxidation by ruthenium photosensitizer, $Ru(bpy)_3(PF_6)_2$, is proposed (Scheme 4.13). Mechanistic investigations revealed that, when the reaction was performed in CD_3CN, no HD or D_2 was observed, implying that the

H$_2$ being generated is solely from the substrates. The authors further report that hydrogen evolution occurred using only the amine; however, the yield of H$_2$ is lower (50 %) than when the diketone is present (88 %). This observation was interpreted as evidence of the diketone being a significant contributor to the H$_2$ generation. When the amino ester was partially deuterated, a mixed H/D product was observed in fitting with a $k_H/k_D = 1.86$ (Scheme 4.13). While the authors interpret this result to mean that the HAT event may be rate-determining, such intramolecular isotope effects result in partitioning regardless of whether the bond breaking is rate-limiting.
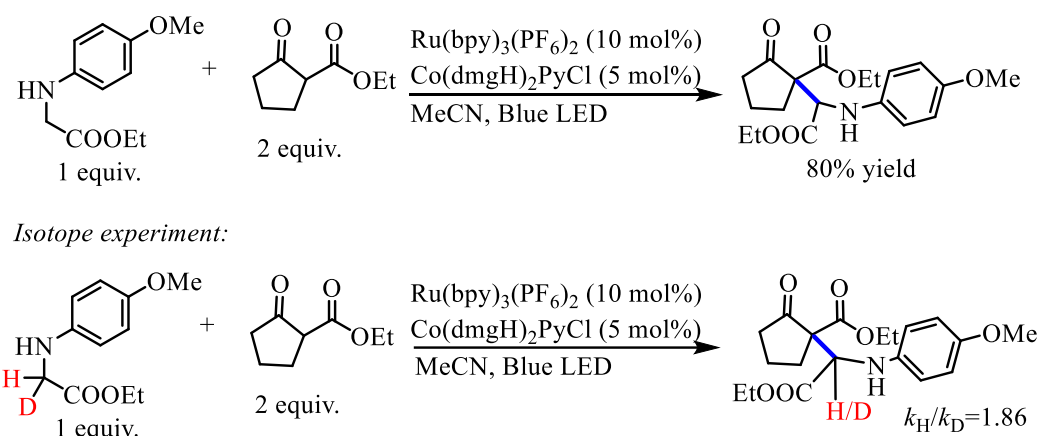
Scheme 4.13: Amino ester/β-keto ester coupling

Wu also demonstrated C(sp^3)–C(sp^3) bond formation with β-keto esters and oxocarbenium ion intermediates generated from isochromans.[167] The activation of the benzylic methylene was accomplished by oxidation of the aromatic system to a radical cation. Subsequent deprotonation is proposed to provide an α-oxy radical intermediate. This is one of the few CDC reactions that is proposed to proceed through a reductive quenching pathway (Scheme 4.14). In order to achieve this oxidation, a strongly oxidizing photocatalyst, Mes-Acr-Me$^+$ ClO$_4^-$, was utilized. The Mes-Acr-Me$^+$ ClO$_4^-$ photosensitizer was paired with a Co(dmgBF$_2$)$_2$(MeCN)$_2$ HE catalyst. Compared to other cobaloximes typically employed, this Co has a much more positive Co$^{II/I}$ reduction potential (–0.55 V vs. SCE, about 0.6 V more positive than Co(dmgH)$_2$ClPy).[144] As such, Co^I intermediates

are possible and indeed are involved in the authors′ proposed mechanism. However, the possibility of a $Co^{III/II}$ sequence cannot be ruled out.
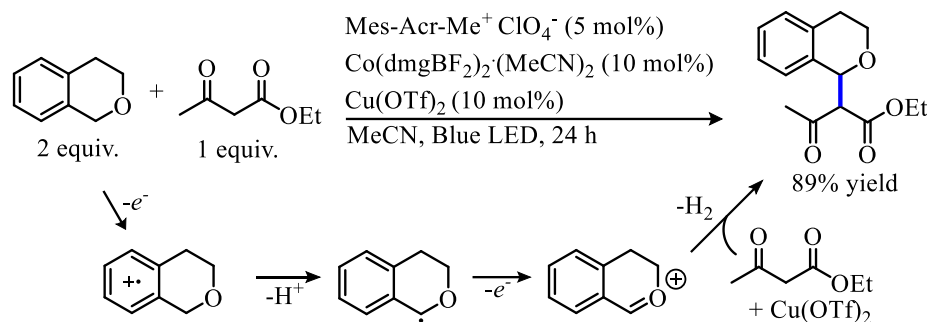
Scheme 4.14: Isochromin/β-keto ester coupling

4.3.4 Additions to Olefins in Cross Dehydrogenative Coupling

The CDC methodology has also been applied to alkenylation reactions for accessing substituted olefins through the formation of $C(sp^2)$–C/N/O bonds. Traditionally, these transformations can be achieved through Heck-type cross-couplings which are dependent on pre-functionalized aryl/vinyl electrophiles. The utilization of CDC reactions not only avoids prefunctionalization, but also allows SET pathways to be exploited for activation of $C(sp^2)$–H systems that are considered inert in standard Heck models.[168]

4.3.4.1 Heteroatom–Carbon Bond Formations

In 2016, Lei reported an elegant Wacker-type anti-Markovnikov oxidation of styrenes.[169] Activation of the styrene via oxidation to the radical cation with a highly oxidizing acridinium catalyst, Mes-Acr-Me$^+$ ClO$_4^-$, allows for a high degree of selectivity for the anti-Markovnikov product. Through merging this strategy with the hydrogen evolution capabilities of the Co(dmgH)$_2$ClPy, the transformation provides carbonyl compounds with water as the O-atom source without an external oxidant (Scheme 4.15).
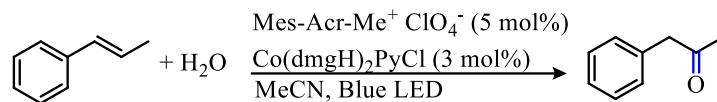
Scheme 4.15: Lei anti-Markovnikov oxidation of styrene

Following this report, in 2017 Lei utilized a similar reaction design to achieve the first

merger of photoredox and cobalt catalysis to achieve alkenylation reactions. Cobaloxime,

$Co(dmgH)_2ClPy$, was employed in conjunction with an acridinium photocatalyst, Mes-Acr-Me$^+$

ClO_4^-, to initiate the cross-coupling of styrenyl derivatives with various oxygen- and nitrogen-

based nucleophiles (Scheme 4.16).[170] The generation of the key radical cation intermediate was

achieved through a SET from the styrene substrate to the excited state photocatalyst. The resulting

radical cations were subsequently intercepted by the nucleophile in an anti-Markovnikov manner.

Acridinium salts were observed to be the only viable photosensitizers for these processes due to

the large positive reduction potential of their excited states.[154f]
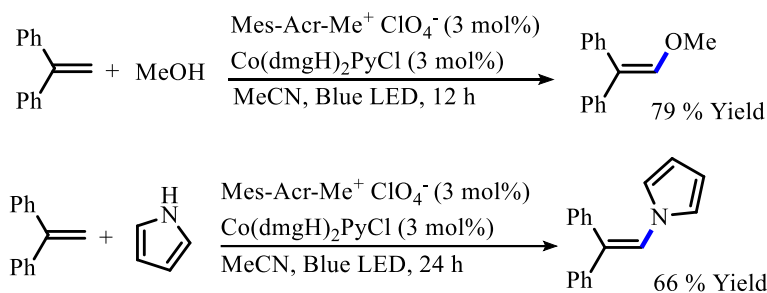
Scheme 4.16: Lei alkenylation reactions

In these 2016/2017 reports, Lei proposed that the carbon-centered radical, resulting from

addition to the activated styrene, was further oxidized by Co^{III} to generate a Co^{II} species. The

benzylic cation that is concomitantly formed then proceeds to produce the olefin through

deprotonation (Scheme 4.17A). Since acridinium salts are not considered to be sufficiently

reducing to facilitate the reduction of Co^{II} to Co^{I} (Figure 4.3), the generation of Co^{III}–H from Co^{II}

through PCET may be more likely (Scheme 4.17B).[145] Throughout their mechanistic studies, the

yield of H$_2$ was observed to be lower than expected (60 % compared to 79 % product yield) which is attributed to hydrogenation of 1,1-diphenylethylene.
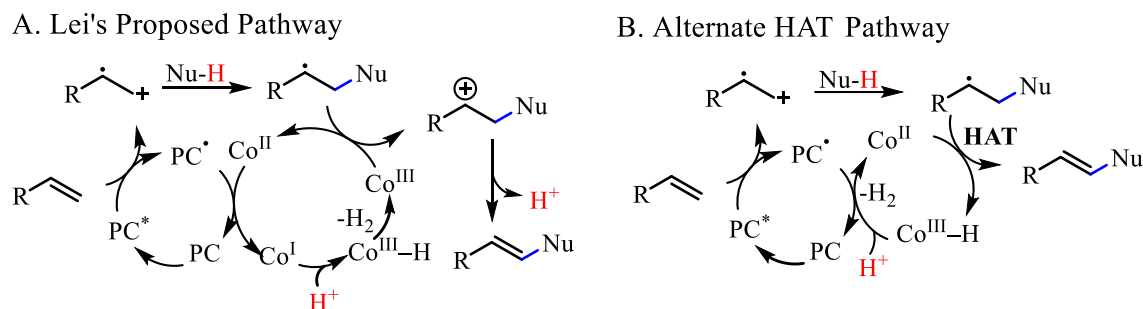
Scheme 4.17: Possible reaction pathways for nucleophilic additions to styrene

In 2019, a tricatalytic activation pathway was discovered that allowed for the dehydrogenative silylation of alkenes resulting in allyl silane products.[171] This represents an unprecedented route to allyl silanes that does not require a stoichiometric oxidant and thus offers a cleaner, more general approach to these molecules. The methodology makes use of the 4CzIPN photosensitizer (Figure 2.3)[44] in conjunction with Co(dmgH)$_2$ClPy and HAT catalyst, quinuclidine. Stern-Volmer quenching studies revealed that the dominant catalytic cycle likely proceeds through a direct oxidative quenching pathway in which the cobaloxime (Co$^{III/II}$ = -0.68 V vs. SCE) quenches 4CzIPN (-1.04 V vs. SCE) out of the excited state (Scheme 4.18). The oxidized 4CzIPN (+1.52 V vs. SCE) is then reduced by quinuclidine (+1.10 V vs. SCE) to close the photocatalytic cycle and provide the amine radical cation. Hydrogen atom abstraction of the Si–H bond by the quinuclidine radical cation gives Si-radical which can add to the alkene reagent to form a new Si–C bond and a C-radical intermediate. The Co^{II} can then trap this radical intermediate and HAT provides the Co^{III}–H and the desired allyl silane product. To turn over the quinuclidine and the cobaloxime, a pyridine assisted proton transfer was necessary to allow for the HE to occur between Co^{III}–H and Py–H (Scheme 4.18). The proposed cobaloxime cycle in this report is a Co$^{III/II}$ process and has a high degree of selectivity for the allyl silane product.
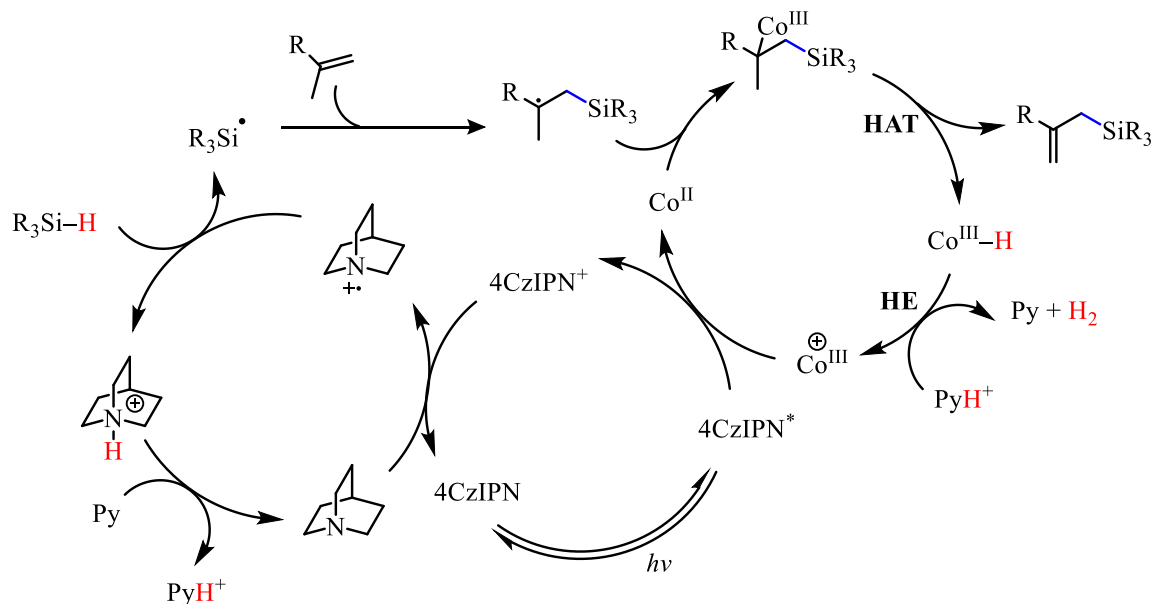
Scheme 4.18: Tricatalytic HAT/HE sequence for the synthesis of allyl silanes

4.3.4.2 Carbon–Carbon Bond Formations

In 2018, Lei reported a $C(sp^2)$–C bond formation which was achieved through the addition of electron-rich aryl nucleophiles.[172] With regards to the cobaloxime catalyst, the use of more electron-donating DMAP as the axial base ligand was vital to achieving high yields and stereo-selectivity (Scheme 4.19). Mechanistically, they propose an alternate pathway to the one depicted in Scheme 4.17A. In this case, they propose that the aryl nucleophile is oxidized to the radical cation by the photocatalyst, as previously shown by Nicewicz.[173] This is followed by radical addition to styrene (Scheme 4.19). The authors favored this pathway based on Stern-Volmer quenching studies that showed 1,3,5-trimethoxybenzene was more inclined to undergo the initial oxidation than styrene.
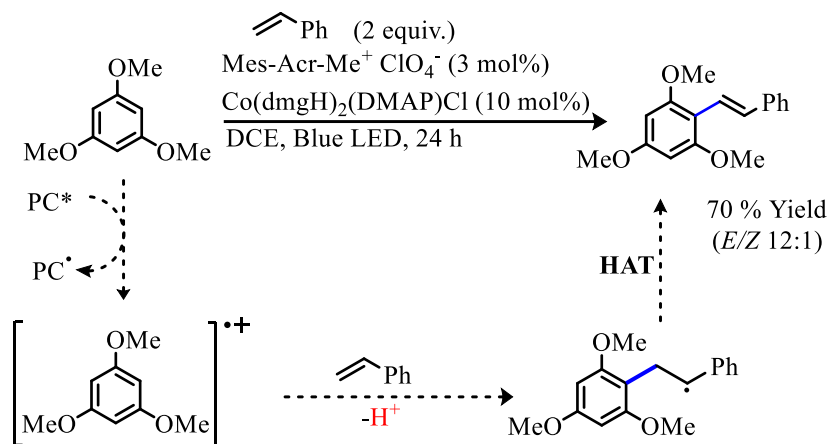
Scheme 4.19: Coupling of styrene with aryl nucleophile

Another Heck-type process reported by Wu and Lui utilizes a decarboxylation pathway to generate a carbon radical intermediate to serve as the nucleophile. The radical generated was then able to be trapped by various styrenyl coupling partners. Subsequent cobaloxime-facilitated removal of a hydrogen atom provided the olefin products (Scheme 4.20A). A Co(dmgH)$_2$Cl(DMAP)/Mes-Acr-Me$^+$ ClO$_4^-$ catalyst system was identified to be best for this process. It is noteworthy that the pyridine axial ligand did provide their desired Heck product in equivalent yield to the DMAP catalyst. However, the more electron-rich species is anticipated to produce a more stable Co(III)–H intermediate with a higher pK_a compared to H–Co(dmgH)$_2$ClPy (pK_a approximately 7) which may have influenced the choice in catalyst system[174]

A. Wu/Lui Decarboxylative Heck-like Coupling
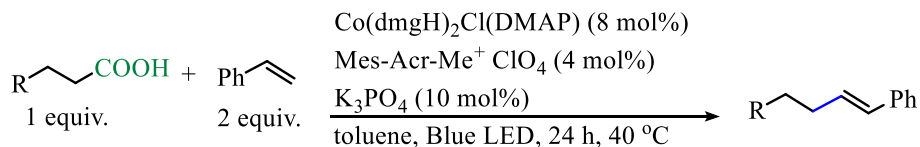
B. Hisaeda/Shimakoshi B12-Catalyzed Heck-type Coupling
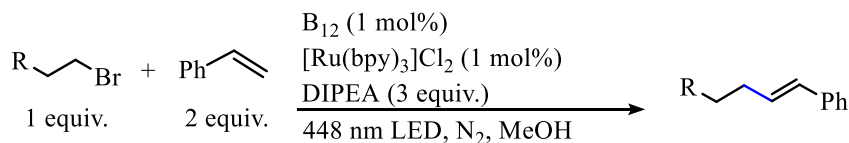
Scheme 4.20: Heck-type coupling of aliphatic carbon nucleophiles with styrene

Around the same time, Hisaeda/Shimakoshi reported an alternative approach to the photoredox/cobaloxime Heck-type process which utilizes alkyl bromides as the radical surrogates instead of carboxylic acids (Scheme 4.20B).[175] In order to access the carbon radical intermediate, a vitamin B12 complex was utilized as the cobalt catalyst as the cobaloxime derivatives did not operate as efficiently in the displacement of the halide. Homolysis of a Co–C intermediate is proposed to release the radical which can subsequently be trapped by styrene. A HAT/HE process liberates the Heck product.

4.3.4.3 Annulation and Radical Cascade Reactions

The photoredox/cobaloxime technology has also been employed with alkenes in various annulation reactions. Several of these invoke styrene radical cations that can be accessed through single electron oxidation by highly oxidizing photosensitizers. Lei highlights this strategy in two reports. In the first report, a $[Co(dmgH)_2Py_2]^+ PF_6^-$/Mes-Acr-Me$^+$ ClO$_4^-$ dual catalytic system was developed from the synthesis of dihydroisoquinolines (Scheme 4.22A).[176] The radical intermediate resulting from oxidation of styrene followed by addition could be intercepted by a dearomatizing cyclization with an adjacent phenyl ring (Scheme 4.22C). It was observed that $[Co(dmgH)_2Py_2]^+$ PF$_6^-$ used in conjunction with fluorine-containing co-solvents (DCE/HFIP) was crucial to obtaining high yields.

Lei's second report showed that these annulations could also be achieved using styrene and alkyne derivatives for the synthesis of substituted naphthalene systems (Scheme 4.22B). Quenching studies found that the styrene substrates were most reactive toward oxidation and electron-rich alkynes promoted reactivity.[177] Rationally, this led to the proposition that the styrene

radical cation is intercepted by an alkyne nucleophile, leading to an alkene radical cation which could readily undergo the dearomatization event (Scheme 4.22C).

A. Annulation towards Dihydroquinilones

71 % Yield
(d.r. > 20:1)
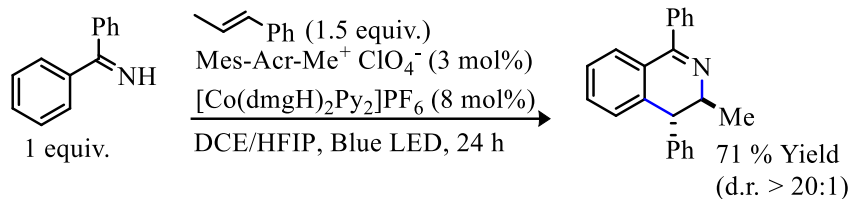
B. Annulation towards Naphthalene Derivatives

93 % Yield
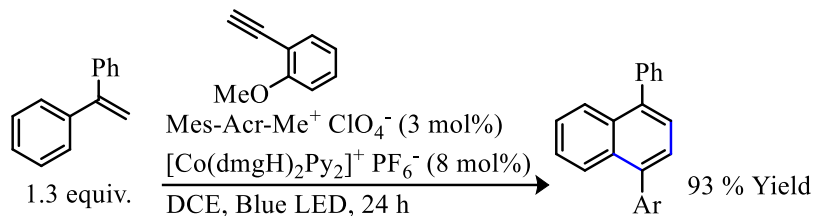
C. Genral Proposed Pathway for Lei's Annulations
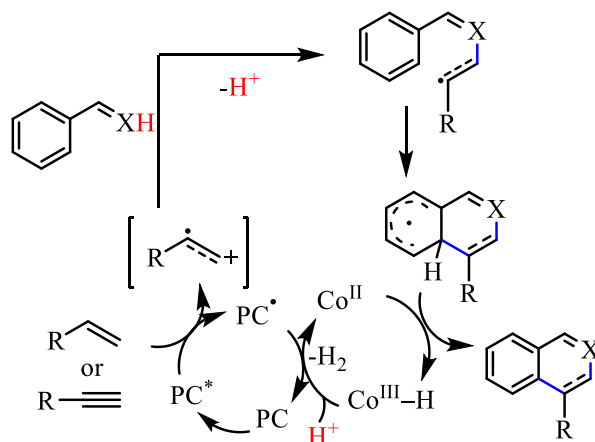
Scheme 4.22: Lei's annulation reactions with styrene

Chen and Wu reported a process in 2018 detailing the dimerization of styrenes through a [4+2] annulation (Scheme 4.23).[178] In the proposed mechanism, the benzylic radical gets oxidized to a cation by the Co^{II} to provide Co^{I}. The Co^{I} is then proposed to perform the deprotonation to establish an olefin. The authors report a similar observation to Wu's 2014 report with amine/indole CDC (Scheme 4.10)[162] in which an absorbance around 550 nm is observed in UV/Vis spectroscopy. This absorbance was attributed to the formation of an anionic Co^{I} complex, lending

credence to their proposed mechanism. As discussed previously, despite this sound logic it is also possible that this observed absorbance is actually a dimeric Co^{II} species.[145] Moreover, this benzylic radical to cation oxidation (+0.37 V vs. SCE) is not favorable.[58a] Thus, the likelihood of an alternate process proceeding through concerted PCET cannot be ruled out.
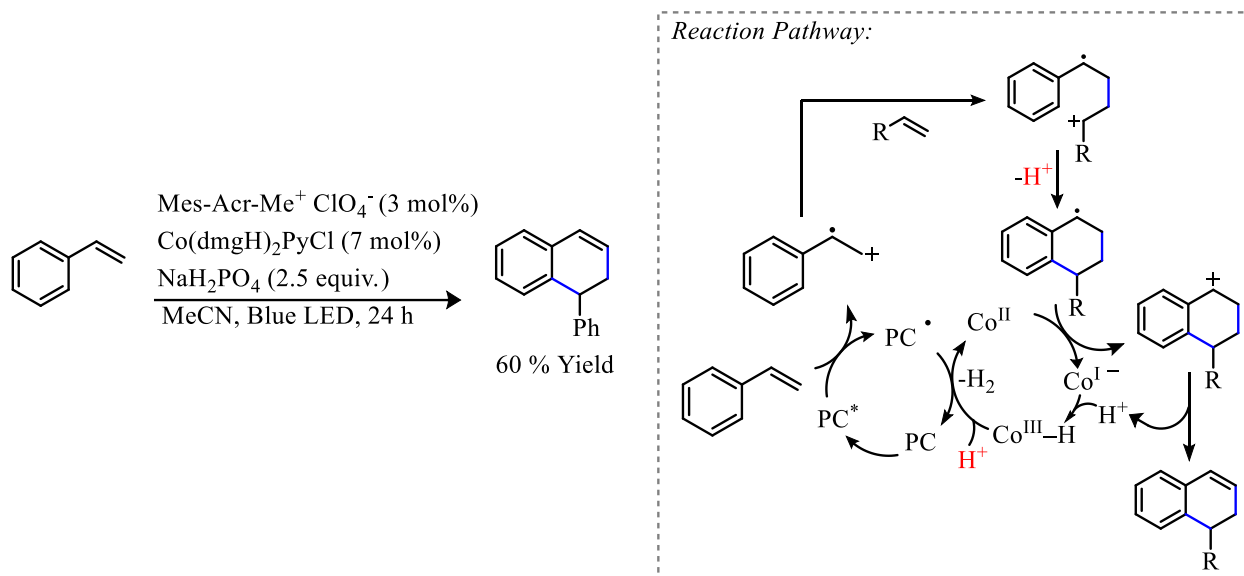
Scheme 4.23: Styrene [4+2] annulation

Xiao and Chen reported the synthesis of dihydropyrazole-fused benzosultams, in the presence of Co(dmgH)$_2$ClPy and a ruthenium-based photocatalyst in 2016 (Scheme 4.24A).[179] They achieved the annulation by initial deprotonation of tosyl-protected allylic hydrazones, where the resulting nitrogen anion is oxidized by the excited state photocatalyst to form an *N*-centered radical. Consequently, this would undergo a radical 5-exo-trig cyclization and the benzosultams were forged following a second dearomative cyclization. HAT-induced rearomatization provided the products.

In 2019, Xiao and Shi also reported the formation of phosphaisocoumarins by utilizing aryl-phosphinite nucleophiles in conjunction with Co(dmgH)$_2$ClPy and an acridinium photocatalyst (Scheme 4.24B).[180] They determined that both the arylphosphinic acid and diphenylacetylene were prone to oxidation by the excited state photocatalyst which led to the

suggestion of two mechanistic pathways. The first of which proposed oxidation of the aryl-phosphinite to the phosphinyloxy radical and subsequent radical addition to the alkyne. The second path involves the interception of the radical cation, formed by oxidation of the alkyne, by the nucleophilic phosphinite. Both pathways show a turnover of the photocatalyst through Co$^{III/II}$ reduction and a subsequent rearomatization event that is achieved through HAT.

A. Bezosultam Synthesis
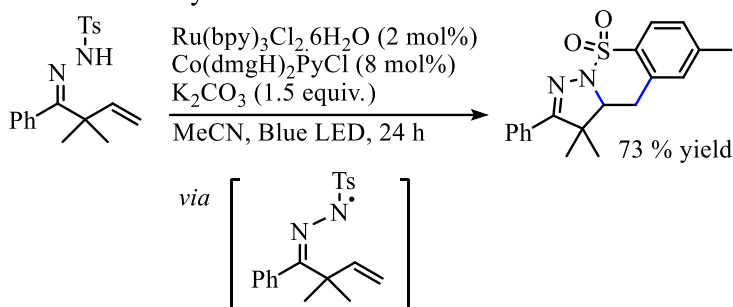
B. Phosphaisocoumarin Synthesis
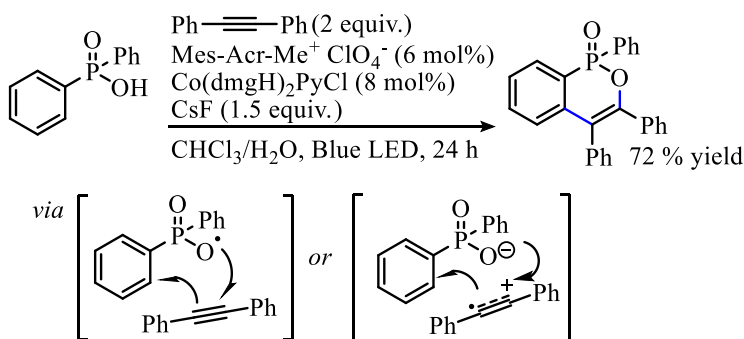
Scheme 4.24: Xiao's dehydrogenative radical cascade reactions

A 2020 report from Lui shows an iminyl-radical-mediated cyclization. This methodology displayed two synthetic possibilities.[181] First, the cyclization event followed directly by a cobalt-facilitated elimination event and second, the cyclization event followed by radical addition to styrene before the cobalt-facilitated elimination event (Scheme 4.25). The aminyl radical is accessed using an activating group that can undergo oxidative decarboxylation and produce acetone as the byproduct of the reaction along with hydrogen gas. To achieve the annulation over

the alkynylation, the conditions had to be modified, most notable the cobaloxime catalyst employed had to be altered.
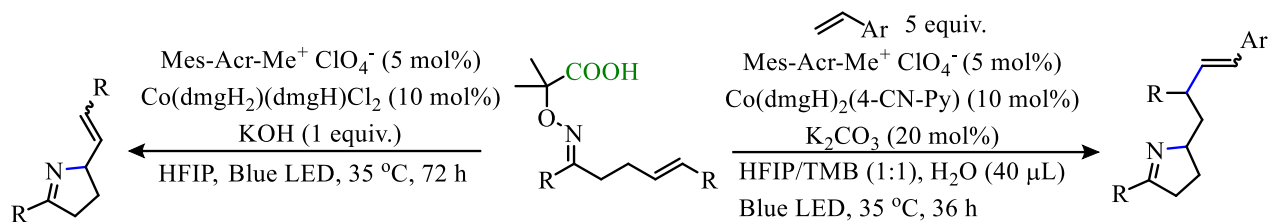
Scheme 4.25: Aza-cyclization for alkene-containing *N*-heterocycles

4.3.5 Additions to Arenes

The CDC manifold has also been successfully applied to the formation of $C(sp^2)$–C/N/O/S bonds using various arene coupling partners with a variety of heteroatom nucleophiles. In this literature, there are two general pathways that are proposed to result in arene functionalization. The first pathway involves the production of a reactive radical heteroatom species that can undergo addition to the arene moiety. The second pathway invokes oxidization of the arene to a radical cation which can then undergo nucleophilic addition.

4.3.5.1 Radical Addition to Arenes

One of the first examples of a CDC in aromatic substitution was reported in 2015 by Wu.[182] In this report, *N*-aryl enamines are converted to indoles through an intramolecular CDC (Scheme 23). Amine oxidation to a radical cation is invoked to access the desired radical intermediate. However, unlike most of the methods previously discussed, this method proposes an oxidative quenching pathway is operable in which the excited state of the Ir(ppy)$_3$ photocatalyst reduces the Co(dmgH)$_2$Cl(4-CO$_2$Me-Py) catalyst to a Co^{II} species. The iridium radical cation returns to its ground state by oxidization of the amine substrate. The resulting amine radical is then in

conjugation with an α,β-unsaturated ester, which places spin density on carbon. The addition of this carbon radical to the aromatic system through a 5-exo-trig cyclization followed by re-aromatization through a HAT process provides the corresponding indole products.

The proposed oxidative quenching pathway is supported by the observation that when the cobaloxime catalyst is irradiated in the presence of Ir(ppy)$_3$, absorbances around 450 nm and 550 nm were noted, indicating the photosensitizer is able to reduce the Co^{III} to Co^{II} and possibly Co^I. However, as previously mentioned, UV/Vis absorbances do not provide definitive proof of anionic Co^I. While Ir(ppy)$_3$ can reduce Co^{II} to Co^I (Figure 4.3), the mechanisms involving HAT to Co^{II} cannot be ruled out (Scheme 4.26).
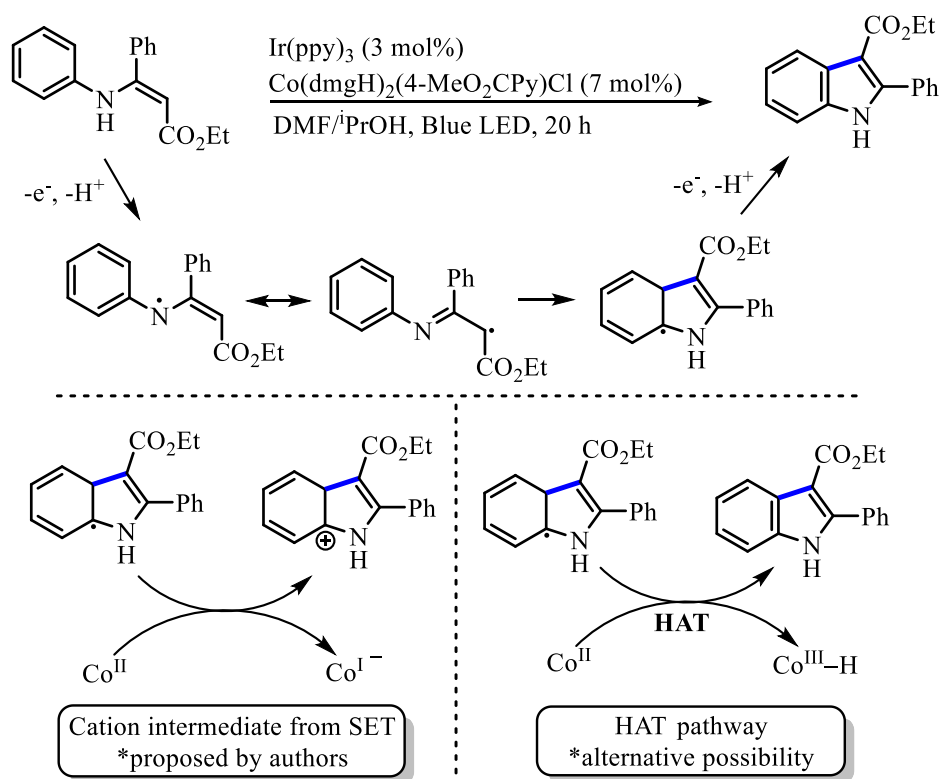
Scheme 4.26: Dehydrogenative synthesis of indoles

In addition to these experiments, there are several other noteworthy observations in this work. For one, the choice of cobaloxime is unique. The carboxymethyl pyridine ligand is one of the only examples of an electron-withdrawing axial base ligand being the optimal choice. This

149

could be a result of a more favorable SET from the excited state Ir^{III} (–0.89 V) to the Co^{III} which

should be less negative compared to the Co(dmgH)$_2$ClPy complex (–0.68 V). Another noteworthy

observation is the improved reaction yields and HE when 1:1 DMF/iPrOH is used as the solvent

system. The possibility of oxidizing the iPrOH was ruled out by the authors and the reason for the

solvent influence remains elusive.

Wu and Lei outlined another intramolecular CDC reaction towards the formation of C–S

bonds in a 2015 report (Scheme 4.27).[183] This was achieved with a

Ru(bpy)$_3$$^{2+}$/Co(dmgH)$_2$Cl(DMAP) catalytic system. The optimal reaction conditions utilize a

stoichiometric loading of sodium glycinate (Na-Gly) as a base and 0.4 equivalents of DMAP. As

was the case in several transformations highlighted previously herein, the authors propose the base

serves as a proton shuttle between the substrate and the cobalt catalyst. The Ru photosensitizer is

proposed to proceed through a reductive quenching pathway in which a SET generates a S-radical

which can then undergo a 5-exo-trig addition to the aromatic moiety. Subsequent HAT would

result in the formation of the Co^{III}–H intermediate. The proposed mechanism shows the Co^{III}–H

being protonated and performing HE but, the highly reducing Ru photosensitizer could potentially

reduce the Co^{III}–H to Co^{II}–H prior to protonation.[140h] The alkaline nature of these reaction

conditions may also influence which order of operations is most favorable.[140h,150]

Ru(bpy)$_3$(PF$_6$)$_2$ (3 mol%)
Co(dmgH)$_2$(DMAP)Cl (8 mol%)
Na-Gly (1 equiv.)
DMAP (0.4 equiv.)
MeCN, Blue LED, 12 h
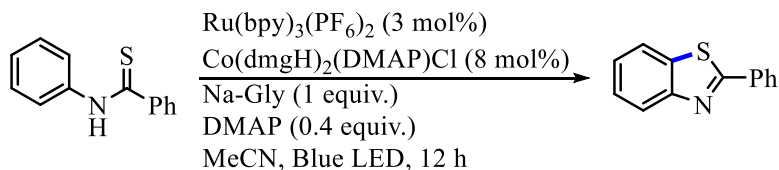
Scheme 4.27: Dehydrogenative thiazole synthesis

In 2018, both Xie and Zhou,[184] as well as Chiang and Lei,[185] reported the synthesis of

lactones through a C–O bond formation in an intramolecular CDC (Scheme 4.28). Both make use

of acridinium photosensitizers to oxidize carboxylate moieties, a process analogous to what is proposed in some of the decarboxylative eliminations (Figure 3.1 & Scheme 4.6). However, unlike in the decarboxylative methods, the rapid loss of CO_2 does not occur to make a radical arene but instead, the O-radical undergoes 6-endo-trig cyclization. The optimization of the method reported by Xie and Zhou details that the presence of a base (0.5 equiv.) was crucial to high reaction yields. Specifically, $PhCOO^- Na^+$ was determined to be optimal. In addition, the $Mes\text{-}Acr\text{-}Ph^+ BF_4^-$ was paired with $Co(dmgH)_2ClPy$, $Co(dmgH)(dmgH_2)Cl_2$, and $Co(dmgBF_2)_2OH_2$ with $Co(dmgH)_2ClPy$ providing superior yields. The authors also screened Ru and Ir photosensitizers but report no product formation with these catalysts, suggesting the strong oxidizing ability of the acridinium is needed for this transformation. In their exploration of the scope, it is notable that yields were lower in certain cases where the aryl moiety undergoing addition was sterically encumbered, particularly with halogens. In cases where yields were not affected by sterics, the C–O bond formation preferentially took place at the more sterically congested bond, leading to ortho-substituted lactones rather than para (Scheme 4.28A).

The Chiang/Lei methodology differs from that discussed above as they do not employ a base and optimize around the use of $Mes\text{-}Acr\text{-}Me^+ ClO_4^-$ (Scheme 4.28B). They screened $Co(dmgH)_2Cl(DMAP)$, $Co(dmgH)_2ClPy$, and $Co(dmgH)(dmgH_2)Cl_2$ under their conditions but, conversely to what was seen by Xie and Zhou, found optimal results with $Co(dmgH)(dmgH_2)Cl_2$. They suggest that the needed deprotonation is achieved using MeCN taking the proton in conjunction with the carboxylate oxidation. Interestingly, Chiang and Lei found that the reaction was inhibited by all sterically encumbering groups in the ortho position on the aryl moiety. Despite this, they did show that with their methodology, the intramolecular C–O bond formation could also be achieved with styrenyl coupling partners in place of biaryl reactants. Additionally, a KIE

study revealed a $k_H/k_D = 1.10$, implying that the C–H bond cleavage event is not the rate determining step.

A. Xie/Zhou Lactonization

Mes-Acr-Ph$^+$ BF$_4^-$ (2 mol%)
Co(dmgH)$_2$PyCl (4 mol%)
PhCOONa (0.5 equiv.)
MeCN, Blue LED, 48 h

96 % Yield

Select examples of steric influence:

87% yield, 3:1   77% yield, 10:1

B. Chiang/Lei Lactonization

Mes-Acr-Me$^+$ ClO$_4$ (1.5 mol%)
Co(dmgH)$_2$Cl$_2$ (2 mol%)
MeCN, Blue LED, 10 h

99% yield

Select examples of steric influence:

70% yield, 15:1   70% yield, 12:1   <5% yield
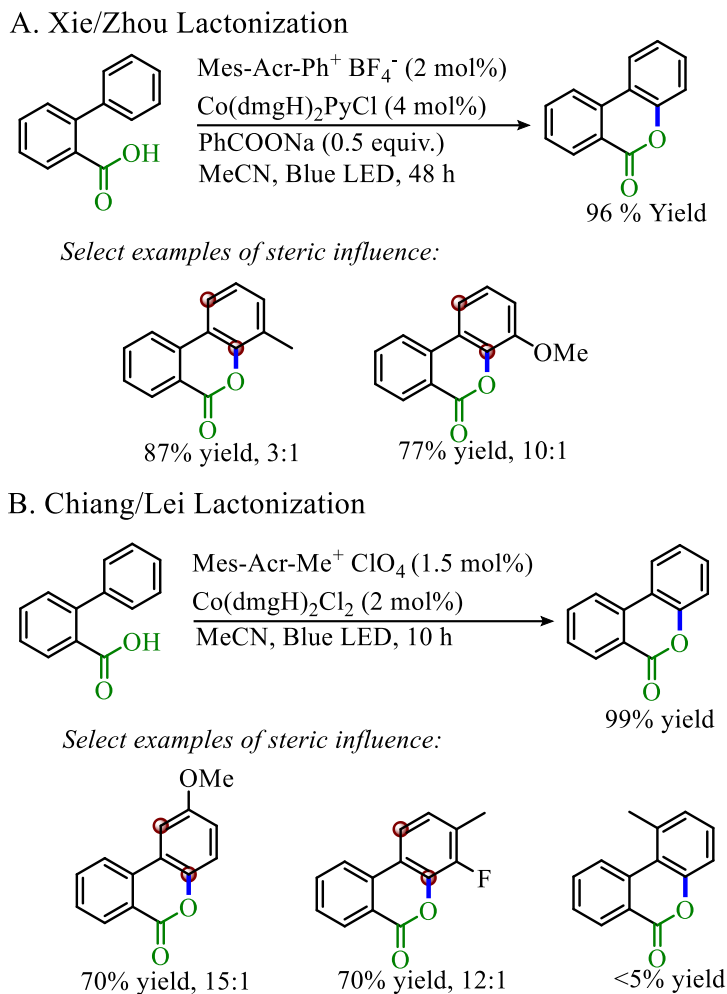
Scheme 4.28: Dehydrogenative lactonization of arylbenzoic acids

The radical additions to arenes thus far have been examples of intramolecular bond formations for the synthesis of heterocycles. In 2019, Li makes use of decarboxylation to produce C-radical coupling partners that subsequently add to heteroarenes in an intermolecular reaction.[186] The method was optimal with a [Co(dmgH)$_2$Py$_2$]$^+$ PF$_6^-$/Ir[dF(CF$_3$)ppy]$_2$dtbbpy catalyst system (Scheme 4.29). Although a variety of carboxylic acids were operable in this chemistry, the highest yields were observed with substrates that are not posed to undergo elimination readily (see *Section 4.3.2* for decarboxylative elimination examples). Stern-Volmer quenching studies revealed that the

carboxylate and the Co^{III} were equally efficient quenchers making the dominant catalytic pathway unclear. Regardless of the order of events, the authors do suggest a sequential HAT process instead of a PCET route but, the possibility of a PCET cannot be ruled out (see Scheme 4.17 for HAT discrepancy). Additionally, the authors suggest that the reduction of the Co^{III}–H to Co^{II}–H before the hydrogen evolution process is possible in this system due to the use of the highly reducing Ir catalyst.
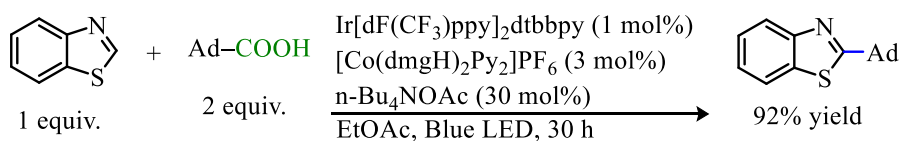
Scheme 4.29: Decarboxylative alkylation of heteroarenes

4.3.5.2 Arene Oxidation

The alternative approach towards arene substitution is to oxidize the arene moiety to a radical cation. The ring is then activated for nucleophilic attack and HAT/HE provides the CDC products. Since the oxidation of the arene moiety is difficult (+1.96 V vs. SCE for benzene), highly oxidizing photosensitizers have been employed in these transformations. Specifically, quinolinium ion and the acridinium photocatalysts are utilized for such oxidations following the reductive quenching pathway (Scheme 4.30). Wu reports in both 2016 and 2017 the use of quinoliniumion, $QuCN^+$, in conjunction with $Co(dmgBF_2)_2(CH_3CN)_2$ to achieve the amination and hydroxylation of benzene[187] as well as etherification of benzene both inter- and intramolecularly.[188] These routes are proposed to proceed through nucleophilic addition to the arene radical cation species followed by the cobaloxime-facilitated removal of an electron and two protons. In both cases, the authors propose a process in which the QuCN radical is re-oxidized through SET to Co^{III}. In 2017, Lei reports a similar coupling between various arene substrates and azoles using a Mes-Acr-Me$^+$ ClO$_4^-$

/Co(dmgH)-(dmgH$_2$)Cl$_2$ catalytic system.[189] Zhou also found this catalyst combination to be optimal for a method reported in 2018 for the amination of aromatic systems with primary amines.[190] Again, the regioselectivity is noteworthy as the C–N bond formation appears to select for the ortho-position to arene substituents. As mentioned previously, this could be an artefact of a preference for the less sterically hindered path for cobaloxime-facilitated HAT.
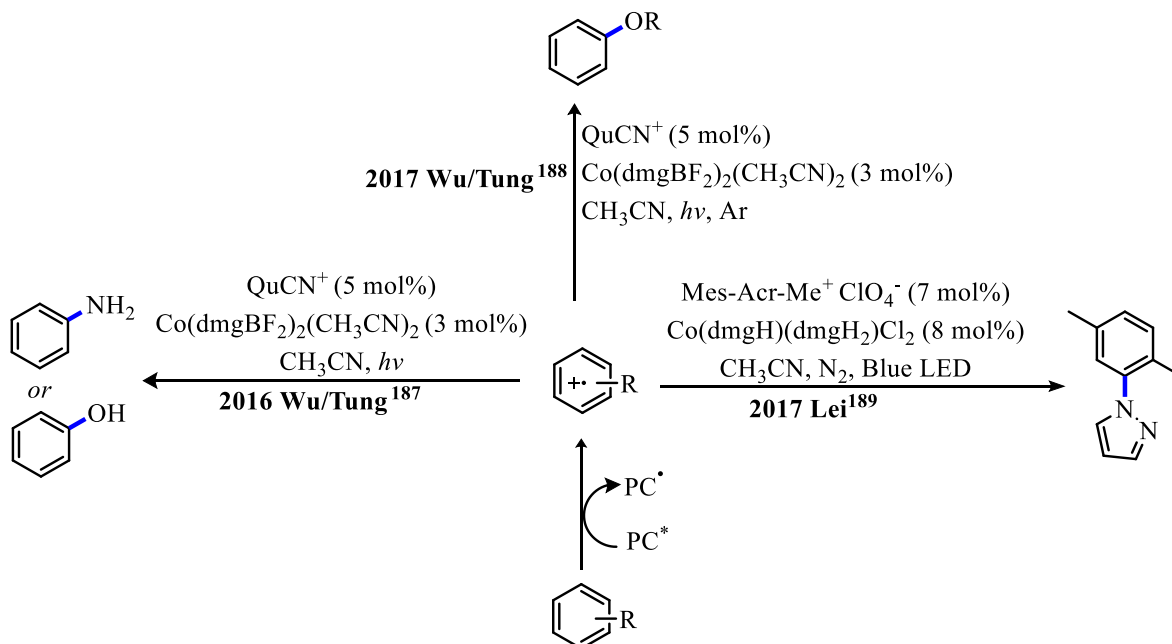
Scheme 4.30: Arene radical cation substitutions

4.4 Conclusion

Thus far, the photo-induced dehydrogenation methodology has proven to have high utility in achieving difficult bond formations. Most notablily, these transformations produce minimal waste and proceed with high chemoselectivity. This approach towards small molecule functionalization is relatively new, only emerging as a synthetic strategy in the past decade. As such, there remains opportunity for new transformations to be discovered. In addition, most of the work outlined in this chapter proposes hypothetical mechanisms, but typically these proposals are

not backed by deailed mechanistic study. As such, much still needs to be invesigated regarding the mechanism(s) by which the photo-induced hydrogen evolutions proceed. For one, the speciation of cobaloximes during catalysis needs to be further investigated. Additionally, the discrepancy between the step-wise SET/deprotonation and the concerted PCET pathways needs to be further explored. In addition to advancing the photoredox/cobaloxime methodology, the use of other reagents capable of proton reduction in dehydrogenative small molecule functionalization is underexplored. Laslty, the application of these methods in the process of building complex molecular scaffolds still needs to be undertaken.

Chapter 5: Acridinium/Cobaloxime Dual Catalysis for the Decarboxylative Elimination of Carboxylic Acids

5.1 Introduction

The direct decarboxylative elimination of carboxylic acids represents a minimal waste producing strategy for the installation of synthetically versatile olefin functionalities from highly abundant carboxylic acids.[191,192] As described in Chapter 3, this type of process was achieved with an acridinium photosensitizer and Cu^{II} as the terminal oxidant to provide enamides and enecarbamates from α-amino acids.[100] However, rendering this process dual-catalytic and redox neutral was desirable. This was achieved by employing an acridinium/cobaloxime cooperative catalytic system that bypasses the need for an oxidant by exploiting hydrogen evolution. Thus, this reaction proceeds without any stoichiometric reagents while producing carbon dioxide and hydrogen gas as the only stoichiometric byproducts.[69,132]

5.2 Decarboxylative Elimination with Acridinium/Cobaloxime Dual Catalysis

When initially considering an external oxidant-free decarboxylative elimination of α-amino acids, Sorensen's dehydrogenation of alkanes served as a source of inspiration for the use of the cobaloxime in a dual-catalytic dehydrogenation (Figure 4.3).[155] The dehydrogenation involves HAT to generate an alkyl radical followed by a second HAT reaction to generate the alkene. The initiation of olefin formation via a HAT reaction limits the reaction scope because it is highly dependent on C−H bond strength and thus not selective when many similar C−H bonds are present. Sorensen recognized this limitation and has utilized aldehydes as initiating groups that can be selectively activated due to their low C−H bond strength (Figure 4.4).[158] Based on these reports, a reaction utilizing carboxylic acids was envisioned. Using an oxidative radical

decarboxylation pathway, a radical intermediate could be generated site-specifically and would obviate the need to rely on differential bond strengths as seen in the Sorenson methodology. A subsequent HAT reaction would provide the alkene product. By employing a photoredox/cobaloxime dual-catalytic system, a reaction that converts feed-stock carboxylic acids into alkenes without the use of any stoichiometric additives while releasing CO_2 and H_2 as the sole stoichiometric byproducts was realized (Scheme 5.1).
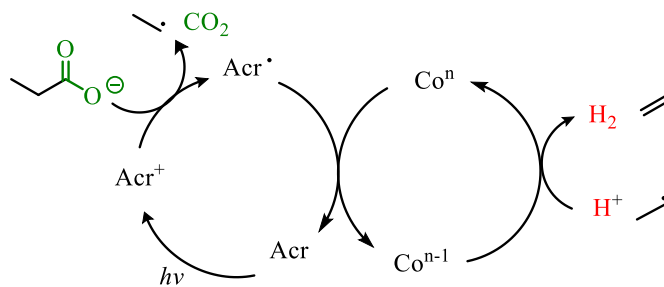
Scheme 5.1: Co/Acr$^+$ decarboxylative elimination pathway

5.2.1 Development of Acr$^+$/Co Catalyzed Decarboxylative Elimination of N-Acyl Amino Acids

Initial focus was directed to the synthesis of enamides and enecarbamates from *N*-acyl amino acids due to the high synthetic value of these functionalities (see discussion in *Section 3.3.1*).[103] As a result of the success of Mes-2,7-Me$_2$-Acr-Ph$^+$ BF$_4^-$ in the Kochi-type elimination (see Chapter 3), this acridinium was predominately used in preliminary experiments. In addition to this acridinium salt, the Co(dmgH$_2$)ClPy was utilized as the co-catalyst initially as it is one of the most common cobaloxime catalysts. Numerous initial experiments paired these catalysts together in a variety of concentrations and solvents with various bases and reductant additives. Results were variable but the alkene product was observed. The initial low conversion (<20%) was attributed to the relatively inert nature of the pre-catalyst which prevented conversion to a catalytically active species. This speculation was evaluated by subjecting the catalyst to reducing conditions before the onset of the reaction in order to obtain a Co^{II} or Co^{I} species. Specifically, a

solution of Zn and NaCl was utilized as a two-electron

reductant was needed for the reduction of Co^{III} to Co^{I}.

It was believed that an anionic Co^{I} species would

immediately deprotonate the carboxylic acid and enter
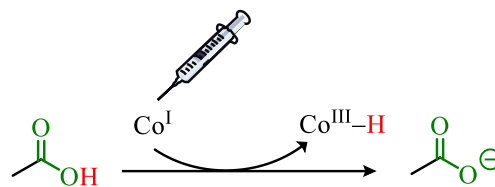
Scheme 5.2: Deprotonation with Co^{I}

the desired catalytic pathway (Scheme 5.2). This pre-activation of the cobaloxime resulted in 20-

40% yields of alkene which led to the further optimization of the decarboxylative elimination

reaction making use of a pre-reduction sequence.

In dual-catalytic processes, the concentrations of each catalyst as well as the ratios of the

catalyst to one another generally is imperative to reaction success. The Co/Acr^+ system was no

exception (Table 5.1).
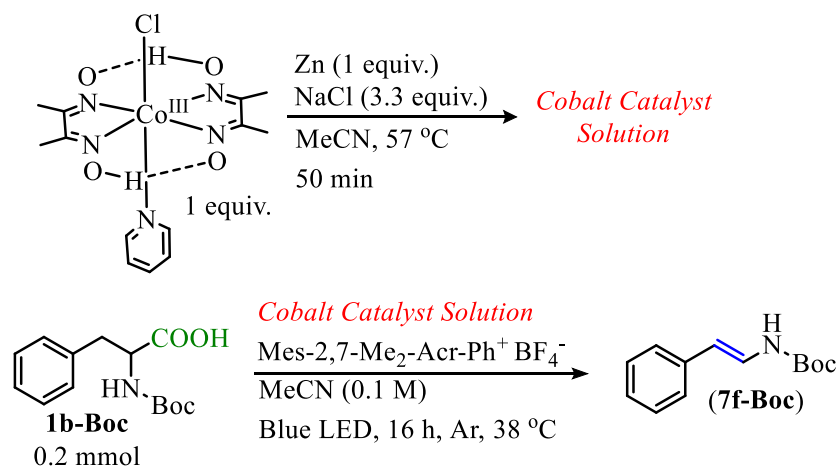
Entry	Co (mol%)	Zn (mol%)	NaCl (mol%)	Acr^+ (mol%)	Isolated Yield
1	3	3	10	3	29%
2	3	3	10	5	38%
3	6	6	20	8	39%
4	6	6	20	10	54%
5	12	12	40	10	49%
6	5	5	17	3	28%
7	1.5	1.5	5	3	30%
8	0.75	0.75	3	1.5	15%

Table 5.1: Catalyst concentrations

For the elimination of *N*-Boc phenyl alanine, enecarbamate yields were highest when a 3:5 ratio of Co(dmgH$_2$)ClPy:Mes-2,7-Me$_2$-Acr-Ph$^+$ BF$_4^-$ was utilized (Table 5.1, Entries 2,4,7,8). In this set of reactions, the highest enecarbamate yield was obtained with a 6 mol% loading of Co and an 8 mol% loading of the acridinium salt (Table 5.1, Entry 4).

Apart from MeCN, the elimination could be performed in other solvent systems (Table 5.2). Acetonitrile was utilized initially due to the success these photoredox-catalyzed reactions tend to have in the solvent, but methanol (MeOH) was found to result in superior yields (Table 5.2, Entry 3). In MeOH, a 3 mol%:5 mol% Co:Acr$^+$ was found to be the optimal catalyst loading.
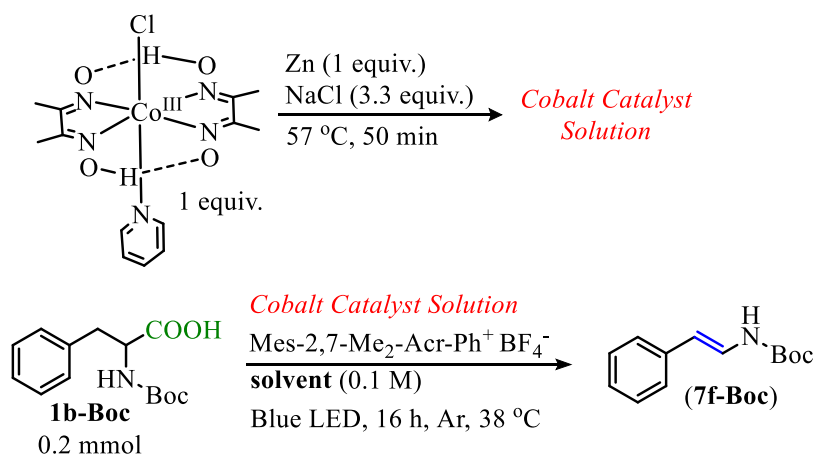
Entry	Co (mol%)	Acr$^+$ (mol%)	Solvent	Isolated Yield
1	3	5	MeCN	38%
2	6	10	MeCN	54%
3	3	5	MeOH	68%
4	6	10	MeOH	40%
5	3	5	Et$_2$O	16%
6	3	5	DMF	-

Table 5.2: Reaction solvent influence

Attention was also given to the optimization of the pre-reduction process (Table 5.3). Although Zn was initially utilized because it is a strong two electron reductant, the reduction of cobaloximes is more commonly reported with borohydride reductants.[193] Among the borohydride reductants screened, sodium triacetoxyborohydride (STAB) produced superior results (Table 5.3,

Entries 1-3). With STAB, the reaction also generally benefits from a catalytic quantity of base in the pre-reduction (Table 5.3, Entries 4-7).

Reductant
Additive
MeOH, 57 °C
50 min

Cobalt Catalyst Solution

1 equiv.

Cobalt Catalyst Solution (3 mol%)
Mes-2,7-Me$_2$-Acr-Ph$^+$ BF$_4^-$ (5 mol%)
MeCN (0.1 M), H$_2$O
Blue LED, 16 h, Ar, 38 °C

1b-Boc
0.2 mmol

(7f-Boc)
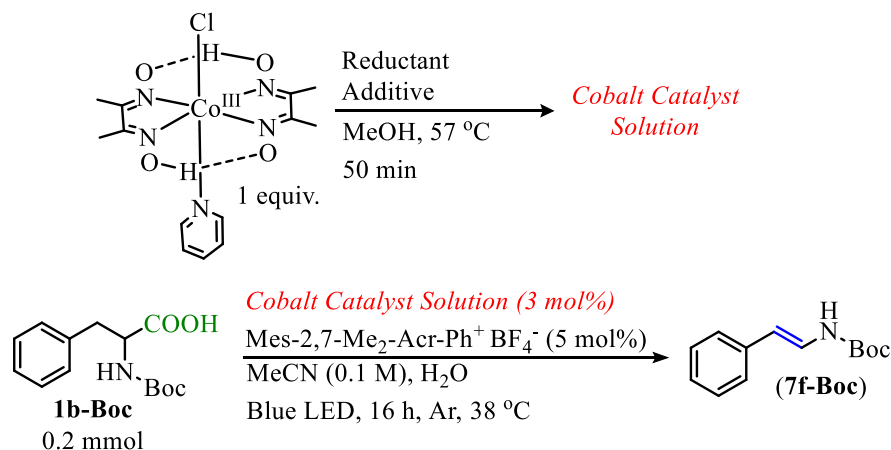
Entry	Reductant	Additive	H$_2$O	Isolated Yield
1	NaBH$_4$ (2 mol%)	-	-	20%
2	NaCNBH$_3$ (7.5 mol%)	-	-	38%
3	STAB (7.5 mol%)	-	-	52%
4	STAB (7.5 mol%)	Na$_2$CO$_3$ (1 mol%)	-	66%
5	STAB (7.5 mol%)	NaOMe (1 mol%)	-	31%
6	STAB (7.5 mol%)	NaOAc (1 mol%)	-	68%
7	STAB (7.5 mol%)	NaOAc (5 mol%)	-	56%
8	STAB (7.5 mol%)	HOAc (3 mol%)	-	61%
9	STAB (7.5 mol%)	-	0.2 mmol	62%
10	STAB (7.5 mol%)	-	7.5 mol%	70%
11	STAB (7.5 mol%)	-	3 mol%	70%
12	STAB (7.5 mol%)	-	9 mol%	65%
13	STAB (7.5 mol%)	-	1.5 mol%	62%
14	STAB (7.5 mol%)	-	11.25 mol%	62%
15	STAB (7.5 mol%)	Na$_2$CO$_3$ (1 mol%)	3 mol%	62%
16	STAB (7.5 mol%)	Na$_2$CO$_3$ (1 mol%)	6 mol%	74%
17	STAB (7.5 mol%)	Na$_2$CO$_3$ (1 mol%)	7.5 mol%	82%

Table 5.3: Reagent optimization

Additionally, the reaction proceeds to higher yields of alkene when water is incorporated into the reaction solvent (Table 5.3, Entries 9-14). When these two additives are used in conjunction, optimal yields were obtained with the best result providing enecarbamate (**7f-Boc**) in 82% yield (Table 5.3, Entries 15-17). It was found that this reaction only produces 1% yield of

(**7f-Boc**) when the Acr$^+$ is omitted from the reaction mixture and no elimination is observed when the reaction is run in the absence of Co. The reaction was found to be operable under air instead of an Ar atmosphere, however a diminished yield was observed (60% under air, 82% under Ar).

Despite being omitted from the optimization tables for clarity, it is important to note that the reaction does produce a mixture of *E/Z* isomers which was found to be a result of a background photoisomerization (see *Section 3.3.3* for discussion of this isomerization). As such, the reaction favors the *E*-isomer at the onset of the reaction but the quantity on *Z*-isomer increases as the reaction progresses. Both isomerization and reaction yield remain constant after the 16-hour irradiation time (Figure 5.3).
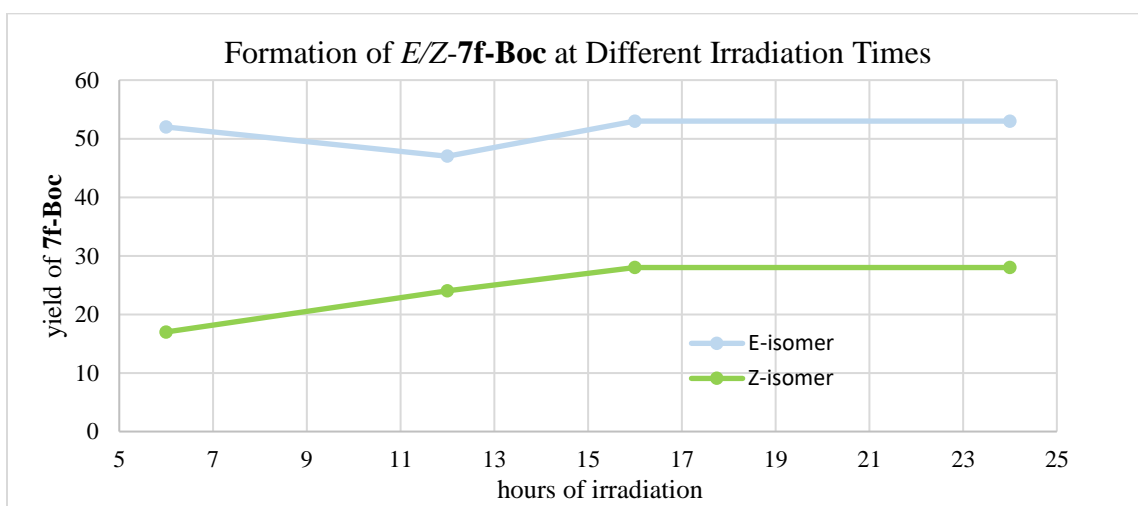
Figure 5.3: Co/Acr$^+$ decarboxylative elimination of **1b-Boc** reaction time

With optimal reaction conditions established, the catalyst system was evaluated. An investigation of the photocatalyst revealed that the Mes-2,7-Me$_2$-Acr-Me$^+$ ClO$_4^-$ catalyst led to higher yields of **7f-Boc** then the Mes-2,7-Me$_2$-Acr-Ph$^+$ BF$_4^-$ but, both of these catalysts result in high yields of the enecarbamate product (Table 5.4). The success of the *N*-Me compared to the *N*-Ph acridinium could be due to the change in redox potentials as the electron donating methyl is

expected to result in a slightly less oxidizing and more reducing photosensitizer compared to the *N*-Ph. Alternatively, the change in counter ion (BF$_4^-$ vs. ClO$_4^-$) could also be a key contributor.[194]
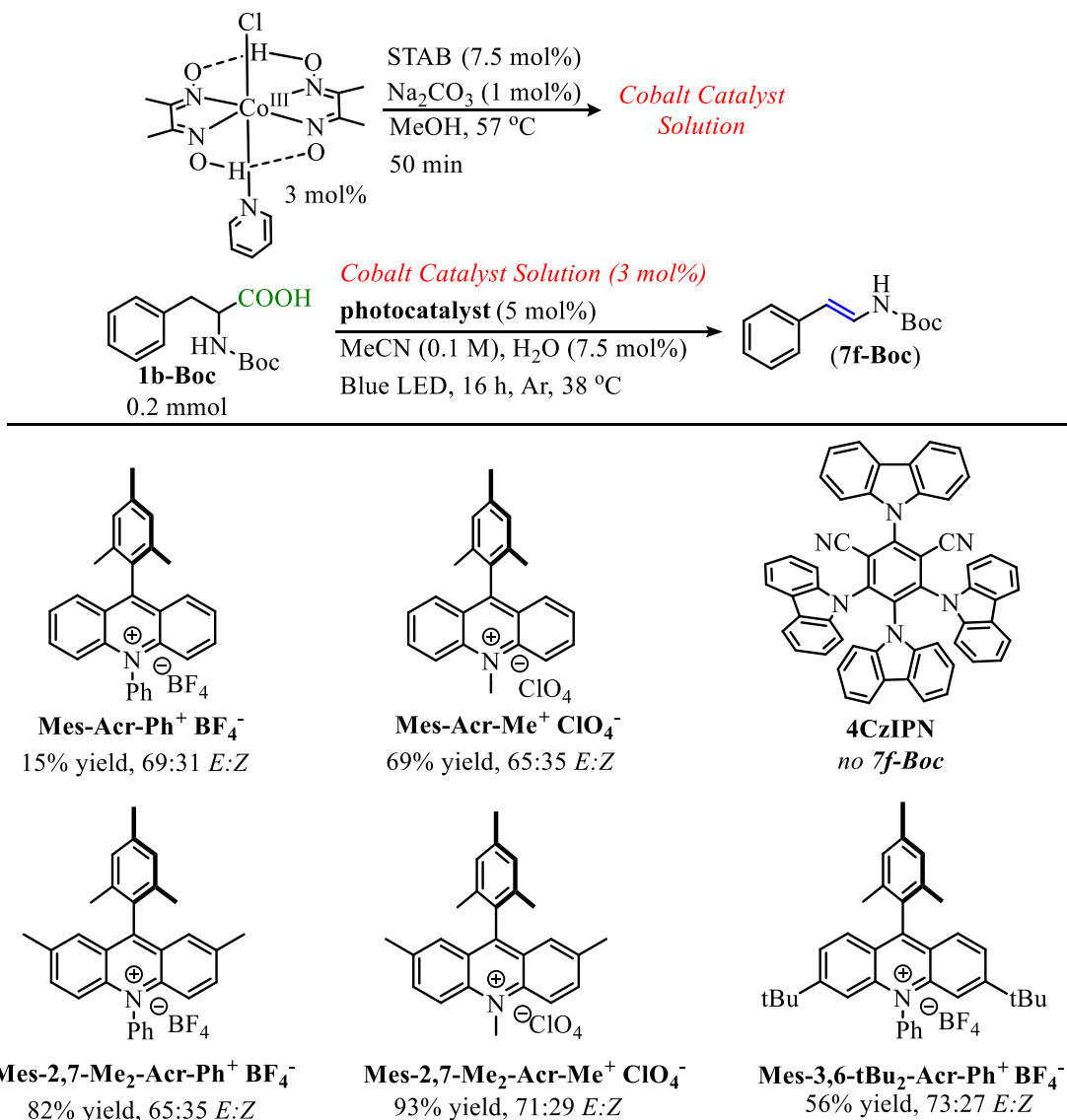
Table 5.4: Photocatalyst investigation

It is important to note that the *N*-Me acridinium salts utilized have perchlorate (ClO$_4^-$) as the counterion and the *N*-Ph salts have tetrafluoroborate (BF$_4^-$) as the counterion. The difference in counterion is expected to influence the photophysics of the photosensitizer which could influence the reaction success.[194] Although which effect is most influential on the decarboxylative elimination system is unclear, it is worth remarking on the greater success of the substituted Mes-

2,7-Me$_2$-Acr-Ph$^+$ BF$_4^-$ and Mes-3,6-(tBu)$_2$-Acr-Ph$^+$ BF$_4^-$ catalysts compared to Mes-Acr-Ph$^+$ BF$_4^-$ which may point to a better redox potential match being achieved with electron donating groups on the acridinium scaffold (Table 5.4). An alternative organophotocatalyst, 4CzIPN, was also utilized but no elimination was observed (Table 5.4).

With the potential to change the photosensitizer to the Mes-2,7-Me$_2$-Acr-Me$^+$ ClO$_4^-$, the reaction conditions were re-evaluated. It was observed that when the reductant and additives were added directly into the reaction mixture without any pre-reduction procedure, **7f-Boc** could be obtained in 86% yield (7% loss from when the pre-reduction process is utilized). Performing the reaction in the absence of STAB resulted in a 74% yield of **7f-Boc** (19% yield loss from optimal conditions) and running the reaction without Na$_2$CO$_3$ and H$_2$O resulted in a 46% yield of **7f-Boc** (47% yield loss from optimal conditions).

Concurrent with to the photosensitizer survey, the cobaloxime catalyst utilized was also evaluated. The synthetic simplicity of this class of compounds allows for the easy modification of both axial ligands as well as the equatorial ligand system (Figure 4.1).[195] Initial explorations evaluated the influence of the change in halide ligand and the bridging ligand system on the cobaloxime in addition to the compatibility of similar cobalt complexes in the elimination (Table 5.5).[196] It was observed that the Co(dmgH)$_2$XPy complexes were superior to the Co(dmgH)(dmgH$_2$)X$_2$ complexes (Table 5.5, Entries 1-2, 4-5). All of these cobaloximes have proton bridges linking the glyoxime macrocycle. When switching to a complex with BF$_2$ bridging ligands, the yield of **7f-Boc** was diminished (Table 5.5, Entry 4). Vitamin B12 was found to produce **7f-Boc** but in very low yield (7%, Table 5.5, Entry 6) and Co(salen) was found to provide the eliminated product but in less than 30% yield (Table 5.5, Entries 7-8). Thus, the cobaloxime

catalysts containing proton bridging equatorial systems and an axial base ligand were determined to be the optimal choices for further derivation.

$$\text{1b-Boc} \xrightarrow[\text{MeOH (0.1 M), H}_2\text{O (7.5 mol\%)}]{\substack{\text{Mes-2,7-Me}_2\text{-Acr-Ph}^+ \text{ BF}_4^- \text{ (5 mol\%)} \\ \text{Co (3 mol\%)}^a \\ \text{Blue LED, 38 }^\circ\text{C, 16 h, Ar}}} \text{7f-Boc}$$
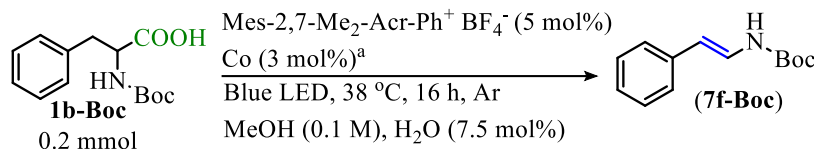
Entry	Cobalt Catalyst	Isolated Yield (E:Z)[b]
1	$Co(dmgH)_2ClPy$	82% (65:35)
2	$Co(dmgH)_2BrPy$	74% (56:44)
3	$Co(dmgBF_2)_2(CH_3CN)_2$	39% (65:35)
4	$Co(dmgH)(dmgH_2)Cl_2$	63% (67:31)
5	$Co(dmgH)(dmgH_2)Br_2$	59% (64:36)
6	B12 [c]	7% (75:25)
7	Co(salen) [c,e]	27% (74:26)
8	Co(salen) [d,e]	21% (88:12)

$Co(dmgH)_2XPy$ $Co(dmgH)(dmgH_2)X_2$ $Co(dmgBF_2)_2(CH_3CN)_2$ Co(salen)
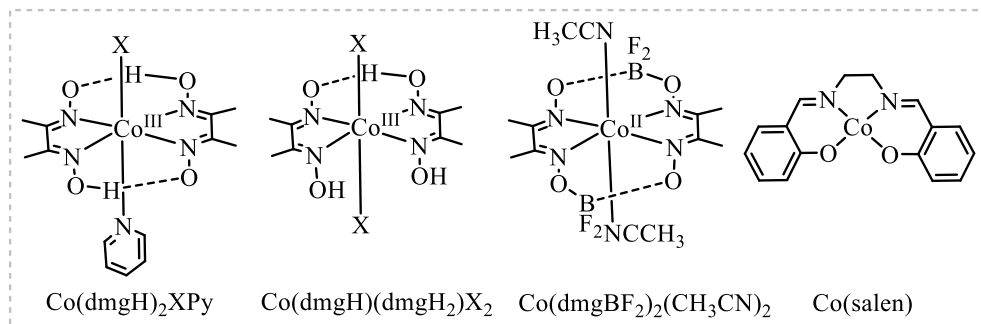
Table 5.5: Cobalt catalyst evaluation
[a] Cobalt catalyst was prepared with STAB (7.5 mol%) and Na_2CO_3 (1 mol%) in MeOH. [b] Isomer ratios determined by ^{1}H NMR. [c] Cobalt was reduced with Zn (3 mol%) in presence of NaCl (10 mol%) in MeOH. [d] No pre-reduction employed. [e] Mes-2,7-Me$_2$-Acr-Me$^+$ ClO$_4^-$ utilized.

A set of cobaloxime complexes were synthesized adhering to the general "Co(RgH)$_2$Cl(L)" structural motif (Figure 5.3).[196] In this set, three different dioxime ligands were utilized: dmgH = dimethylglyoxime, chgH = cyclohexylglyoxime, and dpgH = diphenylglyoxime. The dpgH has been documented to place the most steric demand around the Co center while there is currently conflicting evidence in the literature as to the relative *cis*-steric demand between chgH and dmgH.[198] With each equatorial ligand system, a variety of pyridine bases as well as imidazole bases were incorporated. These axial base ligands have different basicities, which has been

demonstrated to influence the TON and TOF of the cobaloxime when used as catalysts in the context of hydrogen production.[198,199] Although the electronic variation is expected to have the most profound influence, these axial bases also have different steric demands which could also contribute to their catalytic activity in the decarboxylative elimination.
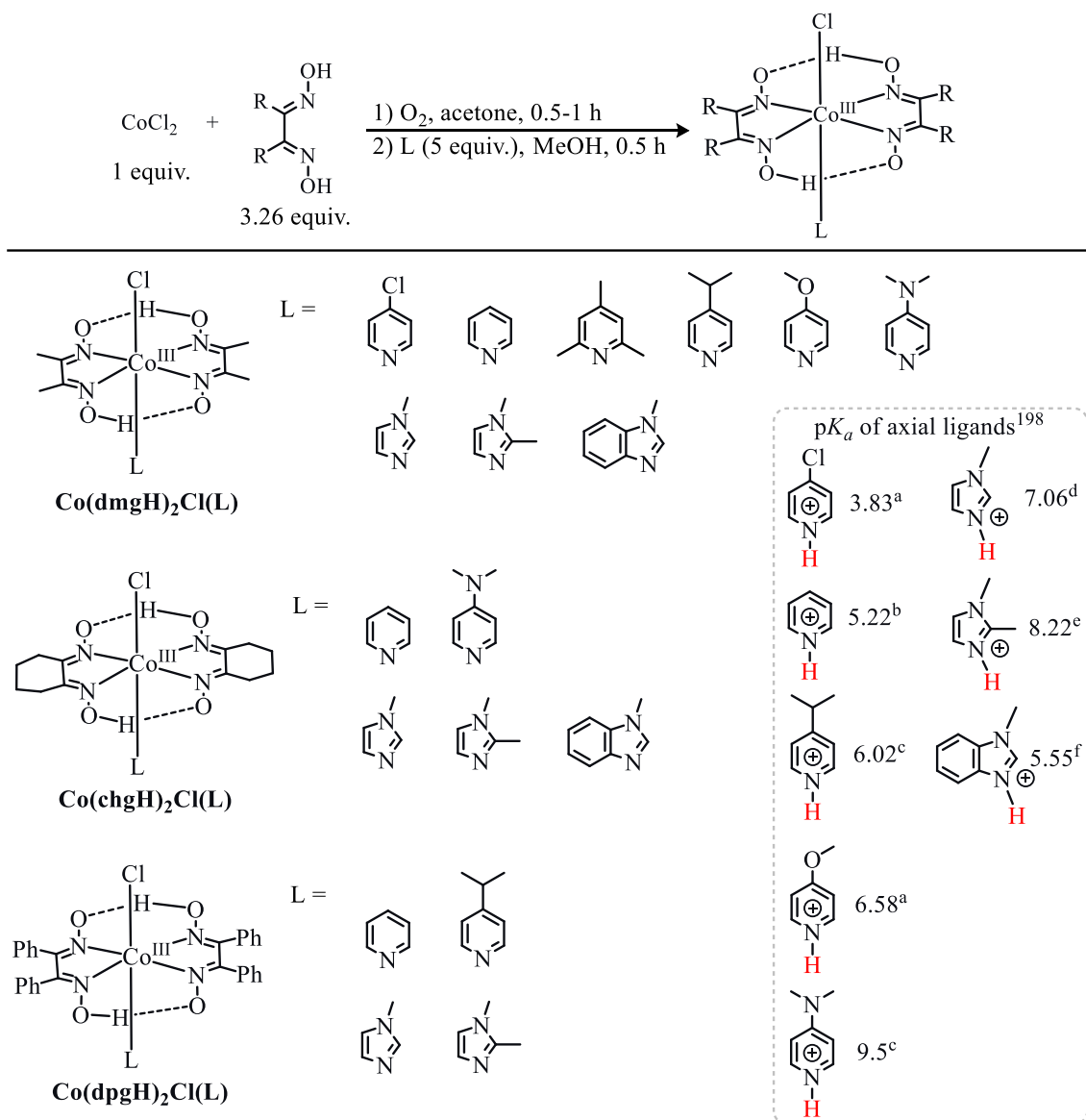
Figure 5.3: Synthesis of Co(RgH)$_2$Cl(L) catalysts

Cobaloxime catalysts with the changes to the ligand system were utilized towards the synthesis of **7f-Boc** under the established Co/Acr$^+$ dual catalytic conditions (Figure 5.4, for catalyst screenings with other amino acid substrates, see Appendix **A5**). What became immediately

apparent is the success of the dmgH ligand system compared to the chgH and dpgH ligands. The higher yields obtained with dmgH-containing catalyst was a result of higher conversion compared to the other equatorial ligands. With the change in axial base ligand, comparable results were observed between pyridine and the 4-substituted pyridines containing electron donating substituents (80-95% yield). Additionally, *N*-Me-imidazole and *N*-benzimidazole also provided comparable yields (80-90% yield). When the 4-substituent on pyridine is replaced with an electron withdrawing Cl, greatly diminished yields are observed (32% yield). Thus, the system appears to be best when the pK_a of the axial base ligand exceeds five. Diminished yields were also observed when the trimethylpyridine axial base was utilized (54% yield). This could be due to the increased steric demand around the nitrogen inhibiting the coordination ability of this ligand relative to the others which appears to have a negative influence on the elimination. The optimal catalyst for this transformation remained the Co(dmgH)$_2$ClPy and was thus utilized in further exploration of this methodology.
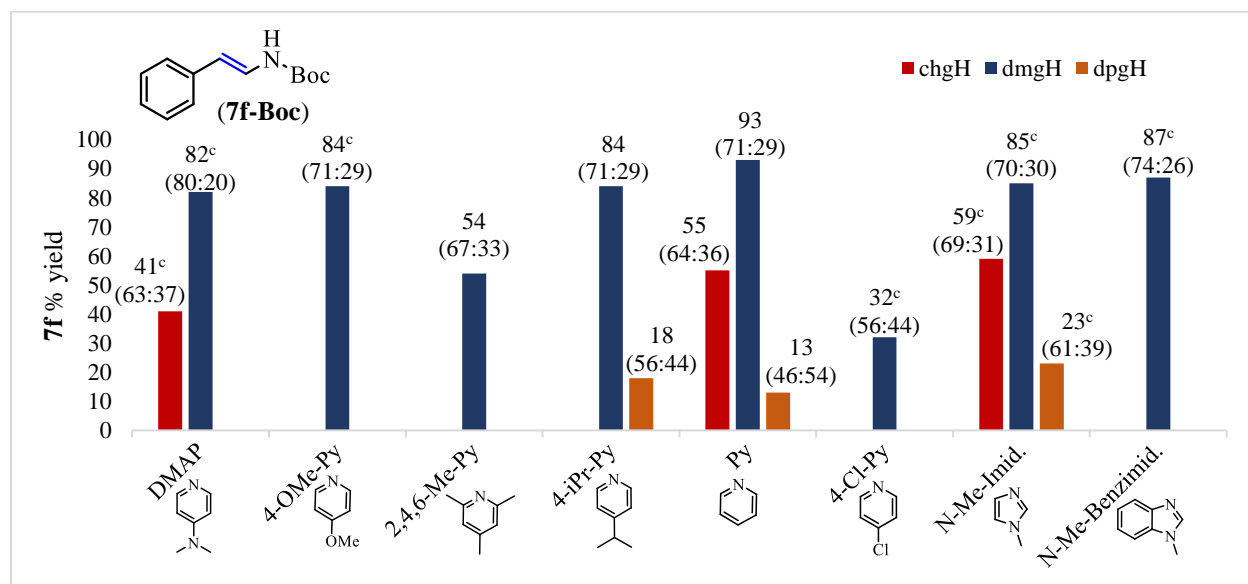
Figure 5.4: Cobaloxime ligand influence on the decarboxylative elimination of **1b-Boc**
[a] Reactions performed with protected amino acids (0.2 mmol), Mes-2,7-Me$_2$-Acr-Me$^+$ (5 mol%), cobaloxime (3 mol %), STAB (7.5 mol %), and Na$_2$CO$_3$ (1 mol %) using the pre-reduction procedure. [b] Isolated yields. [c] Determined by ^{1}H NMR vs. pyridine internal standard. [d] *E:Z* isomer ratios shown in parentheses. [e] All catalysts screened provided elimination product, absent bars indicate no corresponding catalyst. [f] Colored bars correspond to equatorial ligand changes; chgH = red, dmgH = blue, dpgH = yellow.

5.2.2 Synthesis of Enecarbamates and Enamides from N-Acyl Amino Acids

Once the optimal decarboxylative elimination conditions were unveiled, a variety of *N*-acyl amino acids were subjected to the elimination producing enamides and enecarbamates (Table 5.6).[69] Derivatives of phenylalanine were found to be useful substrates for the elimination. Interchanging Boc and acetyl protecting groups with these substrates provided similar yields and *E:Z* selectivity (**7f** & **7g**). Functionalities on the aryl substituent in the para and ortho positions were also tolerated. Having an electron-withdrawing substituent in the para position provided a slight increase in yield and *E*-selectivity compared to an electron-donating para substituent (**7h-7j-Boc**, **7x-7y-Boc**). The tolerance of various side chain functionalities as well as the protecting group identity allowed for the elimination of a simple dipeptide (**7w**). Like in the Kochi-type elimination methodology (Chapter 3), there is the possibility for HAT to occur from the N–H bond as opposed to the C–H bond. However, a tertiary amine still underwent elimination, indicating the N–H HAT pathway is not a requirement for the reaction to proceed (**7p-Boc** & **7v-Ac**). In addition, **7p-Boc** and **7v-Ac** were found to have a high degree of *E*-selectivity (**7v-Ac** does not undergo acridinium facilitated isomerization; see Figure 3.5).

Although the protecting group identity did not influence the elimination efficiency with phenylalanine derivatives, this discrepancy was found to be influential with other amino acids. Evaluating the protecting group influence with norleucine revealed that the *N*-acyl functionality outperformed *N*-carbonate functionalities (**7u**). Although the highest yields were observed with acetyl functionalities, the elimination is tolerant of more diverse acetyl groups (**7w**, **7bb**, **7cc**).

Co(dmgH)$_2$ClPy (3 mol%),
STAB (7.5 mol%), Na$_2$CO$_3$ (1 mol%),
Mes-2,7-Me$_2$-Acr-Ph$^+$ BF$_4^-$ (PC1, 5 mol%)
Mes-2,7-Me$_2$-Acr-Me$^+$ ClO$_4^-$ (PC2, 5 mol%)
MeOH (0.1 M), H$_2$O (7.5 mol%)
32 W Blue LED, Ar, 16 h

0.2 mmol

(7a) PC1: 45% yield, 67:33
PC2: 76% yield, 68:32

(7f-Ac) PC1: 85% yield, 65:35
PC2: 84% yield[e], 64:36
(7f-Boc) PC1: 82% yield, 65:35
PC2: 93% yield, 71:29

(7g-Ac) PC1: 71% yield, 90:10
PC2: 77% yield, 75:25
(7g-Boc) PC1: 59% yield, 80:20
PC2: 78% yield, 74:26

(7h-Boc) PC1: 75% yield, 71:29
PC2: 81% yield, 64:36

(7i-Boc) PC1: 71% yield, 67:33

(7j-Boc) PC1: 85% yield, 81:19
PC2: 72% yield, 78:22

(7l-Ac) PC1: 51% yield
PC2: 84% yield, 30:70

(7m-Ac) PC1: 80% yield, 75:25
PC2: 61% yield, 75:25
(7m-Boc) PC1: 24% yield, >95:5
PC2: 20% yield, 58:42

(7n-Ac) PC1: 54% yield, 76:26
PC2: 60% yield, 66:34
(7n-Boc) PC1: 24% yield, >95:5
PC2: 23% yield, 67:32

(7o-Ac) R = H; PC1: 90% yield, 85:15
(7o-Boc) R = H; PC1: 34% yield, 80:20
(7p-Boc) R = CH$_3$; PC1: 35% yield

(7q-Ac) PC1: 89% yield[e], 60:40
PC2: 85% yield, 60:40

(7r-Cbz) PC1: 61% yield, 55:45

(7u-Ac) PC1: 72% yield, 82:18
PC2: 65% yield, 77:23
(7u-Boc) PC1: 41% yield, 71:29
PC2: 20% yield, 75:25
(7u-Cbz) PC1: 52% yield, 71:29
PC2: 29% yield, 75:25

(7v-Ac) PC1: 52% yield, >95:5
PC2: 65% yield, 86:14

(7w) PC1: 77% yield, 66:34

(7y-Boc) PC1: 58% yield, 67:33
PC2: 55% yield, 69:31

(7x-Boc) PC1: 70% yield, 69:31
PC2: 64% yield, 70:30

(7z-Ac) PC1: 77% yield, 76:24
PC2: 13% yield, 85:15

(7aa-Ac) PC1: 90% yield
PC2: 81% yield

(7bb) PC1: 66% yeild

(7cc) PC1: 73% yield, 64:36[d]

Table 5.6: Scope of Enamides and Enecarbamates

[a] Pre-reduction procedure utilized. [b] All yields reported are isolated yields. [c] Isomer ratios were determined by ^{1}H NMR and are shown as *E:Z*. [d] Major isomer determined by NOESY. [e] Product isolated with aminal side product (>90% purity alkene) and mass adjusted.

168

Variation on the substrate side chain was also well tolerated. The elimination proceeded well with sterically demanding substrates **7l-Ac**, **7q-Ac**, **7aa-Ac**, **7bb**, and **7cc**. Long chain amino acids provided yields between 60-80%. These include straight chain as well as side chains with aryl, carbamate, and ester moieties (**7m-7o, 7r-Cbz**, **7u**, **7z-Ac**).

Generally, the yield and *E/Z* ratio for the alkene product was comparable between the two acridinium photocatalyst utilized (Table 5.6). However, there were a few exceptions to this observation. Although not an exception to the general observation, it is notable that slightly elevated yields were observed for **7f-Boc** when PC2 was utilized compared to PC1. Conversely, in the case of **7u-Boc** and **7u-Cbz**, PC1 provides approximately two-fold the yield as opposed to PC2. This difference is not as great with **7u-Ac**. Tertiary amino acid, **1h-Ac**, performed best with PC2 (**7l-Ac**). Also, aspartic acid-derived **7a-Boc** was obtained in superior yield with PC2. Conversely, **7z-Ac** was obtained in much higher yield with PC1 as opposed to PC2. The factor(s) dictating the yield discrepancy with the photocatalyst change is currently unclear.

Unlike the Kochi-type elimination, these reactions do produce a side product in certain instances. Along with the alkene products, an aminal side product has been observed but did not exceed 10% yield under the optimal reaction conditions (Scheme 5.3). It is worth acknowledging that when the Mes-3,6-(tBu)$_2$-Acr-Ph$^+$ BF$_4^-$ catalyst was used in the synthesis of **7f-Boc**, the aminal side product was obtained in 44% yield (see Table 5.4 for reactions with different photosensitizers). Presumably, this product could be arising from nucleophilic addition of the methanol solvent to an imine or iminium species generated through HAT from N–H or through oxidation of the carbamate by the photocatalyst.[100,127,200]
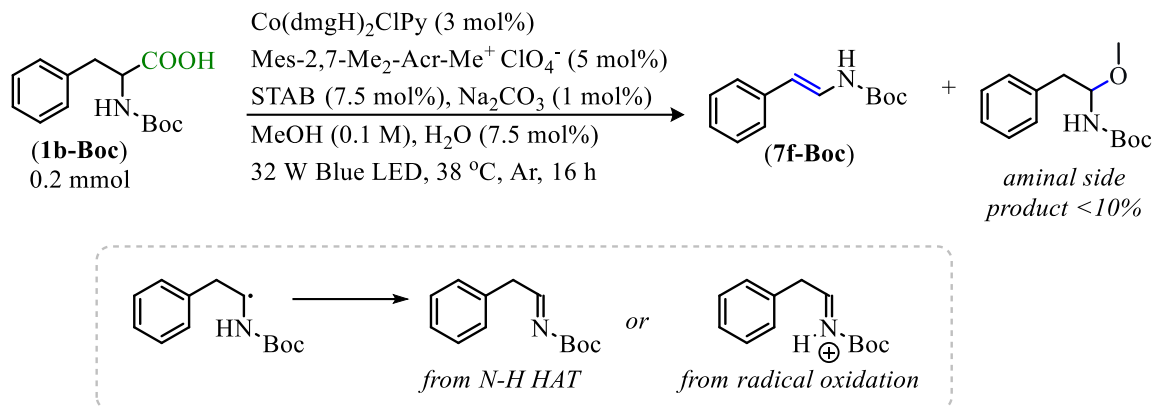
Scheme 5.3: Aminal side product

Many of these reactions were run on the 0.2 mmol scale but these reactions could be scaled to 1 mmol and run in batch efficiently. For example, product **7f-Boc** could be obtained in 83% yield when the reaction is scaled (Scheme 5.4).
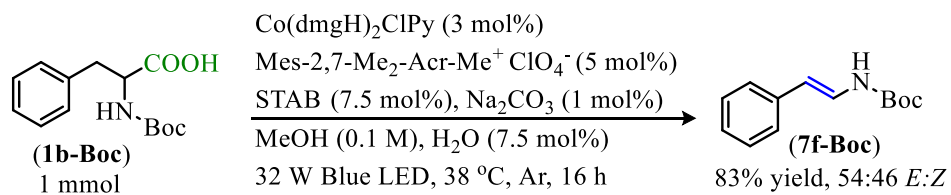
Scheme 5.4: Scalability of decarboxylative elimination protocol

5.2.3 Development of Acr$^+$/Co Catalyzed Decarboxylation of α,α-Disubstituted Carboxylic Acids

Initial interest was in the synthesis of enamides and enecarbamates due to the synthetic value of these molecules and the straightforward approach the decarboxylative elimination provides for their synthesis. But after the development of this reaction with *N*-acyl amino acids, expanding the chemistry to install alkenes in the place of simple carboxylic acids was the objective. Initial attempts utilized the conditions first established for the synthesis of enamides, however, yields were low (17% yield **8d**, Scheme 5.5).[69] Employing the Mes-2,7-Me$_2$-Acr-Me$^+$ ClO$_4^-$ photosensitizer instead of Mes-2,7-Me$_2$-Acr-Ph$^+$ BF$_4^-$ lead to a two fold increase in the alkene yield (38% yield **8d**, Scheme 5.5). This result prompted a reevaluation of the catalyst system.
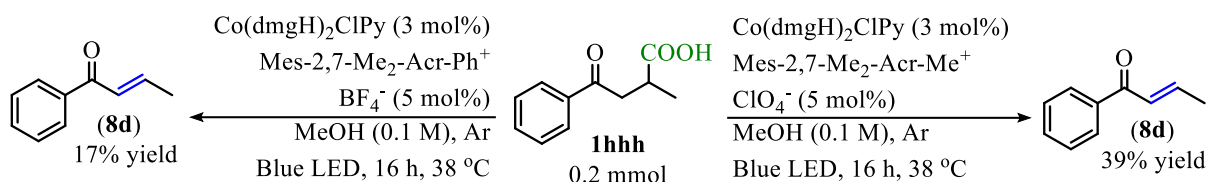

Scheme 5.5: Decarboxylative elimination of **1hhh**
[a] A pre-reduction sequence of the Co with STAB (7.5 mol%) and Na$_2$CO$_3$ (1 mol%) was performed. [b] Yields are only for the *E*-isomer but the *Z*-isomer and alternative regioisomer were isolated separately in <1% yield.

Cobaloxime catalysts with different axial base and equatorial ligand systems were then paired with Mes-2,7-Me$_2$-Acr-Me$^+$ ClO$_4^-$ in the elimination reaction of various α,α-disubstituted carboxylic acids (Figure 5.5, for additional substrate screenings see Appendix **A5**).[196] Variation of the equatorial ligand once again directly influenced the efficiency of the decarboxylative elimination with the chgH and dpgH catalysts exhibiting significantly more reactivity with simple acids than the amino acids. Despite this, dmgH generally was the superior ligand. An exception to this is with **8d** in which the best yield was obtained with dpgH as the equatorial ligand. When the amino acid catalyst screening was conducted, little influence was seen between the axial base ligands explored (Figure 5.4).
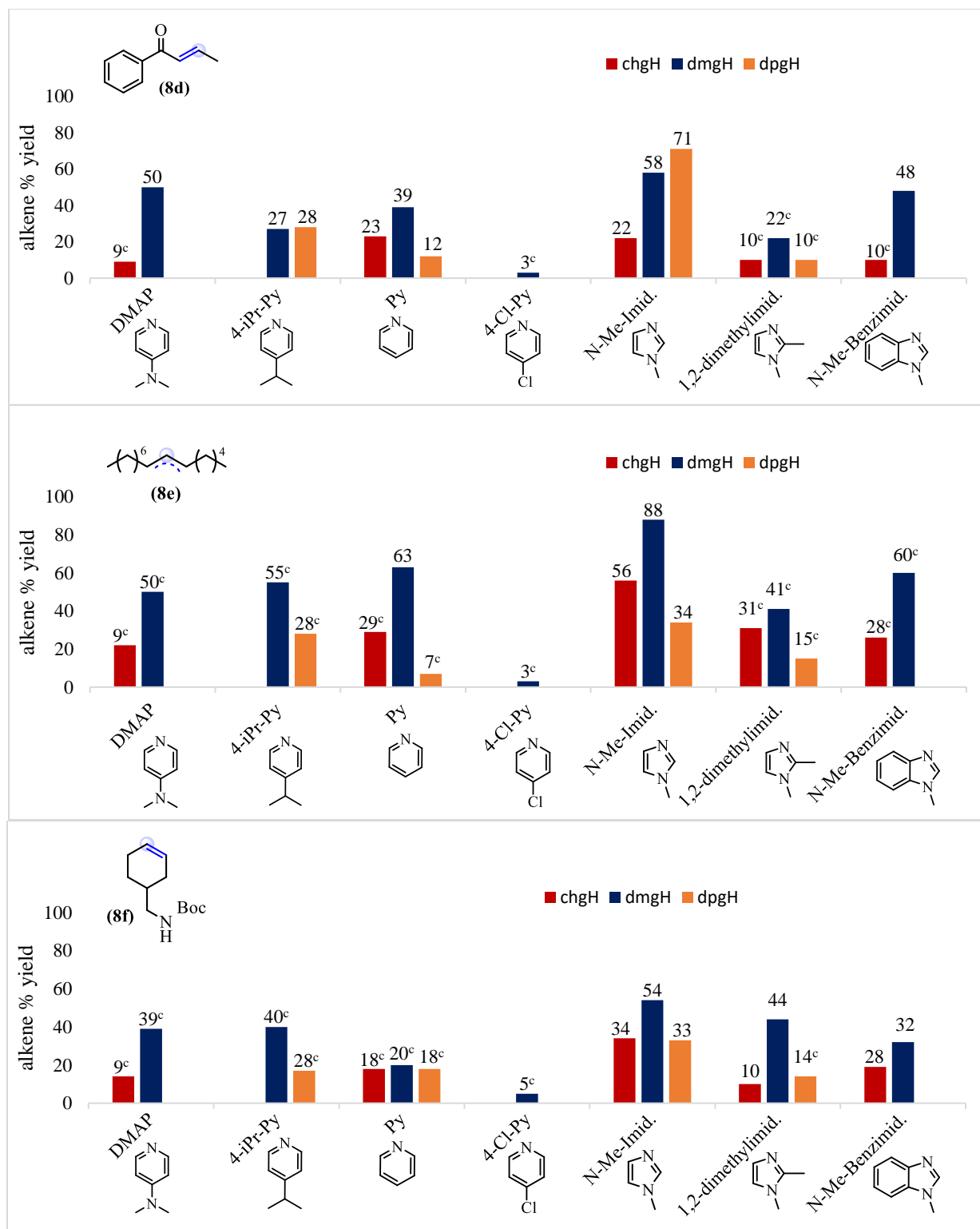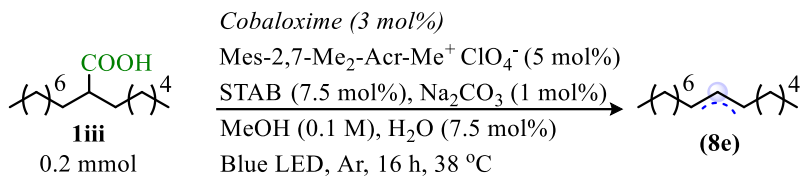
Figure 5.5: Cobaloxime catalyst screen with α,α-disubstituted acids

[a] Reactions performed with protected amino acids (0.2 mmol), Mes-2,7-Me$_2$-Acr-Me$^+$ ClO$_4^-$ (5 mol%), cobaloxime (3 mol%), STAB (7.5 mol%), and Na$_2$CO$_3$ (1 mol%) using the pre-reduction procedure. [b] Isolated yields. [c] determined by q^{1}H NMR with pyridine as the internal reference standard. [d] All ctalyst screened provided elimination product, absent bars are a result of no corresponding catalyst. [e] Colored bars correspond to equitorial ligand changes; chgH = red, dmgH = blue, dpgH = yellow.

Converse to the similar reactivity observed when various axial ligands were utilized with α-amino acid substrates, the axial ligand influence is profound when switching to the α,α-disubstituted class of acids (Figure 5.5). Although catalyst with pyridine as the axial base produced the alkene, the 4-substituted pyridines with higher pK_a values tended to perform better. Overall, the *N*-Me-imidazole proved to be the superior ligand choice. These observations correlate the axial base ligands effect on catalyst stability in hydrogen evolution.[199] Interestingly, *N*-Me-imidazole has been reported to result in the highest TON and TOF in the cobaloxime hydrogen evolution processes.[199]

The difference in yield of the alkene observed with different cobaloxime catalyst appears to be a result of two major factors. First, most reactions fail to reach complete conversion with the extent of conversion fluctuating with the change of cobaloxime. Second, an alkene side product is often observed, which, like reaction conversion, is dependent on the identity of the cobaloxime catalyst. To illustrate this, the product and starting material ratios of the crude reaction mixture as well as the yields have been compiled for **8e** (Table 5.7). The chgH and dmgH ligand systems resulted in relatively comparable conversions however, the chgH complexes produced larger quantities of alkane compared to the dmgH complexes. The increased preference for the alkane product with these complexes explains the lower alkene yields observed with these catalysts. Alternatively, the dpgH ligand system produces very little alkane product compared to dmgH and chgH. Despite this ideal alkene selectivity, the conversion is much lower when this sterically demanding ligand system is utilized. Interesting, the *N*-Me-imidazole axial base ligands leads to the highest alkene selectivity and highest yield of **8e** with chgH, dmgH, and dpgH equatorial ligands.

$Cobaloxime\ (3\ mol\%)$
$Mes\text{-}2,7\text{-}Me_2\text{-}Acr\text{-}Me^+\ ClO_4^-\ (5\ mol\%)$
$STAB\ (7.5\ mol\%),\ Na_2CO_3\ (1\ mol\%)$
$MeOH\ (0.1\ M),\ H_2O\ (7.5\ mol\%)$
Blue LED, Ar, 16 h, 38 °C

COOH

1iii
0.2 mmol

(8e)

Cobalt Catalyst	GC/MS: Alkene	Alkane	Acid	Yield (8e)
Co(chgH)$_2$ClPy	44%	51%	4%	29%
Co(chgH)$_2$Cl(DMAP)	36%	19%	45%	(22%)
Co(chgH)$_2$Cl(*N*-Me-Imidazole)	74%	12%	14%	56%
Co(chgH)$_2$Cl(1,2-dimethylimidazole)	40%	27%	33%	(31%)
Co(chgH)$_2$Cl(*N*-Me-Benzimidazole)	33%	37%	30%	(26%)
Co(dmgH)$_2$ClPy	71%	14%	16%	63%
Co(dmgH)$_2$Cl(4-iPr-Py)	68%	26%	6%	(55%)
Co(dmgH)$_2$Cl(DMAP)	45%	23%	32%	(50%)
Co(dmgH)$_2$Cl(4-Cl-Py)	21%	30%	49%	(3%)
Co(dmgH)$_2$Cl(*N*-Me-Imidazole)	95%	5%	0%	88%
Co(dmgH)$_2$Cl(1,2-dimethylimidazole)	56%	30%	14%	(41%)
Co(dmgH)$_2$Cl(*N*-Me-Benzimidazole)	59%	39%	2%	(39%)
Co(dmgH)$_2$Cl(PPh$_3$)	32%	33%	35%	(32%)
Co(dpgH)$_2$ClPy	18%	13%	69%	(7%)
Co(dpgH)$_2$Cl(4-iPr-Py)	32%	12%	56%	(28%)
Co(dpgH)$_2$Cl(*N*-Me-Imidazole)	28%	0%	72%	34%
Co(dpgH)$_2$Cl(1,2-dimethylimidazole)	23%	28%	49%	(15%)

Table 5.7: Alkane product formation with cobaloxime catalyst variation
[a] Product ratios were determined by GC/MS. [b] (yields) were determined by q^{1}H NMR using 0.2 mmol pyridine as the internal reference standard. All other yields isolated.

To better understand the reaction pathway by which the alkane forms, the decarboxylative elimination reaction for the formation of **8g** was monitored overtime (Scheme 5.6). This substrate was chosen as it was observed to produce significant alkane product. This evaluation revealed that the alkane side product does not begin forming until late in the reaction. The delayed production of alkane likely indicates that the alkane formation results from a decomposed cobaloxime catalyst that is either an effective hydrogenation catalyst or, ineffective at HAT leading to greater disproportionation at later reactions times.
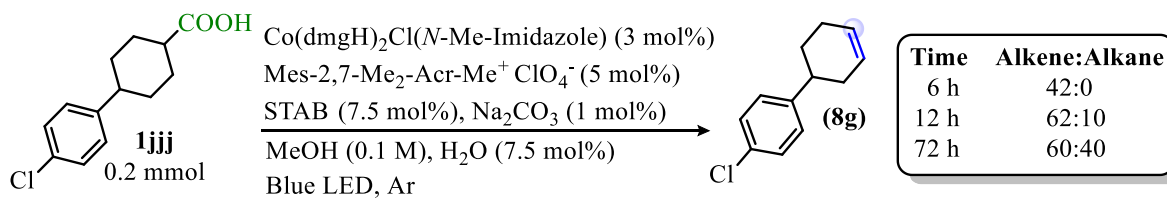
**Scheme 5.6**: Alkane formation over time
[a] Product ratios observed by GC/MS. [b] *In situ* reduction protocol followed.

To further investigate the mechanism of alkane formation, the elimination with a poorly

selective Co(dmgH)$_2$Cl(*N*-Me-benzimidazole) catalyst was undertaken (Scheme 5.7A). In order to

determine if the hydrogen produced leads to hydrogenation of the alkene, gaseous H$_2$ was

continuously removed by maintaining a flow of nitrogen through the headspace of the reaction

vessel. Under these conditions the elimination provided product **8e** in 58% yield and a 77:23

alkene:alkane ratio (Scheme 5.7B). This result is an improvement over the 39% yield, 60:40

alkene:alkane ratio observed under the standard reaction conditions (Scheme 5.7A). Thus, the

lower quantity of alkane produced indicates the increasing [H$_2$] plays a role in the production of

alkane.

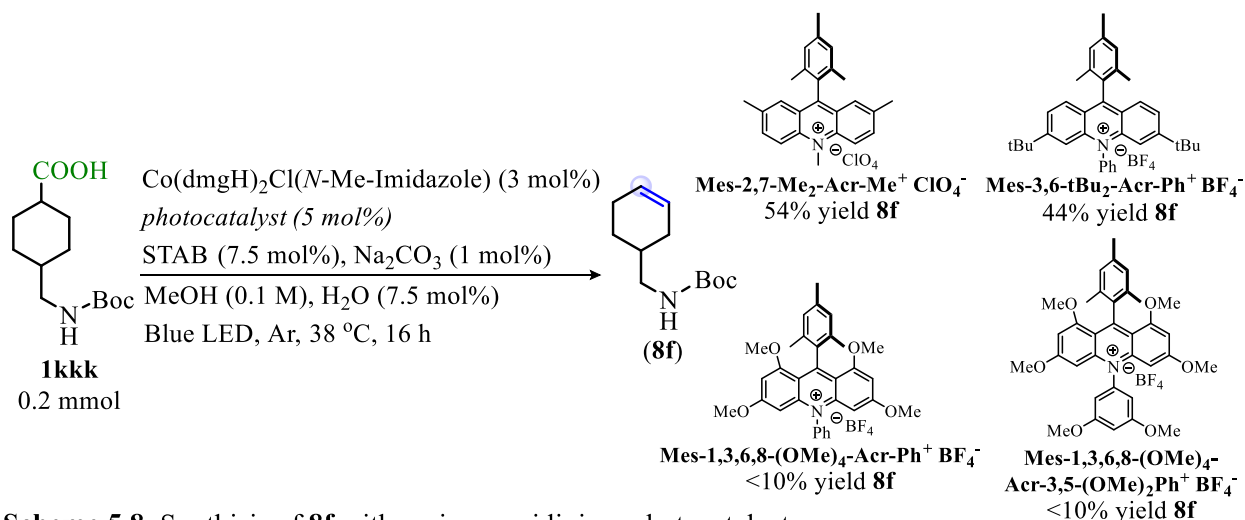A. Standard Elimination Conditions
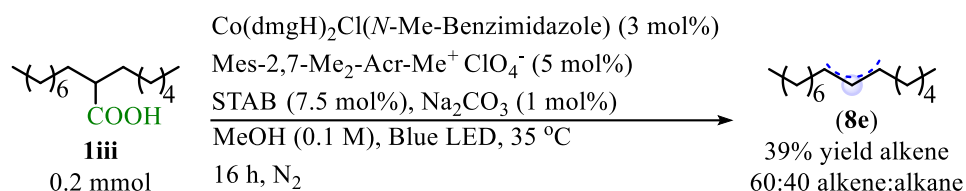
B. Elimination with H$_2$ Removal
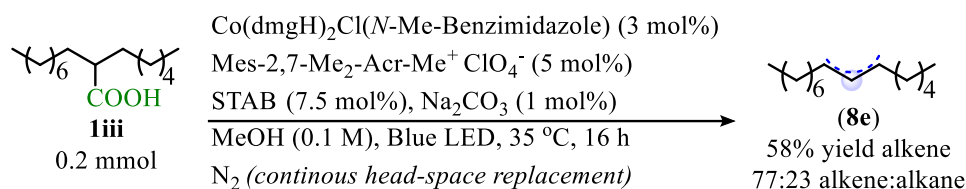
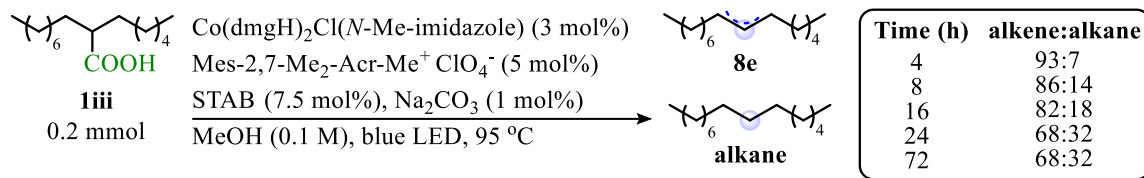**Scheme 5.7**: Effect of H$_2$ on decarboxylative elimination

At this point, several conclusions were made about the system. The yield of the desired

alkene was being influenced by the overall reaction conversion, the formation of an undesired

alkane side product, and the identity of the cobaloxime (Table 5.7). Additionally, extended irradiation time was found to have little impact on alkene yield but resulted in an increased quantity of alkane (Scheme 5.6). Lastly, the alkane product does not begin forming until late in the reaction and its formation can be dampened by removal of the H_2 byproduct (Scheme 5.7). These results suggest a degrading catalyst as the source of low conversion and alkane side product formation.

To address the challenge posed by a degrading catalyst system, several alterations to the reaction matrix and catalyst system were undertaken. First, a return to other acridinium photosensitizers in the elimination was undertaken but Mes-2,7-Me$_2$-Acr-Me$^+$ ClO$_4^-$ remained the superior photocatalyst for this reaction (Scheme 5.8). Heating the reaction was also investigated (Scheme 5.9). Typically, the decarboxylative elimination reactions were performed at 38 ^{o}C, the heat that results from irradiation in the optimal LED light assembly. This temperature can be increased through the use of higher intensity LED lamps providing a 95 ^{o}C reaction temperature for the elimination. The elevated temperature did allow for the rate to be increased but the alkene yield was not improved. Also, the additional heat leads to an elevated rate of alkane formation.
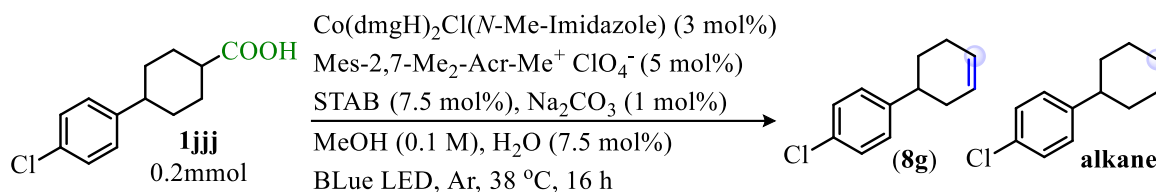

Scheme 5.8: Synthisis of 8f with various acridinium photocatalysts

Co(dmgH)$_2$Cl(N-Me-imidazole) (3 mol%)
Mes-2,7-Me$_2$-Acr-Me$^+$ ClO$_4^-$ (5 mol%)
STAB (7.5 mol%), Na$_2$CO$_3$ (1 mol%)
MeOH (0.1 M), blue LED, 95 °C

Time (h)	alkene:alkane
4	93:7
8	86:14
16	82:18
24	68:32
72	68:32

Scheme 5.9: Decarboxylative elimination at elevated temperature
[a] Product ratios (%) were determined by GC/MS. [b] *In Situ* reduction procedure utilized.

The addition of fresh catalyst(s) was also investigated in hopes that recharging the system with new catalyst would provide additional conversion and for the elimination pathway to remain dominant (Table 5.8). These reactions did not lead to improved yield of alkene product as the catalyst recharge attempts either had little influence on the reaction or resulted in diminished alkene product yields.

Co(dmgH)$_2$Cl(N-Me-Imidazole) (3 mol%)
Mes-2,7-Me$_2$-Acr-Me$^+$ ClO$_4^-$ (5 mol%)
STAB (7.5 mol%), Na$_2$CO$_3$ (1 mol%)
MeOH (0.1 M), H$_2$O (7.5 mol%)
BLue LED, Ar, 38 °C, 16 h

| Co Recharge	Acr$^+$ Recharge	GC/MS: Alkene	Alkane	COOH	Yield (8g)
-	5 mol % after 6h	-	-	-	45%
3 mo1% after 6h	-	-	-	-	62%
3 mol % after 13h	5 mol % after 13h	-	-	-	46%
3 mol % after 15h	-	71%	6%	23%	58%
-	5 mol % after 15h	72%	10%	18%	39%
3 mol % after 15h	5 mol % after 15h	88%	10%	2%	45%

Table 5.8: Catalyst recharge experiments

A 2009 report by Eisenberg proved to be enlightening to overcoming the challenge of a degrading catalyst system.[140h] Eisenberg's report focused on the production of H$_2$ from acidic media with cobaloxime catalyst. In this work, the cobaloxime catalysts were demonstrated to degrade as a result of the hydrogen evolution process. This degradation was speculated to be a result of the relatively labile glyoxime ligand system which was ultimately diminished using additional dimethylglyoxime ligand in the reaction mixture.[140h,201] When this strategy was

employed in the decarboxylative elimination of α,α-disubstituted acids, higher conversions and higher yields of alkene product were able to be obtained (Scheme 5.10).
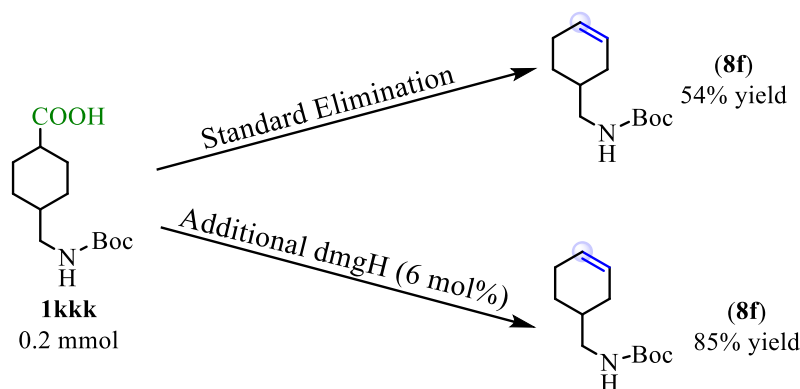
Scheme 5.10: Influence of free dmgH ligand in decarboxylative elimination

Additionally, this strategy for improving catalyst longevity not only improved conversion but also reduced the formation of the alkane side product (Scheme 5.11). The inclusion of free dmgH in the reaction mixture resulted in a two-fold increase of **8e** and a two-fold reduction in alkane formation with the Co(dmgH)$_2$Cl(N-Me-benzimidazole) catalyst. Without the free ligand, this catalyst results in lower conversion and a larger quantity of alkane side product (Table 5.7 & Scheme 5.7).
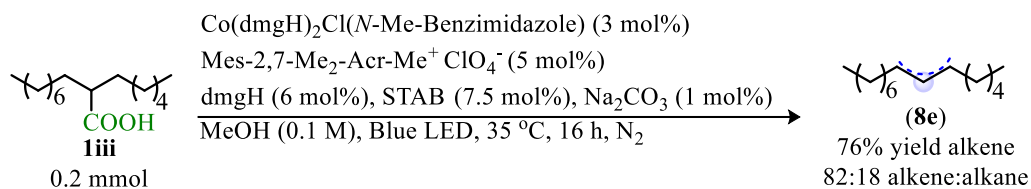
Scheme 5.11: Additional dmgH influence on conversion and alkene selectivity

5.2.4 Synthesis of Olefins from Carboxylic Acids

With conditions established for the decarboxylative elimination of α,α-disubstituted acids, a variety of long chain fatty-acid-type substrates as well as cyclic scaffolds with carboxylic appendages were selected for exploration (Table 5.9 & 5.10). As a result of the high success of the

N-Me-imidazole axial base ligand but the variable results obtained with the equatorial ligand systems (Figure 5.5), the elimination of the selected acids were performed with Co(chgH)$_2$Cl(N-Me-Imidazole), Co(dmgH)$_2$Cl(N-Me-Imidazole), and Co(dpgH)$_2$Cl(N-Me-Imidazole) (Table 5.9). However, apart from **8d** and **8g**, the highest yields were obtained with the Co(dmgH)$_2$Cl(N-Me-Imidazole) catalyst. This exploration of scope also revealed that the architecture of the substrates evaluated had profound influences on the efficiency and regioselectivity of the elimination.

Acyclic carboxylic acids underwent elimination most efficiently when there was less steric hindrance around the reaction site (Table 5.9, **8d**-**8e**, **8h-8l**). The more sterically encumbered reactive sites resulted in lower conversions and lower alkene yields.

Co(R)$_2$Cl(N-Me-Imidazole) (3 mol%)
Mes-2,7-Me$_2$-Acr-Me$^+$ClO$_4^-$ (5 mol%)
STAB (7.5 mol%), Na$_2$CO$_3$ (1 mol%)
MeOH (0.1 M), H$_2$O (7.5 mol%)
Blue LED, Ar, 38 °C, 16 h

0.2 mmol

(8d)
dmgH: 58% yield E
chgH: 22% yield E
dpgH: 71% yield E

(8e)
dmgH: 88% yield, 1:1
chgH: 56% yield, 1:1
dpgH: 34% yield, 1:1

(8h)
dmgH: 88% yield, 66:34, A:B
chgH: 84% yield[d], 60:40 A:B
dpgH: 70% yield[d], 53:47 A:B

(8i)
dmgH: 64% yield, 78:22 A:B[d]
chgH: 60% yield, 80:20 A:B[d]
dpgH: 27% yield, 77:23 A:B[d]

(8j)
dmgH: 52% yield, E/Z, >90:10 A:B[e]
chgH: 40% yield, E/Z, >90:10 A:B[e]
dpgH: 44% yield, E/Z, >90:10 A:B[e]

(8k)
dmgH: 32% yield[f], 74:26 E:Z
chgH: 6% yield[f], 78:22 E:Z
dpgH: 13% yield[f], 73:27 E:Z

(8l)
dmgH: 37% yield, 80:20 E:Z
chgH: 32% yield, 79:21 E:Z
dpgH: 35% yield, 77:23 E:Z

Table 5.9: Decarboxylative elimination of disubstituted acyclic carboxylic acids
[a] Reaction performed using the pre-reduction method and isolated yields are reported unless otherwise denoted.
[b] Regioisomer ratios were determined using ^{1}H & COSY NMR. [c] Yields determined with q^{1}H NMR. [d] Isolated >95:5 E/Z ratio. [e] Mix of E/Z isomers for each regioisomer. [f] Isolated >95:5 regioisomer ratio; isolated with alkane product and yield adjusted accordingly. [g] Geometric isomers were determined with NOESY.
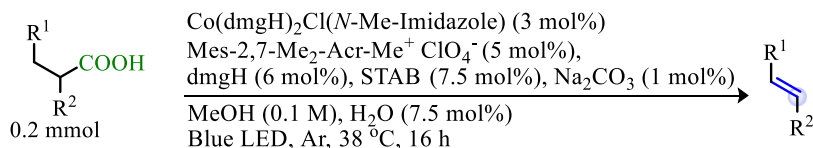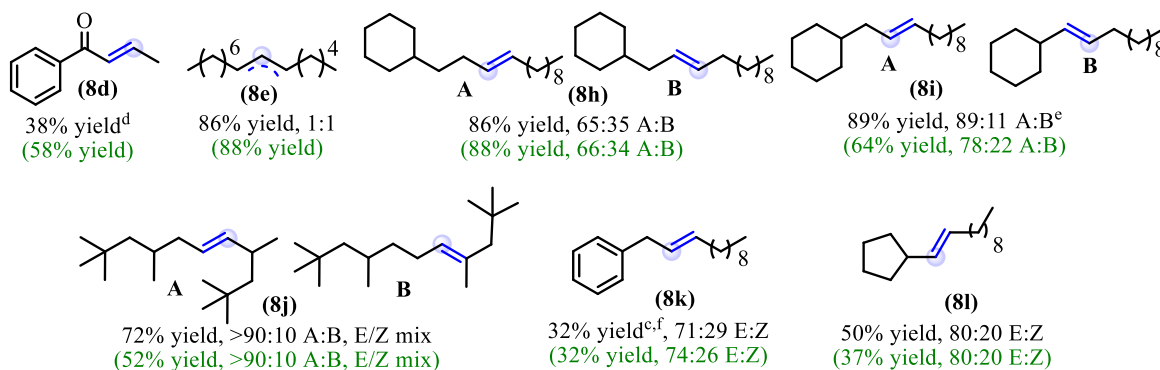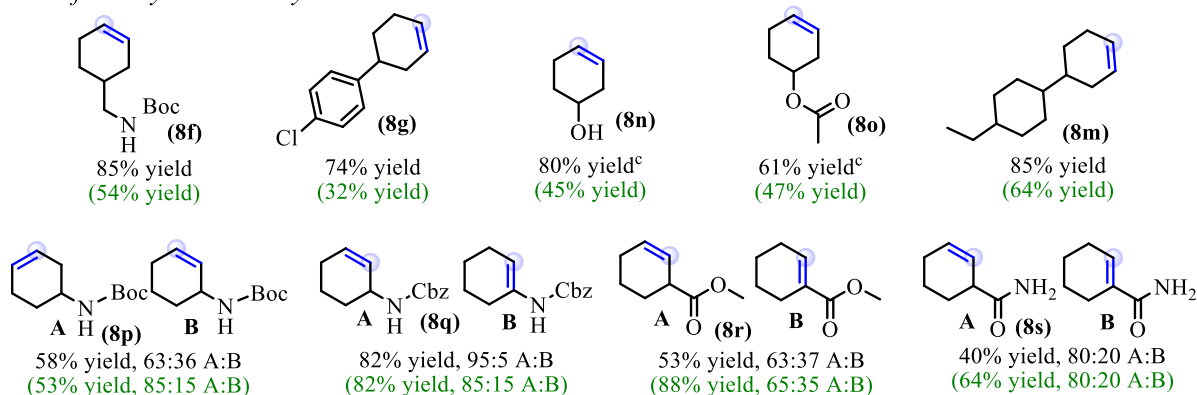
Conversely, the cyclic carboxylic acids benefited from more steric hindrance around the reactive site. Higher conversions and higher alkene yields were obtained when more steric demand was present around the carboxylic acid moiety compared to the less sterically hindered substrates (Table 5.10, **8f-8g**, **8m-8s**). In all cases, the elimination was selective for the Hofmann products and the less sterically encumbered olefin products. Greater regioselectivity arose from increased steric differentiation. In addition to the regioselectivity, certain examples also resulted in a mix of *E/Z*-isomers (Table 5.9, **8j-8l**).[69,100,118]
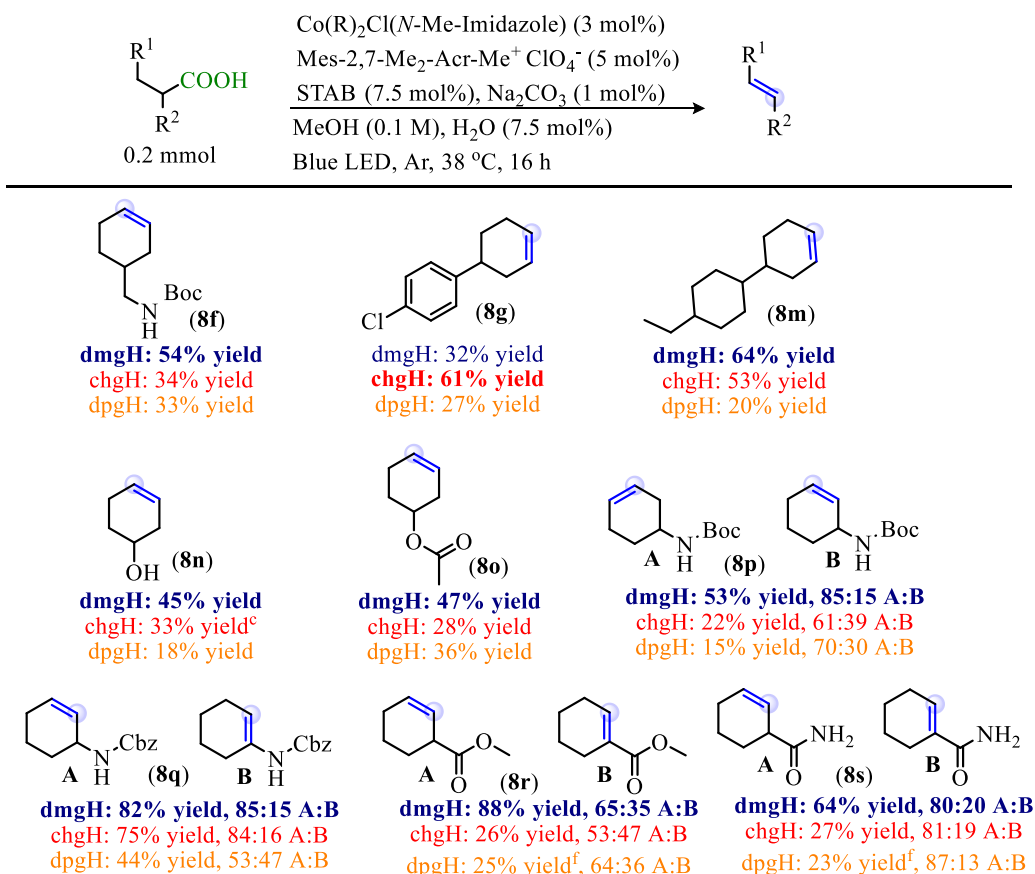
Table 5.10: Decarboxylative elimination of disubstituted cyclic carboxylic acids
[a] Reaction performed using the pre-reduction method and isolated yields are reported unless otherwise denoted. [b] Regioisomer ratios were determined using ^{1}H & COSY NMR. [c] Yields determined with q[1]H NMR. [d] Isolated >95:5 *E/Z* ratio. [e] Mix of *E/Z* isomers for each regioisomer. [f] Isolated >95:5 regioisomer ratio; isolated with alkane product and yield adjusted accordingly. [g] Geometric isomers were determined with NOESY.

The lower yields that result with certain molecular scaffolds were observed to be a result of low conversion. These yields were able to be significantly raised in most cases when the additional dmgH ligand conditions were employed (Table 5.11). Thus, the substrates that resulted in lower alkene yield without the utilization of free dmgH in the reaction matrix were more impacted by catalyst degradation.

Reaction scheme:

R^1–CHR^2–COOH (0.2 mmol) →

Co(dmgH)$_2$Cl(*N*-Me-Imidazole) (3 mol%)
Mes-2,7-Me$_2$-Acr-Me$^+$ ClO$_4^-$ (5 mol%),
dmgH (6 mol%), STAB (7.5 mol%), Na$_2$CO$_3$ (1 mol%)
MeOH (0.1 M), H$_2$O (7.5 mol%)
Blue LED, Ar, 38 °C, 16 h

→ alkene (R^1, R^2)

Alkenes from Acyclic Carboxylic Acids:

(8d)
38% yield[d]
(58% yield)

(8e)
86% yield, 1:1
(88% yield)

(8h) A / B
86% yield, 65:35 A:B
(88% yield, 66:34 A:B)

(8i) A / B
89% yield, 89:11 A:B[e]
(64% yield, 78:22 A:B)

(8j) A / B
72% yield, >90:10 A:B, E/Z mix
(52% yield, >90:10 A:B, E/Z mix)

(8k)
32% yield[c,f], 71:29 E:Z
(32% yield, 74:26 E:Z)

(8l)
50% yield, 80:20 E:Z
(37% yield, 80:20 E:Z)

Alkenes from Cyclic Carboxylic Acids:

(8f)
85% yield
(54% yield)

(8g)
74% yield
(32% yield)

(8n)
80% yield[c]
(45% yield)

(8o)
61% yield[c]
(47% yield)

(8m)
85% yield
(64% yield)

(8p) A / B
58% yield, 63:36 A:B
(53% yield, 85:15 A:B)

(8q) A / B
82% yield, 95:5 A:B
(82% yield, 85:15 A:B)

(8r) A / B
53% yield, 63:37 A:B
(88% yield, 65:35 A:B)

(8s) A / B
40% yield, 80:20 A:B
(64% yield, 80:20 A:B)

Table 5.11: Decarboxylative elimination of α,α-disubstituted carboxylic acids with free dmgH ligand
[a] *In situ* reduction procedure with was utilized. [b] Isolated yields are reported unless otherwise specified; reported ratios for enamide products are *E:Z* isomer ratios determined by ^{1}H NMR. [c] q[1]H NMR yield with 0.2 mmol pyridine as the internal reference standard. [d] Isolated only the *E*-isomer; reaction produces >99:1 *E:Z*. [e] >95:5 *E:Z*. [f] Isolated with alkane and in >95:5 regioisomer ratio. [g] COSY used to determine regio-isomer ratio. [h] NOESY used to determine geometric isomers. [i] () yields are without extra ligand.

181

In the case of acyclic acids, the lower yields with increased steric demand could be a result of a higher energy reaction pathway needing to be accessed to productively eliminate. Thus, the additional hindrance may slow the rate of elimination or allow for off-cycle pathways to be more prevalent. The inverse observation with the cyclic carboxylic acid substrates was intriguing. The improved yields with increased steric demand are possibly indicative of an off-cycle Co–alkyl complex forming which has been shown in other systems to inhibit catalysis.[202] Increasing steric demand presumably allows for homolysis of this species and ultimately a productive pathway to proceed. In sum, structural features that may influence the rate of catalysis appear to result in premature catalyst degradation. But this can generally be overcome through the use of additional dmgH ligand in the reaction.

An additive robustness screening was also completed with **1iii** serving as the model substrate (Figure 5.6).[15] The functionalities in question have been grouped based on the yield of eliminated product **8e** obtained in the presence of each additive (Figure 5.6). Apart from the α,β-unsaturated ketone **A11** and aldehyde **A12**, all of the reactions proceeded without side product formation. The olefin in ketone **A11** was reduced to provide 14% yield of the reduced ketone product and the remaining **A11** was recovered. On the other hand, the aldehyde **A12** produced a complex mixture of side products. Despite the side product formation, the elimination was able to proceed in the presence of these additives to provide moderate yields of **8e**.
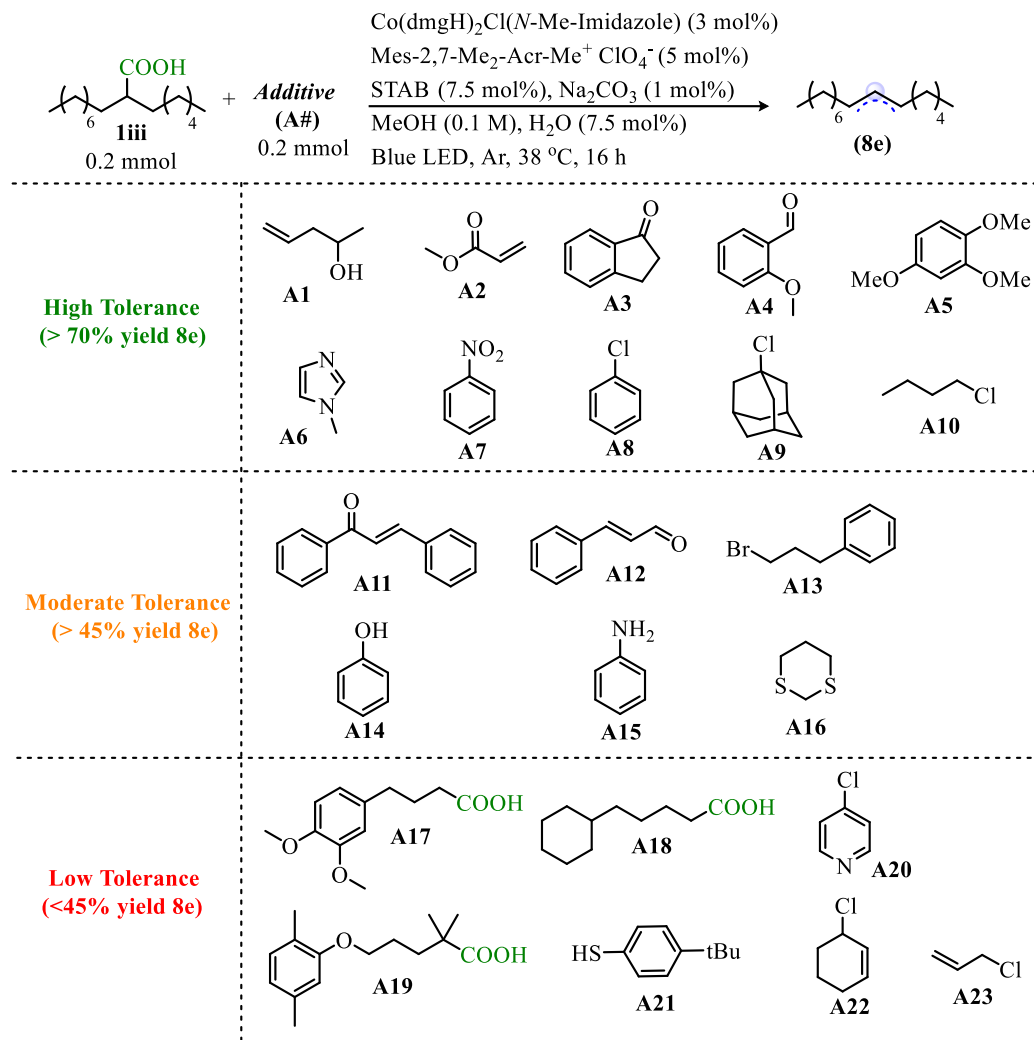
Figure 5.6: Additive robustness screening

[a] Reactions performed with *in situ* reduction procedure. [b] Product(s) were isolated post irradiation.

The reaction was able to proceed with high efficiency in the presence of hydroxyl, carbonyl, aryl, ether, and ester functionalities (**A1-A5**). Interestingly, it was tolerant of both a terminal olefin (**A1**) as well as a Michael acceptor (**A2**). Both of these functionalities have the propensity to react with suspected reactive intermediates in this chemistry. Terminal olefin **A1** was suspected to be posed for isomerization to the more thermo-stable internal olefin by Co–H, a key intermediate proposed in hydrogen evolution chemistry (see *Section 4.2* for Co–H discussion).[141d,142,144,145,147] Michael acceptor **A2** is a known radical trap, but no coupled product was observed.[203] The reaction also performed well in the presence of a good axial base ligand **A6**

and the reaction was highly efficient in the presence of nitroarene (**A7**) as well as various alkyl chlorides **A8-A10**). The tolerance of these chloride reagents was somewhat surprising given the propensity of cobaloximes to react with alkyl halides (see also *Section 2.5*).[61,62]

Although some alkyl halides were well tolerated, others like alkyl bromide **A13** and allylic chlorides **A22** and **A23** lead to an interruption of the elimination. Presumably, these functionalities take the cobaloxime off-cycle (see *Section 2.5*). In addition, moderately Lewis-basic substrates such as **A14-16** and **A20-21** lead to lower alkene formation. It is likely that Lewis-basic functionalities interrupt the catalytic cycle via undesired coordination with the cobalt catalyst, making a less active catalyst. It is worth noting that when **A20** was utilized as the axial base ligand the elimination was poor (Figure 5.5).

Perhaps the most intriguing reactivity interruption resulted from the use of monosubstituted (**A17-18**) or trisubstituted (**A19**) carboxylic acids in the reaction. Although the elimination does not operate efficiently in converting monosubstituted and trisubstitute carboxylic acids to alkenes, these functionalities were not expected to interfere with the elimination of α,α-disubstituted acids. However, both **A17** and **A19** resulted in <10% yield of desired alkene **8e**. The reaction with **A18** lead to product **8e** in 36% yield and the reduced alkane side product in 16% yield. Neither **A17**, **A18**, or **A19** underwent elimination in this reaction. When these acids were subjected to the elimination conditions individually, <20% yield of elimination was observed. These results suggest that the unsubstituted and quaternary acids do not proceed efficiently due to an interruption of the catalytic cycle perpetuated by these substrates.

5.2.5 Exploration into Reaction Mechanism

As discussed in detail in Chapter 4, synthetic methods utilizing photoredox/cobaloxime systems in small molecule functionalizations are on the rise but, the catalytic pathways by which these reactions proceed are not well understood. To further advance the undertanding of the elimination chemistry and to gain insight into photoredox/cobaloxime hydrogen evolving systems, the decarboxylative elimination was probed. First, it is important to note that the decarboxylative elimination does not proceed without the acridinium photocatalyst, light, or the cobaloxime catalyst.[3c]

Due to the high oxidation potential of the carboxylate, the acridinium is expected to be required to facilitate single electron oxidation of the carboxylate.[19] The high excited state reduction potential of the acridiniums ($> +2.0$ V vs. SCE) should allow for the facile oxidation of unsubstituted, α,α-disubstituted, and quaternary carboxylates however, the decarboxylative elimination described herein was found the be most efficient with disubstituted acids (Table 1.1).[102] Thus, the redox potentials do not account for this reactivity difference. It was also observed that an association event can occur between the carboxylate and the acridinium catalyst effectively replacing the ClO_4^- counter-ion with a carboxylate (see Appendix **A6** for spectal data). The counter-ion exchange resulted in a color change from yellow to red (Figure 5.7). In addition to these observations, the reactions were found to be zero order but the rates of elimination are different based on the identity of the acid (Figure 5.8). The reaction order indicates that a photochemical process is likely rate determining which can be expected in photoredox catalysis.[204] However, the rate differences are puzzling as this is not expected for a zero order process. Taken together, its speculated the photophysics of the catalyst is tied to an association event with the

cationic acridinium which could be influenced by carboxylate structure lending to the reactivity differences observed in the elimination.[194,205]
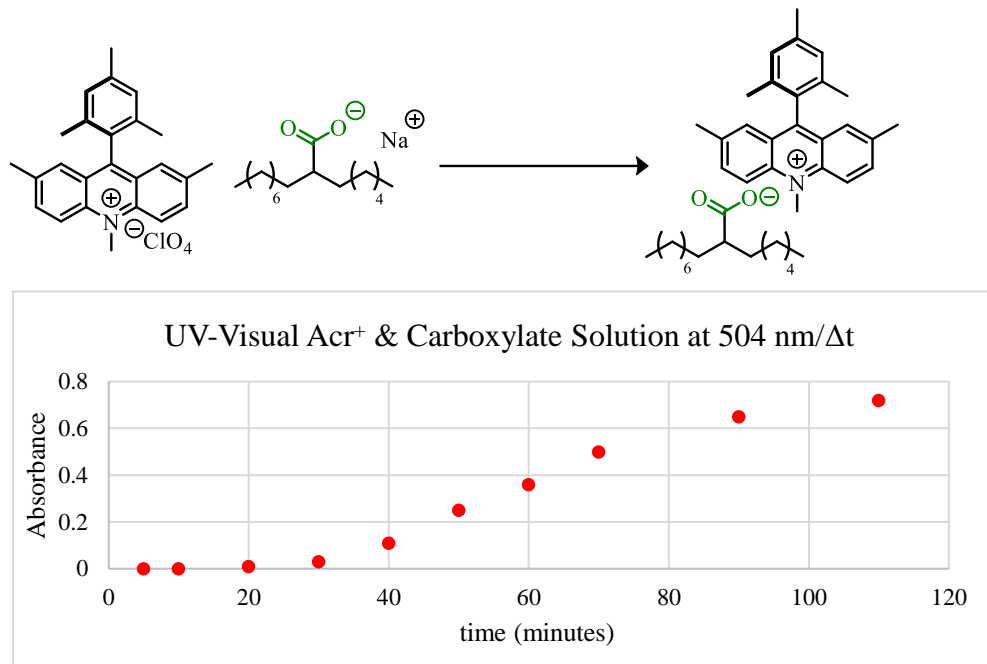
Figure 5.7: UV-visual analysis of association between acridinium and carboxylate in MeCN
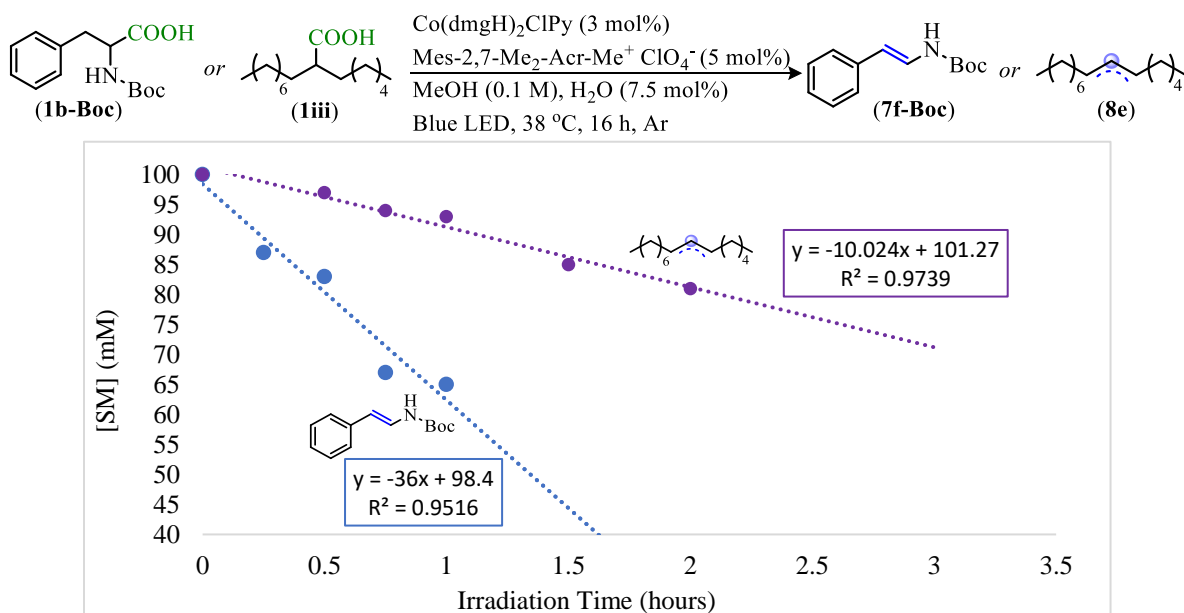
Figure 5.8: Initial decarboxylative elimination rates for **1b-Boc** and **1iii**

Once the acridinium is quenched out of the excited state, it exists as a neutral radical species (Figure 3.1). In order to return the catalyst to the ground state, it will need to be re-oxidized by one electron. The electron could be transferred to the alkyl radical intermediate or the cobaloxime co-catalyst. Due to the large negative reduction potentials of the carbon radicals generated in this reaction ($<$ -1.5 V vs. SCE)[58], in addition to the unproductive reaction pathway that would result, the acridinium catalyst (~ -0.6 V vs. SCE) is suspected to be re-oxidized by a single electron transfer to Co^{III} (-0.68 V vs. SCE)[144] (Figure 4.3). A reduction of $Co^{II/I}$ by the acridinium was also considered but the potential for this reduction is unfavorable (-1.13 V vs. SCE).[144]

To initiate the acridinium's catalytic cycle, the carboxylic acid needs to be deprotonated to liberate carboxylate. By utilizing the proton reduction ability of the cobaloxime catalyst, this can be done without the use of alkaline conditions. However, the Co^{III} catalyst put into the reaction matrix is not capable of performing the needed deprotonation. When considering the reported oxidation states and proposed pathways for proton and electron transfer with cobaloximes, it was postulated that the deprotonation event can be achieved in one of two ways.[146] The first is a deprotonation of the carboxylate by super nucleophilic anionic Co^{I} (equation 1). The second is through protonation of a Co^{III}–H or Co^{II}–H species (equation 4 & 6).

$$\overset{\ominus}{Co^{I}} + HA \longrightarrow Co^{III}\text{–H} + A^{\ominus} \qquad\qquad (1)$$

$$Co^{III}\text{–H} + HA \longrightarrow \overset{\oplus}{Co^{III}} + H_2 + A^{\ominus} \qquad\qquad (4)$$

$$\overset{\bullet\,-}{Co^{II}}\text{–H} + HA \longrightarrow Co^{II} + H_2 + A^{\ominus} \qquad\qquad (6)$$
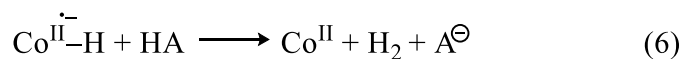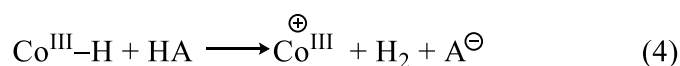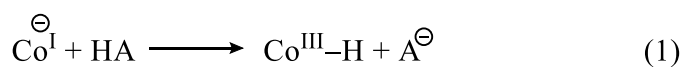
Since the reactivity oberved during inital development of the elimination reaction was sluggish, the pre-reduction protocol was developed in the hopes that injecting Co^{I} into the reaction matrix would allow for the initial deprotonation and begin catalysis (Figure 5.2). This pre-reduction process led to significantly improved reaction yields however, further investigation

revealed that the cobaloxime reduction process likely does not produce an anionic Co^I. The first indication that the product of the reduction was not Co^I was the color of the final reaction mixture (Figure 5.9). The reaction goes from a light yellow heterogeneous mixture to a red homogenous mixture. The red solution is then added into the elimination reaction. Co^I is notoriusly deep blue/purple in color, a far cry from the red that is observed in the reduction process developed for the elimination chemistry. Anionic Co^I was produced in-house but its synthesis required rigorously degassed methanol and highly alkaline conditions (Figure 5.9).[63,195,206] Niether of which were utilized in the decarboxylative elimination reactions. The red color observed post the reduction process is more characteristic of a Co^{II} or Co^{III} species. In fact, it has been reported that many cobaloxime reductions with borohydride reagents actually result in the formation of Co^{II} instead of Co^I.[141c] Thus, its speculated that a Co^{II} species was formed and added to the reaction mixture. Because this does not solve the nessessity for the initial deprotonation event, the increased efficiency gained from the use of catalytic base in the reaction is suspected to provide free carboxylate to start the catalytic cycle (Table 5.3).

Figure 5.9: Reduction of cobaloximes

After decarboxylation, a carbon radical intermediate is produced. For the alkene product to be generated in high yield, the radical intermediate has to undergo HAT with the Co catalyst before being taken off-cycle through homocoupling or dispropostionation. This efficient HAT process is expected to be achieved with a Co^{II} species resulting in the formation of Co^{III}–H (equation 8).

$$\overset{\bullet}{Co}^{II} + \text{alkyl radical} \longrightarrow Co^{III}–H + \text{alkene} \qquad (8)$$
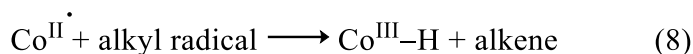
The cobaloxime catalysts utilized also have the ability to couple with the alkyl radical resulting in a Co^{III}–alkyl complx.[128a,147b,202,207] Because this complex is coordinatively saturated, β-hydride elimination is unlikely. Thus, if this off-cycle species forms, efficent homolysis of the Co–C bond is required for the elimination to proceed (Scheme 5.10). Light has been demonstrated to cleave the Co–C bond and thus this species was expected to return to the catalytic cycle under the reaction conditions. In fact, when $Co(dmgH)_2(n\text{-butyl})Py$ was irradiated, 1-butene was observed by ^1H NMR (see Appendix **A7** for spectal data).
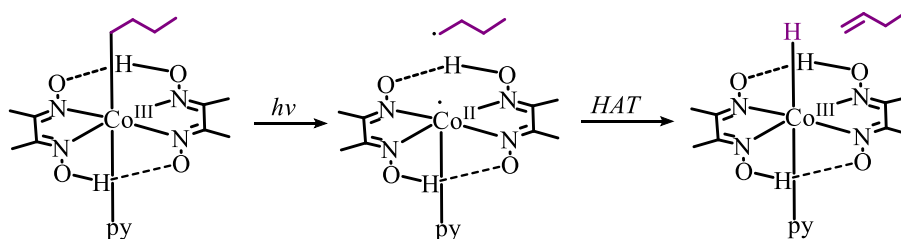
Scheme 5.10: Light-driven homolysis of $Co(dmgH)_2(n\text{-butyl})Py$

The rate of this HAT reaction was probed by competition reactions performed in the presence of one equivalent of TEMPO. Photolysis of a Co–n-nonyl complex along with TEMPO produced a 40:60 ratio of alkene to TEMPO trapped products (Scheme 5.11A). These results indicate that the HAT process is occurring at a rate comparable to the bimolecular radical coupling of the alkyl radical intermediate and TEMPO (~15 x 10^7 $M^{-1}s^{-1}$).[208] A similar ratio of products is observed in a catalytic reaction with a α,α-disubstituted carboxylic acid (Scheme 5.11B).[209] Thus, the trapping of the radical intermediate by the Co catalyst is highly efficient.

A. Photolysis of Co(dmgH)$_2$(*n*-nonyl)(*N*-Me-Imidazole) with TEMPO

1 equiv. + 1 equiv.

MeOH (0.1 M)
Blue LED, 16 h

40:60 olefin:TEMPO adduct[b]

B. Decarboxylative Elimination with TEMPO

1iii
0.2 mmol
COOH

+

0.2 mmol

Co(dmgH)$_2$Cl(*N*-Me-Imidazole) (3 mol%)
STAB (7.5 mol%), Na$_2$CO$_3$ (1 mol%)
Mes-2,7-Me$_2$-Acr-Me$^+$ ClO$_4^-$ (5 mol%)
MeOH (0.1 M), H$_2$O (7.5 mol%)
Blue LED, Ar, 16 h, 38 °C

(8e)

60:40 olefin:TEMPO adduct[c]
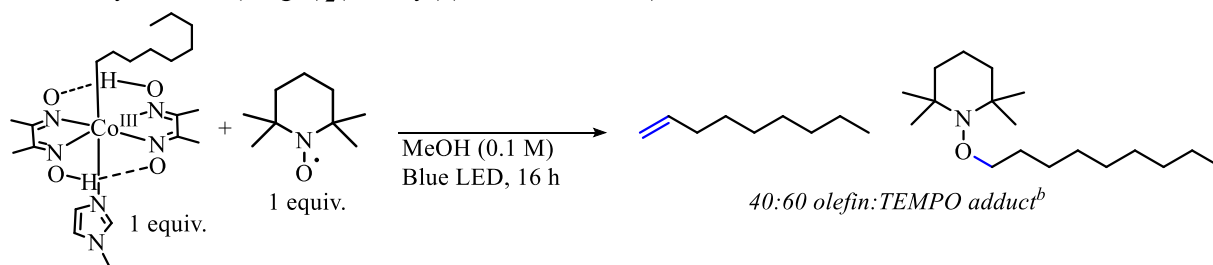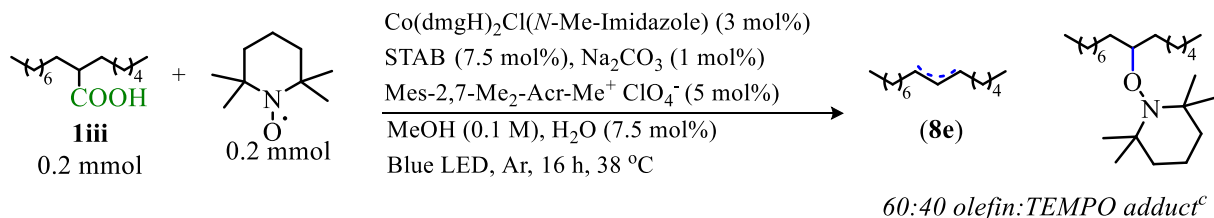
Scheme 5.11: TEMPO-trapping experiements

[a] *In situ* reduction protocol followed. [b] Products were isolated together and the product ratio was determined by GC/MS of the crude reaction mixture.[c] The products were isolated separately and the product ratio shown is an average of three reactions.

At this point, it is important that the nature of the HAT process be addressed. As discussed in Chapter 4, this process between alkyl radicals and Co^{II} has been proposed to proceed through either a proton-coupled electron transfer (PCET) (Scheme 5.12A) or a oxidation of the alkyl radical to a carbocation followed by a deprotonation with the resulting Co^I (Scheme 5.12B).[145,210]

A. Proton-Coupled Electron Transfer

Co^{II} Co^{III}–H
+H$^\bullet$
PCET
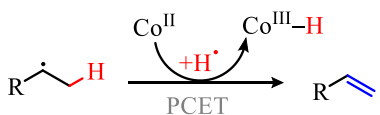
B. Sequential Electron then Proton Transfer

Co^{II} Co^I
-1.13 V

Co^I Co^{III}–H
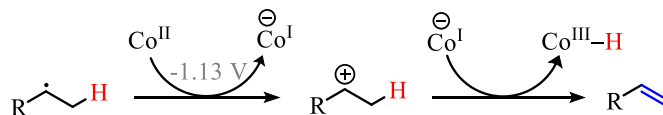
Scheme 5.12: Possible HAT pathways for cobaloximes and alkyl radicals

However, the reduction potentials for the aliphatic radicals are >0 V vs. SCE[58] whereas both the Co$^{III/II}$ and Co$^{II/I}$ potentials (-0.68 V and -1.13 V vs. SCE, respectively)[144b] are too low for this SET to be favorable. Thus, if such radical-polar crossover occurs through oxidation, only the acridinium catalyst employed is sufficiently oxidizing. Nevertheless, oxidation to a cation would lead to E1-type elimination, which is not consistent with the preferred formation of less-substituted

alkenes, nor is it consistent with the catalyst-dependent regioselectivities for elimination. The observed chemistry is consistent with Muckerman's suggestion that HAT through a PCET pathway from Co^{II} to Co^{III} hydride is part of the lowest energy pathway *en route* to cobaloxime-facilitated hydrogen evolution.[146] Thus, a PCET pathway is most likely involved.

In order for the catalytic cycle to continue, a hydrogen evolution process is expected to occur. In sum, the hydrogen gas produced during the elimination is expected to consist of the acidic proton from the carboxylic acid, a hydrogen atom removed from the substrate, and an electron originally arising from the carboxylate. To ensure hydrogen was being evolved in the elimination reaction, and to probe the composition of the H_2 produced, the elimination of **1b** was performed in CD_3OD (Scheme 5.13).[69] Dissolution of the carboxylic acid in deuterated solvent resulted in a rapid H/D exchange effectively deuterating the carboxylic acid. When the decarboxylative elimination was performed, H–D was observed by ^1H NMR indicating the carboxylic acid's deprotonation was part of the hydrogen evolution process. H_2 was also observed but the reaction consisted of ~6:1 HD:H_2.
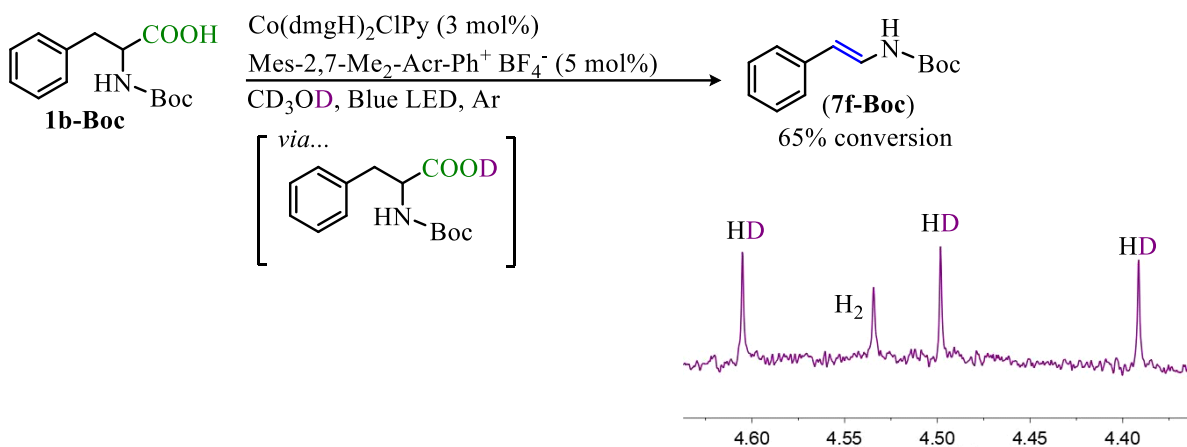
Scheme 5.13: Hydrogen evolution in decarboxylative elimination

Two pathways are possible for the subsequent monometallic hydrogen evolution process that result in the deprotonation event (equations 2 & 3). The Co^{III} hydride can be reduced first by

the photocatalyst to provide Co^{II} hydride and then hydrogen evolution would give Co^{II} and the carboxylate (Co^{III}–H reduction potential is reported to be similar to $Co^{II/I}$ reduction, ~-1.0 V vs. SCE).[140h,141d,211] Alternatively, the Co^{III}–H can perform hydrogen evolution and the resulting Co^{III+} (~-0.68 V vs. SCE)[144] is then reduced by the photocatalyst the Co^{II} closing the catalytic cycle. We favor a hydrogen evolution that involves the Co^{III}–H and carboxylic acid because the potential of our photocatalyst (~-0.6 V vs SCE)[6c,102a,154f] is more suited for the reduction of Co^{III+} as opposed to the reduction of Co^{III}–H (equations 4 & 6).

From the aforementioned experiments, it became apparent that the dominant cycle likely operates through Co^{II} and Co^{III} and appears to have similarities to studies on the cobalt-catalyzed hydrogen evolution using photoacids.[141a,137] To further support this speculation, the elimination reaction was performed with $Co(dmgH)_2(n$-butyl)Py as the pre-catalyst in the absence of base and reductant (Scheme 5.14).
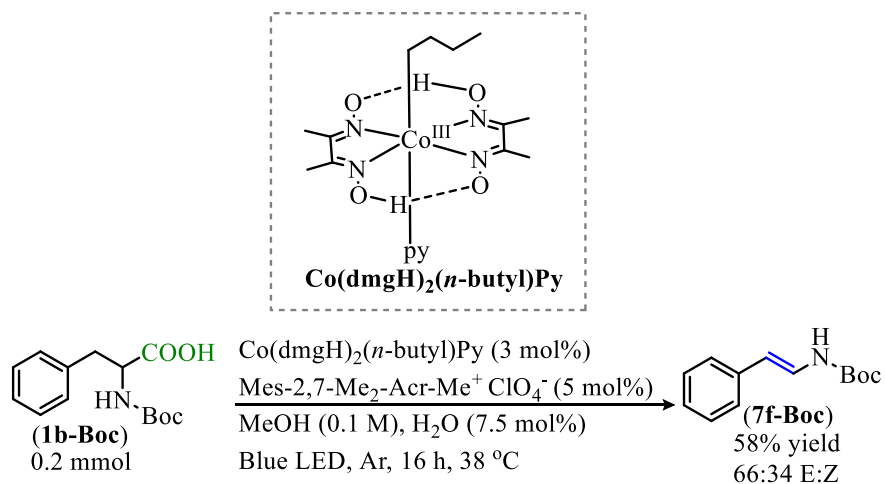
Scheme 5.14: Decarboxylative elimination with Co–alkyl pre-catalyst

The Co–alkyl complex is expected to homolyze and result in Co^{III}–H. This hydride can then enter the catalytic cycle through deprotonating the carboxylic acid to provide the needed carboxylate and, after hydrogen evolution, resulting in a cationic Co^{III} that can undergo acridinium-

facilitated single electron reduction. This reaction did proceed producing the eliminated product in 58% yield (Scheme 5.14).[196]

Using the experimental observations described herein and the cobaloxime hydrogen evolution literature, a mechanistic picture to describe the dominant catalytic cycle was devised (Scheme 5.15).[196] The cycle begins with a single electron oxidation of the carboxylate by the excited state acridinium photocatalyst initiating rapid decarboxylation. The alkyl radical is then trapped by Co^{II} and PCET furnishes Co^{III}–H and the desired alkene. Deprotonation of a molecule of carboxylic acid by the Co^{III}–H liberates more carboxylate as well as allows for the release of hydrogen gas and cationic Co^{III}. The cationic Co^{III} can undergo single electron reduction by the photocatalyst which closes both the Co and acridinium catalytic cycles.

Reduction of Cobaloxime Pre-catalyst:

$$Co^{III} + STAB + Na_2CO_3 \longrightarrow [Co^{II}]$$

Dual Catalytic Pathway:
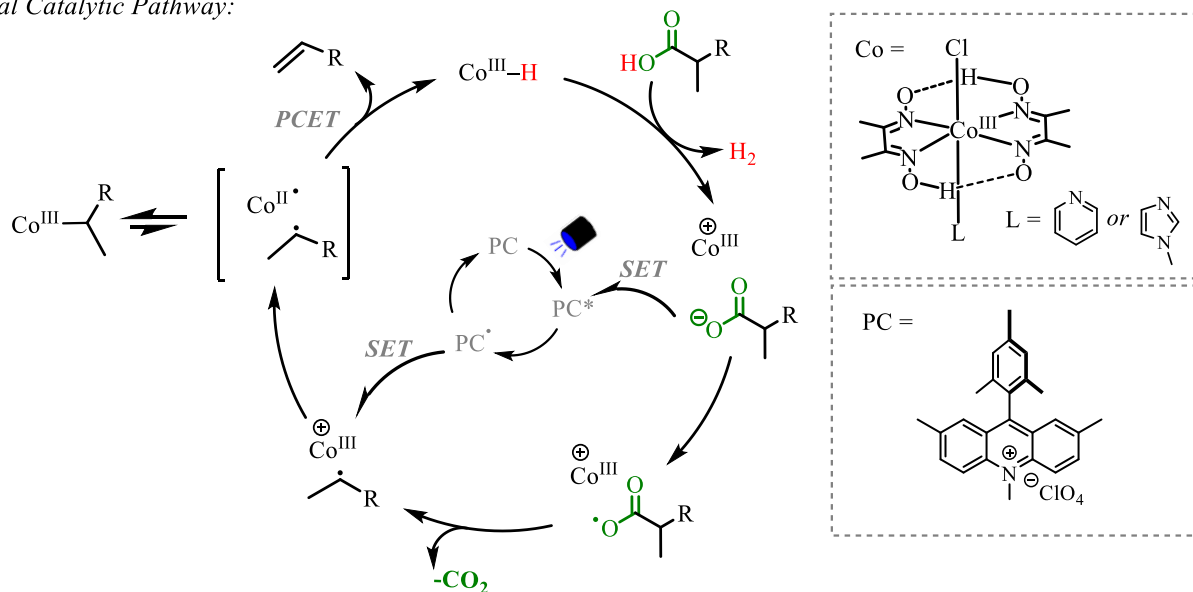
Scheme 5.15: Proposed decarboxylative elimination mechanism

193

5.3 Photoredox/Cobaloxime Decarboxylative Elimination Methodology

Over the course of 2018 and 2019, related photoredox/cobaloxime methodology emerged. Despite the commonality of using decarboxylation and hydrogen evolution in conjunction, these methods have several stark differences in reactivity. One of the first reports to emerge that coincided with the chemistry described in this chapter was from the Ritter group (Scheme 5.16).[128a]
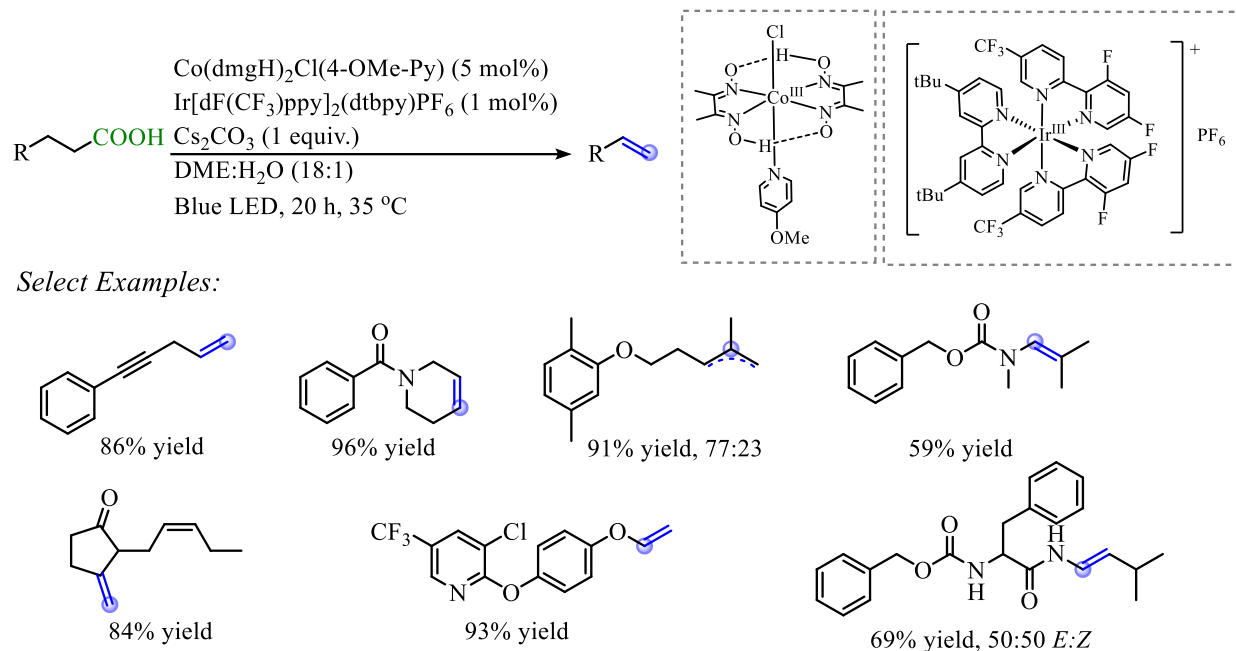
Scheme 5.16: Ritter decarboxylative elimination

Their focus was on the use of cobaloximes with Ir photosensitizers for the decarboxylative elimination of carboxylic acids. It was disclosed that the reaction yields are far superior when the axial ligand on the cobaloxime complex was 4-OMe-Py instead of Py. This reactivity difference stands in stark contrast to what was observed in the Tunge methodology with *N*-acyl amino acids (Figure 5.4).[69,196] However, a similar axial base influence was observed with α,α-disubstituted carboxylic acids which, are more similar the acids employed in the Ritter chemistry (Figure 5.5). Yet, in the Tunge chemistry, *N*-Me-imidazole was the superior ligand. The benefit seen from the

use of 4-OMe-Py as the axial base ligand could be a result of enhanced catalyst stability as opposed to Py.[199] The more stable *N*-Me-imidazole ligand was not instigated in this chemistry.

One of the most notable differences between the two methods is the success the Ritter method has with unsubstituted carboxylic acids which make up the majority of the scope (Scheme 5.16). The Tunge methodology does not perform the decarboxylative elimination of these substrates or in the presence of these substrates (Figure 5.6). As both the Ir photosensitizer used in the Ritter methodology and the acridinium photosensitizer employed in the Tunge methodology are sufficiently oxidizing enough the perform the oxidation, the reactivity difference is suspected to be an artifact of the vastly different oxidation potentials of the reduced photocatalyst species. In the Tunge elimination, a hydrogen evolution process is proposed to occur via the protonation of a Co^{III}–H to liberate cationic Co^{III} and carboxylate as the acridinium (~-0.6 V vs. SCE)[144] is not reducing enough for the Co^{III}–H/Co^{II}–H (~-1.1 V vs. SCE)[144] reduction. Thus, the opportunity for the formation of a Co–carboxylate complex arises in these reactions. In the Ritter elimination, the Ir photosensitizer can perform this reduction (-1.37 V vs. SCE)[154d] and it has been proposed that this route is preferential when allowed.[140h] This would result in Co^{II} and carboxylate which evades the possibility of forming the Co–carboxylate complex. The mechanistic differences that likely exist between the two methods may account for the difference in reactivity. Few amino acid examples and no α,α-disubstituted acids with weak radical stabilization were explored in the Ritter methodology for direct substrate comparison with the Tunge methodology. However, the two α-amino acid examples reported were isolated in 59% and 69% yield (Scheme 5.16). Additionally, the Ritter protocol was attempted to be reproduced in the Tunge lab with 4,4-bis(4-hydroxyphenyl)pentanoic acid. Ritter reports the elimination of this acid in 63% yield however, the best alkene yield obtained in the Tunge lab was 20%.

Also in 2018, Wu/Liu report a decarboxylative Heck-type coupling that utilizes Co(dmgH)$_2$Cl(DMAP) with Mes-Acr-Me$^+$ ClO$_4^-$ (Scheme 5.17A).[128c] Although the DMAP axial base ligand is utilized, this reaction does produce comparable yields of the Heck-type product with Py. The reactivity achieved here is intriguing as it not only functions with unsubstituted acids but also is able to efficiently trap the radical with various styrenes, acrylates, vinyl boronates, and vinyl silanes. This intermolecular coupling would not efficiently out-compete elimination under the Tunge conditions (Scheme 5.11). However, it is important to note that the majority of the carboxylic acid substrates utilized would not undergo elimination (Scheme 5.17). Like the Tunge methodology, a stoichiometric amount of base is utilized which can aid in the generation of carboxylate in the initial reaction mixture, but Wu/Liu also propose that the base can aid in facilitating the hydrogen evolution process through transferring the proton from the carboxylic acid to the Co^{III}–H. The use of K$_3$PO$_4$ in 10 mol% may aid in the reactivity difference between the Wu/Liu and Tunge chemistry.
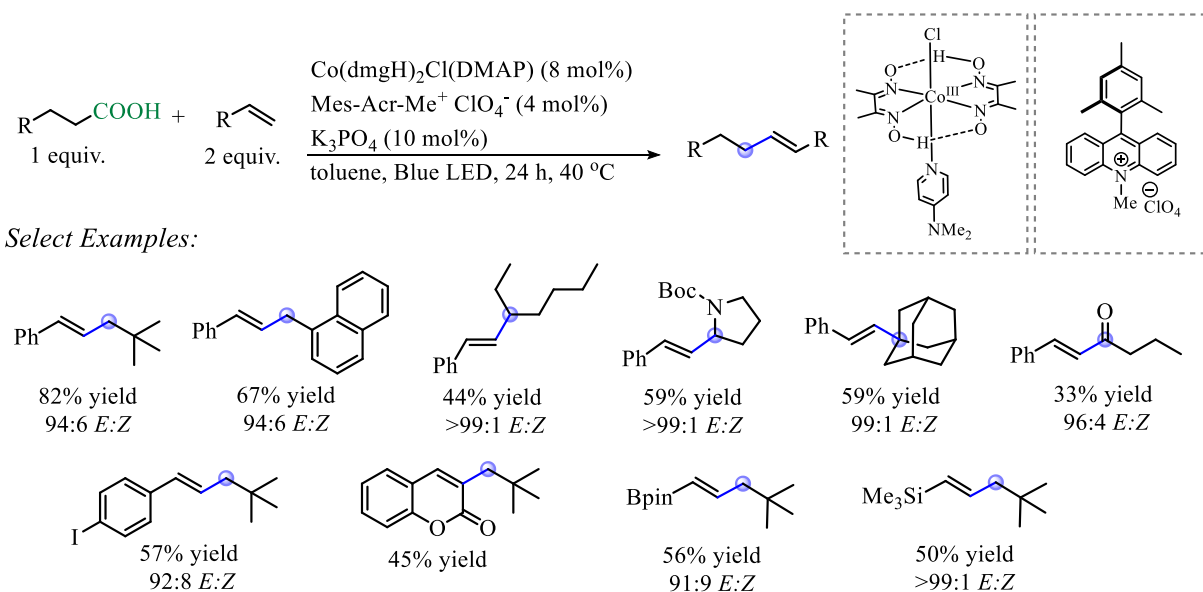
Scheme 5.17: Wu/Liu decarboxylative Heck-like coupling

Shortly after this flurry of reports, Larionov reported a decarboxylative elimination in 2019 utilizing Co(dmgH)$_2$ClPy and acridine (Scheme 5.18).[128b] Like with the Ritter and Wu/Liu methods, this chemistry was predominately explored with unsubstituted carboxylic acids but is shown with α,α-disubstituted and quaternary acids. Unlike the Ritter and Wu/Liu chemistry, this method was applied to an α-amino acid like was utilized in the Tunge chemistry and gave the same yield (Scheme 5.18, Larionov **7a** in 76% yield, 62:38 *E:Z*; Tunge **7a** in 76% yield, 68:32 *E:Z*).

Select Examples:

| 80% yield | 66% yield | 99% yield 88:12 (terminal olefin major) | 72% yield | 76% yield 62:38 *E:Z* |
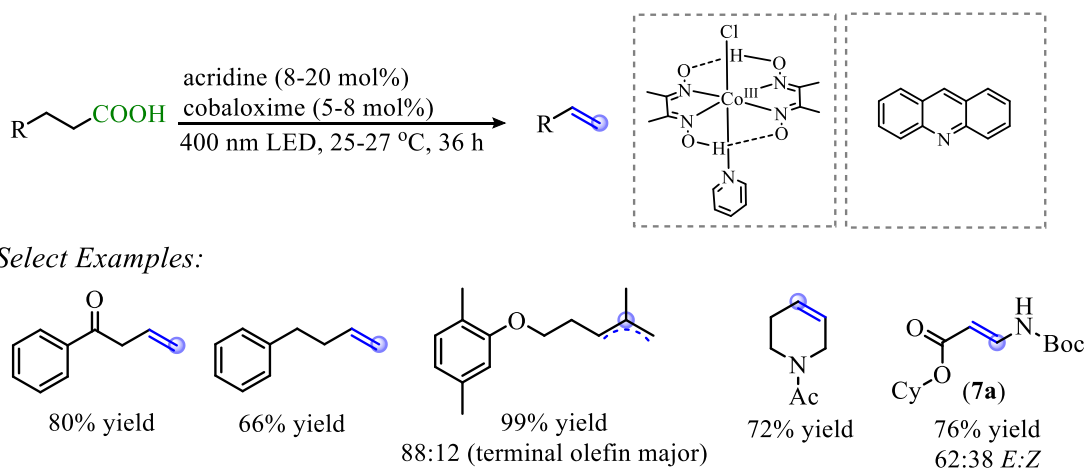
Scheme 5.18: Larionov decarboxylative elimination

Interestingly, this method does not make use of base like others do but instead the acridine is involved in the deprotonation event and subsequent oxidation event of the carboxylic acid. Utilizing this mode of reactivity may aid in the reactivity difference seen with unsubstituted acids compared to the Tunge method (Scheme 5.19).
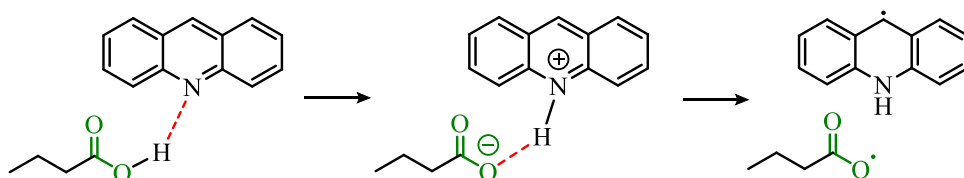
Scheme 5.19: Acridine-facilitated decarboxylation

The differences in scope and reactivity observed through the optimized conditions reached in various laboratories for the decarboxylative elimination is intriguing and requires further study to fully understand.

5.4 Conclusion

The marriage of decarboxylation and hydrogen evolution has allowed for the direct decarboxylative elimination process to proceed without stoichiometric additives under mild and neutral conditions efficiently and with high atom economy. The optimal cobaloxime catalyst for amino acids was identified to be the $Co(dmgH)_2ClPy$ however, these substrates eliminate well with a variety of cobaloximes. Conversely, other carboxylic acid substrates underwent elimination most effectively when $Co(dmgH)_2Cl(N\text{-Me-Imidazole})$ was utilized as the co-catalyst with Mes-Acr-Me$^+$ ClO$_4^-$. The reaction efficiency can be maximized, and the reaction scope expanded, by improving the catalyst longevity via appropriate choice of axial base ligand and through the addition of extra dmgH ligand. Observations also point to the HAT process requiring the cobaloxime catalyst to be in close proximity to the reaction site. One artifact of the steric influences on the elimination is the preference for the less thermodynamically favored Hofmann products and less sterically encumbered alkene products. The dominant catalytic cycle is expected to proceed via a reductive quenching pathway with Co^{II} and Co^{III} intermediates and does not invoke an anionic Co^I species. In addition, an evaluation of potentials has led to the conclusion that a PCET pathway is the preferred route for HAT, and HE via protonation of the Co^{III} hydride is the most likely pathway.

5.5 Experimental

5.5.1 General Considerations

Purification was accomplished with column chromatography using silica gel (60 Å porosity, 230 x 400 mesh, standard grade) which was purchased from Sorbent Technologies (catalog # 30930M-25). TLC analysis was performed (fluorescence quenching and potassium permanganate acid stain) with silica gel HL TLC plates with UV254 purchased from Sorbent Technologies. ^{1}H and ^{13}C NMR spectra were obtained on a Bruker ADVANCE 500 DRX equipped with a QNP cryoprobe. These spectra were referenced to residual protio solvent signals. HRMS data was obtained on an ESI LC-TOF Micromass LCT (Waters). HRMS data was collected using ESI mass spectrometry. Melting points were obtained with Digimelt MPA 160 SRS (# 111278) and samples were loaded with borosilicate glass Kimble tube capillaries (# 34505-9a). GC/MS data was acquired on Shimadzu GCMS-QP2010 SE. UV-visual data was acquired with Ocean Optics DT-MINI-2-GS.

Sodium triacetoxyborohydride was purchased from Oakwood. Photocatalysts 9-mesityl-10-phenylacridinium tetrafluoroborate, 9-mesityl-10-methyllacridinium perchlorate, 9-mesityl-2,7-dimethyl-phenylacridinium tetrafluoroborate, and 9-mesityl-3,6-(tBu)$_2$-10-phenylacridinium tetrafluoroborate were purchased from Sigma-Aldrich. Photocatalyst 9-mesityl-10-methylacridinium perchlorate and 9-mesityl-2,7-Me$_2$-10-methylacridinium perchlorate was purchased from TCI. Cobaloxime, Co(dmgH)$_2$ClPy, was purchased from Sigma-Aldrich. Other cobaloximes were synthesized using CoCl$_2$ from ChemImpex and the respective oxime ligands all purchased from Sigma-Aldrich. All axial base ligands used were commercially available. Anhydrous MeOH was purchased from Acros.

Final decarboxylative elimination reactions were run in a screw-threaded tube from Chemglass (CLS-4208). Kessil H150 Blue LED grow lights provided 450 nm light. Two lights were used in the set-up of these reactions. A 2.0 mL solution of MeOH had an internal temperature of 38 °C after 1 hour under standard reaction conditions.

5.5.2 N-Acylation of Amino Acids

The *N*-acetylation of amino acids was performed following a modification of literature procedure.[212] In a 500 mL round bottom flask with stir bar, a solution of the corresponding amino acid (7.6 mmol) in 70% THF/H$_2$O (0.51 M, 150 mL) was made. Acetic anhydride (42.4 mmol, 4 mL) was added drop wise to the stirring amino acid solution. The reaction was allowed to stir at room temperature for ~16 hours. The reaction mixture was then concentrated and the resulting solid was filtered and washed with H$_2$O (~20 mL) then Et$_2$O (~40 mL) and dried under vacuum to provide the desired products. *N*-Acetyl amino acid products were used without further purification.

The following *N*-acetyl amino acids were synthesized and the products obtained match reported spectroscopic values: *N*-acetyl-phenylalanine[213] (**1b-Ac**), *N*-acetyl-leucine[214] (**1uu-Ac**), *N*-acetyl-cyclohexaneacetic acid[215] (**1eee-Ac**), *N*-Cbz-*N*-acetyl-lysine[216] (**1ddd-Ac**), *N*-acetyl-2-naphthalenepropanoic acid[217] (**1qq-Ac**).
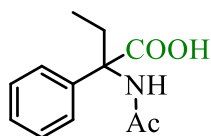
1h-Ac (KC-4-221)

^{1}H NMR (500 MHz, CD$_3$CN): δ 7.35 (m, 5H), 7.24 (s, 1H), [2.37 (m) & 2.28 (m), Σ2H], 2.04 (s, 3H), 0.82 (t, 3H).

^{13}C NMR{^{1}H} (126 MHz, CD$_3$CN): δ 173.4, 172.5, 140.6, 129.3, 128.5, 126.8, 68.0, 29.7, 23.4, 8.7.

IR (film): 3387, 2917, 1730, 1640, 1538, 1270, 1199, 1117 cm^{-1}.

HRMS (ESITOF) m/z: Calc'd $C_{12}H_{14}NO_3Na$ (M+Na) = 244.0950, found 244.0956.

  N-Acylations of amino acids were performed following modified literature procedure.[218] In a 100 mL round bottom flask, a stirring solution of NaOH (14.5 mmol, 2.9 equiv.) in H_2O (15 mL) was made and cooled to 0 °C. The corresponding amino acid (5.0 mmol, 1 equiv.) was added to the basic solution and the reaction mixture was allowed to stir until homogenous. A solution of the corresponding acyl chloride (6.5 mmol, 1.3 equiv.) in dioxane (5 mL) was made and subsequently added to the reaction mixture drop wise. The reaction mixture was allowed to warm to room temperature and stir for ~16 hours. After that time, the reaction mixture was washed with Et_2O (~20 mL 3x) and the resulting aqueous solution was acidified to pH 2 with 2 M HCl. The resulting solution was extracted with Et_2O (~20mL 3x), dried with $MgSO_4$, and concentrated. The resulting solid was purified via recrystallization from Et_2O (~40 mL) to provide the final product.
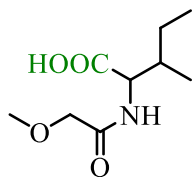
1ggg (KC-4-234)

^{1}H NMR (500 MHz, CDCl$_3$): Mixture of rotamers: δ 7.03 (d, 1H), 4.65 (dd, 1H), 3.96 (q, 2H), [3.48 (s) & 3.45 (s), Σ3H], 2.00 (m, 1H), (1.52-1.23 (m, Σ2H), 0.98 (d, 3H), 0.95 (t, 3H).

^{13}C NMR{^{1}H} (126 MHz, CDCl$_3$): δ 175.5, 170.0, 71.6, 59.2, 55.8, 37.5, 24.9, 15.4, 11.5.

IR (film): 3377, 2963, 2763, 1719, 1627, 1540, 1427, 1363, 1232, 1212, 1121, 998 cm^{-1}.

HRMS (ESITOF) m/z: Calc'd $C_9H_{16}NO_4Na$ (M+Na) 226.1055, found 226.1065.
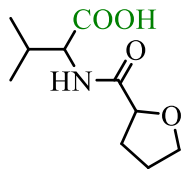
1fff (KC-4-202)

^{1}H NMR (500 MHz, CD$_3$CN): δ 7.08 (s, 1H), 4.30 (m, 2H), 3.98 (m, 1H), 3.84 (m, 1H)], 2.19 (m, 2H), 1.88 (m, 2H), 0.91 (m, 6H).

^{13}C NMR{1H} (126 MHz, CD$_3$CN): δ 174.3, 173.0, 79.1, 70.2, 57.4, 31.5, 31.3, 26.1, 19.5, 17.9.

IR (film): 3380, 2966, 1732, 1637, 1533, 1275, 1261, 1072, 764, 750 cm^{-1}.

HRMS (ESITOF) m/z: Calc'd C$_{10}$H$_{16}$NO$_4$Na (M+Na) = 238.1055, found 238.1046.

5.5.3 N-Methylation of N-Acetyl-Phenylalanine

A flame dried, 100 mL Schlenk flask equipped stir bar under argon was charged with *N*-acetyl-phenylalanine (2.1 mmol, 0.435 g) and dry THF (20 mL, 0.11 M). The resulting solution was cooled to 0 °C. NaH (10.5 mmol, 0.252 g) was added portionwise. Once all NaH had been added, the reaction mixture was allowed to stir for 10 min. Iodomethane (2.5 mmol, 0.16 mL) was then added to the reaction mixture. The reaction was allowed to warm to room temperature and stir for ~16 hours. The reaction mixture was then quenched with H$_2$O and acidified to pH 2 with 2M HCl. This solution was extracted with EtOAc (3x), dried with MgSO$_4$, and condensed to provide a yellow oil. Triteration with Et$_2$O provided a white solid which was collected by vacuum filtration and washed with Et$_2$O.
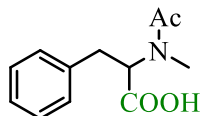
1zz-Ac (KC-4-147)

^{1}H NMR (500 MHz, CD$_3$CN): δ 7.25 (m, 5H), [5.02 (dd) & 4.71 (dd), Σ1H], [3.27 (m) & 3.05 (m), Σ2H], [2.79 (s) & 2.76 (s), Σ3H], [1.90 (s) & 1.66 (s), Σ3H].

^{13}C NMR{^{1}H} (126 MHz, CD$_3$CN): δ 172.3, 139.0, 130.0, 129.9, 129.5, 129.3, 127.7, 127.4, 59.9, 34.9, 29.4, 21.9.

IR (film): 3070, 2939, 1728, 1600, 1496, 1410, 1269, 1215, 785 cm^{-1}.

HRMS (ESITOF) m/z: Calc'd C$_{12}$H$_{15}$NO$_3$Na (M+Na) = 244.0950, found = 244.0962.

5.5.4 Synthesis of α,α-Disubstituted Carboxylic Acids

α,α-Disubstituted carboxylic acids were synthesized from unsubstituted acids following literature procedure.[101a] A solution of diisopropylamine (8.4 mmol, 2.4 equiv., 1.2 mL) in dry THF (40 mL) was made in a 100 mL flame-dried Schlenk flask with stir bar under Ar. The solution was cooled to -78 °C. n-Butyllithium (8.4 mmol, 2.4 equiv., 3.4 mL of 2.5 M solution in hexanes) was added to the stirring solution of diisopropylamine and allowed to stir at -78 °C under argon for 30 min. A solution of primary carboxylic acid (4 mmol, 1 equiv.) in dry THF (5 mL) was made and then added dropwise to the reaction mixture. The reaction mixture was then allowed to warm to room temperature and stir at room temperature for an additional 30 min. The reaction mixture was then cooled to -78 °C and primary alkyl bromide (5 mmol, 1.2 equiv.) was added. The reaction was then allowed to warm to room temperature and stir at room temperature ~14 h before being quenched by 1 M HCl (20 mL) and extracted with EtOAc (3x ~20 mL ea.). Organics were combined, dried with MgSO$_4$, and concentrated. The desired acid was purified by flash column chromatography on silica with 1:5-1:20 EtOAc:Hexanes.
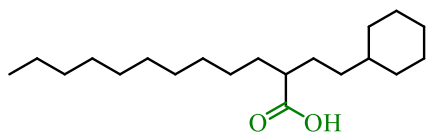
1lll (KC-6-110)

^{1}H NMR (500 MHz, CD$_3$CN): δ9.90 (broad s, 1H), 2.32 (q, 1H), 1.77-1.58 (m, 7H), 1.56-1.46 (m, 2H), 1.32-1.18 (m, 22H), 0.92-0.81 (m, 5H).

^{13}C NMR{^{1}H} (126 MHz, CD$_3$CN): δ 45.9, 37.9, 35.1, 33.5, 33.3, 32.3, 32.1, 29.8, 29.73, 29.66, 29.6, 29.5, 27.5, 26.8, 26.5, 22.8, 14.3.

IR (film): 3220, 2922, 1709, 1467, 1456, 1423 cm^{-1}.

HRMS (ESITOF) m/z: Calc'd C$_{20}$H$_{39}$O$_2$ (M+H) = 311.2950, found 311.2964.
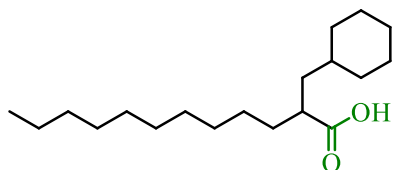
1mmm (KC-6-064)

^{1}H NMR (500 MHz, CD$_3$CN): δ2.47 (broad s, 1H), 1.83-1.75 (m, 1H), 1.72-1.53 (m, 6H), 1.49-1.40 (m, 1H), 1.35-1.07 (m, 22H), 0.93-0.79 (m, 5H).

^{13}C NMR{^{1}H} (126 MHz, CD$_3$CN): δ 40.1, 35.7, 33.7, 33.1, 33.0, 32.1, 29.8, 29.7, 29.6, 29.5, 27.5, 26.7, 26.7, 26.4, 26.3, 22.8, 22.5, 14.3, 14.2.

IR (film): 3542, 2943, 1738, 1464, 1455 cm^{-1}.

HRMS (ESITOF) m/z: Calc'd C$_{19}$H$_{37}$O$_2$ (M+H) = 297.2794, found 297.2799.
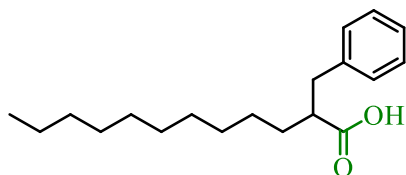
1ppp (KC-6-127)

^{1}H NMR (500 MHz, CDCl$_3$): δ 11.8 (s, 1H), 7.30-7.15 (m, 5H), 2.98 (dd, 1H), 2.76 (dd, 1H), 2.67 (q, 1H), 1.74-1.66 (m, 1H), 1.59-1.52 (m, 1H), 1.39-1.25 (m, 16H), 0.90 (t, 3H).

^{13}C NMR{^{1}H} (126 MHz, CD$_3$CN): δ 181.8, 139.3, 129.0, 128.6, 126.5, 476, 38.3, 32.1, 31.9, 29.7, 29.62, 29.57, 29.6, 27.3, 22.8, 14.3.

IR (film): 3617, 3003, 2944, 1730, 1656, 1635, 1464, 1456, 751 cm^{-1}.

HRMS (ESITOF) m/z: Calc'd C$_{19}$H$_{31}$O$_2$ (M+H) = 291.2324, found 291.2324.
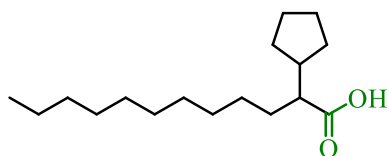
1qqq (KC-6-076)

^{1}H NMR (500 MHz, CD$_3$CN): δ 2.20-2.11 (m, 1H), 2.04-1.91 (m, 1H), 1.90-1.69 (m, 2H), 1.68-1.46 (m, 6H), 1.37-1.09 (m, 18H), 0.87 (t, 3H).

^{13}C NMR{^{1}H} (126 MHz, CD$_3$CN): δ 51.5, 42.7, 32.1, 31.6, 31.0, 30.9, 29.8, 29.6, 29.5, 27.8, 25.1, 25.1, 22.8, 14.3.

IR (film): 3411, 2924, 1733, 1470, 1456, 1419 cm^{-1}.

HRMS (ESITOF) m/z: Calc'd C$_{20}$H$_{39}$O$_2$ (M+H) = 269.2481, found 269.2484.

5.5.5 Synthesis of 2-carbamoylcyclohexane-1-carboxylic acid

2-carbamoylcyclohexane-1-carboxylic acid was synthesized following literature procedure.[219] Ammonium hydroxide (15 mL) was added to 100 mL round-bottom flask with stir bar and cooled to 0 °C. Cyclohexane anhydride (64.9 mmol, 10 g) was added portion wise and then the reaction mixture was allowed to stir overnight. The reaction was then acidified with 12N HCl during which a precipitate formed. The precipitate was collected via vacuum filtration, washed with H$_2$O (~40 mL), then CH$_3$Cl (~40 mL), then Et$_2$O (~40 mL), and dried under vacuum.
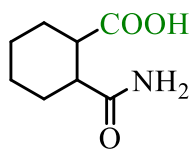
1xxx (KC-5-252)

^{1}H NMR (500 MHz, d$_6$-DMSO): δ 11.89 (broad s, 1H), 7.12 (s, 1H), 6.71 (s, 1H), 2.62 (q, 1H), 2.01-1.86 (m, 2H), 1.68-1.55 (m, 2H), 1.54-1.43 (m, 1H), 1.41-1.22 (m, 3H).

^{13}C NMR{^{1}H} (126 MHz, d$_6$-DMSO): δ 175.6, 175.2, 42.0, 41.7, 27.3, 25.7, 23.7, 23.0.

5.5.6 Synthesis of Cobaloxime Catalysts

Cobaloximes containing chgH and dmgH ligand systems were synthesized via a modification of a literature procedure.[63] To a 100 mL round-bottom flask with stir bar, $CoCl_2$ hydrate (2.3 mmol, 0.54 g) and acetone (15 mL) were added and stirred resulting in a blue homogeneous solution. To this solution, the respective oxime ligand (7.5 mmol) was added and the color changed from blue to purple/pink. Air was passed over this solution via an air inlet line made from Tygon tubing and a 1 mL syringe. Fresh acetone was added when solution became concentrated to maintain constant volume (15 mL). After ~0.5-1 hour, a green precipitate formed. The reaction mixture is cooled to 0 °C and the green solid was filtered via vacuum filtration, then washed with ~10 mL diethyl ether. This solid was then added to a 100 mL round-bottom flask with stir bar and taken up in MeOH (20 mL). To the stirring solution, the respective base ligand was added (4.05 mmol) and the solution turned brown immediately. The reaction mixture was allowed to stir for 30 minutes. After, stirring is stopped and the mixture was cooled to 0 °C. The resulting brown solid was collected via vacuum filtration and washed with water (~10 mL) then diethyl ether (~10 mL). The product was dried under vacuum to yield the desired cobaloxime. The cobaloxime complexes were then utilized without further purification.
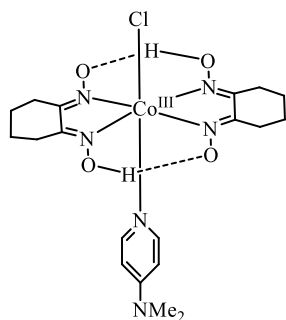
Co(chgH)₂Cl(DMAP) (KC-5-085)

¹H NMR (500 MHz, CD₃CN): δ 7.44 (d, 2H), 6.43 (d, 2H), 2.96-2.86 (m, 4H), 2.92 (s, 6H), 2.81-2.68 (m, 4H), 1.76-1.58 (m, 8H).

¹³C NMR (126 MHz, CD₃CN):{¹H} δ 153.8, 149.3, 109.1, 39.4, 26.7, 22.1.

IR (film): 3445, 3055, 2989, 1687, 1636, 1608, 1422, 763, 749, 653 cm⁻¹.

HRMS (ESITOF) m/z: Calc'd C₁₉H₂₉N₆O₄ClCo (M+H) = 499.1271, found 499.1291.
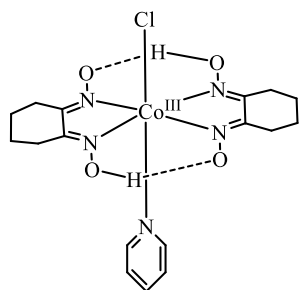
Co(chgH)₂Cl(Py) (KC-5-056)

¹H NMR (500 MHz, CD₃CN): δ 8.11 (d, 2H), 7.79 (t, 1H), 7.30 (t, 2H), 2.97-2.87 (m, 4H), 2.81-2.69 (m, 4H), 1.75-1.58 (m, 8H).

¹³C NMR (126 MHz, CD₃CN):{¹H} δ 154.5, 151.7, 140.4, 126.8, 26.8, 22.0.

IR (film): 3403, 3006, 2945, 1670, 1665, 1422, 763, 701, 638 cm⁻¹.

HRMS (ESITOF) m/z: Calc'd C₁₇H₂₄N₅O₄ClCo (M+H) = 456.0849, found 456.0830.
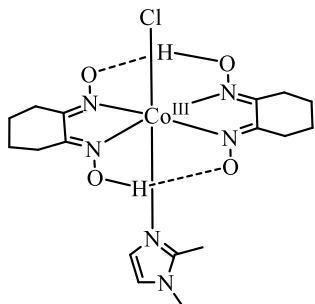
Co(chgH)₂Cl(1,2-dimethylimidazole) (KC-6-040)

^{1}H NMR (500 MHz, CD$_3$CN): δ 7.37-7.29 (m, 13H), 7.25-7.19 (m, 7H), 7.00 (d, 1H), 6.84 (d, 1H), 3.51 (s, 3H), 2.45 (s, 3H).

^{13}C NMR (126 MHz, CD$_3$CN):{^{1}H} δ 154.3, 131.2. 130.7, 130.6, 130.4, 128.9, 128.8, 127.1, 122.5, 35.0, 11.5.

IR (film): 3400, 3055, 2987, 1651, 1634, 1423, 750, 705, 638 cm^{-1}.

HRMS (ESITOF) m/z: Calc'd C$_{17}$H$_{27}$N$_6$O$_4$ClCo (M+H) = 473.1114, found 473.1137.
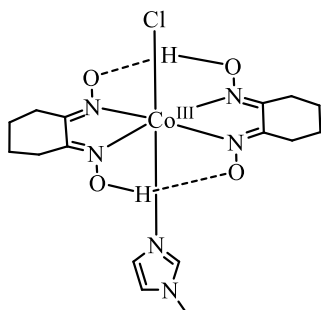
Co(chgH)₂Cl(*N*-Me-Imidazole) (KC-5-162)

^{1}H NMR (500 MHz, CD$_3$CN): δ 7.15 (s, 1H), 6.83 (s, 1H), 6.49 (s, 1H), 3.55 (s, 3H), 2.93-2.84 (m, 4H), 2.84-2.74 (m, 4H), 1.78-1.62 (m, 8H).

^{13}C NMR (126 MHz, CD$_3$CN):{^{1}H} δ 153.5, 139.4, 128.0, 123.6, 35.5, 26.7, 22.1.

IR (film): 3409, 3054, 2987, 1674, 1657, 896, 750, 639 cm^{-1}.

HRMS (ESITOF) m/z: Calc'd C$_{16}$H$_{25}$N$_6$O$_4$ClCo (M+H) = 459.0958, found 459.0973.
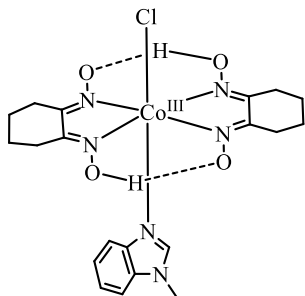
Co(chgH)₂Cl(*N*-Me-Benzimidazole) (KC-6-050)

^{1}H NMR (500 MHz, CD₃CN): δ 8.15 (d, 1H), 7.88 (s, 1H), 7.42 (d, 1H), 7.37-7.26 (d, 2H), 3.76 (s, 3H), 2.97-2.87 (m, 4H), 2.76-2.66 (m, 4H), 1.73-1.63 (m, 4H), 1.63-1.53 (m, 4H).

^{13}C NMR (126 MHz, CD₃CN):{^{1}H} δ 153.4, 145.1, 124.2, 123.6, 111.1, 31.9, 25.8, 21.1.

HRMS (ESITOF) m/z: Calc'd C₂₀H₂₇N₆O₄ClCo (M+H) = 509.1114, found 509.1119.
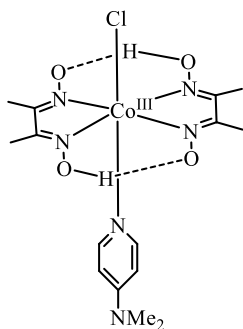
Co(dmgH)₂Cl(DMAP) (KC-5-031)

^{1}H NMR (500 MHz, CD₃CN): δ 7.45 (d, 2H), 6.42 (d, 2H), 2.91 (s, 6H), 2.31 (s, 12H).

^{13}C NMR (126 MHz, CD₃CN):{^{1}H} δ 152.3, 148.5, 108.3, 38.6, 12.1.

IR (film): 3435, 3004, 2945, 1647, 1622, 1436, 1374, 920, 639 cm^{-1}.

HRMS (ESITOF) m/z: Calc'd C₁₅H₂₄N₆O₄ClCo (M+) = 446.0880, found 446.0893.
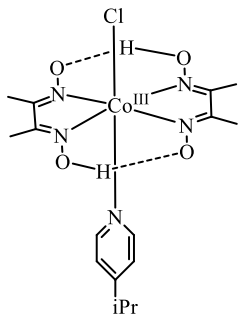
Co(dmgH)₂Cl(4-iPr-Py) (KC-5-014)

^{1}H NMR (500 MHz, CD₃CN): δ 7.97 (d, 2H), 7.17 (d, 2H), 2.86 (q, 1H), 2.31 (s, 12H), 1.13 (d, 6H).

^{13}C NMR (126 MHz, CD₃CN):{^{1}H} δ 162.7, 153.7, 151.2, 125.1, 33.9, 22.7, 13.0.

IR (film): 3397, 3041, 2945, 1652, 1635, 1374, 639 cm^{-1}.

HRMS (ESITOF) m/z: Calc'd C₁₆H₂₆N₅O₄ClCo (M+H) = 446.1005, found 446.1009.
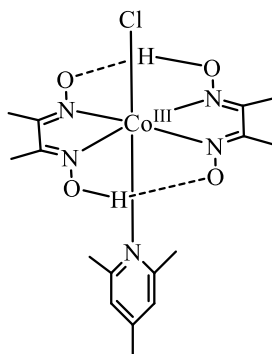
Co(dmgH)₂Cl(2,4,6-trimethylpyridine) (KC-5-016)

^{1}H NMR (500 MHz, CD₃CN): δ 7.39 (s, 2H), 2.43 (s, 9H), 2.39 (s, 12H).
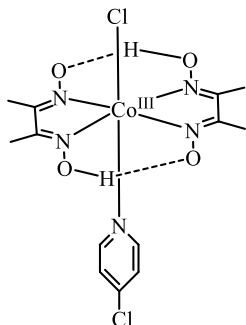
Co(dmgH)₂Cl(4-Cl-Py) (KC-5-148)

4-Cl-Py HCl was basified with sodium carbonate and extracted with DCM before use.

^{1}H NMR (500 MHz, CD₃CN): δ 8.03 (d, 2H), 7.35 (d, 2H), 2.32 (s, 12H).

^{13}C NMR (126 MHz, CD₃CN):{^{1}H} δ 154.0, 152.5, 126.9, 13.0.

IR (film): 3390, 3055, 2987, 1670, 1652, 749, 705, 638 cm^{-1}.

HRMS (ESITOF) m/z: Calc'd $C_{13}H_{29}N_5O_4Cl_2Co$ (M+H) = 448.0929, found 448.0918.
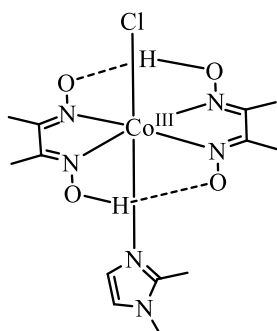
Co(dmgH)₂Cl(1,2-dimethylimidazole) (KC-6-024)

^{1}H NMR (500 MHz, CD₃CN): δ 6.79 (d, 1H), 6.68 (d, 1H), 3.36 (s, 3H), 2.33 (s, 12H), 2.19 (s, 3H).

^{13}C NMR (126 MHz, CD₃CN):{^{1}H} δ 153.3, 127.5, 121.7, 34.7, 12.9, 11.2.

IR (film): 3391, 3005, 2944, 1644, 1637, 1374, 639 cm^{-1}.

HRMS (ESITOF) m/z: Calc'd $C_{13}H_{23}N_6O_4ClCo$ (M+H) = 421.0801, found 421.0822.
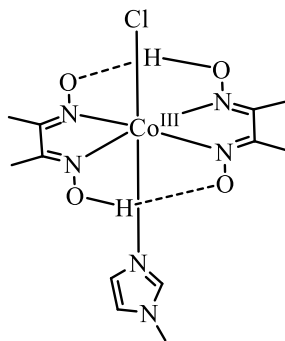
Co(dmgH)₂Cl(*N*-Me-Imidazole) (KC-5-015)

^{1}H NMR (500 MHz, CD₃CN): δ 7.14 (s, 1H), 6.81 (t, 1H), 6.49 (t, 1H), 3.54 (s, 3H), 2.32 (s, 12H).

^{13}C NMR (126 MHz, CD₃CN):{^{1}H} δ 156.0, 152.8, 137.8, 127.5, 31.7, 12.9.

IR (film): 3387, 3055, 2987, 1656, 1634, 1422, 896, 748, 639 cm^{-1}.

HRMS (ESITOF) m/z: Calc'd C₁₂H₂₁N₆O₄ClCo (M+H) = 407.0645, found 407.0630.
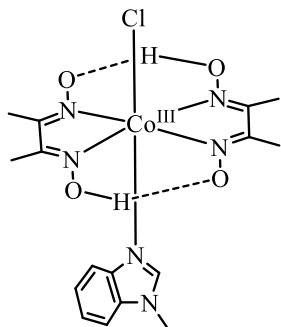
Co(dmgH)₂Cl(*N*-Me-Benzimidazole) (KC-5-190)

^{1}H NMR (500 MHz, CD₃CN): δ 8.17 (d, 1H), 7.88 (s, 1H), 7.40 (d, 1H), 7.31 (m, 2H), 3.75 (s, 3H), 2.29 (s, 12H).

^{13}C NMR (126 MHz, CD₃CN):{^{1}H} δ 153.7, 146.0, 125.0, 124.6, 112.1, 32.9, 13.0.

IR (film): 3536, 3004, 2945, 1641, 1614, 1435, 1375, 919, 639 cm^{-1}.

HRMS (ESITOF) m/z: Calc'd C₁₆H₂₆N₇O₄ClCo (M+NH₄) = 474.1067, found 474.1064.
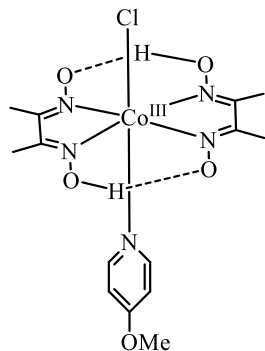
Co(dmgH)₂Cl(4-OMe-Py) (KC-6-191)

^{1}H NMR (500 MHz, CD₃CN): δ 7.85 (d, 2H), 6.82 (d, 2H), 3.80 (s, 3H), 2.31 (s, 12H).

^{13}C NMR (126 MHz, CD₃CN):{^{1}H} δ 153.7, 152.3, 113.0, 57.1, 13.0.

IR (film): 3479, 3005, 2945, 1656, 1616, 1375, 1267, 919, 833, 639 cm^{-1}.

HRMS (ESITOF) m/z: Calc'd C₁₄H₂₁N₅O₅ClCoLi (M+Li) = 440.0723, found 440.0712.

Cobaloximes containing a dpgH ligand system were synthesized from CoCl₂ hexahydrate (0.75 mmol, 1 equiv., 0.1738 g), dpgH (1.5 mmol, 2 equiv., 0.351 g), and the corresponding nitrogen axial base ligand (1.8 mmol, 2.4 equiv.). A stirring solution of CoCl₂ hexahydrate in ethanol (2 mL) was made and then dpgH was added. The reaction mixture was allowed to stir for 20 minutes and then the nitrogen base was added. The reaction was allowed to stir for 20 minutes then H₂O was added, and the reaction stirred for 1 hour. Excess nitrogen base was removed *in vaccuo*. The desired cobaloxime was extracted with CHCl₃ (~10 mL), dried with sodium sulfate, and concentrated. A solid was obtained that was taken in Et₂O then collected via vacuum filtration and dried under vacuum to provide the desired cobaloxime. The cobaloximes synthesized were utilized without further purification.
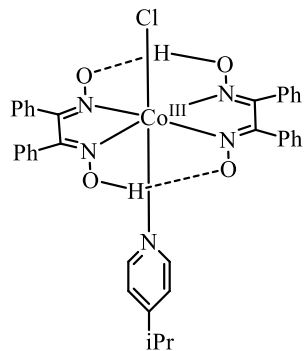
Co(dpgH)₂Cl(4-iPr-Py) (KC-5-014)

^{1}H NMR (500 MHz, CD$_3$CN): δ 8.28 (d, 2H), 7.39-7.28 (m, 14H), 7.21-7.16 (m, 8H), [3.07 (q) &2.97 (q) Σ1H], [1.28 (d) &1.20 (d) Σ6H].

^{13}C NMR (126 MHz, CD$_3$CN):{^{1}H} δ 154.4, 151.1, 130.8, 130.6, 130.5, 129.0, 125.9, 34.0, 22.8.

IR (film): 3565, 3006, 2970, 2925, 1695, 1674, 1652, 1370, 638 cm^{-1}.

HRMS (ESITOF) m/z: Calc'd C$_{36}$H$_{34}$N$_5$O$_4$ClCo (M+H) = 694.1631, found 694.1619.
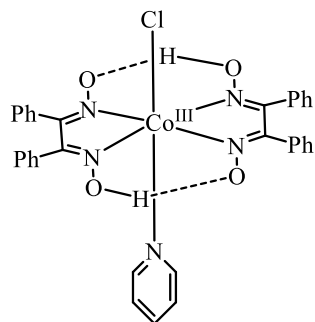
Co(dpgH)₂Cl(Py) (KC-4-210)

^{1}H NMR (500 MHz, CD$_3$CN): δ 8.46 (d, 2H), 7.95 (t,1H), 7.49 (t, 2H), 7.37-7.29 (m, 12H), 7.19-7.17 (m, 8H).

^{13}C NMR (126 MHz, CD$_3$CN):{^{1}H} δ 154.6, 151.7, 141.1, 130.8, 130.5, 129.0, 127.6.

IR (film): 3379, 3055, 2987, 1675, 1651, 1419, 896, 750, 639 cm^{-1}.

HRMS (ESITOF) m/z: Calc'd C$_{33}$H$_{28}$N$_5$O$_4$ClCo (M+H) = 652.1162, found 652.1154.
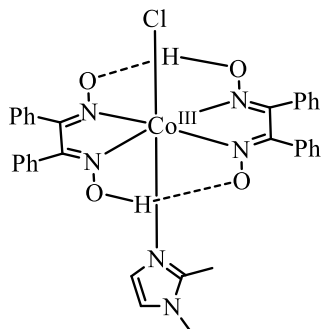
Co(dpgH)₂Cl(1,2-dimethylimidazole) (KC-6-029)

^{1}H NMR (500 MHz, CD$_3$CN): δ 7.36-7.28 (m, 12H), 7.24-7.20 (m, 8H), 7.0 (d, 1H), 6.84 (d, 1H), 3.50 (s, 3H), 2.46 (s, 3H).

^{13}C NMR (126 MHz, CD$_3$CN):{^{1}H} δ 154.8, 131.7, 131.3, 131.1, 131.0, 129.4, 129.3, 127.6, 123.0, 35.5, 12.1.

IR (film): 3375, 3058, 2989, 1671, 1652, 1435, 896, 749, 639 cm^{-1}.

HRMS (ESITOF) m/z: Calc'd C$_{33}$H$_{31}$N$_6$O$_4$ClCo (M+H) = 669.1427, found 669.1434.
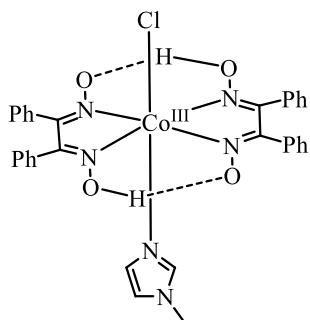
Co(dpgH)₂Cl(*N*-Me-Imidazole) (KC-5-026)

^{1}H NMR (500 MHz, CD$_3$CN): δ [7.71 (s) & 7.55 (s) Σ1H], 7.44-7.28 (m, 12H), 7.25-7.20 (m, 5H), 7.18-7.14 (m, 3H), [7.12 (s) & 6.88 (s) Σ1H], 7.01 (d, 1H), [3.72 (s) & 3.66 (s) Σ3H].

^{13}C NMR (126 MHz, CD$_3$CN):{^{1}H} δ 153.8, 131.1, 130.55, 130.49, 130.0, 129.0, 128.9, 128.0, 36.0.

IR (film): 3522, 3006, 2970, 2925, 1657, 1417, 1370, 908, 638 cm^{-1}.

HRMS (ESITOF) m/z: Calc'd C$_{32}$H$_{29}$N$_6$O$_4$ClCo (M+H) = 655.1271, found 655.1243.

Co(dmgH)₂(butyl)Py was synthesized from a modification of a literature procedure.[63] A 100 mL Schlenk flask was charged with a stir bar and KOH (2.67 mmol, 0.15 g). The flask was

then flame dried and cooled under argon. The flask was charged with MeOH (40 mL from Acros SureSeal) and the KOH/MeOH solution was degassed via 4 sequential freeze and thaw cycles under vacuum. Once rigorously degassed, Co(dmgH)$_2$ClPy (1 mmol, 0.404 g) was added to the reaction flask and the reaction mixture was cooled to -10 ^{o}C via a saltwater ice bath. Sodium borohydride (1.3 mmol, 0.049 g) was then added and after ~10 min the reaction mixture turned dark blue. After this color change occurred, 1-bromobutane (1 mmol, 0.107 mL) was added and after ~1 minutes the reaction mixture became red/orange in color. The reaction was then allowed to warm to room temperature and then stirred for 30 minutes at room temperature. After, acetone (1.5 mL) and water (20 mL) were added. The reaction was removed from inert atmosphere, reduced to half volume, and cooled in an ice bath. Orange precipitate formed and was collected via vacuum filtration. The isolated orange crystalline material was washed with diethyl ether and dried under vacuum to provide the desired alkyl cobaloxime.
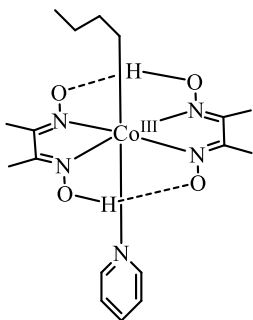
Co(dmgH)$_2$(*n*-butyl)(Py) (KC-6-186)

^{1}H NMR (500 MHz, CD$_3$CN): δ [8.56 (d) & 8.45 (d) Σ2H], [7.82 (t) & 7.74 (t) Σ1H], 7.34 (t) & 7.33 (t) Σ2H], [2.15 (s) & 2.04 (s) Σ12H], 1.48-1.38 (m, 2H), 1.22-1.05 (m, 2H), 0.92-0.73 (m, 2H), 0.80 (t, 3H).

^{13}C NMR (126 MHz, CD$_3$CN):{^{1}H} δ 152.7, 151.7, 150.6, 150.2, 139.7, 139.0, 33.6, 31.2, 24.6, 14.2, 12.5, 12.0.

HRMS: Calc'd C$_{17}$H$_{29}$N$_5$O$_4$Co (M+H) = 426.1552, found 426.1544.

Co(dmgH)$_2$(n-nonyl)(N-Me-Imidazole) was synthesized via the procedure detailed for the synthesis of Co(dmgH)$_2$(n-butyl)Py. Co(dmgH)$_2$Cl(N-Me-Imidazole) (0.31 mmol), KOH (0.83 mmol), NaBH$_4$ (0.40 mmol), and 1-bromononane (0.31 mmol).
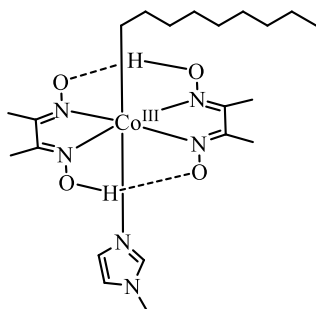
Co(dmgH)$_2$(n-nonyl)(N-Me-Imidazole) (KC-8-047)

^{1}H NMR (500 MHz, CD$_3$CN): δ 7.26 (s, 1H), 6.93 (t, 1H), 6.68 (t, 1H), 3.61 (s, 3H), 2.08 (s, 12H), 1.37–1.05 (m, 14H), 0.90–0.81 (m, 5H).

5.5.7 Co/Acr$^+$ Catalyzed Decarboxylative Elimination of Carboxylic Acids

Reduction of cobaloxime: A dry 10mL Schlenk flask equipped with stir bar was charged with cobaloxime (0.006 mmol, 3 mol%), sodium triacetoxyborohydride (3.2 mg, 0.015 mmol, 7.5 mol%), Na$_2$CO$_3$ (0.2 mg, 0.002 mmol, 1 mol%), and dry MeOH (0.5 mL). The reaction mixture was put under argon and fitted with a reflux condenser. The reaction mixture was stirred and refluxed at 57 °C for 50 minutes, in which time the reaction mixture went from light yellow to red. After 50 minutes, the flask was removed from the heat and allowed to cool for 10 minutes.

Decarboxylation elimination with pre-reduced cobaloxime: An oven-dried screw-threaded glass tube equipped with stir bar was charged with carboxylic acid (0.2 mmol, 1 equiv.) and photocatalyst (0.01 mmol, 5 mol%). A 15 mM stock solution of H$_2$O (1.1 μL) in MeOH (4 mL) was made and 1 mL of the stock solution was transferred to the tube. Then, dry MeOH (0.5 mL) was added and the tube was sealed with a rubber septum and screw cap. After the vial was sealed, it was sparged with argon for 5 minutes through the septum using a 20-gauge needle to bubble gas

through the solvent, and another needle was used to vent the vial. After the flask was sparged, the

sparging needle was removed from the solution but left in the vial during the addition of the cobalt

catalyst solution. Another 20-gauge needle with 5 mL syringe was used to transfer the cobalt

catalyst solution from the Schlenk flask to the reaction tube. After the addition of the cobalt

catalyst, the sparging and venting needles were removed from the septum of the reaction tube, and

the top of the tube was wrapped with parafilm. The reaction was placed in front of two 450 nm 32

W blue LEDs for 16 hours with no distance in between the reaction vessel and the light source.

The reaction mixture was found to reach 38 $^{\circ}$C after 1 hour of irradiation in this LED set-up. After

irradiation, the final reaction mixture was condensed and purified via flash column

chromatography on silica with mixtures of ethyl acetate and hexanes as the eluent. Note: enamide

and enecarbamate products were found to degrade in chloroform.

Decarboxylative elimination with in situ cobaloxime reduction: An oven-dried screw-

threaded glass tube equipped with stir bar was charged with carboxylic acid (0.2 mmol, 1 equiv.),

photocatalyst (0.01 mmol, 5 mol%), cobaloxime (0.006 mmol, 3 mol%), sodium

triacetoxyborohydride (3.2 mg, 0.015 mmol, 7.5 mol%), and Na_2CO_3 (0.2 mg, 0.002 mmol, 1

mol%). A 15 mM stock solution of H_2O (1.1 μL) in MeOH (4 mL) was made and 1 mL of the

stock solution was transferred to the tube. Then, dry MeOH (1 mL) was added and the tube was

sealed with a rubber septum and screw cap. After the vial was sealed, it was sparged with argon

for 5 minutes through the septum using a 20-gauge needle to bubble gas through the solvent, and

another needle was used to vent the vial. The sparging and venting needles were removed from

the septum of the reaction tube and the top of the tube was wrapped with parafilm. The reaction

was placed in front of two 450 nm 32 W blue LEDs for 16 hours with no distance in between the

reaction vessel and the light source. The reaction mixture was found to reach 38 $^{\circ}$C after 1 hour of

irradiation in this LED set-up. After irradiation, the final reaction mixture was condensed and purified via flash column chromatography on silica with mixtures of ethyl acetate and hexanes as the eluent.

The following enamide and enecarbamate products were synthesized using the pre-reduction of cobaloxime procedure and Mes-2,7-Me$_2$-Acr-Ph$^+$ BF$_4^-$ photocatalyst:
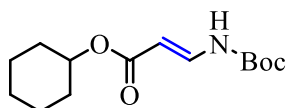

7a-Boc (KC-4-136)

^{1}H NMR (500 MHz, CD$_3$CN): Z-isomer: δ 9.57 (s, 1H), 7.23 (dd, 1H), 4.96 (d, 1H), 4.77 (m, 1H), 1.88-1.67 (m, 4H), 1.48 (s, 9H), 1.58-1.23 (m, 6H). E-isomer: δ 7.93 (s, 1H), 7.64 (dd, 1H), 4.75-4.70 (m, 1H), 1.87-1.67 (m, 4H), 1.46 (s, 9H), 1.56-1.23 (m, 6H).

^{13}C NMR{^{1}H} (126 MHz, CD$_3$CN): Z-isomer: δ 169.4, 141.2, 95.1, 82.6, 73.1, 32.3, 28.2, 26.0, 24.4; E-isomer: δ 167.6, 140.8, 99.3, 82.3, 72.6, 32.4, 28.2, 26.1, 24.5.

IR (film): 3335, 2978, 2936, 2861, 1740, 1680, 1632, 1483, 1454, 1389, 1368, 1207, 1148, 1038, 1017, 970, 860 cm^{-1}.

HRMS (ESITOF) m/z: Calc'd C$_{14}$H$_{24}$NO$_4$ (M+Na)$^+$ = 238.1807, found = 238.1791.
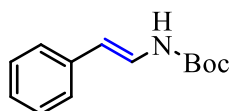
7f-Boc (KC-4-091)

^{1}H NMR (500 MHz, CD$_3$CN): Mix of E/Z-isomers: δ [7.54 (s, E/Z), Σ1H)], [7.38-7.12 (m, E/Z), Σ5H)], [7.13 (ddt, E) & 6.61 (dd, Z), Σ1H], [6.01 (d, E) & 5.56 (d, Z), Σ1H)], [1.46 (s, E/Z), Σ9H].

^{13}C NMR{^{1}H} (126 MHz, CD$_3$CN): Mix of E/Z-isomers: δ 153.9, 138.0, 129.7, 129.5, 128.8, 127.3, 126.8, 125.9, 110.1, 28.4.

IR (film): 3630, 3538, 3368, 3277, 3090, 2980, 2936, 2261, 2114, 1944, 1881, 1701, 1483, 1451, 1370, 1153, 1101, 1030 cm^{-1}.

HRMS (ESITOF) m/z: Calc'd C$_{13}$H$_{17}$NO$_2$Na (M+Na)$^+$ = 242.1157, found = 242.1159.
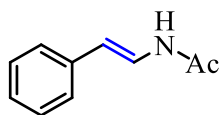
7f-Ac (KC-4-093)

^{1}H NMR (500 MHz, CD$_3$CN): *Z*-isomer: δ 8.17 (s, 1H), 7.41-7.22 (m, 5H), 6.85 (dd, 1H), 5.66 (d, 1H), 1.99 (s, 3H); *E*-isomer: δ 8.45 (s, 1H), 7.44 (dd, 1H), 7.36-7.13 (m, 5H), 6.14 (d, 1H), 1.98 (s, 3H).

^{13}C NMR{^{1}H} (126 MHz, CD$_3$CN): *Z*-isomer: δ 169.3, 136.8, 129.7, 129.1, 127.5, 123.0, 109.9, 23.2; *E*-isomer: δ 168.5, 137.7, 129.6, 127.2, 126.2, 124.2, 112.1, 23.0.

IR (film): 3384, 2925, 1744, 1692, 1510, 1487, 1450, 1372, 1229, 1093, 1027 cm^{-1}.

HRMS (ESITOF) m/z: Calc'd C$_{10}$H$_{11}$NONa (M+Na)$^+$ = 184.0738, found = 184.0735.
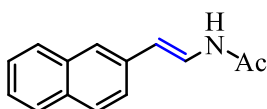
7g-Ac (KC-4-135)

^{1}H NMR (500 MHz, CD$_3$CN): *Z*-isomer: δ 8.34 (s, 1H), 7.88-7.50 (m, 7H), 6.94 (dd, 1H), 5.81 (d, 1H), 2.02 (s, 3H); *E*-isomer: δ 8.50 (s, 1H), 7.80-7.73 (m, 3H), 7.58-7.44 (m, 4H), 7.62-7.58 (m, 1H), 6.30 (d, 1H), 2.01 (s, 3H).

^{13}C NMR{^{1}H} (126 MHz, CD$_3$CN): *Z*-isomer: δ 168.8, 134.0, 133.9, 132.5, 128.5, 128.2, 127.9, 127.2, 127.0, 126.7, 126.2, 123.0, 109.3, 22.; *E*-isomer: δ 168.5, 135.4, 134.8, 133.2, 129.1, 128.5, 128.4, 127.3, 126.3, 125.2, 124.8, 124.1, 112.1. 23.1.

IR (film): 3300, 3090, 2970, 2261, 1646, 1540, 1275, 749 cm^{-1}.

HRMS (ESITOF) m/z: Calc'd C$_{14}$H$_{13}$NONa (M+Na)$^+$ = 234.0895, found = 234.0895.
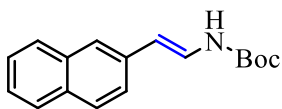
7g-Boc (KC-4-135)

^{1}H NMR (500 MHz, CD$_3$CN): *Z*-isomer: δ 7.89-7.77 (m, 3H), 7.53-7.39 (m, 4H), 7.63 (s, 1H), 6.70 (dd, 1H), 5.69 (d, 1H), 1.47 (s, 9H); *E*-isomer: δ 7.85-7.54 (m, 3H), 7.47-7.38 (m, 4H), 7.80 (s, 1H), 7.32 (dd, 1H), 6.18 (d, 1H), 1.49 (s, 9H).

^{13}C NMR{^{1}H} (126 MHz, CD$_3$CN): Z-isomer: δ 134.6, 133.0, 129.2, 128.6, 128.5, 127.6, 127.3, 127.1, 126.7, 107.9, 28.4; E-isomer: δ 153.9, 135.7, 134.9, 133.0, 129.0, 128.5, 128.3, 127.2, 126.1, 124.7, 124.0, 110.2, 66.2, 28.4.

IR (film): 3630, 3538, 3368, 3279, 3090, 2980, 2261, 2114, 1709, 1695, 1655, 1628, 1508, 1370, 1157, 1030, 858, 847 cm^{-1}.

HRMS (ESITOF) m/z: Calc'd C$_{14}$H$_{16}$NO$_4$ (M-H) = 230.1181, found 230.1187.
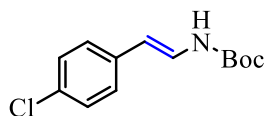
7h-Boc (KC-4-162)

^{1}H NMR (500 MHz, CD$_3$CN): Z-isomer: δ 7.31-7.10 (m, 4H), 7.22 (s, 1H), 6.59 (dd, 1H), 5.53 (d, 1H), 1.46 (s, 9H); E-isomer: δ 7.53 (s, 1H), 7.31-7.01 (m, 4H), 7.11 (dd, 1H), 6.00 (d, 1H), 1.46 (s, 9H).

^{13}C NMR{^{1}H} (126 MHz, CD$_3$CN): Z-isomer: δ 162.6, 160.7, 155.8, 130.4, 124.1, 115.9, 106.5, 78.2, 28.0; E-isomer: δ 163.1, 161.1, 153.9, 134.5, 127.6, 125.7, 116.3, 109.0, 80.9, 28.4.

IR (film): 3320, 2918, 1756, 1683, 1606, 1510, 1368, 1228, 1150, 855 cm^{-1}.

HRMS (ESITOF) m/z: Calc'd C$_{14}$H$_{16}$ClN2O$_2$Na (M+Na)$^+$ = 276.0767, found 276.0778.
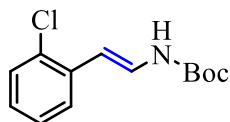
7i-Boc (KC-4-296)

^{1}H NMR (500 MHz, CD$_3$CN): Mix of E/Z-isomers: δ 7.68 (s, E/Z, Σ1H), [7.55 (dd) & 7.44 (ddd) & 7.34 (dd) & 7.22 (m) & 7.12 (td), E/Z, Σ4H], [7.22 (m, E) & 6.74 (dd, Z), Σ1H], [6.38 (d, E) & 5.61 (d, Z), Σ1H], [1.47 (s, E) & 1.44 (s, Z), Σ9H].

^{13}C NMR{^{1}H} (126 MHz, CD$_3$CN): Mix of E/Z-isomers: δ 135.9, 135.0, 133.6, 132.2, 130.9, 130.6, 130.5, 129.2, 128.3, 128.15, 128.08, 126.3, 105.9, 81.1, 28.4.

IR (film): 3304, 2978, 1701, 1653, 1508, 1466, 1368, 1316, 1273, 1246, 1155, 1055, 1034, 716 cm^{-1}.

HRMS (ESITOF) m/z: Calc'd C$_{14}$H$_{16}$ClN2O$_2$Na (M+Na)$^+$ = 276.0767, found 276.0778.
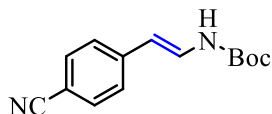
7j-Boc (KC-4-097)

^{1}H NMR (500 MHz, CD$_3$CN): *Z*-isomer: δ 7.68 (d, 2H), 7.45 (d, 2H), 6.73 (dd, 1H), 5.55 (d, 1H), 1.47 (s, 9H); *E*-isomer: δ 7.76 (s, 1H), 7.60 (d, 2H), 7.45 (d, 2H), 7.38 (dd, 1H), 6.05 (d, 1H), 1.50 (s, 9H).

^{13}C NMR{^{1}H} (126 MHz, CD$_3$CN): *Z*-isomer: δ 142.0, 133.5, 129.4, 127.3, 110.0, 106.2, 81.6, 28.3; *E*-isomer: δ 153.4, 143.3, 133.4, 129.4, 126.3, 120.1, 109.1, 108.2, 81.4, 28.4.

IR (film): 3323, 2978, 2226, 1728, 1715, 1653, 1603, 1479, 1395, 1368, 1260, 1236, 1155, 1055, 1024, 764, 750 cm^{-1}.

HRMS (ESITOF) m/z: Calc'd C$_{14}$H$_{16}$N$_2$O$_2$Na (M+Na)$^+$ = 267.1109, found = 267.1115.
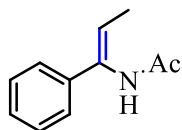
7l-Ac (KC-4-223)

^{1}H NMR (500 MHz, CD$_3$CN): Mix of *E/Z*-isomers: δ 7.60 (s, *E/Z*, Σ1H), 7.41-7.22 (m, *E/Z*, Σ5H), [5.90 (q, *Z*) & 4.70 (q, *E*), Σ1H], 2.05 (s, *E/Z*, Σ3H), 1.72 (d, *E/Z*, Σ3H).

^{13}C NMR{^{1}H} (126 MHz, CD$_3$CN): Mix of *E/Z*-isomers: δ 169.3, 139.6, 135.9, 129.2, 128.2, 126.1, 120.9, 30.2, 23.1, 13.8, 11.2.

IR (film): 3226, 3006, 1656, 1532, 1275, 1261, 764, 750 cm^{-1}.

HRMS (ESITOF) m/z: Calc'd C$_{11}$H$_{13}$NONa (M+Na)$^+$ = 198.0895, found = 198.0896.
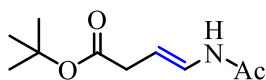
7m-Ac (KC-4-121)

^{1}H NMR (500 MHz, CD$_3$CN): Mix of *E/Z*-isomers: δ [8.16 (s, *E*) & 7.99 (s, *Z*), Σ1H], 6.70 (ddt, *E/Z*, Σ1H), [5.17 (dt, *E*) & 4.77 (dt, *Z*), Σ1H], [3.00 (d, *Z*) & 2.90 (d, *E*), Σ2H], [1.97 (s, *Z*) & 1.90 (s, *E*), Σ3H], [1.43 (s, *Z*) & 1.42 (s, *E*), Σ9H].

^{13}C NMR{^{1}H} (126 MHz, CD$_3$CN): Mix of *E/Z*-isomers: δ 172.2, 171.4, 168.7, 168.2, 126.3, 124.3, 104.9, 103.0, 81.3, 81.0, 36.9, 33.5, 28.2, 22.9.

IR (film): 3284, 3201, 2779, 2933, 1731, 1658, 1529, 1368, 1298, 1256, 1148, 955 cm^{-1}.

HRMS (ESITOF) m/z: Calc'd C$_{10}$H$_{17}$NO$_3$Na = 222.1106, found = 222.1100.
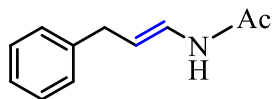
7n-Ac (KC-4-114)

^{1}H NMR (500 MHz, CD$_3$CN): Mix of *E/Z*-isomers: δ 8.10 (s, *E/Z*, Σ1H), 7.33-7.16 (m, *E/Z*, Σ5H), 6.70 (m, *E/Z*, Σ1H), [5.30 (dt, *E*) & 4.82 (dt, *Z*), Σ1H], [3.42 (d, *Z*) & 3.33 (d, *E*), Σ2H], [1.99 (s, *E*) & 1.88 (s, *Z*), Σ3H].

^{13}C NMR{^{1}H} (126 MHz, CD$_3$CN): Mix of *E/Z*-isomers: δ 168.8, 168.1, 142.1, 141.7, 129.43, 129.38, 129.29, 129.1, 126.9, 124.8, 122.7, 111.6, 109.7, 36.5, 32.5, 22.9.

IR (film): 3304, 2923, 1742, 1661, 1532, 1496, 1454, 1373, 1274, 1228, 1040 cm^{-1}.

HRMS (ESITOF) m/z: Calc'd C$_{11}$H$_{13}$NONa (M+Na)$^+$ = 198.0895, found = 198.0897.
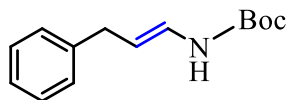
7n-Boc (KC-4-094)

^{1}H NMR (500 MHz, CD$_3$CN): Mix of *E/Z*-isomers: δ 7.34-7.13 (m, *E/Z*, Σ5H), 6.44 (m, *E/Z*, Σ1H), [5.17 (dd, *E*) & 4.71 (q, *Z*), Σ1H], [3.34 (d, *Z*) & 3.30 (d, *E*), Σ2H], [1.45 (s, *Z*) & 1.42 (s, *E*), Σ9H].

^{13}C NMR{^{1}H} (126 MHz, CD$_3$CN): Mix of *E/Z*-isomers: δ 154.0, 142.4, 141.9, 129.4, 129.2, 129.1, 126.9, 125.9, 109.4, 36.5, 28.4.

IR (film): 3621, 3530, 3366, 3090, 2261, 1944, 1881, 1719, 1676, 1495, 1452, 1368, 1236, 1163, 1042 cm^{-1}.

HRMS (ESITOF) m/z: Calc'd C$_{14}$H$_{19}$NO$_2$Na (M+Na)$^+$ = 256.1313, found = 256.1310.
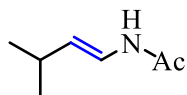
7o-Ac (KC-4-108)

^{1}H NMR (500 MHz, CD$_3$CN): Mix of *E/Z*-isomers: δ 7.97 (s, *E/Z*, Σ1H), [6.61 (ddd, *E*) & 6.48 (ddd, *Z*), Σ1H], [5.13 (dd, *E*) & 4.49 (t, *Z*), Σ1H], [2.60-2.58 (m, *Z*) & 2.30-2.28 (m, *E*), Σ1H], [1.95 (s, *Z*) & 1.88 (s, *E*), Σ3H], [0.98 (d, *E*) & 0.97 (d, *Z*), Σ6H].

^{13}C NMR{^{1}H} (126 MHz, CD$_3$CN): Mix of *E/Z*-isomers: δ 168.0, 121.7, 119.8, 29.7, 26.1, 23.3, 23.2, 22.9.

IR (film): 2824, 2853, 1729, 1660, 1551, 1464, 1377, 1275, 750 cm^{-1}.

HRMS (ESITOF) m/z: Calc'd C$_7$H$_{13}$NO$_2$Na (M+Na)$^+$ = 166.0844, found = 166.0845.
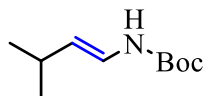
7o-Boc (KC-4-101)

^{1}H NMR (500 MHz, CD$_3$CN): Mix of E/Z-isomers: δ 7.02 (s, *E/Z*, Σ1H), 6.32 (ddd, *E/Z*, Σ1H), 5.00 (dd, *E/Z*, Σ1H), 2.27 (m, *E/Z*, Σ1H), 1.42 (s, *E/Z*, Σ9H), 0.97 (d, *E/Z*, Σ3H).

^{13}C NMR{^{1}H} (126 MHz, CD$_3$CN): Mix of *E/Z*-isomers: δ154.7, 123.3, 121.2, 80.5, 30.1, 28.7, 23.8.

IR (film): 3621, 3530, 3366, 3279, 3090, 2261, 1944, 1881, 1719, 1676, 1494, 1452, 1368, 1236, 1163, 1042 cm^{-1}.

HRMS (ESITOF) m/z: Calc'd C$_{10}$H$_{19}$NO$_2$Na (M+Na)$^+$ = 208.1313, found = 208.1302.
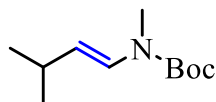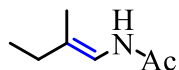
7p-Boc (KC-4-118)

^{1}H NMR (500 MHz, CD$_3$CN): δ 6.88 (broad s, 1H), 4.83 (broad s, 1H), 2.93 (s, 3H, 2.32 (broad s, 1H), 1.46 (s, 9H), 1.00 (d, 6H).

^{13}C NMR{^{1}H} (126 MHz, CD$_3$CN): δ 127.3, 116.8, 81.2, 38.0, 20.3, 28.4, 23.8.

IR (film): 3105, 2959, 2930, 2862, 2358, 2278, 2138, 2083, 1701, 1654, 1388, 1367, 1326, 1150 cm^{-1}.

HRMS (ESITOF) m/z: Calc'd C$_{11}$H$_{21}$NO$_2$Na (M+Na)$^+$ = 222.1470, found = 222.1471.

7q-Ac (KC-4-272)

^{1}H NMR (500 MHz, CD$_3$CN): Mix of *E/Z*-isomers: δ 7.67 (s, E/Z, Σ1H), [6.46 (d, E) & 6.41 (d, Z), Σ1H], [2.07 (q, Z) & 2.03 (q, E), Σ2H], [1.97 (s, E) & 1.95 (s, Z), Σ3H], [1.68 (s, Z) & 1.64 (s, E), Σ3H], 1.01 (m, *E/Z*, Σ3H).

^{13}C NMR{^{1}H} (126 MHz, CD$_3$CN): Mix of E/Z-isomers: δ 168.2, 120.6, 117.5, 30.2, 24.2, 23.0, 19.9, 14.9, 13.2, 12.4.

IR (film): 3294, 2964, 2278, 2137, 1653, 1524, 1371, 1271, 1063, 843 cm^{-1}.

HRMS (ESITOF) m/z: Calc'd C$_8$H$_{15}$NO$_2$Na (M+Na)$^+$ = 180.1000, found 180.0993.
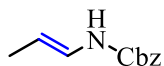
7r-Cbz (KC-4-078)

^{1}H NMR (500 MHz, CD$_3$CN): Mix of *E/Z*-isomers: δ 7.46-7.33 (m, E/Z, Σ5H), 6.42 (m, *E/Z*, Σ1H), [5.15 (s, *E/Z*) & 5.12 (s, *E/Z*), Σ2H], [5.14 (m, *E*) & 4.69 (p, *Z*), Σ1H], [1.62 (ddd, *E/Z*), Σ3H].

^{13}C NMR (126 MHz, CD$_3$CN): Mix *E/Z*-isomers: δ 154.6, 138.0, 129.4, 128.9, 128.7, 67.3, 67.1, 14.9.

IR (film): 3312, 3065, 3032, 2857, 1703, 1682, 1518, 1454, 1294, 1234, 1116, 1028, 947 cm^{-1}.

HRMS (ESITOF) m/z: Calc'd C$_{11}$H$_{13}$NO$_2$Na (M+Na)$^+$ = 214.0844, found = 214.0849.
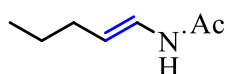
7u-Ac (KC-4-075)

^{1}H NMR (500 MHz, CD$_3$CN): Mix of *E/Z*-isomers: δ [8.01 (s, *E*) & 7.83 (s, *Z*), Σ1H], [6.62 (ddt, *E*) & 6.58 (ddt, *Z*), Σ1H], [5.14 (dt, *E*) & (dt, *Z*), Σ1H], [2.16 (s, *Z*) & 1.88 (s, *E*), Σ3H], [2.05-1.95 (m, *E/Z*), Σ2H], [1.38-1.34 (m, *E/Z*), Σ2H], [0.92 (t, *Z*) & 0.88 (t, *E*), Σ3H].

^{13}C NMR{^{1}H} (126 MHz, CD$_3$CN): Mix of *E/Z*-isomers: δ 167.9, 123.9, 122.1, 112.9, 111.2, 32.5, 28.4, 23.9, 23.4, 22.9, 13.8.

IR (film): 3279, 3200, 3063, 2959, 2928, 2872, 1657, 1528, 1460, 1437, 1371, 1302, 1282, 1172, 1038, 955 cm^{-1}.

HRMS (ESITOF) m/z: Calc'd C$_7$H$_{13}$NONa (M+Na)$^+$ = 150.0895, found = 150.0897.
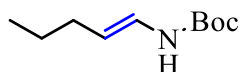
7u-Boc (KC-4-076)

^{1}H NMR (500 MHz, CD$_3$CN): Mix of *E/Z*-isomers: δ [7.58 (s, *E*) & 7.45 (s, *Z*), Σ1H], 6.87-6.84 (m, *E/Z*, Σ1H), [5.54-5.50 (m, *E*) & 5.06-5.02 (m, *Z*), Σ1H], 2.47-2.44 (m, E/Z, Σ2H), [1.95 (s, *Z*) & 1.93 (s, *E*), Σ9H], 1.87 (m, *E/Z*, Σ2H), [1.41 (t, *Z*) & 1.39 (t, *E*), Σ3H].

^{13}C NMR{^{1}H} (126 MHz, CD$_3$CN): Mix of *E/Z*-isomers: δ 154.0, 124.9, 123.2, 110.3, 109.2, 32.5, 32.3, 28.4, 28.1, 24.0, 23.4, 13.9, 13.8.

IR (film): 3327, 2961, 2930, 2872, 1701, 1676, 1508, 1452, 1368, 1242, 1165, 1047, 1022, 951 cm^{-1}.

HRMS (ESITOF) m/z: Calc'd C$_{10}$H$_{19}$NO$_2$Na (M+Na)$^+$ = 208.1313, found = 208.1311.
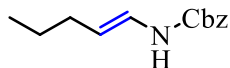
7u-Cbz (KC-4-077)

¹H NMR (500 MHz, CD₃CN): Mix of *E/Z*-isomers: δ 7.45-7.31 (m, *E/Z*, Σ5H), [6.39 (ddt, *E*) & 6.38-6.36 (m, *Z*), Σ1H], [5.12 (s, *E/Z*) & 5.08 (s, *E/Z*), Σ2H], [5.13-5.11 (m, *E*) & 4.62 (q, *Z*), Σ1H], 1.97 (m, *E/Z*, Σ2H), 1.36 (m, *E/Z*, Σ2H), [0.90 (t, *Z*) & 0.88 (t, *E*), Σ3H].

¹³C NMR{¹H} (126 MHz, CD₃CN): Mix of E/Z-isomers: Mix of E/Z-isomers: δ 154.6, 138.0, 129.4, 129.0, 128.8, 124.8, 123.2, 111.6, 110.4, 67.2, 32.4, 28.2, 23.9, 23.4, 13.8.

IR (film): 2963, 2123, 1714, 1679, 1521, 1237, 1051, 831 cm⁻¹.

HRMS (ESITOF) m/z: Calc'd $C_{13}H_{17}NO_4Na$ (M+Na)⁺ = 242.1157, found = 242.1156.
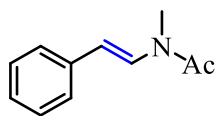
7v-Ac (KC-4-164)

¹H NMR (500 MHz, CD₃CN): Mix of rotamers: δ [8.04 (d) & 7.48 (d), Σ1H], 7.42-7.15 (m, 5H), 6.03 (d, 1H), [3.21 (s) & 3.15 (s), Σ3H], [2.28 (s) & 2.21 (s), Σ3H].

¹³C NMR{¹H} (126 MHz, CD₃CN): δ 170.3, 138.1, 130.6, 129.6, 127.0, 126.4, 110.9, 33.6, 29.6, 22.9, 22.3.

IR (film): 3308, 1675, 1636, 1469, 1387, 1311, 1261, 1141, 1017, 929 cm⁻¹.

HRMS (ESITOF) m/z: Calc'd $C_{11}H_{13}NONa$ (M+Na)⁺ = 198.0895, found 198.0895.
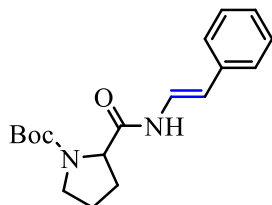
7w (KC-4-109)

¹H NMR (500 MHz, CD₃CN): *Z*-isomer: δ 9.01 (s, 1H), 7.43-7.21 (m, 5H), 6.85 (dd, 1H), 5.75 (s, 1H), [4.27 (s) & 4.18 (s), Σ1H)], 3.36 (s, 2H), 2.23-2.92 (m, 2H), 1.85 (s, 2H), 1.38 (s, 9H); *E*-isomer: δ [8.72 (s) & 8.57 (s), Σ1H], 7.47-7.21 (m, 5H), 7.17 (ddt, 1H), 6.26 (d, 1H), [4.14 (s) & 4.12 (s), Σ1H], [3.46 (m) & 3.40 (m), Σ2H], [2.22 (s) & 2.00 (s), Σ2H], 1.87 (m, 2H), [1.45 (s) & 1.36 (s), Σ9H].

^{13}C NMR{^{1}H} (126 MHz, CD$_3$CN): Z-isomer: δ 136.6, 129.8, 128.9, 127.7, 122.5, 110.7, 100.9, 80.2, 61.1, 48.0, 28.4; E-isomer: δ 137.7, 129.6, 127.3, 126.3, 123.9, 113.3, 80.2, 61.8, 61.3, 48.0, 28.5.

IR (film): 3281, 3061, 2977, 2930, 1699, 1651, 1578, 1536, 1487, 1402, 1247, 1163, 1124, 955 cm^{-1}.

HRMS (ESITOF) m/z: Calc'd C$_{18}$H$_{24}$N$_2$O$_3$Na (M+Na)$^+$ = 339.1685, found = 339.1700.
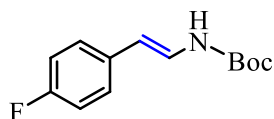
7x-Boc (KC-4-163)

^{1}H NMR (500 MHz, CD$_3$CN): Z-isomer: δ 7.31-7.10 (m, 4H), 7.22 (s, 1H), 6.59 (dd, 1H), 5.53 (d, 1H), 1.46 (s, 9H); E-isomer: δ 7.53 (s, 1H), 7.31-7.01 (m, 4H), 7.11 (dd, 1H), 6.00 (d, 1H), 1.46 (s, 9H).

^{13}C NMR (126 MHz, CD$_3$CN): Z-isomer: δ 163.0, 161.1, 156.1, 130.8, 130.7, 124.5, 124.5, 116.5, 116.3, 106.8, 45.7, 28.3; E-isomer: δ 163.1, 161.1, 153.9, 134.5, 127.6, 127.5, 125.7, 116.3, 116.1, 109.0, 80.9, 28.4.

IR (film): 3320, 2918, 1756, 1683, 1606, 1510, 1368, 1228, 1150, 855 cm^{-1}.

HRMS (ESITOF) m/z: Calc'd C$_{13}$H$_{16}$FNO$_2$Na (M+Na)$^+$ = 260.1063, found = 260.1062.
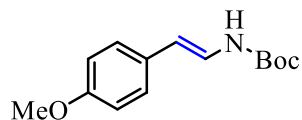
7y-Boc (KC-4-102)

^{1}H NMR (500 MHz, CD$_3$CN): Z-isomer: δ 7.23 (d, 2H), 6.91 (d 2H), 7.14 (s, 1H), 6.51 (dd, 1H), 5.50 (d, 1H), 3.79 (s, 3H), 1.45 (s, 9H); E-isomer: δ 7.45 (s, 1H), 7.22 (d, 2H), 6.84 (d, 2H), 7.03 (dd, 1H), 5.97 (d, 1H), 3.76 (s, 3H), 1.46 (s, 9H).

^{13}C NMR{^{1}H} (126 MHz, CD$_3$CN): Z-isomer: δ 159.1, 130.1, 129.3, 123.1, 115.1, 107.9, 81.0, 55.9, 28.4; E-isomer: δ 159.1, 153.9, 130.5, 127.1, 124.0, 115.0, 110.0, 80.7, 55.8, 28.4.

IR (film): 3296, 2978, 2921, 2849, 1755, 1750, 1603, 1578, 1513, 1460, 1424, 1394, 1369, 1369, 1316, 1258, 1161, 1028 cm^{-1}.
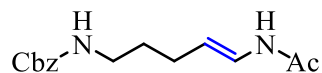
7z-Ac (KC-4-212)

^{1}H NMR (500 MHz, CD$_3$CN): Mix of *E/Z*-isomer: δ 8.02 (s, *E/Z*, Σ1H), 7.34 (m, *E/Z*, Σ5H), 6.65 (m, *E/Z*, Σ1H), 5.64 (s, *E/Z*, Σ1H), [5.14 (dt, *E*) & 4.63 (q, *Z*), Σ1H], 3.09 (m, *E/Z*, Σ2H), 2.09-1.97 (m, *E/Z*, Σ2H), [1.96 (s, *Z*) & 1.88 (s, *E*), Σ3H], 1.51 (m, *E/Z*, Σ2H).

^{13}C NMR{^{1}H} (126 MHz, CD$_3$CN): Mix of *E/Z*-isomers: δ 167.9, 157.3, 138.5, 129.4, 128.7, 124.2, 111.6, 110.5, 66.6, 40.9, 30.9, 30.6, 27.5, 23.6, 22.9.

IR (film): 3617, 3369, 3092, 2937, 2262, 2116, 1692, 1665, 1525, 1372, 1250, 1150, 1037 cm^{-1}.

HRMS (ESITOF) m/z: Calc'd C$_{15}$H$_{20}$N$_2$O$_3$Na (M+Na)$^+$ = 299.1372, found 299.1377.
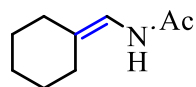
7aa-Ac (KC-4-166)

^{1}H NMR (500 MHz, CD$_3$CN): δ 7.69 (s, 1H), 6.37 (dd, 1H), 2.16-2.05 (m, 4H), 1.92 (s, 3H), 1.52-1.48 (m, 6H).

^{13}C NMR{^{1}H} (126 MHz, CD$_3$CN): δ 168.3, 123.5, 115.1, 34.1, 29.2, 28.0, 27.9, 27.3, 23.0.

IR (film): 3291, 3199, 3034, 2927, 2852, 1653, 1525, 1446, 1373, 1278, 1215, 1154, 968 cm^{-1}.

HRMS (ESITOF) m/z: Calc'd C$_9$H$_{15}$NONa (M+Na)$^+$ = 176.1051, found = 176.1042.
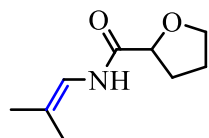
7bb (KC-4-205)

^{1}H NMR (500 MHz, CD$_3$CN): δ 8.04 (s, 1H), 6.39 (dt, 1H), 4.29 (dd, 1H), 3.98-3.83 (m, 2H), 2.24-1.81 (m, 4H), [1.70 (s) & 1.63 (s), Σ6H].

^{13}C NMR{^{1}H} (126 MHz, CD$_3$CN): δ 171.0, 117.0, 78.9, 70.1, 30.9, 26.2, 22.4, 16.6.

IR (film): 3412, 2917, 1681, 1502, 1261, 1233, 1070, 764, 750 cm^{-1}.

HRMS (ESITOF) m/z: Calc'd C$_9$H$_{15}$NO$_2$Na (M+Na)$^+$ = 192.1000, found = 192.0998.
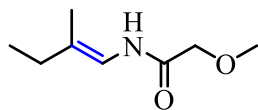
7cc (KC-4-235)

¹H NMR (500 MHz, CD₃CN): Mix of *E/Z*-isomers: δ 7.88 (s, *E/Z*, Σ1H), [6.46 (dq, *E*) & 6.42 (dd, *Z*), Σ1H], [3.88 (s, *E*) & 3.87 (s, *Z*), Σ2H], [3.40 (s, *E*) & 3.40 (s, *Z*), Σ3H], 2.07-2.04 (m, *E/Z*, Σ 2H), [1.70 (d, *E*) & 1.64 (d, *Z*), Σ3H], [1.02-0.99 (m, *E*) & 0.89-0.87 (m, *Z*), Σ3H].

¹³C NMR{¹H} (126 MHz, CD₃CN): Mix of *E/Z*-isomers: δ 167.5, 167.4, 122.9, 122.6, 116.04, 115.99, 72.3, 59.5, 30.1, 24.2, 19.8, 14.7, 13.1, 12.2.

IR (film): 3421, 3306, 2964, 2933, 1679, 1508, 1452, 1198, 1114, 985, 763, 749 cm⁻¹.

HRMS (ESITOF) m/z: Calc'd $C_8H_{15}NO_2Na$ (M+Na)⁺ = 180.1000, found = 180.1001.

The following alkene products were synthesizes via the *in situ* reduction decarboxylative elimination procedure:
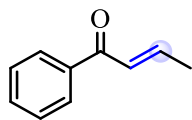
8d (KC-5-024)

¹H NMR (500 MHz, CD₃CN): δ 7.96–7.87 (m, 2H), 7.59–7.50 (m, 1H), 7.47 (dd, 2H), 7.08 (dq, 1H), 6.94–6.87 (m, 1H), 2.00 (dd, 3H).

¹³C NMR{¹H} (126 MHz, CD₃CN): δ 190.7, 144.9, 137.8, 132.5, 128.4, 127.4, 18.5.

IR (film): 3072, 2923, 1718, 1652, 1605, 1454, 935, 750 cm⁻¹.

HRMS (ESITOF) m/z: Calc'd $C_{10}OH_{14}N$ (M+NH₄) = 164.1075, found 164.1077.
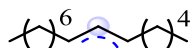
8e (KC-5-206)

¹H NMR (500 MHz, CD₃CN): Mixture of regioisomers (1:1): δ 5.44-5.37 (m) & 5.37-5.31 (m) Σ2H], [2.06-2.00 (m) & 2.00-1.93 (m), Σ4H], 1.4-1.18 (m, 18H), 0.89 (t, Σ6H).

¹³C NMR{¹H} (126 MHz, CD₃CN): Mix of regioisomers (1:1): δ 130.5, 130.0, 32.8, 32.7, 32.08, 32.05, 31.9, 31.6, 30.0, 29.84, 29.80, 29.7, 29.52, 29.49, 29.37, 29.35, 29.3, 29.0, 27.4, 27.3, 22.9, 22.8, 22.7, 14.3.

IR (film): 3005, 2956, 1636, 1466, 1455, 966, 723 cm⁻¹.

See Appendix **A8** for GC/MS data.
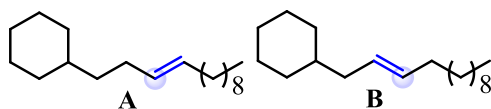
8h (KC-6-128)

^{1}H NMR (500 MHz, CD$_3$CN): Mix of regioisomers (1.95:1 A:B): δ 5.46-5.33 (m, 2H), 2.10-1.97 (m, 3H), 1.97-1.84 (m, 1H), 1.77-1.61 (m, 5H),1.41-1.11 (m, 20H), 0.97-0.81 (m, 5H).

^{13}C NMR{[1]H} (126 MHz, CD$_3$CN): Mix of regioisomers (1.95:1 A:B): δ 131.6, 130.7, 130.3, 128.9, 20.8, 38.3, 37.6, 37.3, 33.5, 32.81, 32.79, 32.1, 29.9, 29.8, 29.71, 29.69, 29.53, 29.52, 29.4, 29.3, 26.9, 26.8, 26.58, 26.56, 22.9, 12.4.

IR (film): 3004, 2925, 1466, 1449, 967, 721 cm^{-1}.

See Appendix **A8** for GC/MS data and Appendix **A9** for COSY data.
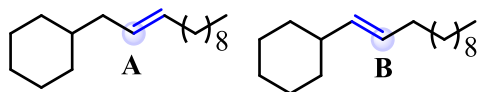
8i (KC-6-070)

^{1}H NMR (500 MHz, CD$_3$CN): Mixture of regioisomers (3.6:1 A:B) and *E/Z* (>95:5): δ [5.43-5.30 (m) & 5.28-5.15 (m) Σ2H], 2.34-1.20 (m, 0.4H, only minor isomer), 2.06-1.83 (m, Σ4H), 1.75-1.58 (m, Σ5H), 1.39-0.98 (m, Σ22H), 0.94-0.75 (m, Σ6H).

^{13}C NMR{[1]H} (126 MHz, CD$_3$CN): Mixture of regioisomers (3.6:1 A:B) and *E/Z* (>95:5): δ 136.5, 131.6, 128.9, 127.9, 40.9, 38.3, 33.5, 33.3, 32.8, 32.1, 29.9, 29.81, 29.78, 29.7, 29.5, 29.34, 29.31, 26.8, 26.6, 26.4, 26.3, 22.9, 14.3.

IR (film): 3055, 2927, 1652, 1634, 1464, 1450, 971, 720 cm^{-1}.

See Appendix **A8** for GC/MS data and Appendix **A9** for COSY data.
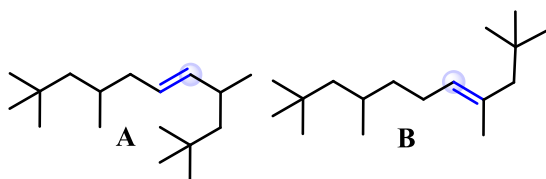
8j (KC-6-035)

^{1}H NMR (500 MHz, CD$_3$CN): Mixture of regioisomers (>90:10) and *E/Z* (86:14): δ [5.43-5.10 (m) Σ2H], [2.58-2.51 (m) 0.15H, only minor isomer)], [2.28-2.19 (m) 0.84H, only major isomer], [2.11-1.98 (m) 0.19H only minor isomer], [1.96-1.88 (m) Σ1H], [1.86-1.78 (m) 0.85H, only major isomer], [1.58-1.39 (m) Σ1H], [1.32-1.13 (m) Σ4H], [1.07-0.79 (m) Σ26H].

^{13}C NMR{^{1}H} (126 MHz, CD$_3$CN): Mixture of regioisomers (>90:10) and *E/Z* (86:14): δ 140.11, 140.08, 126.4, 126.3, 51.4, 50.6, 50.5, 42.7, 34.1, 30.4, 30.3, 30.2, 29.90, 29.86, 24.43, 24.41, 22.8, 22.7.

IR (film): 3053, 2954, 1645, 1464, 1449, 968, 638 cm^{-1}.

See Appendix **A8** for GC/MS data and Appendix **A9** for COSY data.
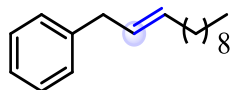
8k (KC-6-175)

^{1}H NMR (500 MHz, CD$_3$CN): Mixture of regioisomers (>95:5) and *E/Z* (3:1); isolated with alkane product (2:1 alkene:alkane): δ 7.32-7.27 (m, 2H), 7.23-7.16 (m, 3H), 5.61-5.46 (m, 2H), [3.41 (d) & 3.34 (d) Σ2H], [2.61 (t) & 2.15 (t) Σ1H], 2.03 (td, 2H), 1.66-1.58 (m, 1H), 1.43-1.21 (m, 20H), 0.89 (t, 4H).

^{13}C NMR{^{1}H} (126 MHz, CD$_3$CN): Mixture of regioisomers (>95:5) and *E/Z* (3:1); isolated with alkane product (2:1 alkene:alkane): δ 143.1, 141.3, 132.3, 131.2, 128.8, 128.6, 128.54, 128.49, 128.46, 128.1, 125.98, 125.94, 125.7, 39.2, 36.2, 33.7, 32.7, 32.1, 31.7, 29.83, 29.76, 29.7, 29.5, 29.4, 27.4, 22.8, 14.3.

IR (film): 3063, 2956, 1699, 1652, 1604, 1464, 1454, 968, 744 cm^{-1}.

See Appendix **A8** for GC/MS data and Appendix **A9** for COSY data.
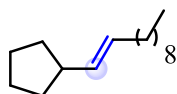
8l (KC-6-084)

^{1}H NMR (500 MHz, CD$_3$CN): Mix of regioisomers (>95:5) and *E/Z* (80:20): δ 5.43-5.31 (m) & 5.30-5.23 (m) Σ2H], [2.73-2.63 (m) & 2.41-2.33 (m) Σ1H], [2.08-2.00 (m) & 1.99-1.92 (m) Σ2H], 1.79-1.70 (m, 2H), 1.69-1.46 (m, 5H), 1.37-1.18 (m, 19H), 0.93-0.83 (m, 4H).

^{13}C NMR{^{1}H} (126 MHz, CD$_3$CN): Mix of regioisomers (>95:5) and *E/Z* (80:20): δ 135.7, 135.4, 128.8, 43.8, 40.6, 38.6, 36.7, 34.2, 33.7, 33.0, 32.3, 30.4, 30.14, 30.12, 30.02, 29.98, 29.8, 29.7, 29.6, 29.2, 27.9, 25.8, 25.6, 25.5, 23.1, 14.5.

IR (film): 3054, 2925, 1660, 1467, 1456, 970, 705 cm^{-1}.

See Appendix **A8** for GC/MS data and Appendix **A9** for COSY data.
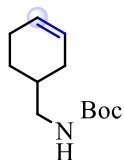
8f (KC-5-138)

^{1}H NMR (500 MHz, CD$_3$CN): δ 5.69-5.60 (m, 2H), 4.61 (broad s, 1H), 3.09-3.00 (m, 2H), 2.13-1.99 (m, 3H), 1.78-1.64 (m, 3H), 1.44 (s, 9H).

^{13}C NMR{^{1}H} (126 MHz, CD$_3$CN): δ 127.5, 126.1, 46.4, 34.7, 29.6, 28.8, 26.7, 25.1.

IR (film): 3343, 2915, 1689, 1519, 1365, 1206, 1150 cm^{-1}.

HRMS (ESITOF) m/z: Calc'd C$_{12}$H$_{22}$O$_2$NNa (M+Na) = 235.1548, found = 235.1560.
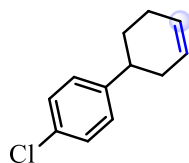
8g (KC-5-073)

^{1}H NMR (500 MHz, CD$_3$CN): δ 7.29 (d, 2H), 7.18 (d, 2H), 5.80-5.76 (m, 2H), 2.85-2.77 (m, 1H), 2.34-2.24 (m, 1H), 2.23-2.08 (m, 3H), 1.96-1.89 (m, 1H), 1.79-1.69 (m, 1H).

^{13}C NMR{^{1}H} (126 MHz, CD$_3$CN): δ 145.6, 131.4, 128.3, 128.1, 126.9, 126.4, 39.4, 22.2, 29.5, 25.6.

IR (film): 3024, 2914, 1665, 1652, 1464, 824, 668, 643 cm^{-1}.

HRMS (ESITOF) m/z: Calc'd C$_{10}$ClH$_{13}$ (M+H) = 168.0706, found = 168.0705.
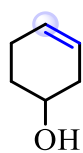
8n (KC-7-039)

^{1}H NMR (500 MHz, CD$_3$CN): δ 5.70-5.62 (m, 1H), 5.61-5.51 (m, 1H), 3.99-3.91 (m, 1H), 2.42-2.30 (m, 1H), 2.23-2.06 (m, 2H), 2.05-1.95 (m, 1H), 1.91-1.81 (m, 1H), 1.08-1.54 (m, 2H).

^{13}C NMR{^{1}H} (126 MHz, CD$_3$CN): δ 126.9, 124.2, 67.1, 34.5, 31.0, 23.7.

IR (film): 3465, 3054, 2987, 1652, 1464, 1421, 1150, 705 cm^{-1}.

HRMS (ESITOF) m/z: Calc'd C$_6$H$_{14}$ON (M+NH$_4$) = 116.1075, found = 116.1070.
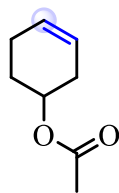
8o (KC-5-193)

^{1}H NMR (500 MHz, CD$_3$CN): δ [6.99-6.96 (m), 5.87-5.82 (m), 5.77-5.72 (m), Σ2H], [3.72 (s), 3.69 (s), 3.65 (s), Σ3H], 3.13-3.07 (m, 1H), [2.28-2.22 (m), 2.2-2.15 (m), Σ2H], 2.08-1.95 (m, 1H), 1.95-1.71 (m, 2H), 1.69-1.54 (m, 2H).

^{13}C NMR{^{1}H} (126 MHz, CD$_3$CN): δ 175.2, 168.2, 139.9, 129.8, 124.4, 51.9, 51.6, 41.2, 29.2, 25.9, 25.4, 24.8, 24.3, 22.2, 21.6, 20.9.

IR (film): 3003, 2944, 1634, 1441, 1224, 1153, 919, 750, 640 cm^{-1}.

HRMS (ESITOF) m/z: Calc'd C$_8$H$_{13}$O$_2$ (M+H) = 141.0916, found 141.0921.

8m (KC-6-007)

^{1}H NMR (500 MHz, CD$_3$CN): δ 5.66 (m, 2H), 2.11-1.95 (m, 3H), 1.83-1.67 (m, 6H), 1.39-1.29 (m, 1H), 1.27-1.14 (m, 3H), 1.12-1.02 (m, 2H), 1.04-0.91 (m, 2H), 0.87 (m, 5H).

^{13}C NMR{^{1}H} (126 MHz, CD$_3$CN): δ 127.3, 127.2, 43.0, 39.9, 39.4, 33.3, 30.2, 30.0, 29.3, 26.4, 26.2.

IR (film): 3022, 2960, 1668, 1447, 896, 705 cm^{-1}.

See Appendix **A8** for GC/MS data.
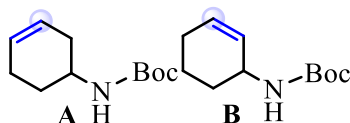
8p (KC-6-244)

^{1}H NMR (500 MHz, CD$_3$CN): Mixture of regioisomers (63:36 A:B) δ [5.81-5.76 (m) & 5.67-5.62 (m) & 5.59-5.55 (m), Σ2H], [4.5 (broad s) & 3.77 (broad s), Σ1H], 2.41-2.32 (m, 1H), 2.17-2.07 (m, 1H), 2.01-1.93 (m, 1H), 1.92-1.79 (m, 2H), 1.69-1.58 (m, 1H), 1.58-1.47 (m, 1H), 1.44 (s, 9H).

^{13}C NMR{^{1}H} (126 MHz, CD$_3$CN): Mixture of regioisomers (63:36 A:B) δ 171.3, 155.5, 130.5, 128.3, 127.1, 124.6, 80.0, 60.5, 45.8, 33.7, 32.2, 29.9, 28.6, 25.7, 24.9, 23.8, 21.2, 19.8, 14.3.

IR (film): 3353, 3025, 2978, 1682, 1652, 1464, 1180, 668 cm^{-1}.

HRMS (ESITOF) m/z: Calc'd C$_{11}$H$_{19}$NO$_2$Na (M+Na) = 220.1313, found 220.1314.
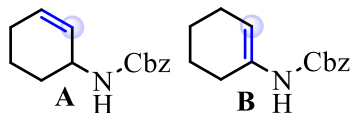
8q (KC-6-091)

^{1}H NMR (500 MHz, CD$_3$CN): Mixture of regioisomers (95:5 A:B) δ 7.47-7.27 (m, 5H), 5.82 (m, 1H), [5.64 (broad s) & 5.53 (broad s) Σ1H], 5.05 (m, 2H), 4.11 (m, 1H), 2.18 (s, 1H), 2.03-1.96 (m, 1H), 1.89-1.82 (m, 1H), 1.74-1.65 (m, 1H), 1.64-1.55 (m, 1H), 1.55-1.46 (m, 1H), [1.36-1.26 (m) & 1.22-1.11 (m) Σ1H].

^{13}C NMR{^{1}H} (126 MHz, CD$_3$CN): Mixture of regioisomers (95:5 A:B) δ 156.7, 138.5, 130.9, 129.4, 129.1, 128.8, 128.7, 66.7, 47.5, 30.4, 25.4, 20.6.

IR (film): 3521, 3061, 3001, 2942, 1716, 1644, 1634, 1463, 1272, 1165, 918, 897, 749, 638 cm^{-1}.

HRMS (ESITOF) m/z: Calc'd C$_{14}$H$_{18}$NO$_2$ (M+H) = 232.1338, found 232.1346.
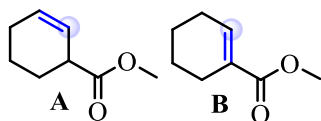
8r (KC-6-037)

^{1}H NMR (500 MHz, CD$_3$CN): Mixture of regioisomers (63:37 A:B) δ [6.99-6.96 (m), 5.87-5.82 (m), 5.77-5.72 (m), Σ2H], [3.72 (s), 3.69 (s), 3.65 (s), Σ3H], 3.13-3.07 (m, 1H), [2.28-2.22 (m), 2.2-2.15 (m), Σ2H], 2.08-1.95 (m, 1H), 1.95-1.71 (m, 2H), 1.69-1.54 (m, 2H).

^{13}C NMR{^{1}H} (126 MHz, CD$_3$CN): Mixture of regioisomers (63:37 A:B) δ 175.2, 168.2, 139.9, 129.8, 124.4, 51.9, 51.6, 41.2, 29.2, 25.9, 25.4, 24.8, 24.3, 22.2, 21.6, 20.9.

IR (film): 3003, 2944, 1634, 1441, 1224, 1153, 919, 750, 640 cm^{-1}.

HRMS (ESITOF) m/z: Calc'd C$_8$H$_{13}$O$_2$ (M+H) = 141.0916, found 141.0921.

8s (KC-5-256)

^{1}H NMR (500 MHz, CD$_3$CN): δ [6.71-6.67 (m), 5.94 (dq), 5.72 (dq), Σ3H], 3.00-2.93 (m, 1H), [2.25-2.20 (m), 2.19-2.14 (m), Σ1H], 2.12-1.97 (m, 1H), 1.96-1.82 (m, 2H), 1.78-1.55 (m, 2H).

^{13}C NMR{^{1}H} (126 MHz, CD$_3$CN): δ 177.7, 170.8, 135.3, 132.4, 131.6, 124.6, 42.7, 26.6, 25.6, 25.0, 24.4, 22.2, 21.5, 20.5.

IR (film): 3345, 3182, 2930, 2833, 1662, 1627, 1412, 1208, 1152, 898, 624 cm^{-1}.

HRMS (ESITOF) m/z: Calc'd C$_7$H$_{12}$NO (M+H) = 126.0919, found = 126.0912.

Appendix

A1. Publication Copyright Credit Line

Reprinted (adapted) with permission from (Cartwright, K. C.; Tunge, J. A. Decarboxylative Elimination of *N*-Acyl Amino Acids via Photoredox/Cobalt Dual Catalysis. *ACS Catal.* **2018**, *8*, 11801-11806.) Copyright (2018) American Chemical Society.

Reprint (adapted) with permission from (Cartwright, K. C.; Lang, S. B.; Tunge, J. A. Photoinduced Kochi Decarboxylative Elimination for the Synthesis of Enamides and Enecarbamates from *N*-Acyl Amino Acids. *J. Org. Chem.* **2019**, 2933-2940.) Copyright (2019) American Chemical Society.

Reproduced (Cartwright, K. C.; Davies, A. M.; Tunge, J. A. Cobaloxime-Catalyzed Hydrogen Evolution in Photoredox-Facilitated Small-Molecule Functionalization. *Eur. J. Org. Chem.* **2020**, 1245-1258.) in part with permission from John Wiley and Sons. License Number: 477571244619; License date: Feb. 23, 2020.

A2. Compound Number Key

Carboxylic Acids (1)

1a

1b-Boc
1b-Ac

1c-Boc

1d-Boc

1e-Boc

1f-Boc

1g-Cbz

1h-Boc
1h-Ac

1i-Boc

1j-Boc

1k-Boc
1k-Ac
1k-Cbz

1l-Boc
1l-Ac
1l-Cbz

1m-Boc

1n-Boc

1o-Boc

1p-Boc

1q

1r

1s

1t

1u

1v

1w

1x

1y

1z

1aa

1bb-Boc

1cc-Boc

1dd

1ee

1ff

1gg

1hh

1ii

1jj

1kk

1ll-Boc

1mm-Boc

1nn-Boc

1oo-Boc

1pp-Boc

1qq-Boc
1qq-Ac

1rr-Boc

1ss-Boc

1tt-Boc
1tt-Ac

1uu-Boc
1uu-Ac

1vv-Boc
1vv-Ac

1ww-Cbz

1xx-Boc

1yy

1zz-Ac

1aaa

1bbb-Boc

1ccc-Boc

1ddd-Ac

1eee-Ac

1fff

1ggg

1hhh

1iii

1jjj

1kkk

1lll

1mmm

1nnn

1ppp

1qqq

1rrr

1sss

1ttt

1uuu-Boc

1vvv-Boc

1www

1xxx

238

Allylic Esters (2)

2a **2b** **2c** **2d** **2e-Boc**

Allylic and Benzylic Carbonates (4)

(4a) **(4b)** **(4c)** **(4d)** **(4e)** **(4e')**

(4f) **(4g)** **(4h)** **(4i)** **(4j)** **(4k)**

(4l) **(4m)** **(4n)** **(4o)** **(4p)** **(4q)**

(4r) **(4s)** **(4t)** **(4u)** **(4v)** **(4w)**

(4x) **(4y)** **(4z)** **(4aa)**

DcA Products (3)

(3a)

(3b-Boc)
(3c-Ac)

(3d)

(3e)

(3f)

(3g)

(3h)

(3i)

(3j)

(3k)

(3l)
(3m)

(3n)

(3o)

(3p)

(3q)

(3r)

(3s)

(3t)

(3u)

(3v)

(3w)

(3x)

(3y)

(3z)

(3aa)

(3bb)

(3cc)

(3dd)

(3ee)

(3ff)

(3gg)

DcA/DcB Products (5)

(5b)   **(5c)**   **(5d)**   **(5e)**

(5f)   **(5e)**   **(5g)**   **(5h)**

(5i)   **(5j)**   **(5k)**   **(5l)**

(5m)   **(5n)**   **(5o)**   **(5p)**

(5q)   **(5r)**   **(5s)**

(5t)   **(5u)**   **(5v)**   **(5w)**

(5x)   **(5y)**   **(5z)**   **(5aa)**

Three-Component Coupled Products (6)

(6a) (6b) (6c) (6d)

(6e) (6f) (6g.1) (6g.2)

(6h) (6i)

Enamide and Enecarbamate Products (7)

(7a-Boc) (7b-Boc) (7c-Boc) (7d-Boc) (7e-Boc) (7f-Boc)
(7f-Ac)

(7g-Boc) (7h-Boc) (7i-Boc) (7j-Boc) (7k-Boc) (7l-Boc)
(7g-Ac) (7l-Ac)

(7m-Boc) (7n-Boc) (7o-Boc) (7p-Boc) (7q-Boc) (7r-Cbz)
(7o-Ac) (7p-Ac) (7q-Ac)

(7s-Boc) (7t-Boc) (7u-Boc) (7v-Ac) (7w)
(7u-Ac)
(7u-Cbz)

(7x-Boc) (7y-Boc) (7z-Ac) (7aa-Ac) (7bb) (7cc)

242
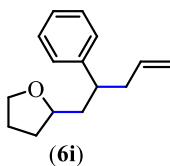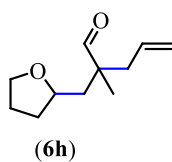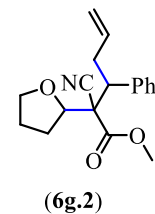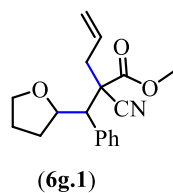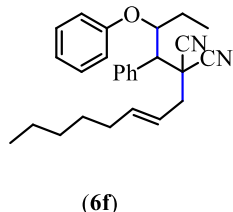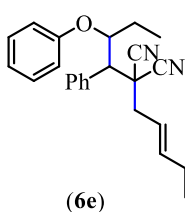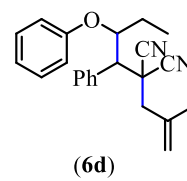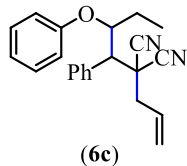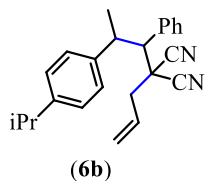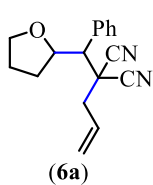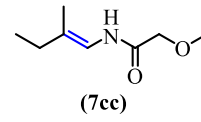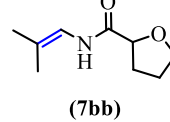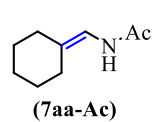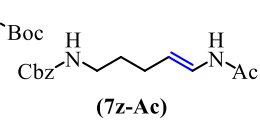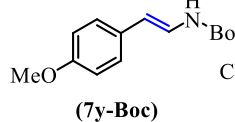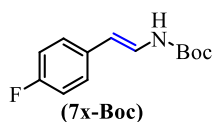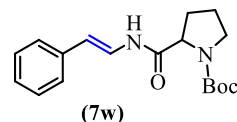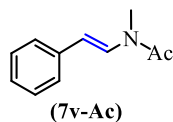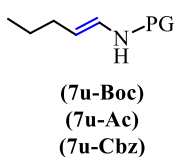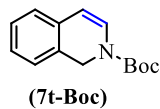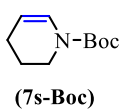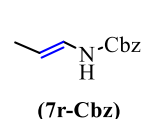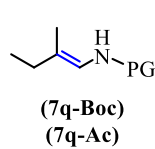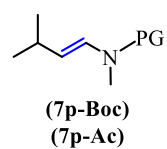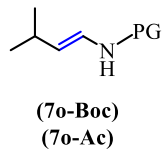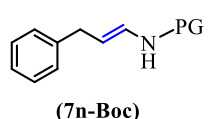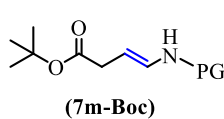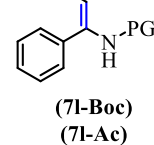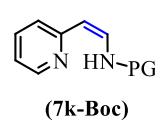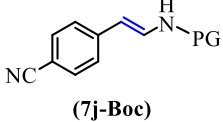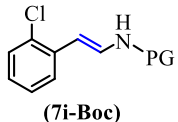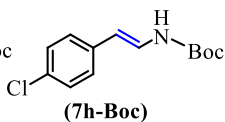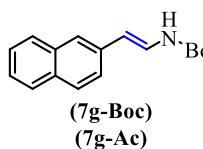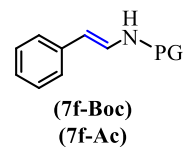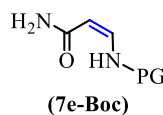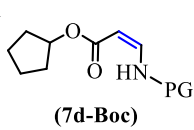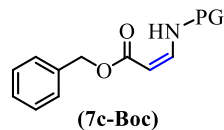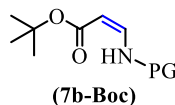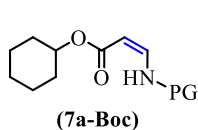
Alkene Products (8)

(8a-Boc)

(8b)

(8c)

(8d)

(8e)

A (8h) B

A (8i) B

A (8j) B

(8k)

(8l)

(8f)

(8g)

(8n)

(8o)

(8m)

A B (8p)

A B (8q)

A B (8r)
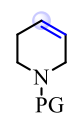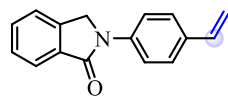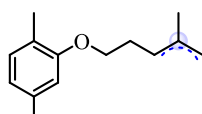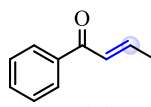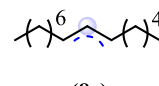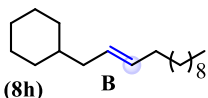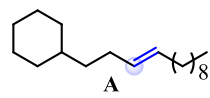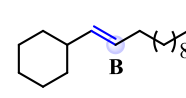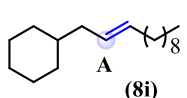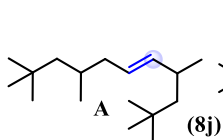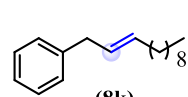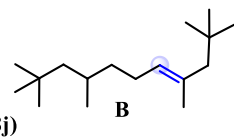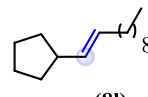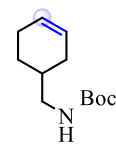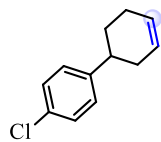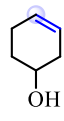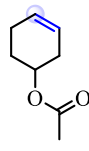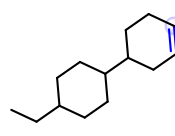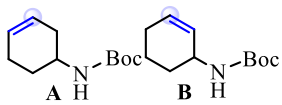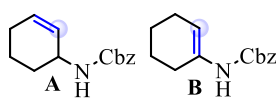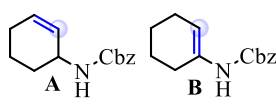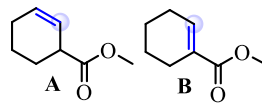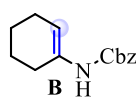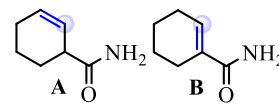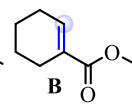
A B (8s)
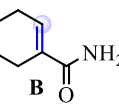
A3. Blue LED Reaction Configuration

Figure A3.1: One Kessil light set-up
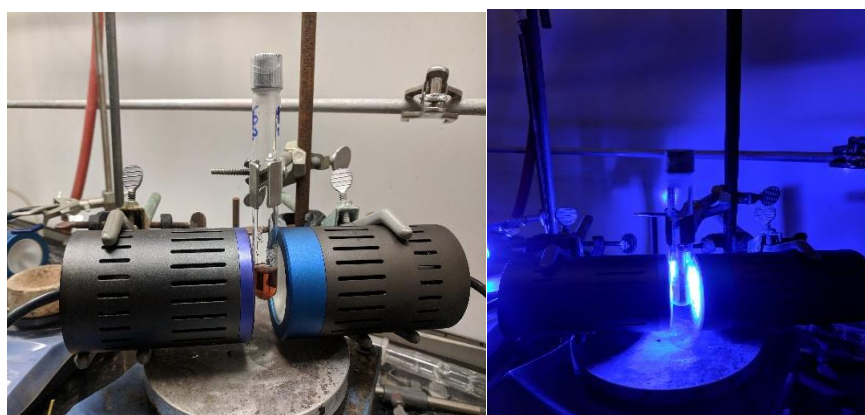
Figure A3.2: Two Kessil light set-up

A4. Isomerization Rate Data and Analysis

Isomerization reactions were performed with 0.038 M of *E*-isomer with a 10 W blue LED bath with Mes-Acr-Ph$^+$ BF$_4^-$ (50 mol%) as the photosensitizer.

E-**7f-Boc** was found to reach 76:24 *E:Z* after 640 minutes of irradiation.

E-**7f-Ac** was found to reach 81:19 *E:Z* after 640 minutes of irradiation.

Note that the plotted data only displays the [Z-isomer]/irradiation time and does not consider the variation in photosteady state between the substrates.

A5. Additional Cobaloxime Catalyst Screenings
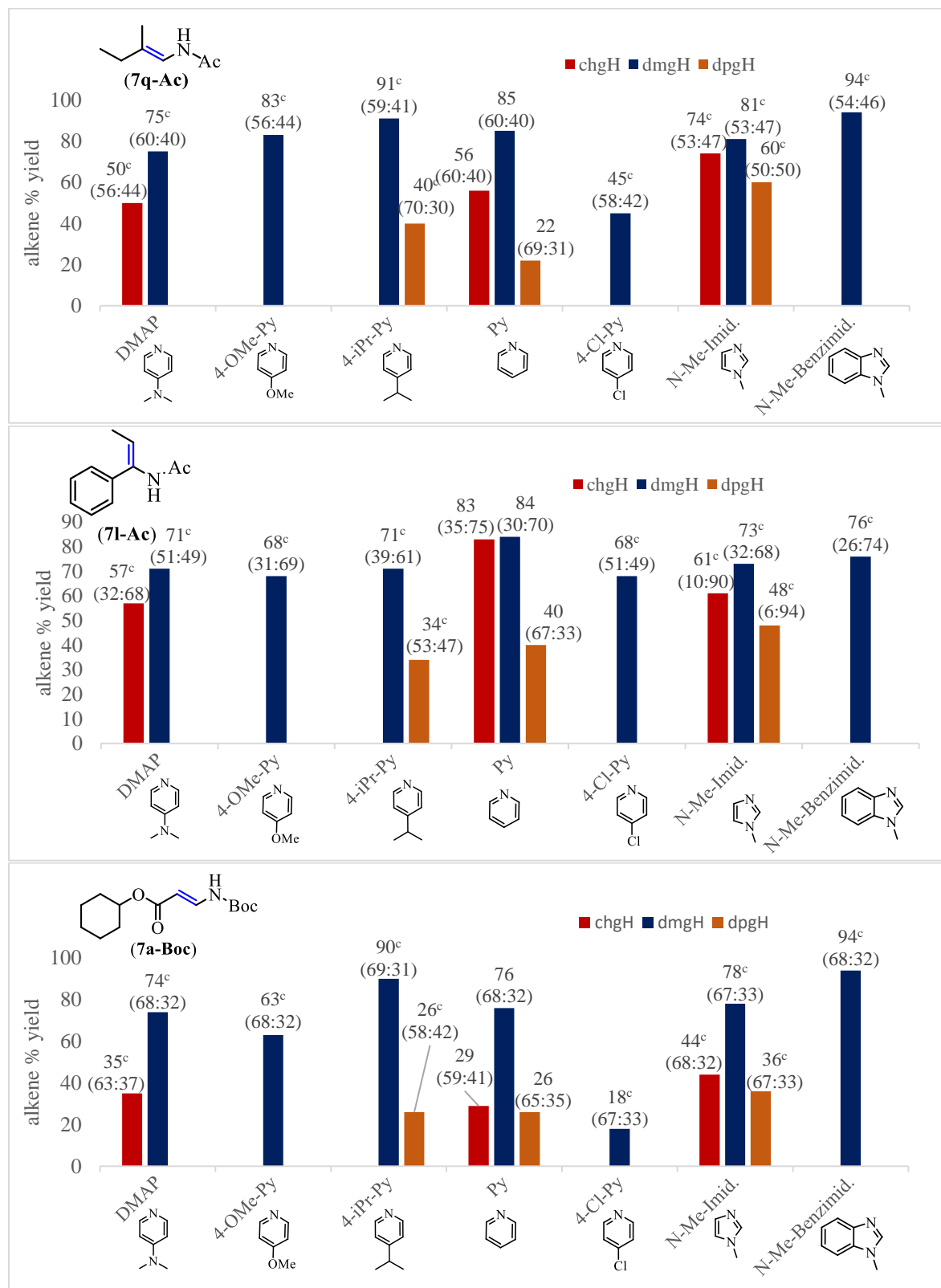
Figure A5.1: Cobaloxime catalyst screen with α-amino acids
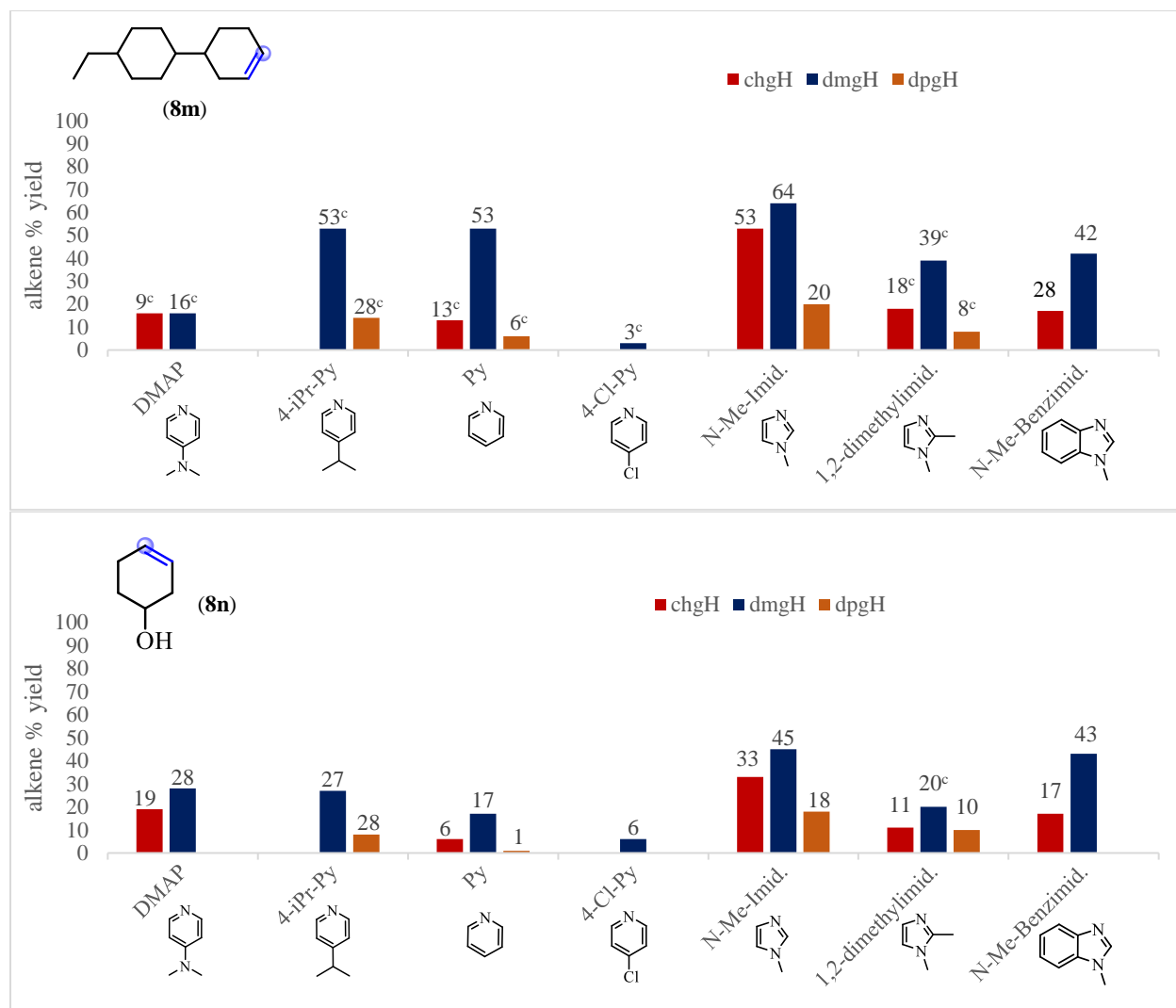
Figure A5.2: Cobaloxime catalyst screen with α,α-disubstituted carboxylic acids

A6. Carboxylate 1ii⁻ Na⁺ and Acridinium Association Spectral Data
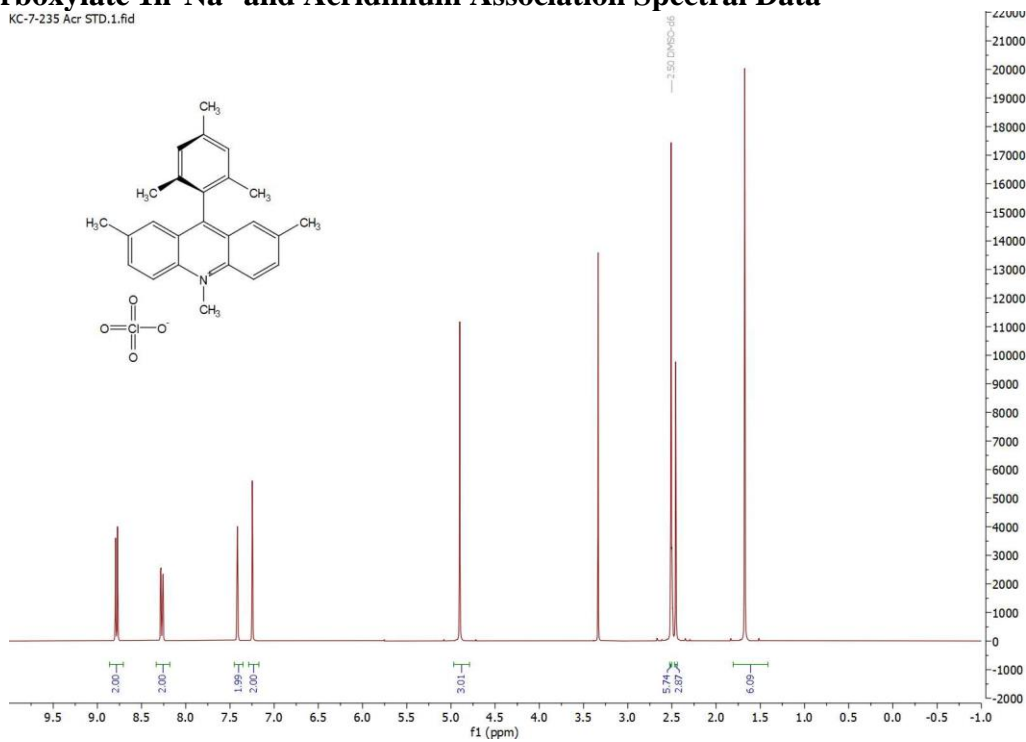
Figure A6.1: ^{1}H NMR of Mes-2,7-Me$_2$-Acr-Me$^+$ ClO$_4^-$
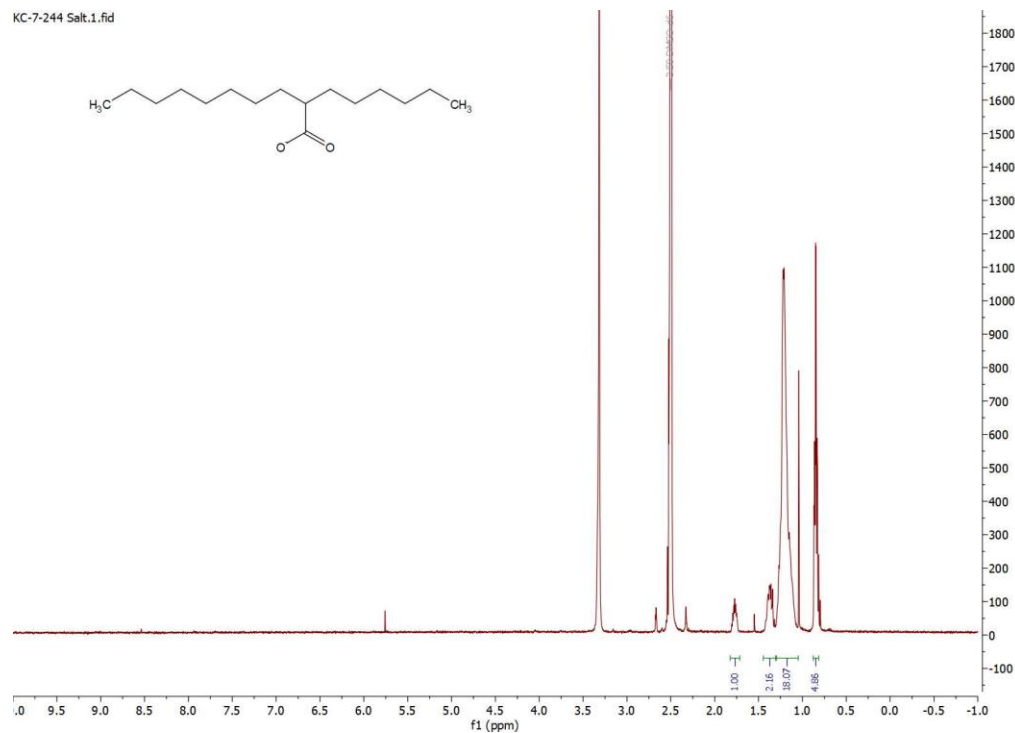
Figure A6.2: ^{1}H NMR of carboxylate salt (**1ii⁻ Na⁺**)
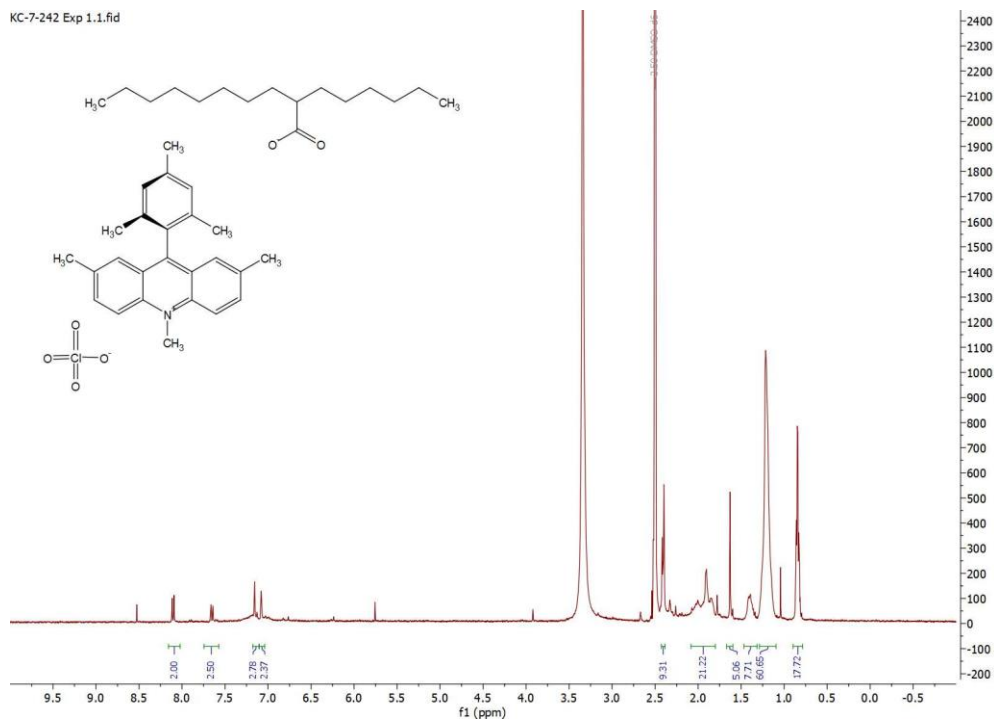
Figure A6.3: Solution of Mes-2,7-Me$_2$-Acr-Me$^+$ ClO$_4^-$ and carboxylate salt (**1ii$^-$ Na$^+$**)

A7. Photolysis of Co(dmgH)$_2$(n-butyl)Py Spectral Data
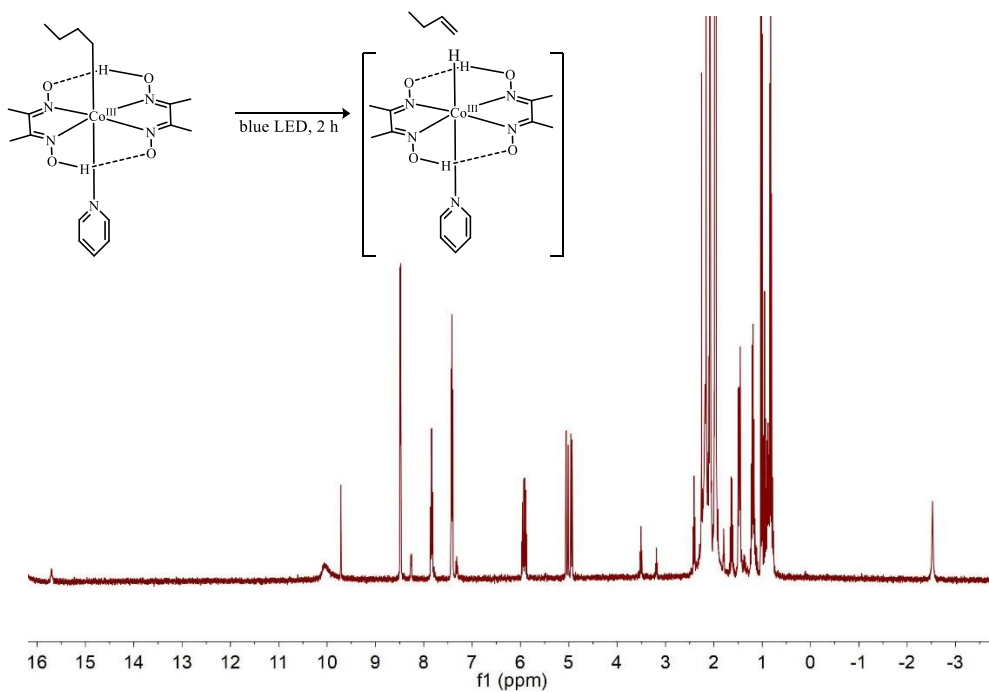
Figure A7.1: ^{1}H NMR of Co(dmgH)$_2$(n-butyl)Py post 2-hour irradiation

Note: identity of resulting cobaloxime complex unknown

A8. GC/MS Data for Alkene Products 8e & 8h-8m

(8e):

Exact Mass: 224.25
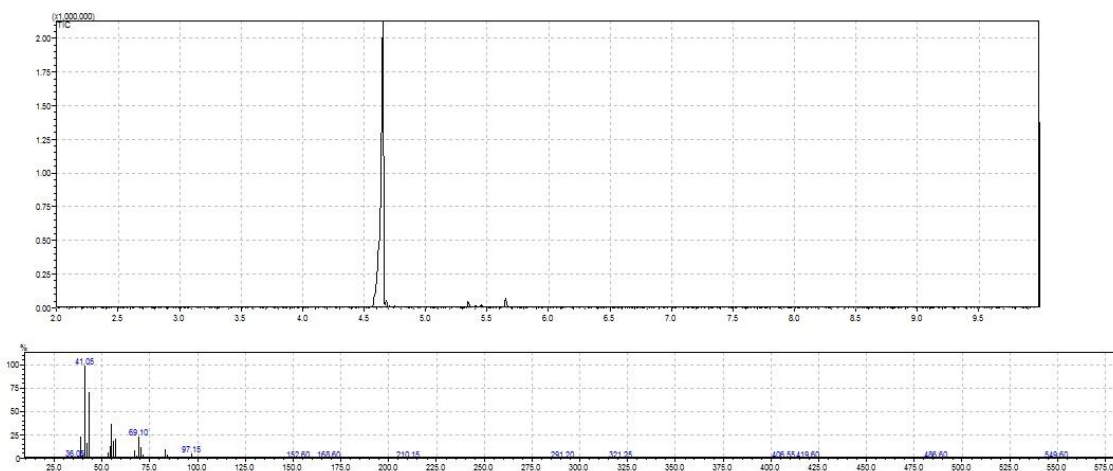
(8h):
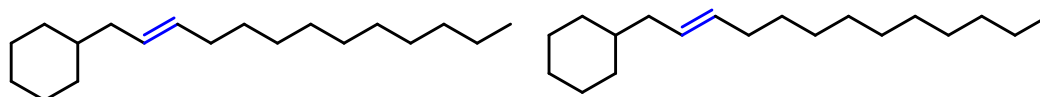
Exact Mass: 264.28
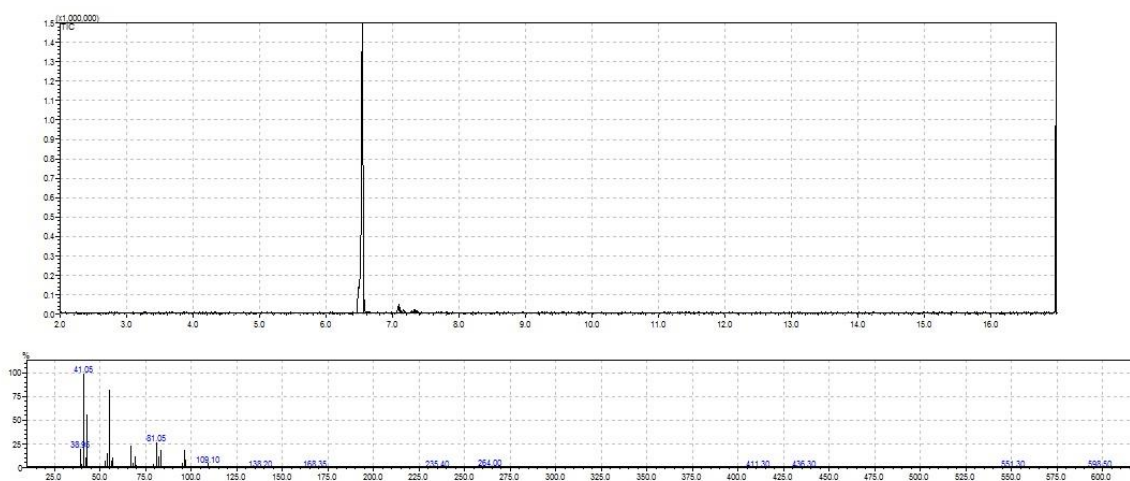
(8i):
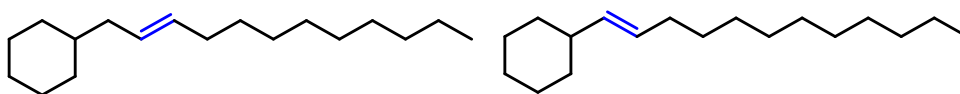
Exact Mass: 250.27

(8j):
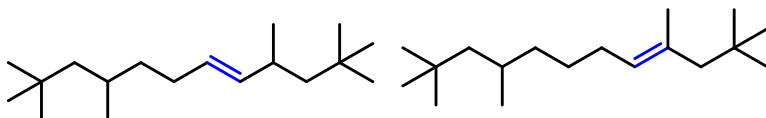
Exact Mass: 238.27
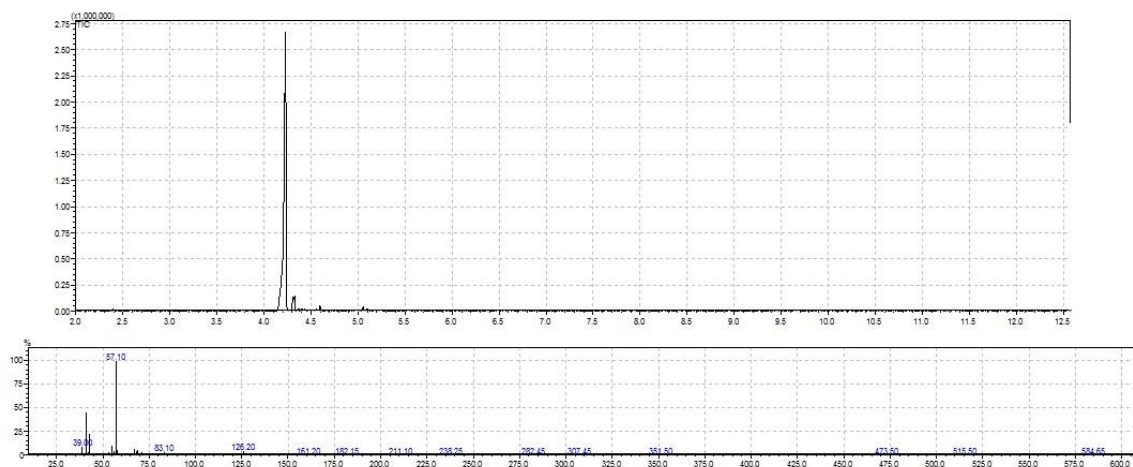
(8k):
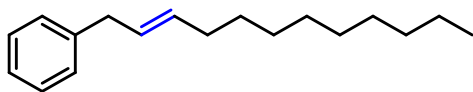
Exact Mass: 244.22
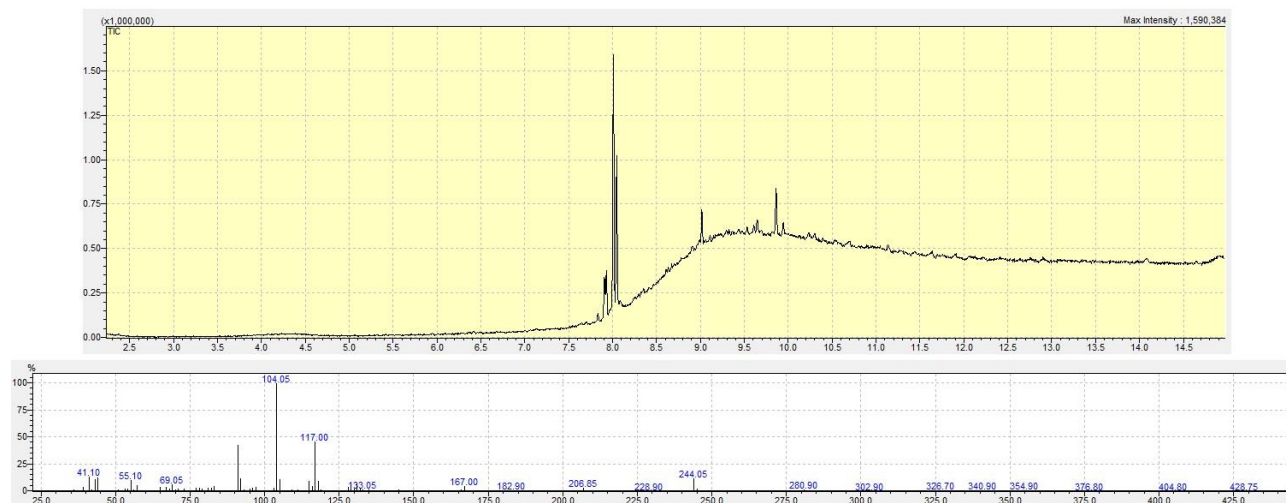
(8l):
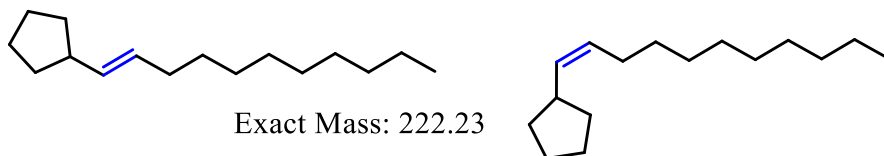
Exact Mass: 222.23
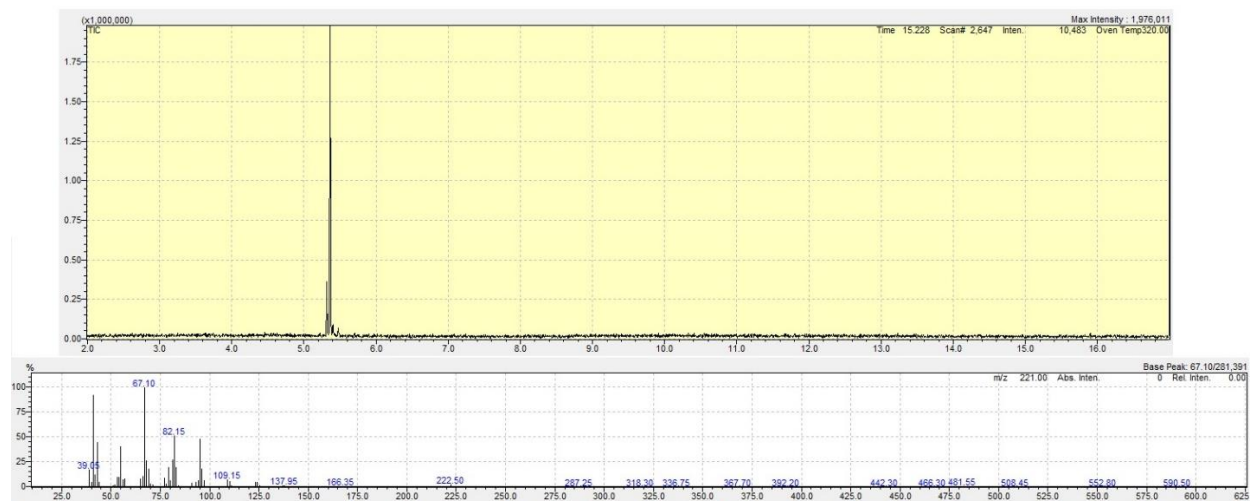
(8m):
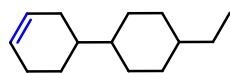
Exact Mass: 192.19
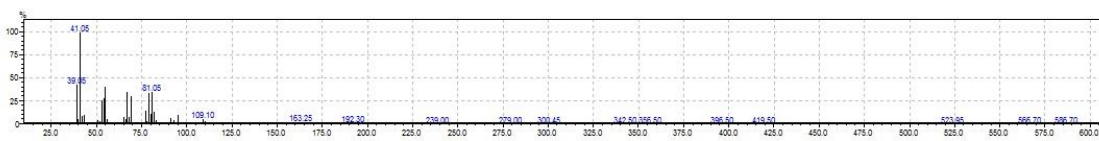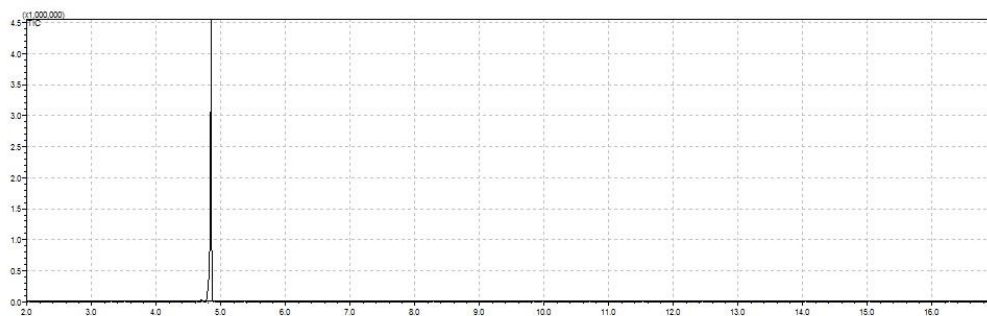
A9. COSY NMR Data for Alkene Products (8h-8l)

(8h) 65:35 regioisomer raito
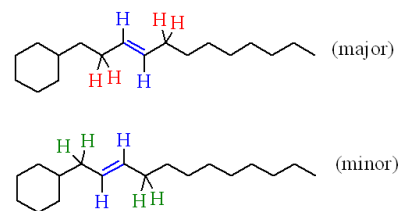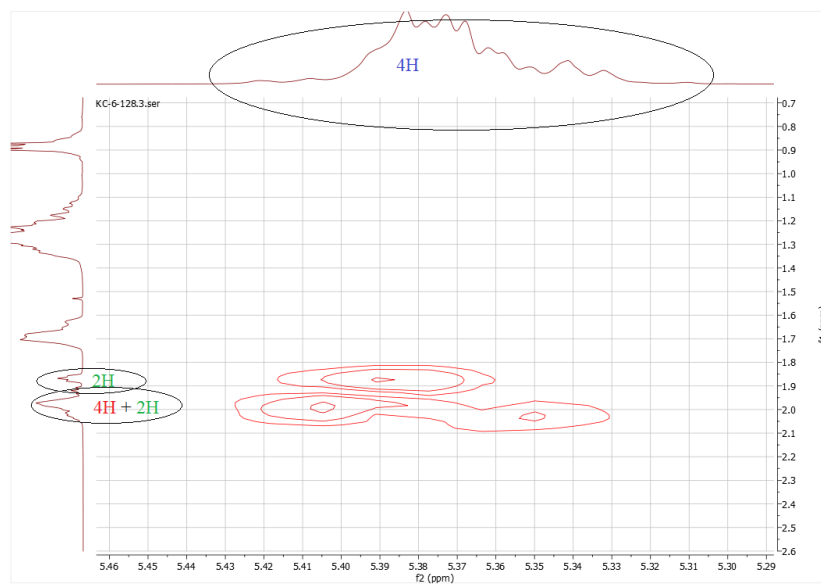
(8i) 89:11 regioisomer ratio
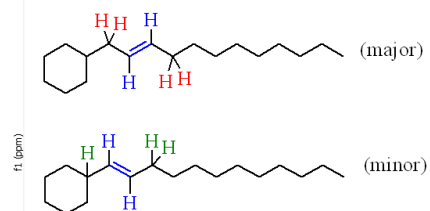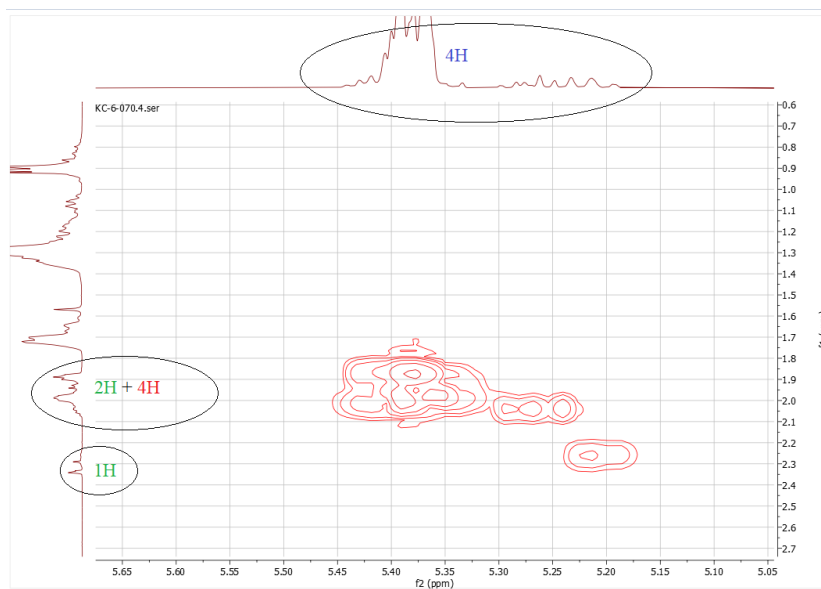
(8j) >90:10 regioisomer ratio; *E/Z* mix
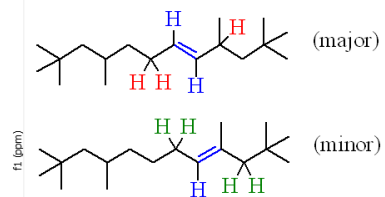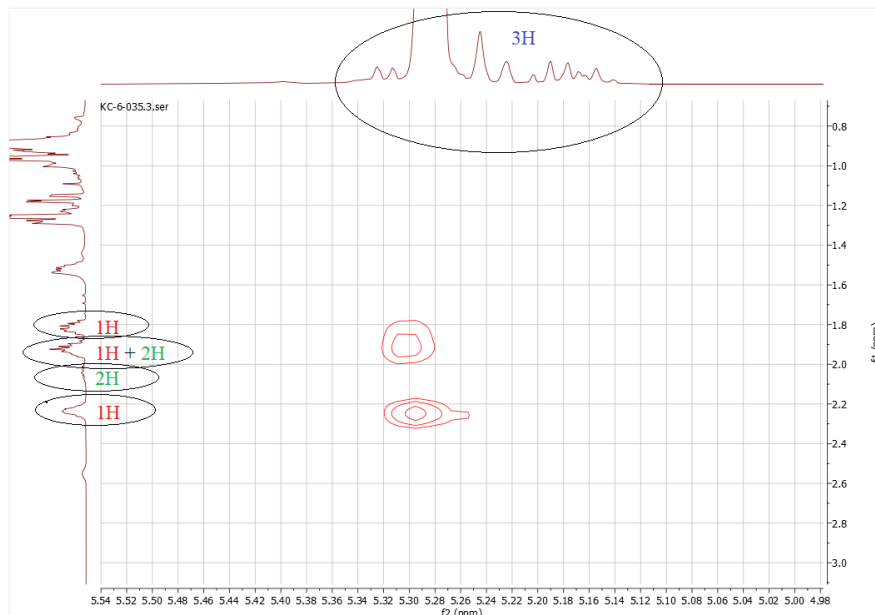
(8k) Single regioisomer; 71:29 *E/Z*
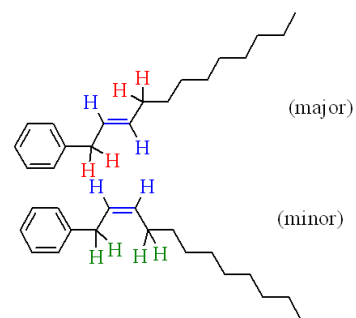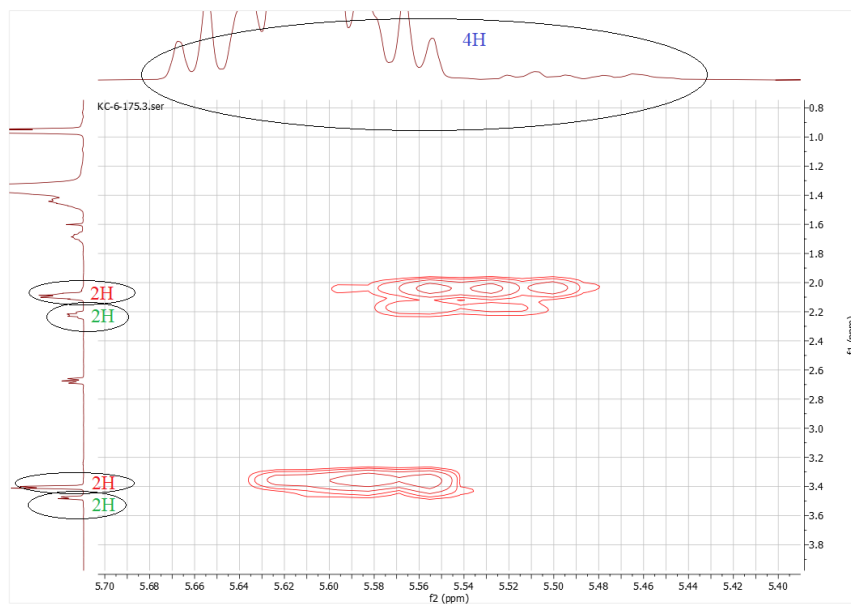
(8l) Single regioisomer; 80:20 *E/Z*.
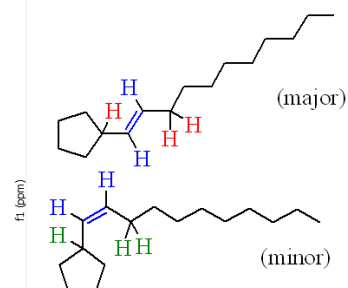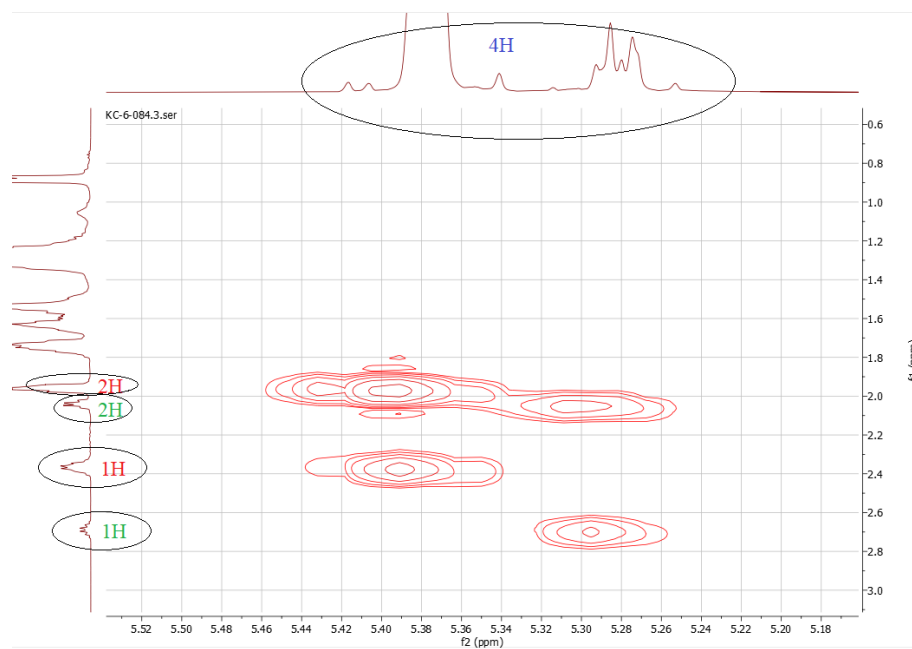
References

Chapter 1:

1. Select early examples of photoredox catalysis in organic synthesis: a) Hedstrand, D. M.; Kruizinga, W. M.; Kellogg, R. M. Light Induced and Dye Accelerated Reductions of Phenacyl onium Salts by 1,4-dihydropyridines. *Tetrahedron Lett*. **1978**, *19*, 1255−1258. b) Van Bergen, T. J.; Hedstrand, D. M.; Kruizinga, W. H.; Kellogg, R. M. Chemistry of Dihydropyridines. 9. Hydride Transfer from 1,4-dihydropyridines to sp^3-Hybridized Carbon in Sulfonium Salts and Activated Halides. Studies with NAD(P)H Models. *J. Org. Chem.* **1979**, *44*, 4953−4962. c) Hironaka, K.; Fukuzumi, S.; Tanaka, T. J. Tris(bipyridyl)ruthenium(II)-Photosensitized Reaction of 1-benzyl-1,4-dihydronicotinamide with Benzyl Bromide. *Chem. Soc., Perkin Trans. 2* **1984**, 1705−1709. d) Fukuzumi, S.; Koumitsu, S.; Hironaka, K.; Tanaka, T. Energetic Comparison between Photoinduced Electron-Transfer Reactions from NADH Model Compounds to Organic and Inorganic Oxidants and Hydride-Transfer Reactions from NADH Model Compounds to *p*-Benzoquinone Derivatives. *J. Am. Chem. Soc.* **1987**, *109*, 305−316. e) Fukuzumi, S.; Mochizuki, S.; Tanaka, T. Photocatalytic Reduction of Phenacyl Halides by 9,10-dihydro-10-methylacridine: Control Between the Reductive and Oxidative Quenching Pathways of tris(bipyridine)ruthenium Complex Utilizing an Acid Catalysis. *J. Phys. Chem.* **1990**, *94*, 722−726. f) Pac, C.; Ihama, M.; Yasuda, M.; Miyauchi, Y.; Sakurai, H. Tris(2,2'-bipyridine)ruthenium(2$^+$)-Mediated Photoreduction of Olefins with 1-benzyl-1,4-dihydronicotinamide: A Mechanistic Probe for Electron-Transfer Reactions of NAD(P)H-Model Compounds. *J. Am. Chem. Soc.* **1981**, *103*, 6495−6497. g) Pac, C.; Miyauchi, Y.; Ishitani, O.; Ihama, M.; Yasuda, M.; Sakurai, H. Redox-Photosensitized Reactions. 11. Ru(bpy)$_3$$^{2+}$-Photosensitized Reactions of 1-benzyl-1,4-dihydronicotinamide with Aryl-Substituted Enones, Derivatives of Methyl Cinnamate, and Substituted Cinnamonitriles: Electron-Transfer Mechanism and Structure-Reactivity Relationships. *J. Org. Chem.* **1984**, *49*, 26−34. h) Ishitani, O.; Ihama, M.; Miyauchi, Y.; Pac, C. Redox-Photosensitised Reactions. Part 12. Effects of Magnesium(II) Ion on the [Ru(bpy)$_3$]$^{2+}$-Photomediated Reduction of Olefins by 1-benzyl-1,4-dihydronicotinamide: Metal-Ion Catalysis of Electron Transfer Processes Involving an NADH Model. *J. Chem. Soc., Perkin Trans. 1* **1985**, 1527−1531. i) Ishitani, O.; Pac, C.; Sakurai, H. Redox-Photosensitized Reactions. 10. Formation of a Novel Type of Adduct between an NADH Model and Carbonyl Compounds by Photosensitization using Ru(bpy)$_3$$^{2+}$. *J. Org. Chem.* **1983**, *48*, 2941−2942. j) Ishitani, O.; Yanagida, S.; Takamuku, S.; Pac, C. Redox-Photosensitized Reactions. 13. Ru(bpy)$_3$$^{2+}$-Photosensitized Reactions of an NADH Model, 1-benzyl-1,4-dihydronicotinamide, with Aromatic Carbonyl Compounds and Comparison with Thermal Reactions. *J. Org. Chem.* **1987**, *52*, 2790−2796. k) Cano-Yelo, H.; Deronzier, A. *Tetrahedron Lett*. **1984**, *25*, 5517−5520. l) Cano-Yelo, H.; Deronzier, A. Photo-oxidation of some Carbinols by the Ru(II) Polypyridyl Complex-Aryl Diazonium Salt System. *J. Chem. Soc., Perkin Trans. 2* **1984**, 1093−1098. m) Cano-Yelo, H.; Deronzier, A. A. Photocatalysis of the Pschorr Reaction by Ru(bpy)$_3$$^{2+}$ *J. Photochem.* **1987**, *37*, 315−321.

2. Reviews on modern photoredox catalysis: a) Melchiorre, P.; Crisenza, G. E. M. Chemistry Glows Green with Photoredox Catalysis. *Nat. Commun.* **2020**, *803*, 1–4. b) McAtee, R. C.;

McClain, E. J.; Stephenson, C. R. J. Illuminating Photoredox Catalysis, *Trends in Chemistry*, **2019**, 111−126. c) Bogdos, M. K.; Pinard, E.; Murphy, J. A. Applications of Organocatalyzed Visible-light Photoredox Reactions for Medicinal Chemistry. *Beilstein J. Org. Chem.* **2018**, *14*, 2035–2064. d) Shaw, M. H.; Twilton, J.; MacMillan, D. W. C. Photoredox Catalysis in Organic Chemistry. *J. Org. Chem.* **2016**, *81*, 6898−6926. e) Romero, N. A.; Nicewicz, D. A. Organic Photoredox Catalysis. *Chem. Rev.* **2016**, *116*, 10075−10166. f) Schultz, D. M.; Yoon, T. P. Solar Synthesis: Prospects in Visible Light Photocatalysis. *Science* **2014**, *343*, 985–995. g) Koike, T.; Akita, M. Visible-Light Radical Reaction Designed by Ru- and Ir-based Photoredox Catalysis. *Inorg. Chem. Front.* **2014**, *1*, 562–576. h) Nicewicz, D. A.; Nguyen, T. M. Recent Applications of Organic Dyes as Photoredox Catalysts in Organic Synthesis. *ACS Catal.* **2014**, *4*, 355–360. i) Yoon, T. P. Visible Light Photocatalysis: The Development of Photocatalytic Radical Ion Cycloadditions. *ACS Catal*. **2013**, 3, 895–902. j) Prier, C. K.; Rankic, D. A.; MacMillan, D. W. C. Visible Light Photoredox Catalysis with Transition Metal Complexes: Applications in Organic Synthesis. *Chem. Rev.* **2013**, 113, 5322−5363. k) Xi, Y.; Yi, H.; Lei, A. Synthetic Applications of Photoredox Catalysis with Visible Light. *Org. Biomol. Chem.* **2013**, *11*, 2387–2403. l) Xuan, J.; Xiao, W.-J. Visible-Light Photoredox Catalysis. *Angew. Chem., Int. Ed*. **2012**, *51*, 6828–6838. m) Narayanam, J. M. R.; Stephenson, C. R. J. Visible Light Photoredox Catalysis: Applications in Organic Synthesis. *Chem. Soc. Rev*. **2011**, *40*, 102–113. n) Fagnoni, M.; Dondi, D.; Ravelli, D.; Albini, A. Photocatalysis for the Formation of the C−C Bond. *Chem. Rev*., **2007**, 107, 2725−2756.

3. Verschueren, R. H.; De Borggraeve, W. M. Electrochemistry and Photoredox Catalysis: A Comparative Evaluation in Organic Synthesis. *Molecules* **2019**, *24*, 2122–2411.

4. Skubi, K. L.; Blum, T. R.; Yoon, T. P. Dual Catalysis Strategies in Photochemical Synthesis *Chem. Rev.* **2016**, *116*, 17, 10035–10074.

5. Cambié, D.; Bottecchia, C.; Straathof, N. J. W.; Hessel, V.; Noël, T. Applications of Continuous-Flow Photochemistry in Organic Synthesis, Material Science, and Water Treatment. *Chem. Rev*. **2016**, *116*, 10276–1034.

6. a) Liu, W., Li, J., Querard, P., Li, C. -J. Transition-Metal-Free, C-C, C-O, and C-N Cross-Couplings Enabled by Light. *J. Am. Chem. Soc.* **2019**, *141*, 6755–6764. b) Srivastava, V.; Singh, P. P. Eosin Y Catalyzed Photoredox Synthesis: A Review. *RSC Adv.* **2017**, *7*, 31377-31392. c) Joshi-Pangu, A.; Lévesque, F.; Roth, H. G.; Oliver, S. F.; Campeau, L. C.; Nicewicz, D.; DiRocco, D. A. Acridinium-Based Photocatalysts: A Sustainable Option in Photoredox Catalysis. *J. Org. Chem.* **2016**, *81*, 7244–7249.

7. a) Miyaura, N.; Suzuki, A. Palladium-Catalyzed Cross-Coupling Reactions of Organoboron Compounds. *Chem. Rev.***1995**, 95, 2457–2483. b) Cahiez, G.; Moyeux, A. Cobalt-Catalyzed Cross-Coupling Reactions. *Chem. Rev.* **2010**, *110*, 1435–1462. c) Hartwig, J. F. Organo-transition Metal Chemistry: from Bonding to Catalysis, University Science Books, Sausalito, **2010**. d) Jana, R.; Pathak, T. P.; Sigman, M. S. Advances in Transition Metal (Pd, Ni, Fe)-Catalyzed Cross-Coupling Reactions Using Alkyl-organometallics as Reaction Partners. *Chem. Rev.* **2011**, *111*, 1417–1492. e) Rosen, B. M.; Quasdorf, K. W.; Wilson, D. A.; Zhang, N.;

Resmerita, A.-M.; Garg, N. K.; Percec, V. Nickel-Catalyzed Cross-Couplings Involving Carbon–Oxygen Bonds. *Chem. Rev.* **2011**, *111*, 1346–1416.

8. a) Patraand, T.; Maiti, D. Decarboxylation as the Key Step in C–C Bond-Forming Reactions. *Chem. Eur. J.* **2017**, *23*, 7382–7401. b) Dzik, W. I.; Lange, P. P.; Goossen, L. J. Carboxylates as Sources of Carbon Nucleophiles and Electrophiles: Comparison of Decarboxylative and Decarbonylative Pathways. *Chem. Sci.* **2012**, *3*, 2671–2678.

9. Select examples of carboxylic acids as carbon nucleophilic equivalents in catalysis: a) Gooßen, L. J.; Deng, G.; Levy, L. M. Synthesis of Biaryls via Catalytic Decarboxylative Coupling. *Science*, **2006**, *313*, 662–664. b) Shang, R.; Xu, Q.; Jiang, Y.-Y.; Wang, Y.; Liu, L. Pd-Catalyzed Decarboxylative Cross Coupling of Potassium Polyfluorobenzoates with Aryl Bromides, Chlorides, and Triflates. *Org. Lett*., **2010**, *12*, 1000–1003. c) Shang, R.; Fu, Y.; Wang, Y.; Xu, Q.; Yu, H.-Z.; Liu, L. Copper-Catalyzed Decarboxylative Cross-Coupling of Potassium Polyfluorobenzoates with Aryl Iodides and Bromides. *Angew. Chem., Int. Ed*., **2009**, *48*, 9350–9354. d) Gooßen, L. J.; Rudolphi, F.; Oppel, C.; Rodrıguez, N. Synthesis of Ketones from α-Oxocarboxylates and Aryl Bromides by Cu/Pd-Catalyzed Decarboxylative Cross-Coupling. *Angew. Chem., Int. Ed*., **2008**, *47*, 3043–3045. e) Collet, F.; Song, B.; Rudolphi, F.; Gooßen, L. J. Development of Decarboxylative Coupling Processes for the Synthesis of Azomethines and Ketones. *Eur. J. Org. Chem.,* **2011**, 6486–6501. f) Shang, R.; Fu, Y.; Li, J.-B.; Zhang, S.-L.; Guo, Q.-X.l Liu, L. Synthesis of Aromatic Esters via Pd-Catalyzed Decarboxylative Coupling of Potassium Oxalate Monoesters with Aryl Bromides and Chlorides. *J. Am. Chem. Soc*., **2009**, *131*, 5738–5739. g) Select examples of carboxylic acids as carbon electrophilic equivalents in catalysis: h) Dai, J.-J.; Liu, J.-H.; Luo, D.-F.; Liu, L. Pd-Catalyzed Decarboxylative Suzuki Reactions and Orthogonal Cu-based O-arylation of Aromatic Carboxylic Acids. *Chem. Commun.*, **2011**, *47*, 677–679. i) Cornella, J.; Lahlai, H.; Larrosa, I. Decarboxylative Homocoupling of (Hetero)aromatic Carboxylic Acids. *Chem. Commun*., **2010**, *46*, 8276–8278. j) Xie, K.; Wang, S.; Yang, Z.; Liu, J.; Wang, A.; Li, X.; Tan, Z.; Guo, C.-C.; Dong, W. Synthesis of Biaryls by Pd-Catalyzed Decarboxylative Homo- and Heterocoupling of Substituted Benzoic Acids. *Eur. J. Org. Chem.*, **2011**, 5787–5790. k) Voutchkova, A.; Coplin, A.; Leadbeater, N.; Crabtree, R. H. Palladium-Catalyzed Decarboxylative Coupling of Aromatic Acids with Aryl Halides or Unactivated Arenes using Microwave Heating. *Chem. Commun.*, **2008**, 6312–6314. l) Wang, C.; Piel, I.; Glorius, F. Palladium-Catalyzed Intramolecular Direct Arylation of Benzoic Acids by Tandem Decarboxylation/C–H Activation. *J. Am. Chem. Soc*., **2009**, *131*, 4194–4195.

10. Select recent examples of decarboxylation in radical-polar cross-over to a carbanion: a) Donabauer, K.; Maity, M.; Berger, A. L.; Huff, G. S.; Crespi, S.; König, B. Photocatalytic Carbanion Generation – Benzylation of Aliphatic Aldehydes to Secondary Alcohols. *Chem. Sci*., **2019**, *10*, 5162–5166. b) Ni, S.; Padial, N. M.; Kingston, C.; Vantourout, J. C.; Schmitt, D. C.; Edwards, J. T.; Kruszyk, M. M.; Merchant, R. R.; Mykhailiuk, P. K.; Sanchez, B. B.; Yang, S.; Perry, M. A.; Gallego, G. M.; Mousseau, J. J.; Collins, M. R.; Cherney, R. J.; Lebed, P. S.; Chen, J. S.; Qin, T.; Baran, P. S. A Radical Approach to Anionic Chemistry: Synthesis of Ketones, Alcohols, and Amines, *J. Am. Chem. Soc.* **2019**, *141*, 6726–6739. c) Shu, C.; Mega, R. S.; Andreassen, B. J.; Noble, A.; Aggarwal, V. K. Synthesis of Functionalized Cyclopropanes from

Carboxylic Acids by a Radical Addition–Polar Cyclization Cascade. *Angew. Chem. Int. Ed.* **2018**, *57*, 15430–15434. Select recent examples of decarboxylation in radical-polar cross over to a carbocation: d) Yasu, Y.; Koike, T.; Akita, M. Three-component Oxytrifluoromethylation of Alkenes: Highly Efficient and Regioselective Difunctionalization of C=C Bonds Mediated by Photoredox Catalysts. *Angew. Chem. Int. Ed*. **2012**, *51*, 9567–9571. e) Yao, C.-J.; Sun, Q.; Rastogi, N.; Kçnig, B. Intermolecular Formyloxyarylation of Alkenes by Photoredox Meerwein Reaction. *ACS Catal*. **2015**, *5*, 2935–2938. f) Dagousset, G.; Carboni, A.; Magnier, E.; Masson, G. Photoredox-Induced Three-Component Azido- and Aminotrifluoromethylation of Alkenes. *Org. Lett.* **2014**, *16*, 4340–4343. g) Carboni, A.; Dagousset, G.; Magnier, E.; Masson, G. Three-Component Photoredox-Mediated Chloro-, Bromo-, or Iodotrifluoromethylation of Alkenes. *Synthesis* **2015**, *47*, 2439–2445. h) Carboni, A.; Dagousset, G.; Magnier, E.; Masson, G. One Pot and Selective Intermolecular Aryl- and Heteroaryl-Trifluoromethylation of Alkenes by Photoredox Catalysis. *Chem. Commun*. **2014**, *50*, 14197–14200. i) Silvi, M.; Sandford, C.; Aggarwal, V. K. Merging Photoredox with 1,2-Metallate Rearrangements: The Photochemical Alkylation of Vinyl Boronate Complexes. *J. Am. Chem. Soc.* **2017**, *139*, 5736–5739. j) Xiao, T.; Li, L.; Zhou, L. Synthesis of Functionalized gem-Difluoroalkenes via a Photocatalytic Decarboxylative/Defluorinative Reaction, *J. Org. Chem*. **2016**, *81*, 7908−7916. k) Phelan, J. P.; Lang, S. B.; Compton, J. S.; Kelly, C. B.; Dykstra, R.; Gutierrez, O.; Molander, G. A. Redox-Neutral Photocatalytic Cyclopropanation via Radical/Polar Crossover. *J. Am. Chem. Soc*. **2018**, *140*, 25, 8037–8047. Select radical-polar crossover reviews: l) Pitzer, L.; Schwarz, J. L.; Glorius, F. Reductive Radical-Polar Crossover: Traditional Electrophiles in Modern Radical Reactions. *Chem. Sci.*, **2019**, *10*, 8285–8291. m) Murphy, J. A. The Radical-Polar Crossover Reaction. In Radicals in Organic Synthesis; Renaud, P., Sibi, M. P., Eds.; Wiley-VCH: Weinheim, **2001**; Vol. 1, pp 298−315.

11. a) Sheldon, R. A.; Kochi, J. K. Oxidative Decarboxylation of Acids by Lead Tetraacetate, *Org. React.* **2011**, *19*, 279– 421. b) Brown, B. R.; Phil, M. A. D. L. The Mechanism of Thermal Decarboxylation, *Q. Rev. Chem. Soc*. **1951**, *5*, 131–146. c) O'Leary, M. H. Transition-State Structures in Enzyme-Catalyzed Decarboxylations, *Acc. Chem. Res*. **1988**, *21*, 450–455. d) Kluger, R.; Mundle, S. O. C. The Role of Pre-Association in Brønsted Acid-Catalyzed Decarboxylation and Related Processes, *Adv. Phys. Org. Chem*. **2010**, *44*, 357–375. e) Kluger, R.; Howe, W.; Mundle, S. O. C. Avoiding CO_2 in Catalysis of Decarboxylation; Advances in Physical Organic Chemistry Chapters 1 & 2, **2013**; Vol. 47, pp. 85–128.

12. a) Huang, H.; Jia, K.; Chen, Y. Radical Decarboxylative Functionalizations Enabled by Dual Photoredox Catalysis, *ACS Catal*. **2016**, *6*, 4983-4988. b) Li, Y.; Ge, L.; Muhammad, M. T.; Bao, H. Recent Progress on Radical Decarboxylative Alkylation for C(sp^3)–C Bond Formation. *Synthesis* **2017**, *49*, 5263–5284.

13. a) Barton, D. H. R.; Serebryakov, E. P.; A Convenient Procedure for the Decarboxylation of Acids. *Proc. Chem. Soc.* **1962**, 309. b) Barton, D. H. R.; Dowlatshahi, H. A.; Motherwell, W. B.; Villemin, D. A. A New Radical Decarboxylation Reaction for the Conversion of Carboxylic Acids into Hydrocarbons. *J. Chem. Soc., Chem. Commun.* **1980**, 732–733. c) Barton, D. H. R.; Crich, D.; Motherwell, W. B. A Practical Alternative to the Hunsdiecker Reaction. *Tetrahedron*

Lett. **1983**, *24*, 4979–4982. d) Barton, D. H. R.; Zard, S. Z. A Novel Radical Decarboxylation Reaction. *Janssen Chim. Acta* **1986**, *4*, 3–9.

14. a) Barton, D. H. R.; Ramesh, M. Generation and Fate of Nondecarboxylating Acyloxy Radicals Derived from the Photolysis of Acyl Derivatives of *N*-hydroxy-2-thiopyridone. *Tetrahedron Lett*. **1990**, *31*, 949–952. b) Barton, D. H. R.; Lacher, B. B.; Zard, S. Z. The Invention of Radical Reactions : Part XVI. Radical Decarboxylative Bromination and Iodination of Aromatic Acids. *Tetrahedron* **1987**, *43*, 4321–4328. c) Saraiva, M. F.; Couri, M. R. C.; Le Hyaric, M.; de Almeida, M. V. The Barton Ester Free-Radical Reaction: A Brief Review of Applications. *Tetrahedron* **2009**, *65*, 3563–3572.

15. a) Okada, K.; Okamoto, K.; Oda, M. A New and Practical Method of Decarboxylation: Photosensitized Decarboxylation of N-acyloxyphthalimides via Electron-Transfer Mechanism. *J. Am. Chem. Soc.* **1988**, *110*, 8736–8738. b) Okada, K.; Okamoto, K.; Morita, N.; Okubo, K.; Oda, M. Photosensitized Decarboxylative Michael Addition Through N-(acyloxy)phthalimides via an Electron-Transfer Mechanism. *J. Am. Chem. Soc*. **1991**, *113*, 9401–9402. c) Okada, K.; Okubo, K.; Morita, N.; Oda, M. Reductive Decarboxylation of N-(acyloxy)phthalimides via Redox-Initiated Radical Chain Mechanism. *Tetrahedron Lett*. **1992**, *33*, 7377−7380. d) Okada, K.; Okubo, K.; Morita, N.; Oda, M. Redox-Mediated Decarboxylative Photo-Phenylselenenylation of N-Acyloxyphthalimides. *Chem. Lett.* **1993**, 22, 2021−2024.

16. Murarka, S. N-(Acyloxy)phthalimides as Redox-Active Esters in Cross-Coupling Reactions. *Adv. Synth. Catal*. **2018**, *360*, 1735–1753.

17. Select examples of stoichiometric amine electron donors: a) Schnermann, M. J.; Overman, L. E. A Concise Synthesis of (−)-Aplyviolene Facilitated by a Strategic Tertiary Radical Conjugate Addition. *Angew. Chem. Int. Ed*. **2012**, *51*, 9576–9580. b) Pratsch, G.; Lackner, G. L.; Overman, L. E. Constructing Quaternary Carbons from N-(Acyloxy)phthalimide Precursors of Tertiary Radicals Using Visible-Light Photocatalysis. *J. Org. Chem.* **2015**, *80*, 6025–6036. c) Hu, C.; Chen, Y. Chemoselective and Fast Decarboxylative Allylation by Photoredox Catalysis Under Mild Conditions. *Org. Chem. Front*. **2015**, *2*, 1352–1355. d) Lackner, G. L.; Quasdorf, K. W.; Overman, L. E. Direct Construction of Quaternary Carbons from Tertiary Alcohols via Photoredox-Catalyzed Fragmentation of *tert*-Alkyl *N*-Phthalimidoyl Oxalates. *J. Am. Chem. Soc*. **2013**, *135*, 15342–15345. e) Lackner, G. L.; Quasdorf, K. W.; Pratsch, G.; Overman, L. E. Fragment Coupling and the Construction of Quaternary Carbons Using Tertiary Radicals Generated from *tert*-Alkyl *N*-Phthalimidoyl Oxalates by Visible-Light Photocatalysis. *J. Org. Chem*. **2015**, *80*, 6012–6024. Select examples of catalytic amine electron donors: f) Jin, Y.; Jiang, M.; Wang, H.; Fu, H. Installing Amino Acids and Peptides on *N*-heterocycles Under Visible-Light Assistance. *Sci. Rep.* **2016**, *6*, 20068(1-7). g) Wang, J.; Qin, T.; Chen, T.-G.; Wimmer, L.; Edwards, J. T.; Cornella, J.; Vokits, B.; Shaw, S. A.; Baron, P. S. Nickel-Catalyzed Cross-Coupling of Redox-Active Esters with Boronic Acids. *Angew. Chem. Int. Ed*. **2016**, *55*, 9676–9679.

18. Ideal synthesis reviews: a) Newhouse, T.; Baran, P. S. Hoffmann, R. W. The Economics of Synthesis. *Chem. Soc. Rev.* **2009**, *38*, 3010–3021. b) Gaich, T; Baran, P. S. Aiming for Ideal Synthesis. *J. Org. Chem.* **2010**, *75*, 4657–4673.

19. Carboxylate oxidation potentials: a) Griffin, J. D.; Zeller, M. A.; Nicewicz, D. A. Hydrodecarboxylation of Carboxylic and Malonic Acid Derivatives via Organic Photoredox Catalysis: Substrate Scope and Mechanistic Insight. *J. Am. Chem. Soc.* **2015**, *137*, 11340−11348. b) Capaldo, L.; Buzzetti, L.; Merli, D.; Fagnoni, M.; Ravelli, D. Smooth Photocatalyzed Benzylation of Electrophilic Olefins via Decarboxylation of Arylacetic Acids. *J. Org. Chem.* **2016**, *81*, 7102–7109. c) Galicia, M.; Gonzalez, F. J. Electrochemical Oxidation of Tetrabutylammonium Salts of Aliphatic Carboxylic Acids in Acetonitrile. *J. Electrochem. Soc.* **2002**, *149*, D46–D50.

20. a) Li, T.; Huo, L.; Pulley C.; Liu, A. Decarboxylation Mechanisms in Biological Systems. *Bioorg. Chem.*, **2012**, *43*, 2–14. b) Chang, G.-G.; Tong, L. Structure and Function of Malic Enzymes, A New Class of Oxidative Decarboxylases. *Biochemistry*, **2003**, *42*, 12721–12733. c) Cleland, W. W. Mechanisms of Enzymatic Oxidative Decarboxylation. *Acc. Chem. Res.*, **1999**, *32*, 862–868.

21. a) Hunsdiecker, H.; Hunsdiecker, C. Über den Abbau der Salze aliphatischer Säuren durch Brom [About the Degradation of Salts of Aliphatic Acids by Bromine]. *Chem. Ber.* **1942**, *75B*, 291-297. b) Johnson, R. G.; Ingham, R. K. The Degradation of Carboxylic Acid Salts by Means of Halogenation. The Hunsdiecker Reaction. *Chem. Rev.* **1956**, *56*, 219–269. c) Wilson, C. V. The Reaction of Halogens with Silver Salts of Carboxylic Acids. *Org. React.* **1957**, 332–387. d) Crich, D. The Hunsdiecker and Related Reactions. *Comp. Org. Synth.* (Eds. Trost, B. M. Fleming, I.), *7*, 717–734. (Pergamon Press, Oxford, **1991**). e) Minisci, F.; Galli, R.; Cecere, M.; Malatesta, V.; Caronna, T. Nucleophilic Character of Alkyl Radicals: New Syntheses by Alkyl Radicals Generated in Redox Processes. *Tetrahedron Lett.* **1968**, 5609-5612. f) Glasstone, S. "Introduction to Electrochemistry," D. Van Nostrand Co., Inc., New York, N. Y. **1942**, pp. 516–519. g) Weedon, B. C. L. Anodic Synthesis with Carboxylic Acids. *Q. Rev. Chem. Soc.* **1952**, *6*, 380–398. h) Kolbe, H. Untersuchungen über die Elektrolyse organischer Verbindungen. *Liebigs Ann. Chem.* **1849**, *69*, 257–294. i) Smith, W. B.; Glide, H. G. The Kolbe Electrolysis as a Source of Free Radicals in Solution. *J. Am. Chem. Soc.* **1959**, 5325–5329.

22. Serguchev, Y. A.; Beletskaya, I. P. Oxidative Decarboxylation of Carboxylic Acids. *Russ. Chem. Rev.* **1980**, *49*, 2257–2285.

23. Miyake, Y.; Nakajima, K.; Nishibayashi, Y. Visible Light-Mediated Oxidative Decarboxylation of Arylacetic Acids into Benzyl Radicals: Addition to Electron-Deficient Alkenes by Using Photoredox Catalysts. *Chem. Commun.*, **2013**, *49*, 7854–7856.

24. Amine oxidation: a) Espelt, L. R.; Wiensch, E. M.; Yoon, T. P. Brønsted Acid Cocatalysts in Photocatalytic Radical Addition of α-Amino C–H Bonds across Michael Acceptors. *J. Org. Chem.*, **2013**, *78*, 4107–4114. b) Zhu, S.; Das, A.; Bui, L.; H.; Zhou, H.; Curran, D. P.; Rueping, M. Oxygen Switch in Visible-Light Photoredox Catalysis: Radical Additions and Cyclizations and Unexpected C–C-Bond Cleavage Reactions. *J. Am. Chem. Soc.*, **2013**, *135*, 1823–1829. c)

Kohls, P.; Jadhav, D.; Pandey, G.; Reiser, O. Visible Light Photoredox Catalysis: Generation and Addition of N-Aryltetrahydroisoquinoline-Derived α-Amino Radicals to Michael Acceptors. *Org. Lett.*, **2012**, *14*, 672-675. d) McNally, A.; Prier. C. K.; MacMillan, D. W. C. Discovery of an α-Amino C–H Arylation Reaction Using the Strategy of Accelerated Serendipity. *Science*, **2011**, *334*, 1114–1117. Ir redox potentials: e) Flamigni, L.; Barbieri, A.; Sabatini, C.; Ventura, B.; Barigelletti, F. Photochemistry and Photophysics of Coordination Compounds: Iridium. *Top. Curr. Chem.* **2007**, *281*, 143–203. f) Dixon, I. M.; Collin, J.; Sauvage, J.; Flamigni, L.; Encinas, S.; Barigelletti, F. A Family of Luminescent Coordination Compounds: Iridium(III) Polyimine Complexes. *Chem. Soc. Rev.* **2000**, *29*, 385–391.

25. Zuo, Z.; MacMillan, D. W. C. Decarboxylative Arylation of α-Amino Acids via Photoredox Catalysis: A One-Step Conversion of Biomass to Drug Pharmacophore. *J. Am. Chem. Soc.* **2014**, *136*, 5257−5260.

26. a) Studer, A. The Persistent Radical Effect in Organic Synthesis. *Chem. Eur. J.* **2001**, *7*, 1159–1164. b) Mori, Y.; Sakaguchi, W.; Hayashi, H. Magnetic Field Effects on Chemical Reactions of Biradical Radical Ion Pairs in Homogeneous Fluid Solvents. *J. Phys. Chem. A.* **2000**, *104*, 4896–4905.

27. a) Dedeian, K.; Djurovich, P. I.; Garces, F. O.; Carlson, G.; Watts, R. J. A New Synthetic Route to the Preparation of a Series of Strong Photoreducing Agents: Fac-Tris-Ortho-Metalated Complexes of Iridium(III) with Substituted 2-Phenylpyridines. *Inorg. Chem.* **1991**, *30*, 1685–1697. b) Tian, N.; Lenkeit, D.; Pelz, S.; Fischer, L. H.; Escudero, D.; Schiewek, R.; Klink, D.; Schmitz, O. J.; Gonzalez, L.; Schaferling, M.; Holder, E. Structure–Property Relationship of Red- and Green-Emitting Iridium(III) Complexes with Respect to Their Temperature and Oxygen Sensitivity. *Eur. J. Inorg. Chem.* **2010**, *30*, 4875–4885.

Chapter 2:

28. Lang, S. B.; O'Nele, K. M.; Tunge, J. A. Decarboxylative Allylation of Amino Alkanoic Acids and Esters via Dual Catalysis. *J. Am. Chem. Soc.* **2014**, *136*, 13606−13609.

29. a) Weaver, J. D.; Recio, A.; Grenning, A. J.; Tunge, J. A. Transition Metal-Catalyzed Decarboxylative Allylation and Benzylation Reactions. *Chem. Rev.* **2011**, *111*, 1846–1913. b) Austeri, M.; Buron, F.; Constant, S.; Lacour, J.; Linder, D.; Muller, J.; Tortoioli, S. Enantio- and Regioselective CpRu-Catalyzed Carroll Rearrangement. *Pure Appl. Chem.* **2008**, *80*, 967–977. c) Mohr, J. T.; Stoltz, B. M. Enantioselective Tsuji Allylations. *Chem. Asian. J.* **2007**, 2, 1476–1491. d) Mohr, J. T.; Ebner, D. C.; Stoltz, B. M. Catalytic Enantioselective Stereoablative Reactions: An Unexploited Approach to Enantioselective Catalysis. *Org. Biomol. Chem.* **2007**, *5*, 3571–3576. e) You, S.-L.; Dai, L.-X. Enantioselective Palladium-Catalyzed Decarboxylative Allylic Alkylations. *Angew. Chem., Int. Ed.* **2006**, *45*, 5246–5248. f) Tunge, J. A.; Burger, E. C. Transition Metal Catalyzed Decarboxylative Additions of Enolates. *Eur. J. Org. Chem.* **2005**, 1715–1726. g) Tsuji, J. Development of β-Keto Ester and Malonate Chemistry. *Proc. Jpn. Acad., B* **2004**, *80*, 349–358.

30. a) Tsuji, J.; Takahashi, H.; Morikawa, M. Organic Syntheses by Means of Noble Metal Compounds XVII. Reaction of π-Allylpalladium Chloride with Nucleophiles *Tetrahedron Lett*. **1965**, 6, 4387–4388. b) Tsuji, J. Carbon-Carbon Bond Formation via Palladium Complexes. *Acc. Chem. Res*. **1969**, *2*, 144–152. c) Tsuji, J. In Handbook of Organopalladium Chemistry in Organic Synthesis; Negishi, E.-I.; Meijere, A.; Eds.; Wiley: New York, **2002**; Vol. 2, pp. 1669.

31. Select examples: a) Trost, B. M.; Self, C. R. On the Palladium-Catalyzed Alkylation of Silyl-Substituted Allyl Acetates with Enolates. *J. Org. Chem*. **1984**, *49*, 468–473. b) Negishi, E.; Matsushita, H.; Chatterjee, S.; John, R. A. Selective carbon-carbon bond formation via transition metal catalysis. 29. A Highly Regio- and Stereospecific Palladium-Catalyzed Allylation of Enolates Derived from Ketones. *J. Org. Chem*. **1982**, *47*, 3188–3190. c) Braun, M.; Meier, T. Tsuji–Trost Allylic Alkylation with Ketone Enolates. *Angew. Chem., Int. Ed*. **2006**, *45*, 6952–6955. d) Trost, B. M.; Schroeder, G. M. Palladium-Catalyzed Asymmetric Alkylation of Ketone Enolates. *J. Am. Chem. Soc*. **1999**, *121*, 6759–6760.

32. a) Shimizu, I.; Yamada, T.; Tsuji, J. Tetrahedron Lett. 1980, 21, 3199. b) Tsuda, T.; Chujo, Y.; Nishi, S.; Tawara, K.; Saegusa, T. Facile Generation of a Reactive Palladium(II) Enolate Intermediate by the Decarboxylation of Palladium(II) β-Ketocarboxylate and its Utilization in Allylic Acylation. *J. Am. Chem. Soc*. **1980**, *102*, 6381–6384.

33. Select examples of enolate allylation: with palladium catalyst: a) Imao, D.; Itoi, A.; Yamazaki, A.; Shirakura, M.; Ohtoshi, R.; Ogata, K.; Ohmori, Y.; Ohta, T.; Ito, Y. Easy Access to Esters with a Benzylic Quaternary Carbon Center from Diallyl Malonates by Palladium-Catalyzed Decarboxylative Allylation. *J. Org. Chem.* **2007**, *72*, 5, 1652–1658. b) Tardibono, L. P.; Patzner, J.; Cesario, C.; Miller, M. J. Palladium-Catalyzed Decarboxylative Rearrangements of Allyl 2,2,2-Trifluoroethyl Malonates: Direct Access to Homoallylic Esters. *Org. Lett*. **2009**, *11*, 4076–4079. c) Chattopadhyay, K.; Jana, R.; Day, V. W.; Douglas, J. T.; Tunge, J. A. Mechanistic Origin of the Stereodivergence in Decarboxylative Allylation. *Org. Lett*. **2010**, *12*, 3042–3045. d) Tsuda, T.; Okada, M.; Nishi, S.; Saegusa, T. J. Palladium-Catalyzed Decarboxylative Allylic Alkylation of Allylic Acetates with β-keto Acids. *Org. Chem*. **1986**, *51*, 421–426. With Mo, Ni, Rh catalysts: e) Tsuji, J.; Minami, I.; Shimizu, I. Synthesis of γ,δ-Unsaturated Ketones by the Intramolecular Decarboxylative Allylation of Allyl β-Keto Carboxylates and Alkenyl Allyl Carbonates Catalyzed by Molybdenum, Nickel, and Rhodium Complexes. *Chem. Lett*. **1984**, *13*, 1721–1724. Asymmetric: f) Burger, E. C.; Tunge, J. A. Asymmetric Allylic Alkylation of Ketone Enolates: An Asymmetric Claisen Surrogate. *Org. Lett.* **2004**, *6*, 4113–4115. g) Trost, B. M.; Xu, J. Regio- and Enantioselective Pd-Catalyzed Allylic Alkylation of Ketones through Allyl Enol Carbonates. *J. Am. Chem. Soc*. **2005**, 127, 2846–2847. h) Mohr, J. T.; Behenna, D. C.; Harned, A. M.; Stoltz, B. M. Deracemization of Quaternary Stereocenters by Pd-Catalyzed Enantioconvergent Decarboxylative Allylation of Racemic β-Ketoesters. *Angew. Chem., Int. Ed*. **2005**, *44*, 6924–6927.

34. a) Recio, A.; Tunge, J. A. Regiospecific Decarboxylative Allylation of Nitriles. *Org. Lett*. **2009**, *11*, 24, 5630-5633. p*K*a in DMSO: b) Matthews, W. S.; Bares, J. E.; Bartmess, J. E.; Bordwell, F. G.; Conforth, F. J.; Drucker, G. E.; Margolin, Z.; McCallum, R. J.; McCollum, G.

J.; Vanier, N. R. Equilibrium Acidities of Carbon Acids. VI. Establishment of an Absolute Scale of Acidities in Dimethyl Sulfoxide Solution. *J. Am. Chem. Soc*. **1975**, *97*, 7006–7014.

35. a) Grenning, A. J.; Tunge, J. A. Rapid Decarboxylative Allylation of Nitroalkanes. *Org. Lett.* **2010**, *12*, 4, 740–742.

36. Weaver, J. D.; Tunge, J. A. Decarboxylative Allylation using Sulfones as Surrogates of Alkanes. *Org. Lett*. **2008**, *10*, 20, 4657–4660.

37. Rayabarapu, D. K.; Tunge, J. A. Catalytic Decarboxylative sp−sp^3 Coupling. *J. Am. Chem. Soc.* **2005**, *127*, 39, 13510–13511.

38. a) Liegault, B.; Renaud, J.-L.; Bruneau, C. Activation and Functionalization of Benzylic Derivatives by Palladium Catalysts. *Chem. Soc. Rev.* **2008**, *37*, 290–299. b) Kuwano, R. Catalytic Transformations of Benzylic Carboxylates and Carbonates. *Synthesis* **2009**, *7*, 1049–1061. c) Legros, J.-Y.; Fiaud, J.-C. Palladium-Catalyzed Nucleophilic Substitution of Naphthylmethyl and 1-Naphthylethyl Esters. *Tetrahedron Lett*. **1992**, *33*, 2509–2510. d) Legros, J.-Y.; Toffano, M.; Fiaud, J.-C. Palladium-catalyzed substitution of esters of naphthylmethanols, 1-naphthylethanols, and analogues by sodium dimethyl malonate. Stereoselective Synthesis from Enantiomerically Pure Substrates. *Tetrahedron* **1995**, *51*, 3235–3246. e) Legros, J.-Y.; Primault, G. l.; Toffano, M.; Riviere, M.-A.; Fiaud, J.-C. Reactivity of Quinoline- and Isoquinoline-Based Heteroaromatic Substrates in Palladium(0)-Catalyzed Benzylic Nucleophilic Substitution. *Org. Lett.* **2000**, *2*, 433–436. f) Kuwano, R.; Kondo, Y.; Matsuyama, Y. Palladium-Catalyzed Nucleophilic Benzylic Substitutions of Benzylic Esters. *J. Am. Chem. Soc*. **2003**, *125*, 12104–12105. g) Kuwano, R.; Kondo, Y. Palladium-Catalyzed Benzylation of Active Methine Compounds without Additional Base: Remarkable Effect of 1,5-Cyclooctadiene. *Org. Lett.* **2004**, *6*, 3545–3547. h) Kuwano, R.; Yokogi, M. Suzuki−Miyaura Cross-Coupling of Benzylic Carbonates with Arylboronic Acids. *Org. Lett*. **2005**, *7*, 945–947. i) Mukai, T.; Hirano, K.; Satoh, T.; Miura, M. Palladium-Catalyzed Direct Benzylation of Azoles with Benzyl Carbonates. *Org. Lett.* **2010**, *12*,1360–1363.

39. Marchini, S.; Passerini, L.; Hoglund, M. D.; Pinno, A.; Nendza, M. Toxicity of aryl- and benzylhalides to Daphnia magna and classification of their mode of action based on quantitative structure–activity relationship. *Environ. Toxicol. Chem.*, **1999**, *18*, 2759–2766.

40. a) Torregrosa, R. R. P.; Mendis, S. N.; Davies, A.; Tunge, J. A. Palladium-Catalyzed Decarboxylative Benzylation of Acetylides and Enolates. *Synthesis* **2018**, *50*, 3205–3216. b) Torregrosa, R. R. P.; Ariyarathna, Y.; Chattopadhyay, K.; Tunge, J. A. Decarboxylative Benzylations of Alkynes and Ketones. *J. Am. Chem. Soc*. **2010**, 132, 9280–9282. c) Fields, W. H.; Chruma, J. J. Palladium-Catalyzed Decarboxylative Benzylation of Diphenylglycinate Imines. *Org. Lett.* **2010**, *12*, 316–319. d) Kuwano, R.; Kusano, H. Benzyl Protection of Phenols under Neutral Conditions: Palladium-Catalyzed Benzylations of Phenols. *Org. Lett*. **2008**, *10*, 1979-1982. e) Rayabarapu, D. K.; Tunge, J. A. Catalytic Decarboxylative sp−sp^3 Coupling. *J. Am. Chem. Soc*. **2005**, *127*, 13510–13511. f) Pi, S.-F.; Tang, B.-X.; Li, J.-H.; Liu, Y.-L.; Liang, Y. Palladium-Catalyzed Decarboxylative Coupling of Allylic Alkynoates with Arynes. *Org. Lett*. **2009**, *11*, 2309–2312.

41. a) Kuwano, R.; Kondo, Y.; Matsuyama, Y. Palladium-Catalyzed Nucleophilic Benzylic Substitutions of Benzylic Esters. *J. Am. Chem. Soc.* **2003**, *125*, 40, 12104–12105. b) Legros, J. Y.; Toffano, M.; Fiaud, J.-C. Palladium-Catalyzed Substitution of Esters of Naphthylmethanols, 1-Naphthylethanols, and Analogues by Sodium Dimethyl Malonate. Stereoselective Synthesis from Enantiomerically Pure Substrates. *Tetrahedron* **1995**, *51*, 3235–3246. c) Legros, J.-Y.; Primault, G.; Toffano, M.; Rivière, M. A.; Fiaud, J.-C. Reactivity of Quinoline- and Isoquinoline-Based Heteroaromatic Substrates in Palladium(0)-Catalyzed Benzylic Nucleophilic Substitution. *Org. Lett.* **2000**, *2*, 433–436. d) Legros, J.-Y.; Boutros, A.; Fiaud, J.-C.; Toffano, M. Asymmetric Palladium-Catalyzed Nucleophilic Substitution of 1-(2-Naphthyl)Ethyl Acetate by Dimethyl Malonate Anion. *J. Mol. Catal. A: Chem.* **2003**, *196*, 21–25.

42. Zhang, W.-W.; Zhang, X.-G.; Li, J.-H. Palladium-Catalyzed Decarboxylative Coupling of Alkynyl Carboxylic Acids with Benzyl Halides or Aryl Halides. *J. Org. Chem.* **2010**, 75, 5259–5264.

43. Lang, S. B.; O'Nele, K. M.; Tunge, J. A. Dual Catalytic Decarboxylative Allylations of α-Amino Acids and Their Divergent Mechanisms. *Chem. Eur. J.* **2015**, *21*, 18589–18593.

44. Luo, J.; Zhang, J. Donor–Acceptor Fluorophores for Visible-Light-Promoted Organic Synthesis: Photoredox/Ni Dual Catalytic C(sp^3)–C(sp^2) Cross-Coupling. *ACS Catal.* **2016**, *6*, 2, 873–877.

45. Zuo, Z.; Ahneman, D. T.; Chu, L.; Terrett, J. A.; Doyle, A. G.; MacMillian, D. W. C. Merging Photoredox with Nickel Catalysis: Coupling of α-Carboxyl sp^3-Carbons with Aryl Halides. *Science*, **2014**, *345*, 437–440.

46. Cartwright, K. C.; Tunge, J. A. Organophotorodox/Palladium Dual Catalytic Decarboxylative Csp^3-Csp^3 Coupling of Carboxylic Acids and π-Electrophiles. *Submitted Manuscript.*

47. Benson, S. W. Disproportiontion of Free Radicals. *J. Phys. Chem.* **1985**, *89*, 20, 4366–4369.

48. a) Ozawa, F.; Kubo, A.; Hayashi, T. Generation of Tertiary Phosphine-Coordinated Pd(0) Species from Pd(OAc)$_2$ in the Catalytic Heck Reaction. *Chem. Lett.* **1992**, 2177-2180. b) Csákai, Z.; Skoda-Földes, R.; Kollá, L. NMR Investigation of Pd(II)–Pd(0) Reduction in the Presence of Mono- and Ditertiary Phosphines. *Inorganica Chimica Acta* **1999**, *286*, 93–97.

49. Sha, S.-C.; Zhang, J.; Carroll, P. J.; Walsh, P. J. Raising the pK_a Limit of "Soft" Nucleophiles in Palladium-Catalyzed Allylic Substitutions: Application of Diarylmethane Pronucleophiles. *J. Am. Chem. Soc.* **2013**, *135*, 17602–17609.

50. Waetzig, S. R.; Tunge, J. A. Palladium-Catalyzed Decarboxylative sp^3−sp^3 Coupling of Nitrobenzene Acetic Esters. *J. Am. Chem. Soc.* **2007**, *129*, 14860–14861.

51. Select examples of thermal DcA with sp^2 and sp carboxylic acids a) Jana, R.; Trivedi, R.; Tunge, J. A. Mild Decarboxylative Allylation of Coumarins. *Org. Lett.* **2009**, *11*, 3434–3436. b) Rayabarapu, D. K.; Tunge, J. A. Catalytic Decarboxylative sp−sp^3 Coupling. *J. Am. Chem. Soc.* **2005**, *127*, 13510–13511.

52. Duan, Y.; Zhang, M.; Ruzi, R.; Wu, Z.; Zhu, C. The Direct Decarboxylative Allylation of *N*-Arylglycine Derivatives by Photoredox Catalysis. *Org. Chem. Front.* **2017**, *4*, 525–528.

53. Lu, J.; Pattengale, B.; Liu, Q.; Yang, S.; Shi, W.; Li, S.; Huang, J.; Zhang, J. Rh(III)-Catalyzed Redox-Neutral Unsymmetrical C–H Alkylation and Amidation Reactions of *N*-Phenoxyacetamides. *J. Am. Chem. Soc.* **2018**, *140*, 42, 13719–13725.

54. Donabauer, K.; Maity, M.; Berger, A. L.; Huff, G. S.; Crespi, S.; König, B. Photocatalytic Carbanion Generation–Benzylation of Aliphatic Aldehydes to Secondary Alcohols. *Chem. Sci.*, **2019**, *10*, 5162–5166.

55. a) Amatore, C.; Jutand, A.; Khalil, F.; Nielsent, M. F. Carbon Dioxide as a C1 Building Block. Mechanism of Palladium-Catalyzed Carboxylation of Aromatic Halides. *J. Am. Chem. Soc.* **1992**, *114*, 7076–7085. b) Amatore, C.; Carré, E.; Jutand, A.; M'Barki', M. A. Rates and Mechanism of the Formation of Zerovalent Palladium Complexes from Mixtures of Pd(OAc)$_2$ and Tertiary Phosphines and Their Reactivity in Oxidative Additions. *Organometallics*, **1995**, *14*, 1818–1826.

56. Zhang, P.; Zhang, W.; Zhang, T.; Wang, Z.; Zhou, W. The Mechanism of the Palladium-Catalyzed Reaction of Allylic Acetates with Carbonyl Compounds via Electrochemical Reduction. *J. Chem. Soc. Chem. Commun.* **1991**, 491–492.

57. Metal carboxylate oxidative decarboxylation select examples: With Ag: a) Lu, P.; Sanchez, C.; Cornella, J.; Larrosa, I. Silver-Catalyzed Protodecarboxylation of Heteroaromatic Carboxylic Acids. *Org. Lett.* **2009**, *11*, 5710−5713. b) Gooßen, L. J.; Lunder, C.; Rodríguez, N.; Lange, P. P.; Fromm, A. Silver-Catalyzed Protodecarboxylation of Carboxylic Acids. *Chem. Commun.* **2009**, 7173−7175. c) Cornella, J.; Sanchez, C.; Banawa, D.; Larrosa, I. Silver-Catalyzed Protodecarboxylation of Ortho-Substituted Benzoic Acids. *Chem. Commun.* **2009**, 7176−7178. d) Gooßen, L. J.; Rodríguez, N.; Linder, C.; Lange, P. P.; Fromm, A. Comparative Study of Copper- and Silver-Catalyzed Protodecarboxylations of Carboxylic Acids. *Chem. Cat. Chem* **2010**, *2*, 430−422. e) Xue, L.; Su, W.; Lin, Z. Mechanism of Silver- and Copper-Catalyzed Decarboxylation Reactions of Aryl Carboxylic Acids. *Dalton Trans.* **2011**, *40*, 11926−11936. f) Seo, S.; Slater, M.; Greaney, M. F. Decarboxylative C–H Arylation of Benzoic Acids under Radical Conditions. *Org. Lett.* **2012**, *14*, 2650−2653. g) Seo, S.; Taylor, J. B.; Greaney, M. F. Protodecarboxylation of Benzoic Acids Under Radical Conditions. *Chem. Commun.* **2012**, *48*, 8270−8272. h) Kan, J.; Huang, S.; Lin, J.; Zhang, M.; Su, W. Silver-Catalyzed Arylation of (Hetero)arenes by Oxidative Decarboxylation of Aromatic Carboxylic Acids. *Angew. Chem., Int. Ed.* **2015**, *54*, 2199−2203. With Pb: i) Kochi, J. K. Oxidation with Lead(IV). I. Mechanism of the Decarboxylation of Pentanoic Acids. *J. Am. Chem. Soc.*, **1965**, *87*, 3609–3619. j) Kochi, J. K.; Sheldon, R. A.; Lande, S. S. Rates of Photochemical and Thermal Decarboxylation of Acids by Lead(IV) Tetraacetate. *Tetrahedron*, **1969**, *25*, 1197–1207. With Ce: k) Sheldon; R. A.; Kochi, J. K. Photochemical and thermal reduction of cerium(IV) carboxylates. Formation and Oxidation of Alkyl Radicals. *J. Am. Chem. Soc.*, **1968**, *90*, 6688–6698. l) Heiba, E. A. I.; Dessau, R. M. Oxidation by metal salts. VIII. Decomposition of Ceric Carboxylates in the Presence of Olefins and Aromatic Hydrocarbons. *J. Am. Chem. Soc.* **1971**, 93, 995–999.

58. Alkyl radical redox potentials (all are reported as V vs. SCE): a) Wayner, D. D. M.; McPhee, D. J.; Griller, D. Oxidation and Reduction Potentials of Transient Free Radicals. *J. Am. Chem. Soc*. **1988**, *110*, 132–137. b) Jaun, B.; Schwarz, J.; Breslow, R. Determination of the Basicities of Benzyl, Allyl, and tert-Butylpropargyl Anions by Anodic Oxidation of Organolithium Compounds. *J. Am. Chem. Soc*. **1980**, *102*, 5741–5748. c) Álvarez-Griera, L.; Gallardo, I.; Guirdo, G. Estimation of Nitrobenzyl Radicals Reduction Potential using Spectro-Electrochemical Techniques. *Electrochimica Acta*. **2009**, *54*, 5098–5108.

58. Trost, B. M.; Van Vranken, D. L. Asymmetric Transition Metal-Catalyzed Allylic Alkylations. *Chem. Rev.* **1996**, *96*, 1, 395–422.

60. a) Cavalcanti, L. N.; Molander, G. A. (**2017**) Photoredox Catalysis in Nickel-Catalyzed Cross-Coupling. In: Correa A. (eds) Ni- and Fe-Based Cross-Coupling Reactions. Topics in Current Chemistry Collections. Springer, Cham. b) Tasker, S. Z.; Standley, E. A.; Jamison, T. F. Recent Advances in Homogeneous Nickel Catalysis. *Nature* **2014**, *509*, 299–309.

61. Giedyk, M.; Turkowska, J.; Lepak, S.; Marculewica, M.; Proinsias, K.; Gryko, D. Photoinduced Vitamin B12-Catalysis for Deprotection of (Allyloxy)arenes. *Org. Lett.* **2017**, *19*, 2670–2673.

62. a) Okabe, M.; Masayoshi, A.; Tada, M. Reductive Cyclization of 2-[(2-propynyl)oxy]ethyl Bromides by a Cobalt Complex, Cobaloxime(I). A New Method for the Aynthesis of α-methylene-γ-butyrolactones. *J. Org. Chem.* **1982**, *47*, 1775–1777. b) Branchaud, B. P.; Detlefsen, W. D. Cobaloxime-Catalyzed Radical Alkyl-Styryl Cross Couplings. *Tet. Lett.* **1991**, *32*, 6273–6276.

63. Jameson, D. L.; Grzybowski, J. J.; Hammels, D. E.; Castellano, R. K.; Hoke, M. E.; Freed, K; Basquill, S.; Mendel, A.; Shoemaker, W. J. Synthesis of Some "Cobaloxime" Derivatives: A Demonstration of "Umpolung" in the Reactivity of an Organometallic Complex. *J. Chem. Ed*. **1998**, *75*, 447–450.

64. Cartwright, K. C.; Forshee, L. M.; Hegarty, M. E.; Tunge, J. A. Organophotoredox/Palladium-Catalyzed Decarboxylative Multicomponent Coupling. *Manuscript in progress.*

65. Select examples of multicomponent decarboxylative coupling: a) Park, K.; Heo, Y.; Lee, S. Metal-Free Decarboxylative Three-Component Coupling Reaction for the Synthesis of Propargylamines. *Org. Lett*. **2013**, *15*, 13, 3322–3325. b) Ariyarathna, Y.; Tunge, J. A. Multicomponent Decarboxylative Allylations. *Chem. Commun*., **2014**, *50*, 14049–14052. c) Mega, R. S.; Duong, V. K.; Noble, A.; Aggarwal, V. K. Decarboxylative Conjunctive Cross-coupling of Vinyl Boronic Esters using Metallaphotoredox Catalysis. *Angew. Chem. Int. Ed.* **2020**, *59*, 4375 –4379.

66. Bortolamei, N.; Isse, A. A.; Gennaro, A. Estimation of Standard Reduction Potentials of Alkyl Radicals Involved in Atom Transfer Radical Polymerization. *Electrochimica Acta.* **2010**, *55*, 8312–8318.

67. Methyl benzalcyanoacetate was synthesized following literature procedure (KC-7-184): Camerino, M. A.; Liu, M.; Moriya, S.; Kitahashi, T.; Mahgoub, A.; Mountford, S. J.; Chalmers, D. K.; Soga, T.; Parhar, S.; Thompson, P. E. Beta amino acid-modified and fluorescently labelled kisspeptin analogues with potent KISS1R activity. *J. Peptide Science* **2016**, *22*, 406–414.

68. Synthetic utility of allylic functionality: a) DeWolfe, R. H.; Young, W. G. Substitution and Rearrangement Reactions of Allylic Compounds. *Chem. Rev.* **1956**, 753–902. Nitrile reactivity: b) Kukushkin, V. Yu.; Pombeiro, A. J. L. Metal-Mediated and Metal-Catalyzed Hydrolysis of Nitriles. *Inorg. Chim. Acta*. **2005**, *358*, 1–21. c) Barrault, J.; Pouilloux, Y. Catalytic Amination Reactions: Synthesis of Fatty Amines. Selectivity Control in Presence of Multifunctional Catalysts. *Catalysis Today*. **1997**, *2*, 137–153. d) Berkoff, C. E.; Rivard, D. E.; Kirkpatrick, D.; Ives, J. L. The Reductive Decyanation of Nitriles by Alkali Fusion. *Synthetic Communications*. **1980**, *10*, 939–945. e) Fleming, F. F.; Zhang, Z. Cyclic Nitriles: Tactical Advantages in Synthesis. *Tetrahedron* **2005**, *6*, 747–789.

69. Cartwright, K. C.; Tunge, J. A. Decarboxylative Elimination of *N*-Acyl Amino Acids via Photoredox/Cobalt Dual Catalysis. *ACS Catal.* **2018**, *8*, 12, 11801–11806

70. Maji, T.; Tunge, J. A. Palladium-Catalyzed Double-Decarboxylative Addition to Pyrones: Synthesis of Conjugated Dienoic Esters. *Org. Lett.*, **2015**, *17*(19), 4766–4769.

71. Trost, B. M.; Miller, J. R.; Hoffman, C. M. A Highly Enantio- and Diastereoselective Molybdenum-Catalyzed Asymmetric Allylic Alkylation of Cyanoesters. *J. Am. Chem. Soc.* **2011**, *133*, 8165–8167.

72. Takizawa, K.; Sekino, T.; Sato, S.; Yoshino, T.; Kojima, M; Matsunaga, S. *Angew. Chem. Int. Ed.* **2019**, *58*, 9199–9203.

73. Zhou, Y.; Breit, B. Rhodium-Catalyzed Asymmetric N−H Functionalization of Quinazolinones with Allenes and Allylic Carbonates: The First Enantioselective Formal Total Synthesis of (−)-Chaetominine. *Chem. Eur. J.* **2017**, *23*, 18156–18160.

74. Chen, H.; Jia, X.; Yu, Y.; Qian, Q.; Gong, H. Nickel-Catalyzed Reductive Allylation of Tertiary Alkyl Halides with Allylic Carbonates. *Angew. Chem. Int. Ed*. **2017**, *56*, 13103–13106.

75. Ye, K.-Y.; Zhang, X.; Dai, L.-X.; You, S.-L. Ruthenium-Catalyzed Regioselective Allylic Trifluoromethylthiolation Reaction. *J. Org. Chem*. **2014**, *79*, 24, 12106–12110.

76. Mi, Z.; Tang, J.; Guan, Z.; Shi, W.; Chen, H. Cleavage of C–C and C–O Bonds to Form C–C Bonds: Direct Cross-Coupling between Acetylenic Alcohols and Benzylic Carbonates. *Eur. J. Org. Chem*. **2018**, 4479–4482.

77. Blessley, G.; Holden, P.; Walker, M.; Brown, J. M.; Gouverneur, V. Palladium-Catalyzed Substitution and Cross-Coupling of Benzylic Fluorides. *Org. Lett*. **2012**, *14*, 11, 2754–2757.

78. Franzoni, I.; Guénéeb, L.; Mazet, C. A General Pd-Catalyzed α- and γ-Benzylation of Aldehydes for the Formation of Quaternary Centers. *Org. Biomol. Chem.*, **2015**, *13*, 6338–6343.

79. Mukai, T.; Hirano, K.; Satoh, T.; Miura, M. Palladium-Catalyzed Direct Benzylation of Azoles with Benzyl Carbonates. *Org. Lett.* **2010**, *12*, 6, 1360–1363.

80. Grignon, J.; Servens, C.; Pereyre, M. Reactivity of Allylic Organotins Towards Halogen Derivatives: Synthetic Aspects and Mechanism. *Journal of Organometallic Chemistry* **1975**, *96*, 225–235.

81. Suh, Y.-G.; Jang, J.; Yun, H.; Han, S. M.; Shin, D.; Jung, J.-K.; Jung, J.-W. Expedient Synthesis of Chiral Homoallylamines via N,O-Acetal TMS Ethers and Its Application. *Org. Lett*. **2011**, *13*, 21, 5920–5923.

83. Romano, C.; Mazet, C. Multicatalytic Stereoselective Synthesis of Highly Substituted Alkenes by Sequential Isomerization/Cross-Coupling Reactions. *J. Am. Chem. Soc.* **2018**, *140*, 13, 4743–4750.

84. Hu, K.-F.; Ning, X.-S.; Qu, J.-P.; Kang, Y.-B. Tuning Regioselectivity of Wacker Oxidation in One Catalytic System: Small Change Makes Big Step. *J. Org. Chem*. **2018**, *83*, 18, 11327–11332.

85. Singh, P. P.; Gudup, S.; Aruri, H.; Singh, U.; Ambala, S.; Yadav, M.; Sawant, S. D.; Vishwakarma, R. D. New Method for C–H Arylation/Alkylation at α-Position of Cyclic Aliphatic Ethers by Iron-Oxide Mediated Reaction. *Org. Biomol. Chem*., **2012**, *10*, 1587–1597.

86. Sittiwong, W.; Richardson, M. W.; Schiaffo, C. E.; Fisher, T. J.; Dussault, P. H. Re_2O_7-Catalyzed Reaction of Hemiacetals and Aldehydes with O-, S-, and C-Nucleophiles. *Beilstein J. Org. Chem.* **2013**, *9*, 1526–1532.

87. Holz, J.; Pfeffer, C.; Zuo, H.; Beierlein, D.; Richter, G.; Klemm, E.; Peters, R. In Situ Generated Gold Nanoparticles on Active Carbon as Reusable Highly Efficient Catalysts for a $C(sp^3)$-$C(sp^3)$ Stille Coupling. *Angew. Chem. Int. Ed.* **2019**, *58*, 10330–10334.

88. Kima, S. H.; Shina, C.; Paea, A. N.; Koha, H. Y.; Changa, M. H.; Chung, B. Y.; Cho, Y. S. $InBr_3$-Catalyzed Deoxygenative Allylation of Benzylic and Allylic Alcohols and Acetates with Allyltrimethylsilane. *Synthesis* **2004**, *10*, 1581−1584.

89. Datta, S.; Chang, C.-L.; Yeh, K.-L.; Liu, R.-S. A New Ruthenium-Catalyzed Cleavage of a Carbon−Carbon Triple Bond: Efficient Transformation of Ethynyl Alcohol into Alkene and Carbon Monoxide. *J. Am. Chem. Soc*. **2003**, *125*, 31, 9294−9295.

90. Wang, G.-Z.; Jiang, J.; Bu, X.-S.; Dai, J.-J.; Xu, J.; Fu, Y.; Xu, H.-J. Copper-Catalyzed Cross-Coupling Reaction of Allyl Boron Ester with 1°/2°/3°-Halogenated Alkanes. *Org. Lett.* **2015**, *17*, 15, 3682−3685.

91. Gonnard, L.; Guørinot, A.; Cossy, J. Cobalt-Catalyzed Cross-Coupling of 3- and 4-Iodopiperidines with Grignard Reagents. *Chem. Eur. J.* **2015**, *21*, 12797–12803.

Chapter 3:

92. a) Mosher. W. A.; Kehr, C. L. The Decomposition of Organic Acids in the Presence of Lead Tetraacetate. *J. Am. Chem. Soc*. **1953**, *75*, 3172–3176. b) Kharasch, M. S.; Friedlander, N.; Urry, W. H. Reactions of Atoms and Free Radicals in Solution. XXVI. Comparison of the Reactions of Lead Tetraacetate and Acetyl Peroxide with Acetic Acid and Isopropyl Ether. *J. Org. Chem*., **1951**, *16*, 533–542. c) Mosher, W. A.; Neidig, H. A. The Oxidation of Benzpinacolyl Alcohol. *J. Am. Chem. Soc.* **1950**, 72, 4452–4454.

93. a) Bacha, J. D.; Kochi, J. K. Alkenes from Acids by Oxidative Decarboxylation. *Tetrahedron*. **1968**, *24*, 2215-2226. b) Kochi, J. K.; Bemis, A. Carbonium Ions from Alkyl Radicals by Electron Transfer. *J. Am. Chem. Soc*. **1968**, *90*, 4038−4051.

94. a) Kochi, J. K. Mechanisms of Organic Oxidation and Reduction by Metal Complexes. *Science*, **1967**, *155*, 422-424. b) Free Radicals in Thermal and Photochemical Oxidative Decarboxylations with Lead(IV). *J. Am. Chem. Soc*. **1967**, *89*, 6538-6547. c) Bacha, J. D.; Kochi, J. K. Oxidation of Alkyl Radicals from Decarboxylation of Acids by Lead(IV) and Copper(II). *J. Org. Chem.* **1968**, *33*, 83−94. d) Davies, D. I.; Waring, C. Free-radical Formation in the Reaction of Lead Tetra-acetate with Monocarboxylic Acids. *Chem. Commun.* **1965**, 263−264. e) Concurrent Carbon-to-Oxygen Rearrangement, Cyclization, and Decarboxylation in the Reaction of 3,3,3-Triarylpropionic Acids with Lead Tetraacetate. *J. Am. Chem. Soc.* **1964**, *86*, 5603−5611. f) Casanova, J.; Corey, E. J. The Formation of Carbonium Ions by Oxidative Decarboxylation of Carboxylic Acids with Lead Tetraacetate. *J. Am. Chem. Soc.* **1963**, *85*, 165.

95. a) Kochi, J. K.; Subramanian, R. V. Kinetics of Electron-Transfer Oxidation of Alkyl Radicals by Copper (II) Complexes. *J. Am. Chem. Soc.* **1965**, *87*, 4855−4866. b) Kochi, J. K.; Bemis, A.; Jenkins, C. L. Mechanism of Electron Transfer Oxidation of Alkyl Radicals by Copper(II) Complexes. *J. Am. Chem. Soc.* **1968**, *90*, 4616−4625.

96. a) Cargill, R. L.; Foster, A. M. The Tricyclo[6.3.0.04,s]undecane System. *J. Org. Chem.* **1970**, *35*, 1971−1973. b) Struble, D. L.; Beckwick, A. L. J.; Gream, G. E. Copper-Ion Catalysed Decomposition of bis-5-(1-cyclohexenyl)pentanoyl Peroxide. *Tet. Lett.* **1970**, 11, 4795−4798.

97. Kochi, J. K.; Bacha, J. D. Solvent Effects on the Oxidation of Alkyl Radicals by Lead(IV) and Copper(II) Complexes. *J. Org. Chem.* **1968**, *33*, 2746−2755.

98. a) McGuirk, P. R., Collum, D. B. Total Synthesis of (+)-Phyllanthocin. *J. Am. Chem. Soc*. **1982**, *104*, 4497-4498. b) Jensen, N. P., Johnson, W. S. A Three-Step Synthesis of Fichtelite from Abietic Acid. *J. Org. Chem.* **1967**, *32*, 2045−2046. c) McMurry, J. E., Blaszczak, L. C. A New Method for the Synthesis of Enones. Total Synthesis of (±)-Mayurone and (i)-Thujopsadiene. *J. Org. Chem*. **1974**, *39*, 2217−2222.

99. a) Sebahar, P. R.; Williams, R. M. The Asymmetric Total Synthesis of (+)- and (-)-Spirotryprostatin B. *J. Am. Chem. Soc.* **2000**, *122*, 5666-5667. b) Li, X.; Danishefsky, S, J. Cyclobutenone as a Highly Reactive Dienophile: Expanding Upon Diels−Alder Paradigms. *J. Am. Chem. Soc.* **2010**, *132*, 11004−11005. c) Mascitti, V.; Corey, E. J. Enantioselective Synthesis of Pentacycloanammoxic Acid. *J. Am. Chem. Soc.* **2006**, *128*, 3118−3119. d) Hancock,

E. N.; Kuker, E. L.; Tantillo, D. J.; Brown, K. Lessons in Strain and Stability: Enantioselective Synthesis of (+)-[5]-Ladderanoic Acid. *Angew. Chem. Int. Ed.* **2020**, *59*, 436−441.

100. Cartwright, K. C.; Lang, S. B.; Tunge, J. A. Photoinduced Kochi Decarboxylative Elimination for the Synthesis of Enamides and Enecarbamates from N-Acyl Amino Acids. *J. Org. Chem.* **2019**, *84*, 2933−2940.

101. a) Similar methodology that arose after the development of the method described in reference 100 that makes use of a redox-active esters in a reductive radical decarboxylation pathway towards alkenes: Tlahuext-Aca, A.; Candish, L.; Garza-Sanchez, R. A.; Glorius, F. Decarboxylative Olefination of Activated Aliphatic Acids Enabled by Dual Organophotoredox/Copper Catalysis. *ACS Catal.* **2018**, *8*, 1715−1719. b) An alternative modern decarboxylative elimination process: Wu, S.-W.; Lui, J.-L.; Liu, F. Metal-Free Microwave-Assisted Decarboxylative Elimination for the Synthesis of Olefins. *Org. Lett.* **2016**, *18*, 1−3.

102. a) Fukuzumi, S.; Kotani, H.; Ohkubo, K.; Ogo, S.; Tkachenko, N. V.; Lemmetyinen, H. Electron-Transfer State of 9-Mesityl-10-methylacridinium Ion with a Much Longer Lifetime and Higher Energy Than That of the Natural Photosynthetic Reaction Center. *J. Am. Chem. Soc.* **2004**, *126*, 1600−1601. b) Romero, N. A.; Margrey, K. A.; Tay, N. E.; Nicewicz, D. A. Site-Selective Arene C-H Amination via Photoredox Catalysis. *Science* **2015**, *349*, 1326−1330.

103. a) Huang, L.; Arndt, M.; Gooßen, K.; Heydt, H.; Gooßen, L. J. Late Transition Metal-Catalyzed Hydroamination and Hydroamidation. *Chem. Rev.* **2015**, *115*, 2596−2697. b) Carbery, D. R. Enamides: Valuable Organic Substrates. *Org. Biomol. Chem.* **2008**, *6*, 3455−3460. Enamides are also privileged structures in bioactive compounds: c) Yet, L. Chemistry and Biology of Salicylihalamide A and Related Compounds. *Chem. Rev.* **2003**, *103*, 4283–4306. d) Kuranaga, T., Sesoko, Y. & Inoue, M. Cu-Mediated Enamide Formation in the Total Synthesis of Complex Peptide Natural Products. *Nat. Prod. Rep.* **2014**, *31*, 514–532.

104. Layer, W. R. The Chemistry of Imines. *Chem. Rev.* **1963**, 63, 489−510.

105. a) Brettle, R.; Mosedale, A. J. Synthesis of Enamides. *J. Chem. Soc., Perkin Trans. 1* **1988**, 2185. b) Kuramochi, K.; Watanabe, H.; Kitahara, T. Synthetic Study on Oximidines: A Concise Synthesis of (*Z*)-Enamides. *Synlett.* **2000**, 397.

106. a) Flitsch, W.; Schindler, S. R. Alkenylation of Imides and Activated Amides. *Synthesis* **1975**, 685. b) Murphy, J. P. Brennan The Wittig olefination reaction with carbonyl compounds other than aldehydes and ketones. *Chem. Soc. Rev.* **1988**, 17, 1.

107. Hansson, C.; Wickberg, B. Preparation of enamines by addition of Grignard reagents to *N,N*-dialkylformamides. *J. Org. Chem.* **1973**, *38*, 3074−3076.

108. a) Venkat, C. R.; Urgaonkar, S.; Verkade, J. G. A Highly Effective Catalyst System for the Pd-Catalyzed Amination of Vinyl Bromides and Chlorides. *Org. Lett.* **2005**, *7*, 4427. b) Pan, X.; Cai, Q.; Ma, D. CuI/*N,N*-Dimethylglycine-Catalyzed Coupling of Vinyl Halides with Amides or Carbamates. *Org. Lett.* **2004**, *6*, 1809.

109. a) Krompiec, S.; Krompiec, M.; Penczek, R.; Ignasiak, H. Double Bond Migration in N-Allylic Systems Catalyzed by Transition Metal Complexes. *Coord. Chem. Rev*. **2008**, *252*, 1819−1841. b) Larsen, C. R.; Grotjahn, D. B. Stereoselective Alkene Isomerization over One Position. *J. Am. Chem. Soc*. **2012**, *134*, 10357− 10360. c) Trost, B. M.; Cregg, J.; Quach, N. Isomerization of *N*-Allyl Amides to Form Geometrically Defined Di-, Tri-, and Tetrasubstituted Enamides. *J. Am. Chem. Soc*. **2017**, *139*, 5133−5139. d) Krompiec, S.; Pigulla, M.; Kuznik, N.; Krompiec, M.; Marciniec, B.; Chadyniak, D.; Kasperczyk, J. J. Highly Selective Isomerization of *N*-Allylamides Catalyzed by Ruthenium and Rhodium Complexes. *J. Mol. Catal. A: Chem.* **2005**, *225*, 91−101. e) Stille, J. K.; Becker, Y. Isomerization of *N*-Allylamides and -Imides to Aliphatic Enamides by Iron, Rhodium, and Ruthenium Complexes. *J. Org. Chem*. **1980**, *45*, 2139−2145. f) Reeves, J. T.; Tan, Z.; Marsini, M. A.; Han, S. Z.; Xu, Y.; Reeves, D. C.; Lee, H.; Lu, B. Z.; Senanayake, C. H. A Practical Procedure for Reduction of Primary, Secondary and Tertiary Amides to Amines. *Adv. Synth. Catal*. **2013**, *355*, 47−52.

110. a) DeKorver, K. A.; Li, H.; Lohse, A. G.; Hayashi, R.; Lu, Z.; Zhang, Y.; Hsung, P. R. Ynamides: A Modern Functional Group for the New Millennium. *Chem. Rev*. **2010**, *110*, 5064−5106. b) Lu, T.; Lu, Z.; Zhang, Y.; Hsung, R. P. Allenamides: A Powerful and Versatile Building Block in Organic Synthesis. *Chem. Rev*. **2013**, *113*, 4862.

111. a) Pohlki, F.; Doye, S. The Catalytic Hydroamination of Alkynes. *Chem. Soc. Rev*. **2003**, *32*, 104−114. b) Alonso, F.; Beletskaya, I. P.; Yus, M. Transition-Metal-Catalyzed Addition of Heteroatom−Hydrogen Bonds to Alkynes. *Chem. Rev*. **2004**, *104*, 3079−3160. c) Severin, R.; Doye, S. The Catalytic Hydroamination of Alkynes. *Chem. Soc. Rev*. **2007**, *36*, 1407−1420. d) Muller, T. E.; Hultzsch, K. C.; Yus, M.; Foubelo, F.; Tada, M. Hydroamination: Direct Addition of Amines to Alkenes and Alkynes. *Chem. Rev*. **2008**, *108*, 3795−3892.

112. a) Evano, G.; Gaumont, A. C.; Alayrac, C.; Wrona, I. E.; Giguere, J. R.; Delacroix, O.; Bayle, A.; Jouvin, K.; Theunissen, C.; Gatignol, J.; Silvanus, A. C. Metal-Catalyzed Synthesis of HeteroSubstituted Alkenes and Alkynes. *Tetrahedron* **2014**, *70*, 1529−1616. b) Matsubara, R.; Kobayashi, S. Enamides and Enecarbamates as Nucleophiles in Stereoselective C−C and C−N Bond-Forming Reactions. *Acc. Chem. Res*. **2008**, *41*, 292−301.

113. a) Garcia-Reynaga, P.; Carrillo, A. K.; VanNieuwenhze, M. S. Decarbonylative Approach to the Synthesis of Enamides from Amino Acids: Stereoselective Synthesis of the (*Z*)-Aminovinyl-d-Cysteine Unit of Mersacidin. *Org. Lett*. **2012**, *14*, 1030−1033. b) Min, K. G.; Hernandez, D.; Lindhardt, A. T.; Skrydstrup, T. Enamides Accessed′ from Aminothioesters via a Pd(0)-Catalyzed Decarbonylative/βHydride Elimination Sequence. *Org. Lett*. **2010**, *12*, 4716−4719.

114. Needles, H. L.; Ivanetich, K. Decarboxylation of *N*-Acetylamino-Acids with Lead Tetra-Acetate in *N'N*-dimethylformamide. *Chem. Ind*. **1967**, 581.

115. Furniss, B. S.; Hannaford, A. J.; Smith, P. W. G.; Tatchell, A. R. Vogel's Textbook of Practical Organic Chemistry, 5th ed.; Pearson Prentice Hall: Essex, England, **1989**; pp 156−164.

116. Prices were obtained from https://www.sigmaaldrich.com/united-states.html on 3/7/2020 and prices per gram listed where approximated. Sigma-Aldrich lists $Cu(OAc)_2$ as a green alternative for adhering to one or more of the principle of green chemistry.

117. a) Sawyer, D. T. Electrochemical transformations of metals, metal compounds, and metal complexes: invariably (ligand/solvent)-centered. *J. Mol. Catal. A: Chem*. **2003**, *194*, 53−67. b) Fontanet, M.; Popescu, A.-R.; Fontrodona, X.; Rodriguez, M.; Romero, I.; Teixidor, F.; Viñas, C.; Aliaga-Alcalde, N.; Ruiz, E. Design of Dinuclear Copper Species with Carboranylcarboxylate Ligands: Study of Their Steric and Electronic Effects. *Chem. - Eur. J.* **2011**, *17*, 13217−13229. c) McCann, S. D.; Stahl, S. S. Copper-Catalyzed Aerobic Oxidations of Organic Molecules: Pathways for Two-Electron Oxidation with a Four-Electron Oxidant and a One-Electron Redox-Active Catalyst. *Acc. Chem. Res*. **2015**, *48*, 1756−1766. Potentials in this reference for Cu halides were reported vs. NHE and were converted to SCE for redox potential comparisons in Chapter 3.

118. a) Singh, K.; Staig, S. J.; Weaver, J. D. Facile Synthesis of Z-Alkenes via Uphill Catalysis. *J. Am. Chem. Soc*. **2014**, *136*, 5275−5278. b) Singh, A.; Fennell, C. J.; Weaver, J. D. Photocatalyst Size Controls Electron and Energy Transfer: Selectable E/Z Isomer Synthesis via C−F Alkenylation. *Chem. Sci*. **2016**, *7*, 6796−6802.

119. Quenching of photocatalysts by amines: a) Lalevee, J.; Tehfe, M.-A.; Dumur, F.; Gigmes, D.; Blanchard, N.; Morlet-Savary, F.; Fouassier, J. P. *ACS Macro Lett*. **2012**, *1*, 286. b) Beatty, J. W.; Stephenson, C. R. Amine Functionalization via Oxidative Photoredox Catalysis: Methodology Development and Complex Molecule Synthesis. *Acc. Chem. Res*. **2015**, *48*, 1474−1484. c) Ghosh, T.; Das, A.; Konig, B. Photocatalytic *N*-Formylation of Amines via a Reductive Quenching Cycle in the Presence of Air. *Org. Biomol. Chem*., **2017**, *15*, 2536-2541. d) Chen, J.-R.; Hu, X.-Q.; Lu, L.-Q.; Xiao, W.-J. Visible Light Photoredox-Controlled Reactions of *N*-Radicals and Radical ions. *Chem. Soc. Rev.*, **2016**, *45*, 2044-2056.

120. Potentials for amine single electron oxidation: a) Jonsson, M.; Wayner, D. D. M.; Lusztyk, J. Redox and Acidity Properties of Alkyl- and Arylamine Radical Cations and the Corresponding Aminyl Radicals. *J. Phys. Chem*. **1996**, *100*, 17539-17543. Potential for amide single electron oxidation: b) O'Donnell, J. F.; Mann, C. K. Controlled-Potential Oxidation of Aliphatic Amides. *J. Electroanal. Chem.* **1967**, *13*, 157-162.

121. Lu, Z.; Yoon, T. P. Visible Light Photocatalysis of [2+2] Styrene Cycloadditions by Energy Transfer. *Angew. Chem. Int. Ed*. **2012**, *51*, 10329-10332.

122. a) Hofbeck, T.; Yersin, H. The Triplet State of *fac*-Ir(ppy)₃. *Inorg. Chem*. **2010**, *49*, 9290-9299. b) Teegardin, K.; Day, J. I.; Chan, J.; Weaver, J. Advances in Photocatalysis: A Microreview of Visible Light Mediated Ruthenium and Iridium Catalyzed Organic Transformations. *Org. Process Res. Dev*. **2016**, *20*, 1156-1163.

123. Benniston, A. C.; Harriman, A.; Li, P.; Rostron, J. P.; van Ramesdonk, H. J.; Groeneveld, M. M.; Zhang, H.; Verhoeven, J. W. Charge Shift and Triplet State Formation in the 9-Mesityl-10-methylacridinium Cation. *J. Am. Chem. Soc*. **2005**, *127*, 16054-16064.

124. T. L. Cottrell, The Strengths of Chemical Bonds, 2d ed., Butterworth, London, 1958.

125. Šakić, D.; Zipseb, H. Radical Stability as a Guideline in C–H Amination Reactions. *Adv. Synth. Catal.* **2016**, *358*, 3983–3991.

126. Unpublished reactions performed by Dr. Sameera Senaweera 9/14/2017.

127. Senaweera, S.; Cartwright, K. C.; Tunge, J. A. Decarboxylative Acetoxylation of Aliphatic Carboxylic Acids. *J. Org. Chem.* **2019**, *84*, 12553−12561.

128. Select examples of photoredox-catalyzed decarboxylative elimination: a) Sun, X.; Chen, J.; Ritter, T. Catalytic Dehydrogenative Decarboxyolefination of Carboxylic Acids. *Nat. Chem.* **2018**, *10*, 1229–1233. b) Nguyen, V. T.; Nguyen, V. D.; Haug, G. C.; Dang, H. T.; Jin, S.; Li, Z.; Flores-Hansen, C.; Benavides, B. S.; Arman, H. D.; Larionov, O. V. *ACS Catal.* **2019**, *9*, *10*, 9485−9498. c) H. Cao, H. Jiang, J. M. C. Kwan, X. Liu, J. Wu, *J. Am. Chem. Soc.* **2018**, *140*, 16360-16367.

129. Li, G.; Qu, J. Enantioselective Friedel−Crafts Reactions between Phenols and *N*-Tosylaldimines Catalyzed by a Leucine-Derived Bifunctional Catalyst. *Chem. Commun.* **2012**, *48*, 5518−5520.

130. Bennasar, M. L.; Roca, T.; Monerris, M.; García-Díaz, D. Sequential *N*-Acylamide Methylenation−Enamide Ring-Closing Metathesis: Construction of Benzo-Fused Nitrogen Heterocycles. *J. Org. Chem.* **2006**, *71*, 7028-7034.

131. Ogiwara, Y.; Uchiyama, T.; Sakai, N. Reductive Amination/Cyclization of Keto Acids Using a Hydrosilane for Selective Production of Lactams versus Cyclic Amines by Switching of the Indium Catalyst. *Angew. Chem. Int. Ed.* **2015**, *55*, 1864-1867.

Chapter 4:

132. Cartwright, K. C.; Davies, A. M.; Tunge, J. A. Cobaloxime-Catalyzed Hydrogen Evolution in PhotoredoxFacilitated Small-Molecule Functionalization. *Eur. J. Org. Chem.*, **2020**, 1245-1258. Cover article, Very Important Paper, and part of a ChemPhotoChem virtual collection on photochemical synthesis, Burkhard König, Geraldine Masson, Tehshik Yoon, Zhiwei Zuo Eds.

133. Green chemistry reviews: a) Li, C.-J.; Trost, B. M. Green Chemistry for Chemical Synthesis. *Proc. Natl. Acad. Sci.* **2008**, *105*, 13197-13202. b) Anastas, P. T.; Warner, J. C. Green Chemistry: Theory and Practice; Oxford University Press: New York, **1998**.

134. Photoredox/transition metal dual catalysis: a) Ravelli, D.; Dondi, D.; Fagnoni, M.; Albini, A. Photocatalysis. A Multi-faceted Concept for Green Chemistry. *Chem. Soc. Rev.*, **2009**, *38*, 1999-2011. b) Xuan, J.; Xiao, W-J. Visible-Light Photoredox Catalysis. *Angew. Chem. Int. Ed.* **2012**, *51*, 6828–6838. c) Twilton, J.; Le, C.; Zhang, P.; Shaw, M. H.; Evans, R. W.; MacMillan, D. W. The Merger of Transition Metal and Photocatalysis. *Nature Reviews Chemistry* **2017**, *1*, 0052. d) C. K. Prier, D. A. Rankic, D. W. C. MacMillan, *Chem. Rev.* **2013**, *11*, 5322-5363. e) Zhu, C.; Zhang, Y.-F.; Liu, Z.-Y.; Zhou, L.; Liu, H.; Feng, C. Selective C–F

Bond Carboxylation of *gem*-Difluoroalkenes with CO_2 by Photoredox/Palladium Dual Catalysis. *Chem. Sci.*, **2019**, *10*, 6721-6726.

135. Select reviews on CDC: a) Li, C-J. Cross-Dehydrogenative Coupling (CDC): Exploring C−C Bond Formations beyond Functional Group Transformations. *Acc. Chem. Res.* **2009**, *42*, 335-344. b) Yeung, C. S.; Dong, V. M. Catalytic Dehydrogenative Cross-Coupling: Forming Carbon−Carbon Bonds by Oxidizing Two Carbon−Hydrogen Bonds. *Chem. Rev.* **2011**, *111*, 1215–1292. c) Siemsen, P.; Livingston, R. C.; Diederich, F. Acetylenic Coupling: A Powerful Tool in Molecular Construction. *Angew. Chem., Int. Ed.* **2000**, *39*, 2632-2657. d) Beccalli, E. M.; Broggini, G.; Martinelli, M.; Sottocornola, S. C−C, C−O, C−N Bond Formation on sp^2 Carbon by Pd(II)-Catalyzed Reactions Involving Oxidant Agents. *Chem. Rev.* **2007**, *107*, 5318-5365.

136. a) Benniston, A. C.; Harriman, A. Artificial photosynthesis. *Mater. Today* **2008**, 11, 26–34. b) Gust, D.; Kramer, D.; Moore, A.; Moore, T. A.; Vermaas, W. Engineered and Artificial Photosynthesis: Human Ingenuity Enters the Game. *MRS Bull.* **2008**, *33*, 383–387. c) J. Barber, *Chem. Soc. Rev.* **2009**, *38*, 185–196.

137. Fajrina, N.; Tahir, M. A Critical Review in Strategies to Improve Photocatalytic Water Splitting Towards Hydrogen Production. *Int. J. Hydrog. Energy* **2019**, *44*, 540-577.

138. Szajna-Fuller, E.; Bakac, A. Catalytic Generation of Hydrogen with Titanium Citrate and a Macrocyclic Cobalt Complex. *Eur. J. Inorg. Chem.* **2010**, 2488–2494.

139. a) Lewis, N. S.; Nocera, D. G. Powering the Planet: Chemical Challenges in Solar Energy Utilization. *Proc. Natl. Acad. Sci.* **2007**, *103*, 15729-15735. b) Esswein, A. J.; Nocera, D. G. Hydrogen Production by Molecular Photocatalysis. *Chem. Rev.* **2007**, *107*, 4022–4047. c) Bard, A. J.; Fox, A. M. Artificial Photosynthesis: Solar Splitting of Water to Hydrogen and Oxygen. *Acc. Chem. Res.* **1995**, *28*, 141–145.

140. a) Wang, M.; Na, Y.; Gorlov, M. Light-driven Hydrogen Production Catalyzed by Transition Metal Complexes in Homogeneous Systems. *Dalton Trans.* **2009**, 6458–6467. b) Krishnan, C. V.; Brunschwig, B. S.; Creutz, C.; Sutin, N. Sun, L. C. Homogeneous Catalysis of the Photoreduction of Water. 6. Mediation by Polypyridine Complexes of Ruthenium(II) and Cobalt(II) in Alkaline Media. *J. Am. Chem. Soc.* **1985**, *107*, 2005–2015. c) Creutz, C.; Sutin, N. Light Induced Electron Transfer Reactions of Metal Complexes. *Coord. Chem. Rev.* **1985**, *64*, 321–324. d) Probst, B.; Rodenberg, A.; Guttentag, M.; Hamm, P.; Alberto, R. A Highly Stable Rhenium−Cobalt System for Photocatalytic H_2 Production: Unraveling the Performance-Limiting Steps. *Inorg. Chem.* **2010**, *49*, 6453–6460. e) Zhang, P.; Wang, M.; Dong, J.; Li, X.; Wang, F.; Wu, L.; Sun, L. Photocatalytic Hydrogen Production from Water by Noble-Metal-Free Molecular Catalyst Systems Containing Rose Bengal and the Cobaloximes of BF_x-Bridged Oxime Ligands. *J. Phys. Chem. C* **2010**, *114*, 15868–15874. f) Probst, B.; Kolano, C.; Hamm, P.; Alberto, R. An Efficient Homogeneous Intermolecular Rhenium-Based Photocatalytic System for the Production of H_2. *Inorg. Chem.* **2009**, *48*, 1836–1843. g) Du, P. W.; Knowles, K.; Eisenberg, R. A Homogeneous System for the Photogeneration of Hydrogen from Water Based on a Platinum(II) Terpyridyl Acetylide Chromophore and a Molecular Cobalt Catalyst. *J. Am. Chem. Soc.* **2008**, *130*, 12576–12577. h) Lazarides, T.; McCormick, T.; Du, P. W.; Luo, G. G.;

Lindley, B.; Eisenberg, R. Making Hydrogen from Water Using a Homogeneous System Without Noble Metals. *J. Am. Chem. Soc*. **2009**, *131*, 9192–9194. i) Okura, I.; Kaji, N.; Aono, S.; Kita, T. Photoinduced Hydrogen Evolution Using Bipyridinium Salts as Electron Carrier. *Inorg. Chem.* **1985**, *24*, 451–453. j) Okura, I. Hydrogenase and its Application for Photoinduced Hydrogen Evolution. *Coord. Chem. Rev*. **1985**, *68*, 53-99. k) Adar, E.; Degani, Y.; Goren, Z.; Willner, I. Photosensitized Electron-Transfer Reactions in β-Cyclodextrin Aqueous Media: Effects on Dissociation of Ground-State Complexes, Charge Separation, and Hydrogen Evolution. *J. Am. Chem. Soc.* **1986**, *108*, 4696–4700. l) Ho, P.-Y.; Wang, Y.; Yiu, S.-C.; Yu, W.-H.; Ho, C.-L.; Huang, S. Starburst Triarylamine Donor-Based Metal-Free Photosensitizers for Photocatalytic Hydrogen Production from Water. *Org. Lett*. **2017**, *19*, 1048–1051.

141. a) Artero, V.; Chavarot-Kerlidou, M.; Fontecave, M. Splitting Water with Cobalt. *Angew. Chem. Int. Ed.* **2011**, *50*, 7238–7266. b) Connolly, P.; Espenson, J. H. Cobalt-Catalyzed Evolution of Molecular Hydrogen. *Inorg. Chem*. **1986**, *25*, 2684–2688. c) Hu, X.; Brunschwig, B. S.; Peters, J. C. Electrocatalytic Hydrogen Evolution at Low Overpotentials by Cobalt Macrocyclic Glyoxime and Tetraimine Complexes. *J. Am. Chem. Soc*. **2007**, *129*, 8988–8998. d) Razavet, M.; Artero, V.; Fontecave, M. Proton Electroreduction Catalyzed by Cobaloximes: Functional Models for Hydrogenases. *Inorg. Chem*. **2005**, *44*, 4786–4795. e) Baffert, C.; Artero, V.; Fontecave, M. Cobaloximes as Functional Models for Hydrogenases. 2. Proton Electroreduction Catalyzed by Difluoroborylbis(dimethylglyoximato)cobalt(II) Complexes in Organic Media. *Inorg. Chem*. **2007**, *46*, 1817–1824. f) Hu, X. L.; Cossairt, B. M.; Brunschwig, B. S.; Lewis, N. S.; Peters, J. C. Electrocatalytic Hydrogen Evolution by Cobalt Difluoroboryl-diglyoximate Complexes. *Chem. Commun*. **2005**, 4723–4725. g) Pantani, O.; Anxolabehere-Mallart, E.; Aukauloo, A.; Millet, P. Electroactivity of Cobalt and Nickel Glyoximes with Regard to the Electro-Reduction of Protons into Molecular Hydrogen in Acidic Media. *Electrochem. Commun*. **2007**, *9*, 54–58.

142. a) Gridnev, A. A.; Ittel, S. D. Catalytic Chain Transfer in Free-Radical Polymerizations. *Chem. Rev*. **2001**, *101*, 3611–3659. b) Li, G; Pulling, M. E.; Estes, D. P.; Norton, J. R. Evidence for Formation of a Co–H Bond from (H₂O)₂Co(dmgBF₂)₂ under H₂: Application to Radical Cyclizations. *J. Am. Chem. Soc*. **2012**, *134*, 14662–14665.

143. Razavet, M.; Artero, V.; Fontecave, M. Proton Electroreduction Catalyzed by Cobaloximes: Functional Models for Hydrogenases. *Inorg. Chem*. **2005**, *46*, 1817–1824.

144. Dempsey, J. L.; Brunswig, B. S.; Winkler, J. R.; Gray, H. B. Hydrogen Evolution Catalyzed by Cobaloximes. *Acc. Chem. Res*. **2009**, *42*, 1995–2004.

145. a) Lacy, D. C.; Robers, G. M.; Peters, J. C. The Cobalt Hydride that Never Was: Revisiting Schrauzer's "Hydridocobaloxime". *J. Am. Chem. Soc.* **2015**, *137*, 4860–4864. b) Estes, D. P.; Grills, D. C.; Norton, J. R. The Reaction of Cobaloximes with Hydrogen: Products and Thermodynamics. *J. Am. Chem. Soc*. **2014**, *136*, 17362–17365.

146. Muckerman, J. T.; Fujita, E. Theoretical Studies of the Mechanism of Catalytic Hydrogen Production by a Cobaloxime. *Chem. Commun*. **2011**, *47*, 12456–12457.

147. a) Gridnev, A. A.; Ittel, S. D. Catalytic Chain Transfer in Free-Radical Polymerizations. *Chem. Rev*. **2001**, *101*, 3611–3659. b) Li, G.; Pulling, M. E.; Estes, D. P.; Norton, J. R. Evidence for Formation of a Co–H Bond from $(H_2O)_2Co(dmgBF_2)_2$ Under H_2: Application to Radical Cyclizations. *J. Am. Chem. Soc*. **2012**, *134*, 14662–14665.

148. Reviews containing PC/Co H_2 evolution in cross-couplings: a) Tang, S.; Zeng, L.; Lei, A. Oxidative R^1–H/R^2–H Cross-Coupling with Hydrogen Evolution. *J. Am. Chem. Soc.* **2018**, *140*, 13128–13135. b) Chen, B.; Wu, L.-Z.; Tung, C.-H. Photocatalytic Activation of Less Reactive Bonds and Their Functionalization via Hydrogen-Evolution Cross-Couplings. *Acc. Chem. Res.* **2018**, *51*, 2512–2523. Review on HAT in photocatalyzed organic synthesis: c) Capaldo, L.; Ravelli, D. Hydrogen Atom Transfer (HAT): A Versatile Strategy for Substrate Activation in Photocatalyzed Organic Synthesis. *Eur. J. Org. Chem*. **2017**, 2056–2071.

149. Panagiotopoulos, A.; Ladomenou, K.; Sun, D.; Artero, V.; Countsolelos, A. Photochemical Hydrogen Production and Cobaloximes: The Influence of the Cobalt Axial *N*-Ligand on the System Stability. *Dalton Trans.* **2016**, *45*, 6732–6738.

150. Du, P.; Schneider, J.; Luo, G.; Brennessel, W. W.; Eisenberg, R. Visible Light-Driven Hydrogen Production from Aqueous Protons Catalyzed by Molecular Cobaloxime Catalysts. *Inorg. Chem*. **2009**, *48*, 4952–4962.

151. Creutz, C.; Chou, M. H.; Fujita, E.; Szalda, D. J. Reactions of Hydroxymethyl and Hydride Complexes in Water: Synthesis, Structure and Reactivity of a Hydroxymethyl–Cobalt Complex. *Coord. Chem. Rev*. **2005**, *249*, 375–390.

152. a) Felton, G. A. N.; Glass, R. S.; Lichtenberger, D. L.; Evans, D. H. Iron-Only Hydrogenase Mimics. Thermodynamic Aspects of the Use of Electrochemistry to Evaluate Catalytic Efficiency for Hydrogen Generation. *Inorg. Chem.* **2006**, *45*, 9181–9184. b) Izutsu, K. Acid-Base Dissociation Constants in Dipolar Aprotic Solvents; Blackwell Scientific Publications: Oxford, U. K.,1990.

153. a) Banerjee, T.; Haase, F.; Savasci, G.; Gottschling, K.; Ochsenfeld, C.; Lotsch, B. V. Single-Site Photocatalytic H_2 Evolution from Covalent Organic Frameworks with Molecular Cobaloxime Co-Catalysts. *J. Am. Chem. Soc.* **2017**, *139*, 16228–16234.

154. Potentials in Figure 4.3 are measured with SCE in MeCN. a) All Co potentials from reference 144. b) Co(III)–H pKa 7.7: Natali, M. Elucidating the Key Role of pH on Light-Driven Hydrogen Evolution by a Molecular Cobalt Catalyst. *ACS Catal*. **2017**, *7*, 1330–1339. c) pK_a suspected to be for Co(I)–H tautomer of Co(III)–H: See reference 141e. Ru and Ir photosesitizers: d) Narayanam, J. M R.; Stephenson, C. R. J. Visible Light Photoredox Catalysis: Applications in Organic Synthesis. *Chem. Soc. Rev*. **2011**, 40, 102–113. e) Teegardin, K.; Day, J. I.; Chan, J.; Weaver, J. Advances in Photocatalysis: A Microreview of Visible Light Mediated Ruthenium and Iridium Catalyzed Organic Transformations. *Org. Process Res. Dev*. **2016**, *20*, 1156–1163. Acr^+ photocaalyst: f) Fukuzumi, S.; Kotani, H.; Ohkubo, K.; Ogo, S.; Tkachenko, N. V.; Lemmetyinen, H. Electron-Transfer State of 9-Mesityl-10-methylacridinium Ion with a Much Longer Lifetime and Higher Energy Than That of the Natural Photosynthetic

Reaction Center. *J. Am. Chem. Soc*. **2004**, *126*, 1600-1601. g) Ohkubo, K.; Kobayashi, T.; Fukuzumi, S. Direct Oxygenation of Benzene to Phenol Using Quinolinium Ions as Homogeneous Photocatalysts. *Angew. Chem. Int. Ed*. **2011**, *50*, 8652-8655. For a review on organic photoredox catalysis: h) Romero, N. A.; Nicewicz, D. A. Organic Photoredox Catalysis. *Chem. Rev.* **2016**, *116*, 10075-10166. i) Hari, D. P.; König, B. Synthetic Applications of Eosin Y in Photoredox Catalysis. *Chem. Commun*. **2014**, *50*, 6688–6699. j) Neumann, M.; Fuldner, S; König, B.; Zeitler, K. Metal-Free, Cooperative Asymmetric Organophotoredox Catalysis with Visible Light. *Angew. Chem. Int. Ed.* **2011**, *50*, 951–954. k) Ohkubo, K.; Kobayashi, T.; Fukuzumi, S. Direct Oxygenation of Benzene to Phenol Using Quinolinium Ions as Homogeneous Photocatalysts. *Angew. Chem. Int. Ed*. **2011**, *50*, 8652–8655. l) Ohkubo, K.; Suga, K.; Morikawa, K.; Fukuzumi, S. Selective Oxygenation of Ring-Substituted Toluenes with Electron-Donating and -Withdrawing Substituents by Molecular Oxygen via Photoinduced Electron Transfer. *J. Am. Chem. Soc*. **2003**, *125*, 12850–12859.

155. West, J. G.; Huang, D.; Sorensen, E. J. Acceptorless Dehydrogenation of Small Molecules through Cooperative Base Metal Catalysis. *Nat. Commun*. **2015**, *6*, 10093.

156. Tzirakis, M. D.; Lykakis, I. N.; Orfanopoulos, M. Decatungstate as an Efficient Photocatalyst in Organic Chemistry. *Chem. Soc. Rev*. **2009**, *38*, 2609–2621.

157. Zhang, X.-M. Homolytic Bond Dissociation Enthalpies of the C−H Bonds Adjacent to Radical Centers. *J. Org. Chem.* **1998**, *63*, 1872–1877.

158. Abrams, D. J.; West, J. G.; Sorensen, E. J. Toward a Mild Dehydroformylation Using Base-Metal Catalysis. *Chem. Sci*. **2017**, *8*, 1954–1959.

159. He, K.-H.; Tan, F.-F.; Zhou, C.-Z.; Zhou, G.-J.; Yang, X.-L.; Li, Y. Acceptorless Dehydrogenation of *N*-Heterocycles by Merging Visible-Light Photoredox Catalysis and Cobalt Catalysis. *Angew. Chem. Int. Ed*. **2017**, *56*, 3080–3084.

160. Sahoo, M. K.; Saravanakumar, K.; Jaiswal, G.; Balarman, E. Photocatalysis Enabling Acceptorless Dehydrogenation of Diaryl Hydrazines at Room Temperature. *ACS Catal*. **2018**, *8*, 7727–7733.

161. Related methods involving iminium and oxonium ion intermediates generated by photoredox catalysis employing a sacrificial H-atom acceptor/oxidant: a) Tucker, J. W.; Narayanam, J. M. R.; Shah, P. S.; Stephenson, C. R. J. Oxidative Photoredox Catalysis: Mild and Elective Deprotection of PMB Ethers Mediated by Visible Light. *Chem. Commun*. **2011**, *47*, 5040–5042. b) Condie, A. G.; Gonzalez-Gomez, J. C.; Stephenson, C. R. J. Visible-Light Photoredox Catalysis: Aza-Henry Reactions via C−H Functionalization. *J. Am. Chem. Soc*. **2010**, *132*, 1464–1465.

162. Zhong, J.-J.; Meng, Q.-Y.; Liu, B.; Li, X.-B.; Gao, X.-W.; Lei, T.; Wu, C.-J.; Li, Z.-J.; Tung, C.-H.; Wu, L.-Z. Cross-Coupling Hydrogen Evolution Reaction in Homogeneous Solution without Noble Metals. *Org. Lett*. **2014**, *16*, 1988–1991.

163. Jia, Z.; Yang, Q.; Zhang, L.; Luo, S. Photoredox Mediated Acceptorless Dehydrogenative Coupling of Saturated *N*-Heterocycles. *ACS Catal*. **2019**, *9*, 3589–3594.

164. Niu, L.; Wang, S.; Liu, J.; Yi, H.; Liang, X.-A.; Liu, T.; Lei, A. Visible Light-Mediated Oxidative C(sp^3)–H Phosphonylation for α-Aminophosphonates Under Oxidant-Free Conditions. *Chem. Commun*. **2018**, *54*, 1659–1662.

165. Roth, H. G.; Romero, N. A.; Nicewicz, D. A. Experimental and Calculated Electrochemical Potentials of Common Organic Molecules for Applications to Single-Electron Redox Chemistry. *Synlett* **2016**, *27*, 714-723.

166. Gao, X.-W.; Meng, Q.-Y.; Li, J.-X.; Zhong, J.-J.; Lei, T.; Li, X.-B.; Tung, C.-H.; Wu, L.-Z. Visible Light Catalysis Assisted Site-Specific Functionalization of Amino Acid Derivatives by C–H Bond Activation without Oxidant: Cross-Coupling Hydrogen Evolution Reaction. *ACS Catal.* **2015**, *5*, 2391–2396.

167. Xiang, M.; Meng, Q.-Y.; Li, J.-X.; Zheng, Y.-W.; Ye, C.; Li, Z.-J.; Chen, B.; Tung, C.-H.; Wu, L.-Z. Activation of C–H Bonds through Oxidant-Free Photoredox Catalysis: Cross-Coupling Hydrogen-Evolution Transformation of Isochromans and β-Keto Esters. *Chem. Eur. J*. **2015**, *21*, 18080–18084.

168. Tang, S.; Liu, K.; Liu, C.; Lei, A. Olefinic C–H Functionalization through Radical Alkenylation. *Chem. Soc. Rev*. **2015**, *44*, 1070–1082.

169. Zhang, G.; Hu, X.; Chiang, C.-W.; Yi, H.; Pei, P.; Singh, A. K.; Lei, A. Anti-Markovnikov Oxidation of β-Alkyl Styrenes with H$_2$O as the Terminal Oxidant. *J. Am. Chem. Soc*. **2016**, *138*, 12037−12040.

170. Yi, H.; Niu, L.; Song, C.; Li, Y.; Dou, B.; Singh, A. K.; Lei, A. Photocatalytic Dehydrogenative Cross-Coupling of Alkenes with Alcohols or Azoles without External Oxidant. *Angew. Chem. Int. Ed*. **2017**, *56*, 1120–1124.

171. Yu, W.-L.; Luo, Y.-C.; Yan, L.; Liu, D.; Wang, Z.-Y.; Xu, P.-F. Dehydrogenative Silylation of Alkenes for the Synthesis of Substituted Allylsilanes by Photoredox, Hydrogen-Atom Transfer, and Cobalt Catalysis. *Angew. Chem. Int. Ed.* **2019**, *131*, 11057-11061.

172. Hu, X.; Zhang, G.; Bu, F.; Luo, X.; Yi, K.; Zhang, H.; Lei, A. Photoinduced Oxidative Activation of Electron-Rich Arenes: Alkenylation with H$_2$ Evolution under External Oxidant-Free Conditions. *Chem. Sci.* **2018**, *9*, 1521–1526.

173. Tay, N. E. S.; Nicewicz, D. A. Cation Radical Accelerated Nucleophilic Aromatic Substitution via Organic Photoredox Catalysis. *J. Am. Chem. Soc*. **2017**, *139*, 16100–16104.

174. Cao, H.; Jiang, H.; Feng, H.; Kwan, J. M. C.; Liu, X.; Wu, J. Photo-induced Decarboxylative Heck-Type Coupling of Unactivated Aliphatic Acids and Terminal Alkenes in the Absence of Sacrificial Hydrogen Acceptors. *J. Am. Chem. Soc.* **2018**, *140*, 16360–16367.

175. Chen, L; Hisaeda, Y.; Shimakoshi, H. Visible Light-Driven, Room Temperature Heck-Type Reaction of Alkyl Halides with Styrene Derivatives Catalyzed by B12 Complex. *Adv. Synth. Catal*. **2019**, *361*, 2877–2828.

176. Hu, X.; Zhang, G.; Bu, F.; Lei, A. Selective Oxidative [4+2] Imine/Alkene Annulation with H_2 Liberation Induced by Photo-Oxidation. *Angew. Chem. Int. Ed*. **2018**, *57*, 1286–1290.

177. Zhang, G.; Lin, Y.; Luo, X.; Hu, X.; Chen, C.; Lei, A. Oxidative [4+2] Annulation of Styrenes with Alkynes under External-Oxidant-Free Conditions. *Nat. Commun.* **2018**, *9*, 1225.

178. Cao, W.; Wu, C.; Lei, T.; Yang, X.; Chen, B.; Tung, C.; Wu, L. Photocatalytic Hydrogen-Evolution Dimerization of Styrenes to Synthesize 1,2-dihydro-1-arylnaphthalene Derivatives using Acr$^+$-Mes and Cobaloxime Catalysts. *Chin. J. Catal*. **2018**, *39*, 1194–1201.

179. Zhao, Q.-Q.; Hu, X.-Q.; Yang, M.-N.; Chen, J.-R.; Xiao, W.-J. A Visible-Light Photocatalytic *N*-radical Cascade of Hydrazones for the Synthesis of Dihydropyrazole-Fused Benzosultams. *Chem. Commun*. **2016**, 52, 12749–12752.

180. Qiao, M.-M.; Liu, Y.-Y.; Yao, S.; Ma, T.-C.; Tang, Z.-L.; Shi, D.-Q.; Xiao, W.-J. Photoredox/Cobalt-Catalyzed Phosphinyloxy Radical Addition/Cyclization Cascade: Synthesis of Phosphaisocoumarins. *J. Org. Chem*. **2019**, *84*, 6798–6808.

181. Tu, J.-L.; Liu, J.-L.; Tang, W.; Ma, S.; Liu, F. Radical Aza-Cyclization of α-Imino-oxy Acids for Synthesis of Alkene-Containing N-Heterocycles via Dual Cobaloxime and Photoredox Catalysis. *Org. Lett*. **2020**, *22*, 1222−1226.

182. Wu, C.-J.; Meng, Q.-Y.; Lei, T.; Zhong, J.-J.; Liu, W.-Q.; Zho, L.-M.; Li, Z.-J.; Chen, B.; Tung, C.-H.; Wu, L.-Z. An Oxidant-Free Strategy for Indole Synthesis via Intramolecular C–C Bond Construction under Visible Light Irradiation: Cross-Coupling Hydrogen Evolution Reaction. *ACS Catal*. **2016**, *6*, 4635–4639.

183. Zhang, G.; Liu, C.; Yi, H.; Meng, Q.-Y.; Bian, C.-L.; Chen, H.; Jian, J.-X.; Wu, L.-Z.; Lei, A. External Oxidant-Free Oxidative Cross-Coupling: A Photoredox Cobalt-Catalyzed Aromatic C–H Thiolation for Constructing C–S Bonds. *J. Am. Chem. Soc*. **2015**, *137*, 9273–9280.

184. Zhang, M.; Ruzi, R.; Li, N.; Xie, J.; Zhu, C.-J. Photoredox and Cobalt Co-Catalyzed C(sp^2)–H Functionalization/C–O Bond Formation for Synthesis of Lactones under Oxidant- and Acceptor-Free Conditions. *Org. Chem. Front*. **2018**, *5*, 749–752.

185. Shao, A.; Zhan, J.; Li, N.; Chiang, C.-W.; Lei, A. External Oxidant-Free Dehydrogenative Lactonization of 2-Arylbenzoic Acids via Visible-Light Photocatalysis. *J. Org. Chem*. **2018**, *83*, 3582–3589.

186. Tian, W.-F.; Hu, C.-H.; He, K.-H.; He, X.-Y.; Li, Y. Visible-Light Photoredox-Catalyzed Decarboxylative Alkylation of Heteroarenes Using Carboxylic Acids with Hydrogen Release. *Org. Lett*. **2019**, *21*, 6930−6935.

187. Zheng, Y.-W.; Chen, B.; Ye, P.; Feng, K.; Wang, W.; Meng, Q.-Y.; Wu, L.-Z.; Tung, C.-H. Photocatalytic Hydrogen-Evolution Cross-Couplings: Benzene C–H Amination and Hydroxylation. *J. Am. Chem. Soc.* **2016**, *138*, 10080–10083.

188. Zheng, Y.-W.; Chen, B.; Ye, P.; Feng, K.; Wang, W.; Meng, Q.-Y.; Wu, L.-Z.; Tung, C.-H. Benzene C–H Etherification via Photocatalytic Hydrogen-Evolution Cross-Coupling Reaction. *Org. Lett.* **2017**, *19*, 2206–2209.

189. Niu, L.; Yi, H.; Wang, S.; Liu, T.; Liu, J.; Lei, A. External Oxidant-free Electrooxidative [3 + 2] Annulation Between Phenol and Indole Derivatives. *Nat. Commun.* **2017**, *8*, 1–7.

190. Zhao, F.; Yang, Q.; Zhang, J.; Shi, W.; Hu, H.; Liang, F.; Wei, W.; Zhou, S. Photocatalytic Hydrogen-Evolving Cross-Coupling of Arenes with Primary Amines. *Org. Lett.* **2018**, *20*, 7753–7757.

Chapter 5:

191. Gooßen, L. J.; Rodríguez, N.; Gooßen, K. Carboxylic Acids as Substrates in Homogeneous Catalysis. *Angew. Chem., Int. Ed.* **2008**, *47*, 3100−3120.

192. a) Miller, J. A.; Nelson, J. A.; Byrne, M. P. A Highly Catalytic and Selective Conversion of Carboxylic Acids to 1-Alkenes of One Less Carbon Atom. *J. Org. Chem.* **1993**, *58*, 18−20. b) Maetani, S.; Fukuyama, T.; Suzuki, N.; Ishihara, D.; Ryu, I. Efficient Iridium-Catalyzed Decarbonylation Reaction of Aliphatic Carboxylic Acids Leading to Internal or Terminal Alkenes. *Organometallics* **2011**, *30*, 1389−1394. c) Miranda, M. O.; Pietrangelo, A.; Hillmyer, M. A.; Tolman, W. B. Catalytic Decarbonylation of Biomass-Derived Carboxylic Acids as Efficient Route to Commodity Monomers. *Green Chem.* **2012**, *14*, 490−494. d) Murray, R. E.; Walter, E. L.; Doll, K. M. ACS Catal. 2014, 4, 3517−3520. e) Liu, Y.; Kim, K. E.; Herbert, M. B.; Fedorov, A.; Grubbs, R. H.; Stoltz, B. M. Tandem Isomerization-Decarboxylation for Converting Alkenoic Fatty Acids into Alkenes. *Adv. Synth. Catal.* **2014**, *356*, 130−136. f) John, A.; Hillmyer, M. A.; Tolman, W. B. Anhydride-Additive-Free Nickel-Catalyzed Deoxygenation of Carboxylic Acids to Olefins. *Organometallics* **2017**, *36*, 506−509.

193. a) X. Hu, B. S. Brunschwig, J. C. Peters, *J. Am. Chem. Soc.* **2007**, *129*, 8988-8998. b) C. Creutz, M. H. Chou, E. Fujita, *Coord. Chem. Rev.* **2005**, *249*, 375- 390. c) G. N. Schrauzer, E. Deutsch, *J. Am. Chem. Soc.* **1969**, *91*, 3341-3350.

194. Beaumont, T. G.; Davis, K. M. C. Charge-Transfer Complexes. Part IX. Charge-Transfer Mechanisms in the Quenching of the Fluorescence of the *N*-methylacridinium Ion by Counter-Ions. *J. Chem. Soc. B*, **1970**, 456–459.

195. Brown, T. M.; Dronsffeld, A. T. Cobaloximes as Vehicles for College Teaching. *J. Chem. Ed.* **1990**, *67*, 973-974.

196. Cartwright, K. C.; Joseph, E.; Comadoll, C. G.; Tunge, J. A. Photoredox/Cobalt Dual Catalyzed Decarboxylative Elimination of Carboxylic Acids: Development and Mechanistic Insight. *Chem. Eur. J.* **2020.** DOI: 10.1002/CHEM.202001952.

197. a) Dutta, G.; Laskar, M.; Gupta, B. D. Molecular Oxygen Insertion in Benzylcobaloximes with Mixed Dioximes. *Organometallics* **2008**, *27*, 3338–3345. b) Bhuyan, M.; Laskar, M.; Mandal, D.; Gupta, B. D. Co−C Bond Reactivity and *Cis* Influence Relationship in Benzylcobaloximes with Glyoxime and Dimesitylglyoxime. *Organometallics* **2007**, *26*, 3559-3567. c) Gupta, B. D.; Yamuna, R.; Mandal, D. Cobaloximes with Mixed Dioximes of Glyoxime and Diphenylglyoxime: Synthesis, Characterization, CV, X-ray Studies, and Crystal Packing. *Organometallics* **2006**, *25*, 706-714. c) Mandal, D.; Gupta, B. D. Cobaloximes with Dimesitylglyoxime: Synthesis, Characterization, and Spectral Correlations with the Related Cobaloximes. *Organometallics,* **2005**, *24*, 1501-1510. d) Gupta, B. D.; Singh, V.; Yamuna, R.; Barclay, T.; Cordes, W. Organocobaloximes with Mixed Dioxime Equatorial Ligands: A Convenient One-Pot Synthesis. X-ray Structures and Cis−Trans Influence Studies. *Organometallics* **2003**, *22*, 2670-2678. e) Branchaud, B. P.; Choi, Y. L. Effect of a Remote Ligand Substituent on Premature β-H Elimination in a Cobaloxime-Mediated Radical Alkyl-Alkenyl Cross Coupling. *Tet. Lett.* **1988**, *29*, 6037-6038.

198. a) David R. Lide, ed., *CRC Handbook of Chemistry and Physics, Internet Version,* <http://www.hbcpnetbase.com>, CRC Press, Boca Raton, FL, **2005**. b) Andon, R. J. L.; Cox, J. D.; Herington, E. F. G. The Ultra-Violet Absorption Spectra and Dissociation Constants of Certain Pyridine Bases in Aqueous Solution. *Trans. Faraday Soc.,* **1954***, 50,* 918-927. c) Chrystiuk, E.; Williams, A. A Single Transition-State in the Transfer of the Methoxycarbonyl Group Between Isoquinoline and Substituted Pyridines in Aqueous Solution. *J. Am. Chem. Soc.,* **1987**, *109*, 3040-3046. d) Dean, J. A.; Lange, N. A. *Lange's Handbook of Chemistry*; McGraw-Hill, **1934**. e) Buckingham, J. *Dictionary of Organic Compounds*; Chapman & Hall, **1996**. f) Hensel, S.; Megger, N.; Schweizer, K.; Müller, J. Second Generation Silver(I)-Mediated Imidazole Base Pairs. *Beilstein J. Org. Chem.* **2014***, 10,* 2139–2144. g) Allman, T.; Goel, R. G. The Basicity of Phosphines. *Can. J. Chem.,* **1982***, 60,* 716-722.

199. a) Panagiotopoulos, A.; Ladomenou, K.; Sun, D.; Artero, V.; Coutsolelos, A. G. Photochemical Hydrogen Production and Cobaloximes: The Influence of the Cobalt Axial *N*-Ligand on the System Stability. *Dalton Trans.*, **2016**, *45*, 6732-6738. b) Lawrence, M. A. W.; Celestine, M. J.; Artis, E. T.; Joseph, L. S.; Esquivel, D. L.; Ledbetter, A. J.; Cropek, D. M.; Jarrett, W. L.; Bayse, C. A.; Brewer, M. L. Holder, A. A. Kinetics and Mechanism of the Oxidation of a Cobaloxime by Sodium Hypochlorite in Aqueous Solution: Is it an Outer-Sphere Mechanism? *Dal. Trans,* **2016**, *45*, 10326-10342. c) Mirra, S.; Strianese, M.; Pellecchia, C.; Bertolasi, V.; Monaco, G.; Milione, S. Influence of Coordinated Ligands in a Series of Inorganic Cobaloximes. *Inorganica Chimica Acta*, **2016**, *444*, 202-208. d) Yamazaki, N.; Hohokabe, Y. Studies on Cobaloxime Compounds. I. Synthesis of Various Cobaloximes and Investigation on Their Infrared and Far-Infrared Spectra. *Bulletin of the Chemical Society of Japan,* **1971***, 44*, 63-69. e) Kilic, A.; Durgun, M.; Yorulmaz, N.; Yavuz, R. The Synthesis and Investigation of Different Cobaloximines by Spectroscopic Methods. *J. Molecular Structure,* **2018**, *1174,* 25-31. f) Stewart, R. C.; Marzilli, L. G. *J. Am. Chem. Soc.* **1977**, *111,* 817-822.

200. Lee, B. J.; DeGlopper, K. S.; Yoon, T. P. Site-Selective Alkoxylation of Benzylic C−H Bonds by Photoredox Catalysis. *Angew. Chem. Int. Ed.* **2020**, *59*, 197-202.

201. Additional reports of additional dmgH improving HE: a) Eckenhoff, W. T.; McNamara, W. R.; Du, P.; Eisenberg, R. Cobalt Complexes as Artificial Hydrogenases for the Reductive Side of Water Splitting. *Biochim. Biophys. Acta, Bioenerg*. **2013**, *1827*, 958−973. b) McCormick, T. M.; Han, Z.; Weinberg, D. J.; Brennessel, W. W.; Holland, P. L.; Eisenberg, R. Visible Light-Driven Hydrogen Production from Aqueous Protons Catalyzed by Molecular Cobaloxime Catalysts. *Inorg. Chem.* **2011**, *50*, 10660−10666. c) Banerjee, T.; Haase, F.; Savasci, G.; Gottschling, K.; Ochenfeld, C.; Lotsch, B. V. Single-Site Photocatalytic H_2 Evolution from Covalent Organic Frameworks with Molecular Cobaloxime Co-Catalysts. *J. Am. Chem. Soc.* **2017**, *139*, 16228−16234.

202. Reactivity of Co-alkyls under photochemical conditions: a) Branchaud, B. P.; Meier, M. S.; Choi, Y. Alkyl-Alkenyl Cross Coupling via Alkyl Cobaloxime Radical Chemistry. An Alkyl Equivalent to the Heck Reaction Compatible with Common Organic Functional Groups. *Tet. Lett*. **1988,** *29*, 167-170. b) Branchaud, B. P.; Detlefsen, W. D. Cobaloxime-Catalyzed Radical Alkyl-Styryl Cross Couplings. *Tet. Lett*. **1991**, *32*, 6273-6276. c) Vranchaud, B. P.; Choi, Y. L. Synthesis of Monensin. Reconstruction from Degradation Products. *J. Org. Chem.* **1988**, *53*, 4641-4643.

203. a) Giese, B. *Radicals in Organic Synthesis: Formation of Carbon–Carbon Bonds*, Pergamon Press, Oxford, 1986. b) Acr$^+$-promoted Giese-type reaction with carboxylic acids: Ramierz, N. P.; Gonzalez-Gomez, J. C. Photocatalytic Dehydrogenative Lactonization of 2-Arylbenzoic Acids. *Eur. J. Org. Chem.* **2016**, *2017*, 2154-2163.

204. Moore, D. E. Kinetic Treatment of Photochemical Reactions. *International Journal of Pharmaceutics*, **1990**, *63*, R5-R7.

205. Kochi, J. K. Charge-Transfer Excitation of Molecular Complexes in Organic and Organometallic Chemistry. *Pure & Appl. Chem*., **1991**, *63*, 2, 255-264.

206. a) Trogler, W. C.; Stewart, R. C.; Epps, L. A.; Marzilli, L. G. *Inorg. Chem.* **1974**, *13*, 1564–1570. b) Bulkowski, J.; Cutler, A.; Dolphin, D.; Silverman, R. B. Cis and Trans Effects on the Proton Magnetic Resonance Spectra of Cobaloximes. *Inorg. Synth*. **1980**, *20*, 127–134.

207. Shevick, S. L.; Obradors, C.; Shenvi, R. A. Mechanistic Interrogation of Co/Ni-Dual Catalyzed Hydroarylation. *J. Am. Chem. Soc*. **2018**, *140*, 12056-12068.

208. Rate estimate based on nonyl radical and TEMPO coupling rate in acetonitrile: Beckwith, A. L. J.; Bowry, V. W.; Ingold, K. U. Kinetics of Nitroxide Radical Trapping. 1. Solvent Effects. *J. Am. Chem. Soc.* **1992**, *114*, 4983-4992.

209. The possibility of a Co-Carboxylate complex leading to the Co catalyst being in close proximinty to the alkyl radical formed should be considered: Lande, S. S.; Kochi, J. K. Formation and Oxidation of Alkyl Radicals by Cobalt(III) Complexes. *J. Am. Chem. Soc.* **1968**, 90, 19, 5196-5207.

210. See page 11 for discussion on Co oxidation of alkyl radicals: Lande, S. S.; Kochi, J. K. Formation and Oxidation of Alkyl Radicals by Cobalt(III) Complexes. *J. Am. Chem. Soc.* **1968**, 90, 19, 5196-5207.

211. McCormick, T. M.; Calitree, B. D.; Orchard, A.; Kraut, N. D.; Bright, F. V.; Detty, M. R.; Eisenberg, R. Reductive Side of Water Splitting in Artificial Photosynthesis: New Homogeneous Photosystems of Great Activity and Mechanistic Insight. *J. Am. Chem. Soc*. **2010**, *132*, 15480–15483.

212. Shindo, K.; Suzuki, H.; Okuda, T. Paecilopeptin, a New Cathepsin S Inhibitor Produced by *Paecilomyces carneus. Biosci. Biotechnol. Biochem*., **2002**, *66*, 2444–2448.

213. Fukuzawa, S-I.; Oura, I.; Shimizu, K.; Minoru, K.; Ogata, K-I. Is the Elimination of Lithium Alkoxide Easier from a Vinyllithium or from an Alkyllithium? A DFT Study of the Aromatization of 3-Vinylidene-2,3-dihydrobenzofurans to Benzofurans. *Eur. J. Org. Chem.* **2009**, *5,* 726-720.

214. Wang, X-J.; Yang, Q.; Liu, F.; You, Q-D. Microwave-Assisted Synthesis of Amide Under Solvent-Free Conditions. *Synthetic Communications,* **2008**, *38*, 1028-1035.

215. Hamasaki, A.; Liu, X.; Makoto, T. Amidocarbonylation of Aldehydes Utilizing Cobalt Oxide-Supported Gold Nanoparticles as a Heterogeneous Catalyst. *Chem. Lett.*, **2008**, *37*, 1292-1293.

216. LeTiran, A.; Stables, J. P.; Kohn, H. Design and Evaluation of Affinity Labels of Functionalized Amino Acid Anticonvulsants. *J. Med. Chem.*, **2002**, *45*, 4762-4773.

217. Tang, W.; Zhang, X. A Chiral 1,2-Bisphospholane Ligand with a Novel Structural Motif: Applications in Highly Enantioselective Rh-Catalyzed Hydrogenations. *Angew. Chem. Int. Ed.*, **2002**, *41*, 1612-1614.

218. Engle, K. M.; Wang, D-H.; Yu, J-Q. Ligand-Accelerated C-H Activation Reactions: Evidence for a Switch of Mechanism. *J. Am. Chem. Soc.*, **2010**, *132*, 14137-14151.

219. Potevien, B.; Tordjman, C.; Pastoureau, P.; Bonnet, J.; De Nanteuil, G.1,3-Diaryl-4,5,6,7-tetrahydro-2*H*-isoindole Derivatives: A New Series of Potent and Selective COX-2 Inhibitors in Which a Sulfonyl Group Is Not a Structural Requisite. *J. Med. Chem.* **2000**, *43*, 4582-4593.

220. Anslyn, E. V.; Dougherty, D. A. *Modern Physical Organic Chemistry*, 1ˢᵗ ed.; University Science Books: **2006**; pp. 388-389.